ANTIFOULING PHYSICALLY SMALL CARBON ELECTRODES FOR DOPAMINE DETECTION

By

Shajahan Siraj

Master of Science, University of Dhaka

A thesis submitted in fulfilment of the requirements for the degree of

Doctor of Philosophy

Department of Chemistry and Biomolecular Sciences

Macquarie University

Sydney, Australia

19 August 2016

Abstract

In this work, we have developed physically small carbon electrodes that show antifouling behaviour during detection of the neurotransmitter dopamine in a biological medium to achieve meaningful detection results. In such an experiment, amphiphilic proteins, peptides and lipids present in extracellular fluid can easily adsorb on a hydrophilic electrode surface. This prevents dopamine from making direct contact with the electrode for electron transfer reactions, leading to electrode fouling in which a gradually diminishing transient detection signal is observed. In this study, we have developed antifouling conical-tip carbon electrodes by hydrogenating the carbon using an *n*-butylsilane or a diethylsilane reduction method, followed by a 4-sulfobenzene layer. These modified electrodes were subjected to dopamine detection in the presence of a simulated biological environment to assess their effectiveness in such a detection experiment. In addition, we have also discovered in this work that the *n*-butylsilane reduction method is capable of activating non-functioning carbon electrodes by removing carbon-oxygen functionalities from an electrode surface prior to terminating the defect sites with carbon-hydrogen.

In our laboratory, physically small conical-tip carbon electrodes are routinely fabricated by thermally pyrolysing acetylene in a nitrogen atmosphere to deposit carbon at the tip and on the shank of quartz capillaries already pulled down to a tapered end, typically ~2 μm in tip diameter and ~15 μm axial length. These electrodes were characterised by a sigmoidal-shaped cyclic voltammogram of $[Ru(NH_3)_6]^{3+}$ with a small charging current between the forward and backward scan. Occasionally, a non-sigmoidal shaped cyclic voltammogram with an appreciable charging current was obtained, indicating a non-functioning conical-tip carbon electrode. These electrodes were then treated in a one-pot reaction involving *n*-butylsilane reduction capable of reducing carbon–oxygen functionalities present on a carbon surface, *e.g.* aldehydes, ketones and primary, secondary and tertiary alcohols, polycarboxylic acid group to their corresponding alkyl functionalities, leaving carbon–carbon double bonds and the graphitic structure undisturbed. Phenolic hydroxyl groups, however, were not reduced but were instead silanised to form a dendrimeric butylsiloxane. After such a hydrogenation treatment,

these electrodes were found to yield an expected sigmoidal-shaped cyclic voltammogram of $[Ru(NH_3)_6]^{3+}$ with negligible charging current, indicating a characteristic functioning microelectrode. In this way, the fabrication success rate of carbon microelectrodes was improved to nearly 100%. X-ray photoelectron spectroscopy was used to systematically characterise the surface of hydrogenated carbon electrodes. We also studied the electrochemistry of anthraquinone-2,6-disulfonate (AQDS) at these hydrogenated carbon electrodes to provide evidence for the removal of the carbon-oxygen functionalities from the electrode surface. In addition, after a one-week storage in air and in a pH 7.4 citrate/phosphate buffer, there was a minimal change in the corresponding $[Ru(NH_3)_6]^{3+}$ reduction signal of ~1.1% and ~2.8%, respectively, observed at these hydrogenated carbon electrodes.

The *n*-butylsilane hydrogenated carbon electrodes were further characterised using $[Fe(CN)_6]^{3-}$ and dopamine as redox markers. To support the cyclic voltammetric results, electrochemical impedance spectroscopy was also conducted at the hydrogenated carbon electrodes. The results obtained indicated sluggish electron transfer kinetics for both redox markers at the electrodes due to the formation of an sp^3 enriched, defect free hydrophobic surface. The electrode surface was also examined using atomic force microscopy. Raman spectroscopic results also confirmed a larger proportion of sp^3 hybridised carbon at these hydrogenated carbon electrodes, compared to the corresponding carbon electrodes that were not hydrogenated. Hydrogenated carbon electrodes with such a hydrophobic surface have demonstrated their capability in determining dopamine with minimal interference from ascorbic acid at concentration as high as 500 μM generally expected in an extracellular fluid. Upon incubating hydrogenated carbon electrodes in a synthetic fouling solution containing 1.0% (v/v) caproic acid (a lipid), 4% (w/v) bovine serum albumin and 0.01% (w/v) cytochrome C (both are proteins), and 0.002% (w/v) human fibrinopeptide B (a peptide) for 30 min, they were used in the cyclic voltammetric detection of dopamine in order to assess their degree of antifouling capability. A ~35% decrease in dopamine oxidation current was observed. However, the magnitude of this oxidation current remained almost unchanged even after incubating the electrodes in the same synthetic fouling solution

for one week. The dopamine oxidation product, dopamine-*o*-quinone, is itself a well-known fouling reagent. However, there was no observable interference at the hydrogenated carbon electrodes when the dopamine concentration was kept below 1.0 μM, which is a 100-fold higher concentration than that generally expected in the central nervous system. These results support minimal fouling at *n*-butylsilane hydrogenated electrodes during dopamine detection *in vitro*.

Next, a 4-sulfobenzene layer was immobilised on hydrogenated conical-tip carbon electrodes to achieve improved dopamine detection sensitivity and to further enhance the fouling resistance at the electrodes. Cyclic voltammetry and X-ray photoelectron spectroscopy confirmed the grafting of 4-sulfobenzene on *n*-butylsilane modified electrodes. Similar results in the voltammetric studies of $[Fe(CN)_6]^{3-}$ at the electrodes to *n*-butylsilane hydrogenated electrodes were obtained. However, a ~4% improved $[Ru(NH_3)_6]^{3+}$ detection signal and a ~10% improved dopamine detection signal were estimated at 4-sulfobenzene modified electrodes that were hydrogenated by *n*-butylsilane reduction, compared to hydrogenated electrodes without any 4-sulfobenzene modification. The former electrodes also displayed a ~13% higher dopamine detection sensitivity over the latter electrodes. We have attributed all these observations to electrostatic attraction between the negatively charged 4-sulfobenzene groups on the electrode surface and positively charged $[Ru(NH_3)_6]^{3+}$ and dopamine (a cation under physiological pH). By assessing the antifouling property of the 4-sulfobenzene modified electrodes in the same fouling solution described above, there was only a 15% sensitivity loss, compared to ~38% at hydrogenated electrodes without 4-sulfobenzene modification. In addition, a limit of detection of 52 ± 8 nM was estimated at 4-sulfobenzene modified electrodes, which is approximately a three-fold improvement relative to 138 ± 12 nM estimated at hydrogenated electrodes without any 4-sulfobenzene modification.

In this work, we have also conducted carbon electrode hydrogenation using a branch-chained alkylsilane, diethylsilane, in place of the linear-chain n-butylsilane, to evaluate their antifouling capability. These diethylsilane hydrogenated carbon electrodes

showed a ~36% decrease in the dopamine oxidation signal after a one-week incubation in the fouling solution, which is comparable to 35% obtained at *n*-butylsilane hydrogenated carbon electrodes. In a similar experiment, a 38% decrease in dopamine signal was observed at a 4-sulfobenzene layer immobilised carbon electrodes that were hydrogenated by diethylsilane reduction. We have also observed faster electron transfer kinetics at both diethylsilane hydrogenated carbon electrodes and those that were subsequently modified by 4-sulfobenzene compared to all other electrodes studied in this work. More significantly, 100% 4-sulfobenzene modified carbon electrodes that were hydrogenated by diethylsilane reduction (compared to 66% of diethylsilane hydrogenated, 33% *n*-butylsilane hydrogenated, and 33% 4-sulfobenzene modified carbon electrodes that were hydrogenated by *n*-butylsilane reduction) were found to be stable and demonstrated consistent fouling resistance throughout the experiments after being incubated in the fouling solution for 0, 10, 30 min and 1 week.

Finally, all electrodes studied in this work were assessed in their feasibility in the analysis of dopamine in a real-life human serum sample, into which dopamine was spiked and then the recovery was evaluated. In this way, a 97.2 – 129% recovery of dopamine was obtained at all modified electrodes. These results support the potential applications of all the above modified electrodes for determination of dopamine in real-life samples.

Acknowledgements

I would firstly like to thank my supervisor, Dr Danny K.Y. Wong, for allowing me to work independently, however always being available to offer advice and assistance when required. He taught me how to effectively deliver research presentation to a wide scientific community. I have also learned from him how to systematically solve seemingly complex problems. His enthusiasm and encouragement have helped me throughout my candidature. Working with him all these years will undoubtedly assist me in further development as a researcher in future years.

Sincere thanks to my associate supervisor, Dr Christopher R. McRae, who assisted me in acquiring a good understanding of the silane hydrogenation process. I would also like to thank my research group members, Thomas Somerville, Mominul Haque, and Benjamin Pendleton for all their assistance and laughter in the laboratory over the years. Particularly, I like to express my gratitude to Thomas for his general advice and help in instrument setup. Thanks to Krystyna Drozdowicz-Tomsia at the Optical Characterisation Facility, Macquarie University, for her help in examining electrode surface by Raman spectroscopy.

Thank you to all the colleagues I have met at Macquarie University, Ketan, Nirmal, Kavita, Tareq, Imam, Rashid, Raha, Yvonne, Mohammed Hashemi, Rita, Dithi, Tony, Mark, Hong and anyone I may have inadvertently missed.

To the most important people in my life who made the biggest sacrifices – my parents, my wife, my son (**Ayaan**), my siblings, for their unconditional support and encouragement to pursue my interests.

Last but not least, I extend my gratitude to Macquarie University, for providing me the prestigious “International Macquarie University Research Excellence Scholarship”, and to my work institution, Bangladesh Council of Scientific and Industrial Research, for supporting me during my PhD candidature.

This thesis is dedicated to my parents, who always wish to see my success.

Declaration

I hereby declare that this thesis represents my own work and efforts in its entirety, and has not been submitted for a higher degree or otherwise at any other university, or institution.

	19 August, 2016
Shajahan Siraj	**Date**

Table of Contents

Chapter 1

Introduction

1.1 Neurotransmission and neurotransmitters

In the mammalian brain, the central nervous system processes a tremendous amount of information received from the surrounding through senses such as sight, hearing, and touch, which is then integrated within the body. Signalling in the brain is transmitted between the neurons using small biomolecules as messengers and this transmission is known as neurotransmission. A neurotransmission process occurs in the central nervous system by cell-to-cell communication upon an electrical or a chemical stimulation. The process involves exocytotic events through which chemicals are released by presynaptic cells, followed by reuptake by presynaptic reuptake carrier proteins embedded in the membrane of the nerve terminal.[1] In this way, information from the surroundings is extracted through an action potential triggered neurotransmission, resulting in corresponding behavioural changes.[2] Dopamine, serotonin, γ-aminobutyric acid (GABA), glutamate, epinephrine and norepinephrine (their structures are shown in Table 1.1) are some of the common chemicals involved in the neurotransmission process. Each of these neurotransmitters has its unique source or generation site as well as its characteristic removal or degradation process within the tissue. For example, there are three major dopamine systems well presented in a mammalian brain[3] including (i) the cell bodies of the nigrostriatal pathway that reside in the substantia nigra pars compacta and project to dorsal striatum (caudate-putamen); (ii) the mesolimbic pathway that originates in the ventral tegmental area and terminates in the nucleus accumbens; (iii) the mesocortical pathway that originates in the ventral tegmental area but terminates in the prefrontal cortex. The brain anatomy in terms of the projection of neurotransmitters described by Berke *et al.*[4] is reproduced in Figure 1.1. For example, the flow of dopamine to the striatum is mostly obtained by a dense network of axon terminals arising from cell bodies in the substantia nigra pars compacta and ventral tegmental area. The striatum receives glutamatergic input from all cortical areas, while GABA is projected to globus pallidus-external and subthalamic nucleus

from striatal neurons as ninety percent of these neurons are medium-sized GABAergic cells.[4] In a review on vesicular exocytosis and microelectrode arrays, Amatore *et al.*[5] described the neurotransmitter release process in the extracellular medium. Accordingly, the arrival of an appropriate stimulation increases the intracellular Ca^{2+} concentration, which in turn causes the vesicles to move from the cell cytoplasm toward the cell membrane, where they dock through protein assemblies called soluble N-ethylmaleimide sensitive fusion protein attachment receptors. These vesicles then fuse through the membrane to release their content in extracellular medium. As described by Xu *et al.*[6], an amperometric system comprising of a recording system and a stimulation system are often employed in dopamine detection *in vivo*. The recording system includes an amplifier, a filter and an AD/DA converter. Electrical stimulation (*e.g.* potential pulses) can then be easily generated through the AD/DA converter and an isolator. In the experiment, a sensing / working electrode is positioned in the striatum area of interest, while a bipolar stimulation electrode is placed in the medial forebrain bundle in a rat brain. In this way, stimulating pulses are applied to trigger dopamine release in the striatum and the corresponding signals are recorded by adjusting the depth of the working electrode.

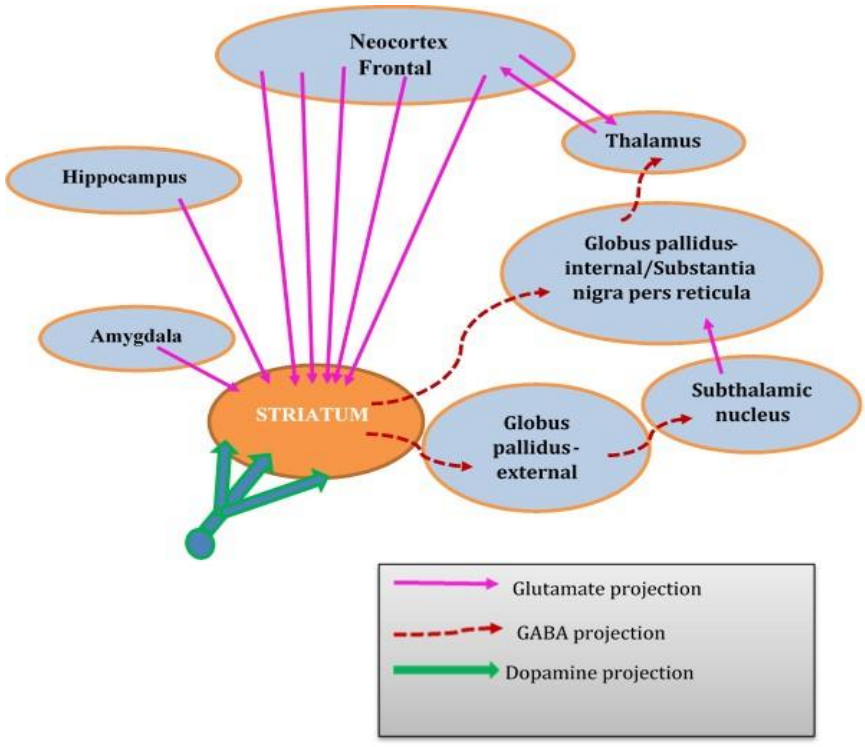

Figure 1.1. Anatomy of cortex-basal ganglia circuits. Adapted from reference 4.

Table 1.1 Redox reactions for electrochemically detectable neurotransmitters in the brain. Adapted from reference 7.

Molecule	Electrochemical oxidation	Oxidation potential (versus Ag|AgCl)
Dopamine	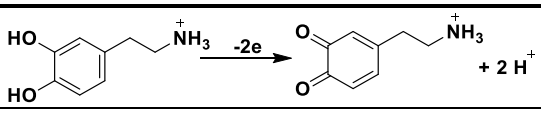	+ 0.2 V
L-DOPA*	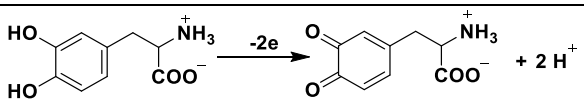	+ 0.4 V
Norepinephrine	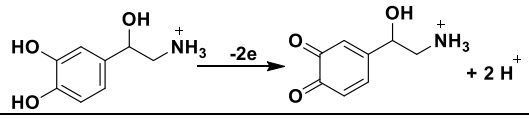	+ 0.2 V
Epinephrine	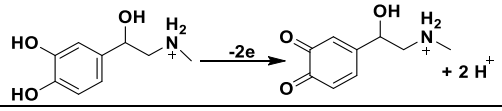	+ 0.2 V
DOPAC**	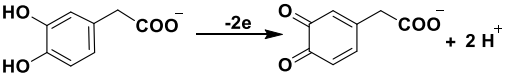	+ 0.2 V
Serotonin	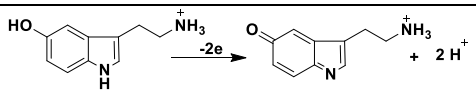	+ 0.35 V
5-Hydroxy indolacetic acid	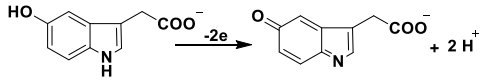	+ 0.35 V
Adenosine	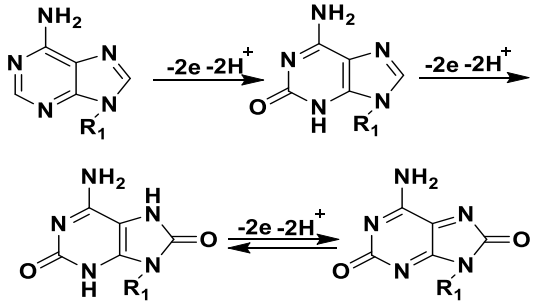	First step + 1.2 V
Ascorbic acid	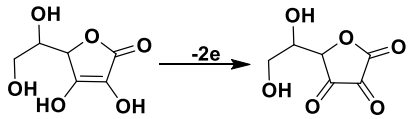	+ 0.2 V
Uric acid	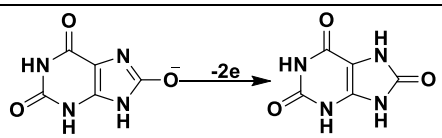	+ 0.3 V

* L-3,4-dihydroxyphenylalanine; ** 3,4-Dihydroxyphenylacetic acid

Neurotransmitters play a crucial role in the central and peripheral nervous system. They play a key communication process between neurons. They are also involved in action initiation, timing, control, learning and memory via striatal generation of neuronal activity that initiates and terminates action sequences.[7] Any disorder of neurotransmitters, *e.g*. glutamate, acetylcholine, dopamine, and serotonin, in a specific brain region may cause many neurodegenerative diseases.[8] These disorders may be caused by primary and secondary defects in the biosynthesis, degradation, or transport of neurotransmitters.[9] While there are many types of neurotransmitter, the majority of researches involving direct electrochemical detection are concentrated on mononamines including dopamine, serotonin, epinephrine and norepinephrine because they are easily oxidised.

Dopamine is a neurotransmitter belonging to a catecholamine group present in the dopaminergic area.[10] It is strongly implicated in higher-order cognitive and motor functioning[11] and it also plays important physiological roles in the peripheral nervous system as the regulator of olfaction, retinal processes, hormonal regulation cardiovascular functions, sympathetic regulations, immune system and renal functions[12]. The main dopamine source is the dopaminergic cells located in the midbrain region called the substantia nigra pars compacta. The number of dopaminergic cell bodies varies from 45,000 in the rat, 165,000 in the macaca monkey, and as high as 590,000 in the fourth decade of human life.[13] However, this number drops to 350,000 during the sixth decade of life.[13] Decrease in concentration of dopamine in striatum may cause extrapyramidal disorders and neuropsychiatric diseases such as Parkinson's Disease, addiction, schizophrenia, obsessive compulsive disorder, and Tourette's syndrome.[9-10] Dopamine also acts as a modulator of mood and depressive symptoms.[14] Dopamine concentration in striatum can also be triggered by psychomotor stimulants such as cocaine and amphetamine.[4] Additionally, dopaminergic neurons in the ventral tegmental area are activated by several types of aversive stimuli and dopamine release is triggered in the dorsal striatum and nucleus accumbens core by tail pinch.[15] In the central nervous system, dopamine is found in basal ganglia where its concentration is approximately 10 nM, while fast burst can

increase dopamine concentration from 0.1 µM to 1 µM.[16] Under stress, dopamine concentration in urine may rise several times higher than the physiological concentration of 1.3 µM.[17,18] On the other hand, dopamine concentration in blood may lie between 0.07 to 0.13 nM depending on diet.[19] Dopamine concentration can also dramatically reach 50 µM in the caudate nucleus after drug consumption.[18]

Serotonin, otherwise known as 5-hydroxytryptamine (5-HT), is also an indoleamine that acts as a modulator of gastrointestinal motility, peripheral vascular tone, cerebral vascular tone, and platelet function. It has been implicated in the pathophysiology of mood disorders, emesis, migraine, irritable bowel syndrome, and pulmonary and systemic hypertension.[20] Irregular serotonin concentration is responsible for the development of neurological disorders such as anxiety and depression.[21] It is predominantly found in gastrointestinal tract released by enterochromaffin cells located in the mucosa.[22]

Two other neurotransmitters are norepinephrine and epinephrine. Norepinephrine is a biochemical messenger and one of the major central nervous system effectors of the human stress response. It has a potential role in panic, anxiety and posttraumatic stress disorder.[23,24,] A progressive degeneration of norepinephrine in the basal forebrain and of noradrenergic nuclei in the brain stem causes Alzheimer's diseases.[25] Epinephrine, also known as adrenaline, is a neurotransmitter secreted by the medulla of the adrenal glands. It is a catecholamine (pKa 8.55)[26] existing as a cation in a physiological environment. This neurotransmitter is triggered into the bloodstream under physiological stress and low blood sugar level.[27] It is also secreted in responding to fear, anger or excitement. Thus, a quantitative determination of epinephrine concentration, such as in human plasma and urine, is significant for developing nerve physiology, pharmacological research and life sciences.[28]

1.2 Neurotransmitters detection *in vitro* and *in vivo*

1.2.1 Significance of neurotransmitters detection

The above discussion has demonstrated the importance of neurotransmitter analysis, particularly with respect to the rapid and early detection of neural disorders. Appropriate analysis would contribute to addressing many important issues of interest to neuroscientists, for example,

- the quantity of neurotransmitters released in an individual action potential and if this is a quantised amount;
- the half-lives of neurotransmitters;
- possible effects of pharmaceutical agents on neurotransmitter release and reuptake.[29]

An improved understanding of the chemical interactions that play key roles in the functioning brain may be understood by *in vivo* measurement of neurotransmitter and related compounds.[30] Most of the techniques for *in vivo* measurements involve microdialysis sampling techniques, followed by analysis using liquid chromatography – mass spectrocopy, fluorescence technique or electrochemical methods.[31,32]

1.2.2 Microdialysis and chromatographic determination of neurotransmitters

Microdialysis sampling is among the techniques used to collect sample from a brain. Microdialysis sampling is therefore readily applied to neuroscience, particularly the neuro-intensive care of brain-injured human patients. Moreover, in microdialysis, the simultaneous implantation of multiple probes in different brain regions enables the technique in revealing region-dependent dynamics of released neurotransmitters.[33] Segovia *et al*.[34] monitored dopamine release in the nucleus accumbens and in the striatum of a rat brain to elucidate the effects of environmental enrichment in adulthood on dopamine release. In such an experiment, a microdialysing probe of 2 mm length with active dialysis membrane was accommodated in a bilateral guide-cannulae and was implanted in the nucleus accumbens. The probe was implanted such that the dialysis membrane of the probe ran almost through the core of the nucleus accumbens.

The probe was perfused with artificial cerebrospinal fluid for 3 h and the sample was subsequently collected over a 20-min period and was stored at -80^{o}C until analysed. Finally, the collected sample was analysed by reverse-phase high performance liquid chromatography (HPLC) using a C18 column, where a mobile phase consisting of an actate-citrate buffer, EDTA, sodium octyl sulfonate and methanol was used. In this work, a limit of detection of 0.15 nM dopamine was estimated. In other work, a method based on liquid chromatography-mass spectrometry/mass spectrometry (LC-MS/MS) was developed to simultaneously determine dopamine, adenosine, acetylcholine, and 5-HT in mouse brain microdialysates. The limit of quantification was estimated to be 0.05 nM.[35] Suominen *et al*.[36] validated an ultra-performance LC-MS/MS method for the determination of serotonin, dopamine, and their metabolites in human brain dialysate and cerebrospinal fluid sample. Meanwhile, dopamine and enkephalins were monitored in rat globus pallidus by implanting a probe of 2 mm dialysing membrane and the dialysate was subsequently analysed by capillary liquid chromatography/mass spectrometry.[37] In a separate work, a probe of 4 mm dialysing membrane was implanted in the striatum in a dyskinetic rat and the probe was perfused for approximately 12 h with artificial cerebrospinal fluid.[38] The dialysate was analysed by HPLC and LC-MS/MS using reverse-phase column to measure dopamine and L-DOPA. Ferry *et al*.[39] employed electrochemical detection coupled with HPLC for monitoring norepinephrine, dopamine, and serotonin in brain dialysate. The experiment was carried out in a single run using micro-volumes of dialysate obtained from dorsal hippocampus and basolateral amygdala in a rat brain. However, the technique has limitation in temporal and spatial resolution and also considerable tissue damage arising from the implantation of a ~200 μm diameter dialysing probe that triggers gliosis and ischemia.[40,41,42,43] To minimise penetration injury, Jaquins-Gerstl *et al*.[43] conducted dialysis in a rat brain using already synthesised glucocorticoid dexamethasone, an anti-inflammatory and immunosuppressant substance, in the perfusion fluid. After 5 days of dialysis to collect a dopamine sample, dexamethasone was found to reduce penetration injury by almost 100% around the probe track and minimise both gliosis and ischemia. Notably, the probe has no significant effect on dopamine flux. However, Wang *et al*.[44] found a significant disruption on dopaminergic activity near the probe track where a

dialysing probe of 200 μm diameter and 4 mm active length was positioned in the rat striatum. In this work, they have found that, although the cells survived around the probe track, the dopamine terminals experienced altered presynaptic inhibition. The method involves a two-step process, extraction of analyte from the dialysate and then purification by capillary electrophoresis or chromatography before the actual measurement. Hence, the measurement process was slow and it required a considerable time scale from minutes to hours. Thus, this technique is not quite suitable for real-time measurement *in vivo* as the analyte concentration is known to fluctuate within fractions of seconds.[45]

1.2.3 Fluorescence techniques for neurotransmitter detection

Fluorescent probes have recently been found as promising tools in life science research owing to their ultrasmall size and biocompatible property. They have a wide range of applications as biosensors, in molecular imaging, as optoelectronics and nanomedicine.[46] Wu *et al*.[47] reported a fluorescence quenching based dopamine and other catecholamine detection method where they used phosphate-modified titanium dioxide nanoparticles and fluorescein for sensing the catecholamines. By measuring fluorescence quenching of fluorescein occurring in the presence of dopamine, the limit of detection was estimated as 33.5 nM. Liu *et al*.[48] developed a fluorescence probe consisting of $CuInS_2$ ternary quantum dots functionalised with 3-aminophenyl boronic acid that emits fluorescence at 736 nm. The reaction between the boronic acid group of the probe and dopamine caused fluorescence quenching that was quantitatively related to dopamine. A fluorescent nanosensor capable of quenching and recovering the photoluminescence was constructed by Xiangzhao *et al*.[49] for the simultaneous detection of dopamine and glutathione. In this work, the binding of the oxidised form of dopamine (dopamine-*o*-quinone) to a silica-coated CdTe quantum dot surface caused the quenching of fluorescence. In the next step, glutathione recovered the luminescence by reducing the adsorbed dopamine-*o*-quinone. The authors found a linear relationship between dopamine concentration and glutathione and the intensity of the photoluminescence of the quantum dots during both quenched and regenerated forms.

CdSe/ZnS quantum dots were modified by adenosine for selective and sensitive detection of dopamine in human urine samples without any interference from amino acid, ascorbic acid, and uric acid at a 100-fold higher concentration than dopamine.[50] The fluorescence of the modified probe was quenched when dopamine was non-covalently bound to the receptor adenosine on quantum dots. Another fluorescence probe consisting of 3-aminopropyl triethoxylsilane modified ZnO quantum dots was developed and performed with similar fluorescence quenching mechanism to detect dopamine in serum samples.[51] No effect was detected on fluorescence of emission was observed when the interference experiment was conducted using ascorbic acid, uric acid, and several other amino acids. A bovine serum albumin stabilised Au nanocluster fluorescent probe was prepared to detect dopamine down to as low as 10 nM.[52] The probe displayed fluorescence at 615 nm, which was completely quenched upon addition of dopamine to the probe. The developed probe also demonstrated selectivity towards dopamine as no emission from the probe was found in the presence of dopamine, when the sample was excited by a UV trans-illuminator but emission was observed in the presence of ascorbic acid, uric acid, and DOPAC. In other work, DNA mediated silver nanostructures were used as a platform for sensitive and selective detection of dopamine.[53] In the presence of dopamine, silver nanoparticles were found to be released from the DNA scaffold and dopamine was chemisorbed on the silver nanoparticles. Next, Genefinder dye was intercalated in DNA caused approximately 20% increase in fluorescence, which was then used as a dopamine detection signal. Zhang *et al*.[54] developed a (3-aminopropyl) trimethoxysilane silicon nanoparticle based fluorescent probe that was used to selectively determine dopamine. In this work, only dopamine was found to quench the fluorescence of the probe and the diminishing fluorescence intensity was directly proportional to the dopamine concentration. This work has demonstrated an excellent method with a limit of detection as low as 0.3 nM of dopamine.

1.2.4 Electrochemical detection of neurotransmitters

In conjunction with anatomical, physiological, and pharmacological evidence, neurotransmitters are easily analysed by electrochemical techniques because they offer high sensitivity, rapid response, simple operation, real time detection, and low expense. The main challenge of such a detection technique is to achieve adequate sensitivity as the concentration of biomolecules of interest *in vivo* is often in the nanomolar to picomolar range. Another challenge is that a bare electrode often does not exhibit sufficient selectivity towards analyte of interest because of other similar coexisting species in a complex biological environment can easily interfere with the detection. Therefore, modified electrodes are of great physiological importance to obtain meaningful determination of analyte. In the last decade, there is a significant improvement of electrochemical techniques with considerable modification processes.

1.2.4.1 Electrochemical detection of neurotransmitters by modified conventional/macro-electrodes

Carbon materials are widely used in electrochemistry due to their wide potential window (generally +3V to -3V) and low cost. Carbon-based electrodes are extensively used for *in vivo* and *in vitro* electrochemical analysis of neurotransmitters. Owing to the presence of various functional groups on a carbon surface, carbon nanomaterials can be chemically modified with ease so that different molecules are immobilised on the surface for diverse applications. In addition, their inherent electrocatalytic activity will aid in enhancing the detection sensitivity of electrochemical techniques. Therefore, carbon nanotube-based microelectrodes may be useful for modification because of their high detection sensitivity arising from the large surface area, antifouling property, and high conductivity, rapid electron transfer kinetics compared to bare electrodes. In contrast, carbon nanotubes display extraordinary mechanical and electronic properties. Coupled with their electrocatalytic activity, nanometre-sized dimension, good electrical conductivity, and low capacitance, carbon nanotubes have also been incorporated on electrodes for neurotransmitter sensing to achieve high sensitivity through improved electron transfer kinetics.[16] For instance, a polylysine-functionalised single walled

carbon nanotube-modified glassy carbon electrode was demonstrated to measure dopamine at nanomolar level concentration due to dopamine preconcentration facilitated by carbon nanotubes.[18] In their work, poly(lysine) was used to increase the dispersion of the single walled carbon nanotube in H_2O:EtOH (2:1, v/v). As ascorbic acid was unable to penetrate the layer and it was poorly adsorbed on the modified electrode surface, no signal was observed at 1.0 mM concentration of ascorbic acid. A per-6-amino-β-cyclodextrin-modified glassy carbon electrode that was then coated with carboxyl functionalised single-walled carbon nanotubes was also used to determine dopamine in the presence of ascorbic acid.[55] The catalytic activity of functionalised single-walled carbon nanotubes and π-π interactions between the phenyl group of dopamine and the hexagonal carbon structure of single-walled carbon nanotubes was responsible for the enhanced electron transfer reaction. The dextrin derivative improved the selectivity towards dopamine by forming an inclusion complex with dopamine as a guest molecule. In a separate work, multi-walled carbon nanotubes were functionalised with C_{60}-fullerene and enhanced dopamine detection signal with high specificity was obtained with no interference even in the presence of 10 mM ascorbic acid.[56] A carbon nanotube modified screen-printed electrode was coated by an electrochemically polymerised polythionine film to determine L-DOPA, a precursor of dopamine in undiluted human serum.[57] This electrode was further modified by the enzyme tyrosinase that catalyses the oxidation of L-DOPA to ortho-quinone. The electrode was finally coated by a Nafion film to enhance its fouling resistance during the detection of L-DOPA in human serum.

Among the other modified electrodes, using a 10-nm porosity carbon material modified glassy carbon electrode, Veerakumar *et al*.[58] obtained an extraordinary sensitivity of 2.56 mA μm^{-1} cm^{-2} to dopamine with a desirable limit of detection of 2.9 nM. High surface area (approximately 2660 m^2 g^{-1}) of the carbon porous materials, synthesised from carbon precursors consisting of formaldehyde and resorcinol, contributed to the enhanced detection sensitivity. In other work, a natural clay doped with zinc hexacynoferate modified glassy carbon electrode was used to detect dopamine.[59] The doped zinc hexacynoferate has reportedly increased the sensitivity towards dopamine,

accompanied by approximately a 5% reduced overpotential along with a 160 mV peak separation between the oxidation signal of dopamine and uric acid and 400 mV between the oxidation signal of uric acid and tryptophan. Suresh *et al.*[60] modified a glassy carbon electrode with Ni-doped V_2O_5 to obtain enhanced sensitivity towards dopamine detection. The modified electrode also demonstrated selectivity towards dopamine in the presence of uric acid. Sun *et al*. modified a glassy carbon electrode with a gold nanoparticle impregnated MoS_2 nanocomposite for the simultaneous determination of dopamine, ascorbic acid, and uric acid by differential pulse voltammetry with a peak separation of 151 mV and 137 mV.[61] The modified electrode exhibited a recovery of 98-102% of dopamine spiked in human serum. In other work, a hybrid material consisting of silver nanoparticles in a SiO_2/graphene oxide composite was immobilised on a glassy carbon electrode for the simultaneous detection of dopamine and epinephrine.[62] The modified electrode was capable of detecting dopamine and epinephrine with no interference in the presence of a 30-time higher concentration of uric acid and ascorbic acid. Also, a recovery of 99-101% and 99-100% of dopamine and epinephrine, respectively, was obtained in applying the electrode to their detection in human urine as a real-life sample.

Tan *et al.*[63] compared the effectiveness of dopamine oxidation at an sp^3 hybridised boron doped diamond electrode relative to that at an sp^2 hybridised boron doped graphene electrode. These authors found that a more positive dopamine oxidation potential of 0.628 V at diamond electrode, compared to 0.272 V at the corresponding graphene electrode. It was determined that the dopamine was less sensitive to H-terminated diamond surface, in contrast to surface oxide/oxygen functionalities present on graphene surfaces. Porous diamond-like carbon was deposited on vertically aligned multi-walled carbon nanotubes from *n*-hexane as a source material by a plasma enhanced chemical vapour deposition method.[64] When a diamond-like carbon-vertically aligned multi-walled carbon nanotube modified electrode was applied to determining dopamine and epinephrine, the authors obtained a high analytical sensitivity (0.2-0.3 μA mol^{-1}) and a limit of detection (2.9 μmol L^{-1} for dopamine and 4.5 μmol L^{-1} for epinephrine) arising from the high surface area of the composite on the

electrode. Diamond nanowires were grown on a planar silicon substrate by microwave plasma enhanced chemical vapour deposition using 6% CH_4/94% N_2 gas as a source.[65] The voltammetric signals of co-existing ascorbic acid (0.0 V), dopamine (at 0.15 V), and uric acid (0.28 V) in a solution were found to be well-resolved at these diamond nanowires. This electrochemical property was accounted by the presence of sp^2 graphitic phase and new C-N bonds at the diamond grains, which increase the electrical conductivity at the grain boundary of the developed wires.

Graphene, an allotrope of carbon, has recently attracted tremendous research interest in electrode modification because of its large specific surface area, superior mechanical strength, excellent thermal or chemical conductivity, high stability, and environmentally friendly nature.[66] Accounted by the π-π stacking interaction between dopamine and graphene surface that accelerates dopamine electron transfer, but weakens the ascorbic acid oxidation, the graphene modified electrode surface exhibited selective dopamine detection in the presence of ascorbic acid.[67] A disposable screen-printed graphene electrode displaying a wide potential window (-1.8 - +1.8 V) in different buffer electrolytes including 0.1 M KCl, 1.0 M HCl, 0.5 M NaOH, 0.1 M acetate buffer (pH 4.5), and 0.1 M phosphate buffer (pH 7.0), low background current and fast electron kinetics was developed by Ping *et al*.[68] A high density of defect sites at the edge planes of chemically reduced graphene oxide provides remarkable properties in electron transfer kinetics that permit the simultaneous differential pulse voltammetric detection of ascorbic acid, dopamine, and uric acid at the corresponding oxidation potential of -50 mV, 150 mV, and 300 mV. Three-dimensional reduced graphene oxide was employed for selective sensing of dopamine in the presence ascorbic acid and uric acid.[69] Initially, a hybrid of graphene oxide and polystyrene spheres was prepared through π-π interaction, before graphene oxide in the hybrid was reduced by hydrazine. The polystyrene spheres were then removed and three dimensional reduced graphene oxide was obtained. Owing to the high surface area and open pore structures, three dimensional graphene oxide has offered more advantageous features than other graphene materials. Yu *et al*.[70] used the electrochemically reduced three-dimensional graphene oxide for simultaneous determination of dopamine,

ascorbic acid, and uric acid. They obtained a recovery of 99.7% in detecting dopamine in human serum without any observable interference by proteins and amino acids in the serum. In other work[71], a graphene derivative of ferulic acid was synthesised by a condensation reaction of graphene oxide and ferulic acid. Next, the electrochemically reduced derivative was employed to determine dopamine in the presence of interfering species including serotonin, glucose, ascorbic acid, hydrogen peroxide, and uric acid. While glucose, hydrogen peroxide, and uric acid have no influence on determination of dopamine, the presence of 20 μM of serotonin and 20 μM ascorbic acid have contributed a ~17% increased dopamine signal. Gutierrez *et al*.[72] successfully used a graphene paste electrode for quantification of 60 μM dopamine using differential pulse voltammetry-adsorptive stripping technique in the presence of 1.0 mM ascorbic acid and 2 mM serotonin. A graphene/Pt composite modified glassy carbon electrode was used to simultaneously determine ascorbic acid, dopamine and uric acid by cyclic voltammetry and differential pulse voltammetry.[73] In their work, 1.7-nm diameter Pt particles were self-assembled by allowing 10 μL of the graphene/Pt composite to air dry on a-graphene surface at room temperature. At this modified electrode, a potential separation of 160 mV was observed between ascorbic acid and dopamine, 120 mV between dopamine and uric acid, and 280 mV between ascorbic acid and uric acid. A tryptophan/graphene composite modified glassy carbon electrode was also developed for the simultaneous detection of dopamine, ascorbic acid and uric acid in a human serum sample and a urine sample.[74] The composite material also demonstrated electrocatalytic activities and enhanced sensitivity towards the analytes, which was attributed to the high density of defect sites at the edge plane on the composite.

1.2.4.2 Electrochemical detection of neurotransmitters by microelectrodes

In neurotransmitters detection, advanced electroanalytical methods and devices are readily applicable to precise studies of exocytotic events at a single-cell and an individual-vesicular level in real time. However, an existing challenge in this field is to obtain micrometres/nanometres of spatial resolution as the distance between a neuronal

synapse are approximately 20 nm and distances between blood capillaries are approximately 30-70 μm.[31] Also, neurotransmitters in extracellular fluid often exhibit a millisecond time scale lifespan before their concentrations are rapidly restored to their originally low levels by metabolism or cellular uptake.[75] To-date, electroanalytical techniques are among the most promising techniques used to study exocytosis at a single-cell level. In these techniques, a micro/nanometric electrode is positioned at the top and near the emitting cell. An appropriate constant potential is applied to the electrode so that species released by exocytosis (mainly catecholamines) will be readily oxidised at the electrode surface to yield a current peak for each individual vesicular release. As a consequence, the cell release at the cell apex will correspond to a succession of amperometric peaks. Detailed analysis of the entire set of current peaks during amperometric analysis will present important data related to the whole cell activity, the dynamics and the quantity of biomessengers released for each exocytotic event.[5] The main features of this amperometric technique are (i) very high temporal resolution even at sub-millisecond, (ii) the high signal-to-noise ratio, which allows estimation of the quantity of released molecules and the fusion pore formation, and (iii) the ability to provide a direct measure of exocytosis.[76]

In amperometric experiments conducted *in vivo*, carbon fibre microelectrodes are widely used for neurotransmitter detection because of their availability, excellent electrical conductivity, and biocompatibility. They are also amenable to diameter miniaturisation (5-30 μm in diameter), which aids in spatially and temporally resolved determination of neurotransmitters in a subsecond time frame to facilitate a real time analysis. In the following sections, a review on some of the recent work involving the detection of dopamine at various types of carbon microelectrodes will be presented. For example, a 10-μm diameter carbon fibre microelectrode was first time employed to amperometrically determine the exocytotic event at BON, a cell line derived from a metastatic human carcinoid tumour of the pancreas.[77] Wightman's group[78] measured dopamine at a 5-μm diameter carbon fibre electrode in zeptomole quantities released from individual vesicle of dopaminergic amacrine cells isolated from genetically modified mouse retina. Park *et al.*[79] employed fast-scan cyclic voltammetry at a carbon

fibre microelectrode to study the role of dopaminergic and noradrenergic transmission within the caudal nucleus accumbens shell in regulating the behavioural and physiologic responses associated with drug abuse, physical stressors and other rewarding and aversive stimuli. Their results indicated a weaker exocytotic activity of neurotransmitters in BON cells than that in chromaffin cells. An adsorption and desorption kinetic study of dopamine by the same group at a bare carbon fibre microelectrode found a delayed response to concentrations of species that adsorbed on the electrode surface. Estimation of the response time by such experiment is crucial in the acceptable interpretation of the transient dopamine release and reuptake in biological systems.[80] However, the detection sensitivity of dopamine by fast scan cyclic voltammetry is limited by adsorption or diffusion of dopamine on the electrode surface, and as the scan repetition frequency increases, the sensitivity of the carbon fibre microelectrode dramatically decreased.[81] In other work, a 1,2-phenylenediamine modified carbon fibre microelectrode was used to simultaneously detect dopamine and ascorbic acid *in vitro*.[82] At this modified electrode, dopamine was determined without any interference from ascorbic acid (0.3 mM) when 0.7%(w/w) human serum protein was deliberately added, indicating that the modified electrode can potentially be used in *in vivo* and *in vitro* measurements of dopamine and ascorbic acid in brain.

Jacobs *et al*.[81] discovered that dopamine oxidation at a carbon nanotube yarn microelectrode was independent of scan repetition frequency of a fast scan cyclic voltammetric experiment. In such an experiment, a temporal resolution of two orders of magnitude was obtained compared to that using a carbon fibre microelectrode in the corresponding fast scan cyclic voltammetry experiment. In a separate work, the sensitivity of carbon fibre disc microelectrode to dopamine was enhanced 36-fold by growing an aligned single-walled carbon nanotube forest using a chemical self-assembly method.[83] Carboxyl acid functionalised single-walled carbon nanotubes were assembled from a dimethylformamide suspension on a carbon disc that was initially modified by a thin iron hydroxide-decorated Nafion film.[83] The modified electrode was capable of determining dopamine in the ventral nerve cord of the fruit fly, *Drosophila melanogaster*, with a high oxidation current sensitivity of 29 nA μM^{-1} of

dopamine and very low limit of detection of 17 nM. The high sensitivity of the electrode was ascribed to the exposure of the carbon nanotube terminals to the analyte.

In addition, a chitosan modified carbon fibre microelectrode was employed to determine serotonin in live embryonic zebrafish intestine.[84] Chitosan was considered as an alternative to Nafion for measuring serotonin with minimal interference from anionic ascorbic acid due to electrostatic repulsion at the negatively charged chitosan film. Using differential pulse voltammetry, the limit of detection was estimated as 1.6 nM with a sensitivity of 5.12 nA μM^{-1}. The chitosan film on the carbon fibre microelectrode was found to be stable even after four consecutive implantations *in vivo*. A vertically aligned carbon nanotube modified carbon fibre electrode was developed to monitor ascorbate in the striatum of a rat brain, while the ascorbate was evoked by intracerebral infusion of glutamate.[85] This electrode was reproducibly fabricated by growing vertically aligned carbon nanotubes on carbon fibre on a carbon fibre via the pyrolysis of iron(II) phthalocyanine at 800–1100^{o}C. This strategy was reported to have avoided variations from person-to-person or electrode-to-electrode by eliminating such manual manipulations as dip-coating and drop-coating techniques. A vertically aligned carbon nanotube-sheathed carbon fibre microelectrode of 20-30 μm diameter was developed by pyrolysising iron(II) phthalocyanine on a carbon fibre support.[85] After coating this microelectrode with an eletropolymerised film of 3-amino-5-mercapto-1,2,4-triazole (*p*-AMTa), it was implanted in the striatum of a Sprague-Dawley rat to selectively determine ascorbate with coexisting neurotransmitters including dopamine, uric acid, and serotonin.[86] A gold nanoparticle deposited carbon fibre disc electrode that was modified by the enzymes, acetaylcholinesterase and choline oxidase, was employed to determine the nonelectroactive neurotransmitter acetylcholine in an artificially formed single cell.[87] The 30-μm diameter electrode selectively determined acetylcholine in the presence of other neurotransmitters, *e.g*. dopamine, norepinephrine, glutamate, and ascorbic acid at lower physiologically relevant concentrations (sub-μM to low μM). The modified electrode exhibited a stable sensor response after repeated 15-20 acetylcholine injections over the course of a 4-h experiment.

In the last decade, diamond based biosensors have attracted a lot of attention in neuroscience research as doped diamond has demonstrated excellent electrochemical properties, especially with a wide potential window, yet it is chemically inert but biocompatible and exhibited long-term stability in contact with biomolecules.[65] Additionally, owing to a relatively oxygen free surface, there is a low background current at diamond electrodes, negating any pretreatment before use. The electrochemical characteristics of a diamond electrode surface are also independent of solution pH.[88,89] Suzuki *et al*.[90] deposited a diamond film on a 5-μm diameter tungsten wire from acetone/methanol in the presence of B_2O_3 by microwave plasma assisted chemical vapour deposition. The anodically oxidised electrode was implanted into the corpus striatum of a mouse brain to detect dopamine by differential pulse voltammetry, while 100 pulses at 50 Hz for 2 s were applied to a stainless bipolar stimulating electrode positioned in the medial forebrain bundle. In other work, a diamond-coated 76-μm diameter Pt wire microelectrode was employed to determine serotonin from the intestinal mucosal layer of enterochromaffin cells by continuous amperometry.[88] An ultrananocrystalline diamond microsensor was implanted in the dopamine-rich striatal region of the forebrain of an anesthetised rat to measure dopamine.[91] Simultaneously, a stimulation electrode was implanted in the medial forebrain bundle to electrically activate action potentials in dopamine neuronal axons in the striatum so that after exocytotic event dopamine is released in extracellular fluid. The implanted electrode was capable of monitoring extracellular dopamine in real-time in the implanted area and this demonstrates its viability as a brain-implantable sensor. Moreover, the electrode exhibited a limit of detection as low as 27 nM of dopamine.

Apart from carbon based electrodes, there were also many other materials used to fabricate electrodes before they were applied to dopamine detection. A self-assembled monolayer of 3-mercaptopropionic acid was immobilised on a gold-ring microelectrode to improve the specificity and sensitivity toward dopamine with a limit of detection of 50 nM.[92] The same electrode was used for recording neurochemical release from a rat striatum that was stimulated by locally injected high KCl concentration. An ultrasensitive indium tin oxide-based microsensor was fabricated by immobilising

already synthesised carbon nanotubes on the electrode by chemical vapour deposition.[93] The modified electrode exhibited a three-fold improvement in sensitivity compared to a corresponding bare electrode in the amperometric monitoring of dopamine release from single PC12 cultured cells at 300 mV versus a Ag|AgCl reference electrode. In such an experiment, the cells were stimulated by a K^+ saline solution filled micropipette introduced within 100 µm in proximity to the cells.

1.2.4.3 Electrode arrays for neurotransmitter detection

The detection of neurotransmitters by a single electrode, *e.g.*, a carbon fibre microelectrode, is limited to single-cell experiments and is therefore difficult to obtain a quantitative view of the regional diversities of cells. This limitation can be overcome by using an electrode array that simultaneously records exocytotic events from different cells. Such a multi-site array capable of detecting secretion from a single cell will improve the spatial resolution of secretory events. Thereby, a clear picture of cell to cell communication can be well understood by analysis in depth on spatial diversity of biological events. In a microelectrode array, the electrodes are connected together and the individual electrodes can identify secretion from individual cells. In this respect, a large-scale integrated amperometric sensor array was developed by Abe *et al.*[94] to measure dopamine from three dimensionally cultured PC12 cells. The device was composed of 400 sensing electrodes positioned 5 µm away from PC12 cells. The device was also able to identify the effect of dopaminergic drugs L-DOPA and reserpine on dopamine release from PC12 cells. A fast scan cyclic voltammetry compatible microelectrode array with 16 channels was developed by Zachek *et al.*[95] to investigate heterogeneous release of dopamine in the striatum of an anesthetised rat. The fabricated electrode array was capable of studying the dopamine release from multiple brain locations *in vivo*. However, the planar electrode geometry has limited the diffusion of analyte to electrode surface compared to a single carbon fibre electrode. A polystyrene sulfonate anion doped polypyrrole film modified interdigitated gold microelectrode was employed to measure dopamine released from rat PC12 cells.[96] Using polystyrene sulfonate anion, the modified electrode exhibited electrostatic

attraction towards dopamine and yielded a 2.6-fold signal amplification compared to that at a bare electrode. Patel *et al*.[97] fabricated a gold microelectrode array to measure electrically evoked dopamine released at multi-sites of single neuron isolated from dopaminergic somas from pond snail. The array with twelve 25 × 150 μm gold electrodes was demonstrated in conducting a 4-h experiment without a significant signal attenuation and yielding an 11 nM limit of detection. Kim *et al*.[98] designed a disposable array consisting of 2400 gold ultramicroelectrodes that were divided into two sets, each set with a gold counter electrode and a reference electrode. The 15-mm diameter circle of electrodes was employed to simultaneously determine nitric oxide and peroxynitrite in HL-60 cells. This disposable unit can also be integrated within cell culture wells and plates, resulting in an easy-to-handle tool for cellular biology. A planar nanocrystalline diamond electrode array consisting of nine ultra-microelectrodes was developed for amperometric detection of dopamine and several other neurotransmitters.[76] Using this array, single quantal exocytotic events were recorded in mouse and bovine chromaffin cells. This electrode array was suitable for multi-site recording within single living cells and was able to determine micromolar level concentration of neurotrasmitters by both chronoamperometric and voltammetric methods. Ewing's group developed a thin-film platinum ultramicroelectrode array consisting of 16, 25, and 36 square electrodes on a glass substrate.[99] PC12 cells were cultured on a poly(dimethylsiloxane) and a collagen IV modified platinum array was used to measure dopamine released at every exocytotic event in the PC12 cells. The same group developed an array with a tuneable number of 8-15 electrodes, with each electrode corresponded to a carbon ring electrode formed by depositing pyrolysed carbon on already pulled and bevelled tip of glass capillary that was then insulated.[100] The array of 10 to 50 μm dimeter electrodes was employed to measure dopamine release at individual neuronal cells or cell networks. A total mapping of exocytotic events of PC12 cells was also determined by electrochemical imaging, while each cell was addressed by individual electrodes of the developed array. Individually addressable array of Ti/Pt (5 nm/45 nm) microwells was also fabricated on a glass wafer for spatially and temporally resolved neurotransmitter release across a single PC12 cells.[101] Each photoresist microwell was constructed such that it would

accommodate only one cell to record the subcellular heterogeneity in that single cell. During a 5-s amperometric recording of exocytosis of stimulated cells, the events were produced by different vesicles simultaneously released at different membrane regions in the single cell, which would otherwise be not possible to be recorded by traditional carbon microelectrodes. Another advantage of this array is that it was able to record the events even when it was further than 700 nm away from cells. On the other hand, the sensing capability at a carbon fibre microelectrode decreased rapidly when the electrode edge was also away from cells at a similar distance. A Pt microelectrode array was modified by dipping it in Nafion to repel ascorbate before it was used for detecting glutamate in the prefrontal cortex of awake rats.[102] After depositing poly(3,4-ethylenedioxythiophene) (PEDOT)-carbon nanotube (CNT) composite on a gold microelectrode array, the array demonstrated excellent biocompatibility and adhesion to cultured cells.[103] In this modification, PEDOT was electropolymerised from ethylenedioxythiophene in an aqueous suspension containing 1% poly(sodium *p*-styrenesulfonate) and a CNT suspension (0.3 wt%). Using the modified electrode, a doubled signal-to-noise ratio was achieved compared to that at PEDOT modified electrode.

1.3 Fabrication of microelectrodes

Microelectrodes are defined as electrodes having at least one dimension that is smaller than 100 μm.[104] The diverse applications of microelectrodes can be found in, for example, electrochemistry, neurophysiology, and scanning probe microscopy. Very often, they are applied to monitor the secretion from single cells, neurons, membrane pores, and liposome. Notably, the rate of damage of cells can be reduced by using smaller probes in such work. For example, a microdialysis probe of ~250 μm in diameter causes damage to local cells and blood vessels during an *in vivo* detection experiment, resulting in tissue ischemia and initiation of an inflammatory cascade.[105] On the other hand, the rate of damage is reportedly much smaller around a carbon fibre microelectrode of ~7 μm diameter.[106] In addition, the small dimensions of sensing electrodes allow investigations at single cells or single vesicle in cells during an

exocytosis event.[106] At these small electrodes, the concentration changes during chemical events within an intact animal can also be monitored.[75] Besides, there are well-known advantageous features associated with microelectrodes[107]:

(a) the small size allows the measurement of analyte in very small volumes ranging from nanolitres to picolitres;

(b) radial diffusion of an analyte towards the electrode results in a rapid steady state signal for a Faradaic process, which then permits time-independent measurements of analyte;

(c) an improved Faradaic-to-charging current ratio will assist in measuring analyte of interest at very low concentrations;

(d) small Faradaic currents result in a small Ohmic potential drop between the working electrode and the reference electrode, permiting a two electrode arrangement used during *in vivo* analysis;

(e) an improved signal-to-noise ratio is attained due to convergent or edge diffusion of analyte, especially when the diffusion layers are overlapped in a microelectrode array;

(f) amperometric current is enhanced at microelectrode arrays through recharging depletion layer during detection of analyte in flowing liquids.

1.3.1 Fabrication of carbon microelectrodes

Nobel Laureate Hubel is widely known to be the first scientist credited with fabricating the first metal microelectrode over 50 years ago.[108] Since then, many techniques have been developed to fabricate microelectrodes. During microelectrode fabrication, several aspects including the electrode size to minimise cellular damage, the compatibility in biological environment, the stability of the insulator in the electrolyte so that it does not contaminate the analyte and the geometry to obtain enhanced sensitivity during analysis, and also the simplicity of the fabrication technique must be taken into consideration. A neuronal synapse is a ~20 nm gap. As a result, the sensing electrode must be at least smaller than the synaptic gap to conduct an uninterrupted experiment in the synapse.[31] High sensitivity and high spatial resolution can be

obtained during non-invasive analysis of single living cells and intracellular detection of neurotransmitter using nanometer-sized electrodes. Moreover, the flux of the analyte to the electrode surface from the target source also depends on the size and geometry of electrode.[109] Carbon fibre microelectrodes are widely used in electrochemical detection because of their availability, excellent electrical conductivity, and biocompatibility. They are also amenable to miniaturisation (5-30 μm in diameters), which aids in spatially and temporally resolved measurement of analyte in a microenvironment. Recently, there is a growing interest on carbon nanomaterials that include carbon nanohorns[110], carbon nanofibres[111], different forms of graphene on metal wires[112], and carbon nanospikes[113] have been considered as an alternative to carbon fibre microelectrodes owing to their high sensitivity, anti-fouling property, and high conductivity, which can lead to rapid electron transfer reactions. In this respect, Zestos *et al.*[113] grew a uniform layer of carbon nanospikes on different metal wires, *e.g.*, tantalum, niobium, palladium, and nickel of ~25 μm diameter in a DC plasma-enhanced chemical vapour deposition chamber, where ammonia gas at 100 cm^3 min^{-1} and acetylene at 80 cm^3 min^{-1} were used as a carbon source. Ewing's group[114] has pioneered the development of nanotip conical carbon fibre microelectrodes by thermally etching a carbon fibre in a blue butane flame for less than 2 s to obtain 50-100 nm tip diameter. This represents a significant advancement in microelectrode fabrication as these electrodes have now enabled the direct quantification of vesicular transmitter content in the intracellular environment. In other work, a single carbon fibre microelectrode was modified with branched carbon nanotubes for enhanced sensing performance.[115] Initially, a carbon fibre was annealed at 250^{o}C for 3 h. Fe was then introduced on the fibre by reducing Fe(III) acetylacetonate. The fibre was next carbonised at 850^{o}C for 30 min. Finally, hexane vapour at 600 mL min^{-1} together with argon carrier gas was delivered into the furnace at 700^{o}C to grow carbon nanotubes on the carbon fibre. At the end of this process, an electrode with a 10-15 μm tip diameter was obtained. Similarly, a carbon nitride film of ~150 nm thick was deposited on 10 – 100 μm diameter glass capillary from a graphite target in a plasma of an argon-nitrogen mixture.[116] In other work, the biopolymer chitosan was used to modify a carbon fibre electrode before it was used to detect serotonin in live embryonic zebrafish intestine.[84]

Low toxicity and biocompatibility of chitosan make the modified carbon fibre electrode to function more satisfactorily as an implantable device. Cheng *et al.*[117] modified a 9-μm diameter carbon fibre microelectrode with an already assembled nanocomposite of thionine/ketjen black for the determination of ascorbic acid in the cortex of a living rat brain. In a separate work, a nanostructured carbon electrode was obtained by pyrolysing photoresist SU-8 in combination with polystyrene and poly(styrene)-block-poly(dimethylsiloxane) on silicon wafer as a substrate and the kinetics of the modified electrode was compared with that at the electrode modified by only pyrolysing photoresist SU-8.[118]

1.3.2 Fabrication of diamond microelectrodes

More recently, diamond microelectrodes have emerged as electrodes that offer superior analytical advantages in terms of linear dynamic range, wide potential window, improved signal to noise ratio, limit of detection, response precision, and stability, compared to carbon fibre and other metal microelectrodes. Several diamond microelectrode fabrication approaches[119] have been reported including (i) conformal diamond coatings on small-diameter wires, (ii) coatings on the end of capillary columns, (iii) deposition of diamond on lithographically patterned substrates, and (iv) oxygen-based ion beam plasma etching of bulk diamond material. Notably, a great deal of work involving diamond microelectrodes has been reported by Swain's group[119,120,121,122]. As an example, using chemical vapour deposition from a 0.5%(v/v) CH_4/H_2 source, a diamond film was deposited on a 76 μm diameter platinum substrate. In their work, B_2H_6 mixed with H_2 gas was also incorporated as a boron doping source in the deposited diamond film. Very recently, the same group[123] demonstrated enhanced selectivity and sensitivity of a hemin-polymerised 3,4-ethylenedioxythiophene film modified diamond electrode (76 μm diameter) towards detection of peroxynitrite. In other report, diamond films were grown on a sharp tungsten filament tip by chemical vapour deposition.[124] Here, a hydrogen rich CH_4-H_2 gas was used as a source of diamond and B_2O_6 dissolved in ethanol carried by argon gas to facilitate boron doping in the diamond film to enhance conductivity. This

diamond film was subsequently exposed in a hydrogen stream to convert the diamond to an H-terminated surface if there were any C–O impurities present on the diamond surface. This electrode was reported to be ~15 μm in axial length and ~2 μm in tip diameter. An all-diamond microprobe was firstly reported by Silva *et al*.[125], where an 800 nm thick undoped diamond film was coated around the tip of a conducting boron doped diamond electrode. Finally, the tip of the electrode was cut using focused ion beam to expose an electroactive boron doped diamond disc of ~1.5 μm diameter. Macpherson's group[126] also pioneered work involving diamond hydrodynamic flow microelectrodes for electroanalysis. After insulating both sides of a 90-μm thick layer of polycrystalline boron doped diamond disc by mechanical grade diamond, a 10-mm diameter disc was cut from the prepared diamond wafer. A 500-μm diameter hole was introduced at the centre of the disc to facilitate analyte flow. Ultrananocrystalline diamond microsensors on a tantalum and a tungsten substrate of 50 μm and 1 μm diameter, respectively, were reported by Arumugam *et al*.[91]. These electrodes were fabricated by chemical vapour deposition from a CH_4/H_2 gaseous mixture as the diamond source and trimethylboron for doping in nanocrystalline diamond.

1.3.3 Fabrication of gold microelectrodes

Although gold electrodes are not as ideal as carbon electrodes for neurotransmitter detection *in vivo*, they have strong affinity with molecules containing thiol/amine groups.[92] Therefore, a great deal of work has also been carried out to develop gold microelectrodes for measurements *in vitro* and *in vivo*. A 5-μm thick gold microring was fabricated on an aminated polycarbonate rod by Wu *et al*.[127]. Initially, gold nanoparticles were deposited on the rod by chemically reducing $HAuCl_4$ by $NaBH_4$. Next, a thin gold film was plated on the deposited gold nanoparticles. The rod was then insulated by epoxy glue. A fresh electroactive ring was exposed by successively cutting the rod. Lin *et al*.[92] developed a gold-ring microelectrode of 15–50 μm diameter at the tip of a pulled glass capillary. These authors initially treated a pulled glass capillary in piranha solution to obtain a hydroxyl group functionalised surface followed by grafting adhesive polydopamine film on hydroxyl group surface. Then, a

monolayer of gold nanoparticles was deposited by reducing $HAuCl_4$ on polydopamine and the monolayer of gold nanoparticles was covered by a thin gold layer. In other report[128], a gold substrate was electrochemically etched to obtain a 6-nm diameter nanodisc electrode housed in a borosilicate capillary that was sealed using electrophoretic paint and polyimide. Nanoband microelectrodes consisting of a 100-nm thick gold or copper film was fabricated on poly(dimethylsiloxane).[129] The gold or copper conducting film was sandwiched in between two layers of poly(dimethlsiloxane) so that the cross section of the band was used as an electrode, which was then used to detect amino acid, protein and neurotransmitter molecules. Jiang *et al.*[130] introduced a nanopurous gold microelectrode from an alloy phase of gold and zinc. A 50-μm diameter gold disc was positioned in a glass pipette before Zn was electrochemically deposited to prepare a gold–zinc alloy. In the next step, Zn was selectively oxidised, leaving 100-500 nm pores on gold surface. Chu *et al.*[131] fabricated an integrated microelectrode accommodating an IrO_2 working electrode, a Ag|AgCl reference electrode, and a counter electrode eliminate the electrode size limitation during microscale measurement *in vivo*.

1.4 Fabrication of microelectrodes of different geometry

1.4.1 Disc/Ring-shaped microelectrodes

In the conventional design of microelectrodes, they are very commonly fabricated as a disc shaped electrode embedded in an insulating substrate. For example, a gold disc or a platinum disc microelectrode is fabricated by sealing a corresponding gold wire and platinum wire, in a glass pipette, followed by polishing the end of the electrode to expose the electroactive surface.[132] The wire was then connected to a Ni/Cr wire with a silver ink conductive paint to obtain electrical conductivity. Harvey *et al.*[133] developed a Pt ring-disc microelectrode on a polyimide insulated platinum substrate. In their process, the substrate was mounted in a furnace of high negative voltage (2.5 kV), where argon was ionised. The ionised argon atom collided with a platinum target material in the furnace to produce a cloud of platinum. The insulated substrate was then passed through the cloud so that the vaporised platinum was deposited at the tip

and around the substrate. Upon coating with platinum, the wire was cut into 3-cm axial lengths. For electrical conductivity, the inner metal disc and the outer ring was separately connected with silver wires.

Lin *et al.*[100] fabricated an electrode array, as shown in Figure 1.2, consisting of 10-15 carbon-ring microelectrodes to individually address the secretion of single cells. In this fabrication process, the required number of capillaries was packed and held together using epoxy. A butane / oxygen torch was used to heat up the middle of the capillaries so that they were separated into two bundles. Then a mixed stream of nitrogen and acetylene gas was delivered through these pulled capillaries while acetylene was pyrolysed to obtain pyrolytic carbon as a shiny carbon ring on the inner wall of the capillaries. The ring thickness was demonstrated to increase proportionally with pyrolysis time.

In other work, a platinum wire insulated in a quartz capillary was pulled to produce a platinum disc as small as 3 nm diameter.[134] The tip of the assembly was then polished by a variable speed polisher rotating at 400 rpm to expose the platinum disc. The glass substrate and the disc was thermally sealed at 685ºC for 40 s. A copper wire was connected to the platinum wire to accomplish electrical conductivity.

A metal trilayer consisting of Ti, Ni, and Au and SiO_2 or Si_3N_4 was deposited on a silicon wafer by Laczka *et al.*[135] The microdisc-ring shaped electrode of deposited metals of 10 µm diameter was then exposed after applying a series of photolithographic steps on the device. Approximately eighty microdisc-rings were then stacked on top of each other with a 200-µm gap to form a comprehensive device for application. Xiao *et al.*[136] fabricated a random array of nano boron doped diamond discs that were coated by molybdenum (IV) dioxide nanoparticles. Then, an insulating 4-nitrophenyldiazonium film was deposited on top of the assembly. Finally, the disc was exposed by dissolving away the molybdenum oxide nanoparticles such that remaining part of diamond platform was covered by the 4-nitrophenyldiazonium film.

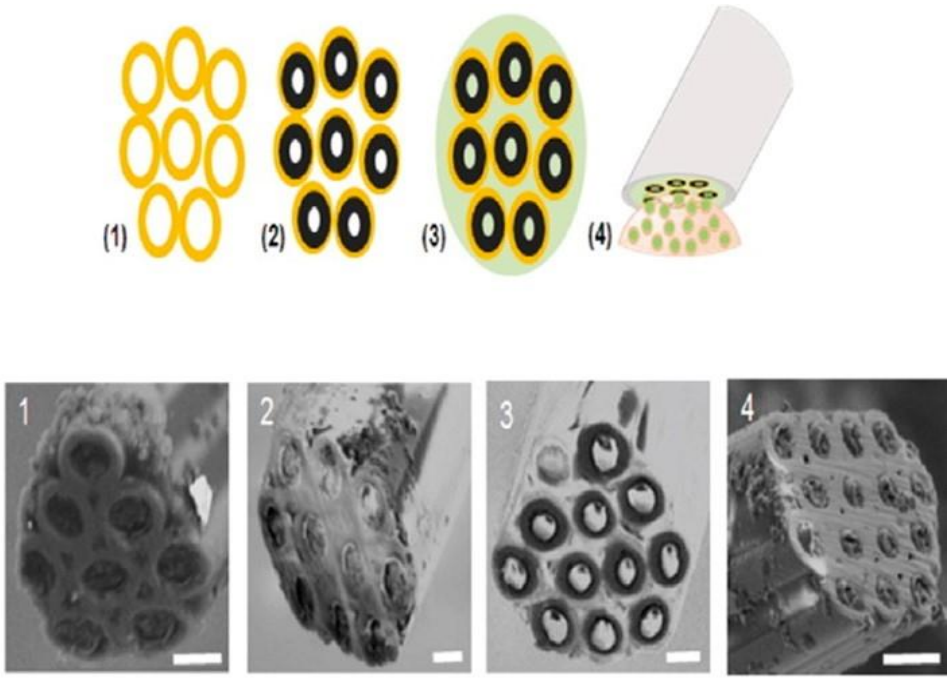

Figure 1.2. (A) Fabrication of a carbon-ring microelectrode array that includes (1) fused silica multibarreled capillary, (2) a carbon film deposited in the inner-side of the capillary by pyrolysis of acetylene, (3) epoxy sealing between the capillaries, (4) electrode array positioned at a single cell. (B) Scanning electron micrographs of a carbon-ring microelectrode array consisting of (1) 8, (2) 10, (3) 12, and (4) 15 microring electrodes. Adapted from reference 100.

A gold ring-disc ultramicroelectrode array consisting of seven individually addressable electrodes was reported by Kim *et al.*[137] In their work, a 50-µm diameter gold disc surrounded by a 200-µm diameter gold ring was deposited on a glass substrate. Copper was then electrochemically deposited on the gold disc to obtain a Au/Cu ring-disc ultramicroelectrode. However, electrochemical study at the disc-shaped electrode is sometimes difficult as the two dimensional geometry and the disc-insulator boundary of the electrode produce an edge effect that restricts mass transport of analyte towards the electrode surface.[138] This prompted Ellison *et al.*[139] to study the effect of insulating sheath thickness on the steady state current at micro-disc electrodes. As shown in Figure 1.3, they found that the thinner the insulating sheath, the higher the mass transport of the analyte to the electrode surface was observed. Results from the modelling at carbon micro-disc electrodes suggested that, to obtain a reasonable steady

state current, the insulating sheath thickness was required to be at least two times smaller than the disc radius. This conclusion supported Daniele *et al.*'s[140] earlier study involving a similar investigation on a platinum microdisc electrode and on a cylindrical platinum wire electrode.

Figure 1.3. A micro-disc electrode with (A) an infinite sheath and (B) an infinitesimal sheath. Adapted from reference 139.

1.4.2 Conical shaped microelectrodes

The geometry of an electrode dictates the nature of mass transport to its surface. In general, the diffusion-limited current is enhanced dramatically at a conical shaped electrode owing to the nonplanar diffusion at both the edge and the apex of the cone.[141] Therefore, conical shaped electrodes are often considered an alternative choice to disc shaped electrodes for electrochemical detection to obtain enhanced sensitivity in a resistive biological environment. Hermans *et al.*[142] prepared a conical tip tungsten substrate by the etching the metal in a saturated solution of $NaNO_3$ in 1 M NaOH using an AC potential of 10 V. The tip was then placed in a photoresist, which was pyrolysed to deposit carbon on the tip. Before depositing the pyrolysed carbon, oxide functionalities on tungsten (which may aid in increasing the resistance between the substrate and the deposited carbon) was removed by treating with concentrated hydrofluoric acid. The entire electrode was finally insulated with epoxylite but leaving the tip undisturbed. Similarly, Morton *et al.*[143] have also developed a carbon electrode using parylene as a carbon source. They conducted the pyrolysis in a furnace of 900^{o}C

for 1 h to deposit carbon on the tip of a pulled pipette with an inner diameter of 150 nm. The process was repeated twice to minimise possible pinhole leaks. The remaining body of the pipette was insulated by poly(dimethylsiloxane). Park *et al.*[121] electrochemically etched a platinum wire to obtain a conical tip and then deposited electrically-conducting diamond by a microwave plasma chemical vapour deposition method from a $CH_4/H_2/B_2H_6$ source gas mixture. In other work, a silicon microtip array was fabricated by anisotropic etching and a deep reactive ion etching process to attain a high aspect ratio of the probe.[144] A conducting indium tin oxide layer was then deposited on each tip to form a modified electrode array. A NH_2-terminated silane monolayer and single walled carbon nanotube modified conical glass/platinum micropore electrode was developed to achieve an electrocatalytic effect and a low background current when the electrode was used to detect dopamine.[145] Rees *et al.*[146] fabricated a carbon electrode using already pulled conical tip glass nanopipette of 50 to 400 nm diameter. In this work, the already pulled pipette was placed in a chemical vapour deposition chamber with a flow of methane and argon at 900^{o}C such that carbon selectively deposited inside the pipette. Finally, the tip was etched using buffered hydrofluoric acid for 1 min to expose carbon of 5 to 10 μm length. A nanotip conical carbon-fibre micorelectrode of 50-100 nm diameter and 30-100 μm length was developed by Li *et al.*[114] for quantitative measurement of transmitters in individual vesicles. As shown in the schematic fabrication process in Figure 1.4, a 5-μm diameter carbon fibre was aspirated into a borosilicate glass capillary that was then pulled. The protruded fibre was next evenly etched in the blue part of a butane flame before the fibre was sealed in the capillary using epoxy. The electrode demonstrated good electrochemical characteristics and showed high sensitivity to the analyte. For electrochemical measurement, this electrode was demonstrated to show minimal damage to a cell after penetrating the cell membrane. Only electrodes that showed a steady-state diffusion limited current were used in further experiments.

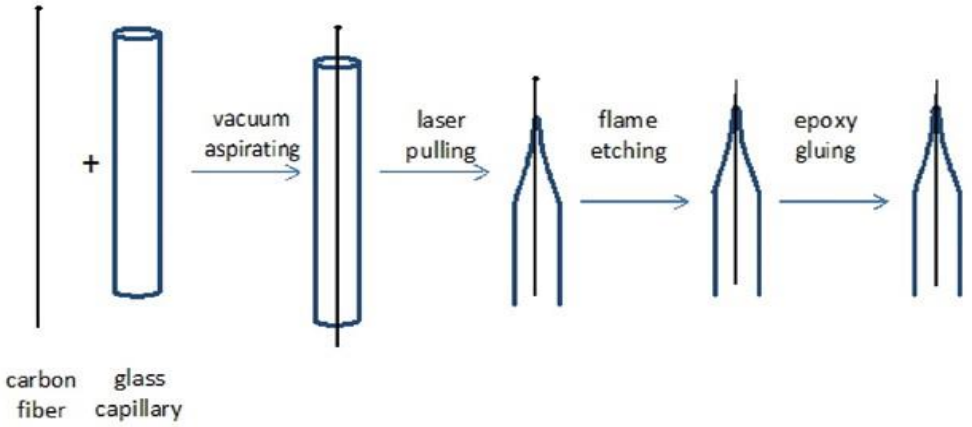

Figure 1.4. A schematic diagram showing the processes for fabrication of nano-tip conical carbon fibre microelectrodes. Adapted from reference 106.

1.5 Advantages of conical-tip carbon electrodes over carbon fibre electrodes

A carbon fibre microelectrode is a significant development in the history of bio-electrochemistry owing to several advantages. They have been used for decades to understand basic neurobiological mechanisms as they are biocompatible, non-toxic to cells and have good electrochemical properties. A miniaturised fibre (5-35 μm in diameter) is clearly more suitable for implantation with minimum cell damage compared to a larger conventional-sized electrode. During the fabrication process of carbon fibre microelectrodes, the fibre is aspirated through a glass capillary such that approximately 100 μm of the fibre in length protrudes the capillary. Epoxy is usually applied to the fibre-glass junction to secure the fibre in the glass capillary.[147] However, unsatisfactory sealing and leakage of epoxy often compromise the quality of carbon fibre electrodes, resulting in high noise, low sensitivity, short electrode life span and sometimes contamination of solution of interest.[148]

Our research group has previously reported on the development of conical-tip carbon electrodes.[149] Briefly, in constructing such an electrode, we initially house a quartz capillary that has already been pulled down to a fine tip before C_2H_2 is thermally pyrolysed to form carbon that is deposited both at the tip (~2 μm diameter) and on the

shank (~15 μm axial length) of the capillary. Graphite powder and a conducting wire are introduced through the larger end of the pulled capillary to complete the construction of a conical-tip carbon electrode. Compared to carbon fibre electrodes, the quartz substrate of conical-tip carbon electrodes provides the mechanical strength, whilst the sharp tips aid in easy biological membrane penetration during implantation.[150] In addition, the open-ended base edge on a conical-tip electrode is more accessible to the mass transport of analyte to the electrode, compared to an insulating plane at the finite fibre-capillary junction on carbon fibre electrodes. Therefore, conical-tip carbon electrodes of a similar dimension to carbon fibre electrodes were found to show an improved signal-to-noise ratio in detecting dopamine *in vivo*.[151] Notably, there is also no epoxy sealing at the carbon-capillary junction, which could otherwise have polluted solution of interest in a biological environment.[148] A physical comparison of carbon fibre and conical-tip carbon electrodes is presented in Figure 1.5.

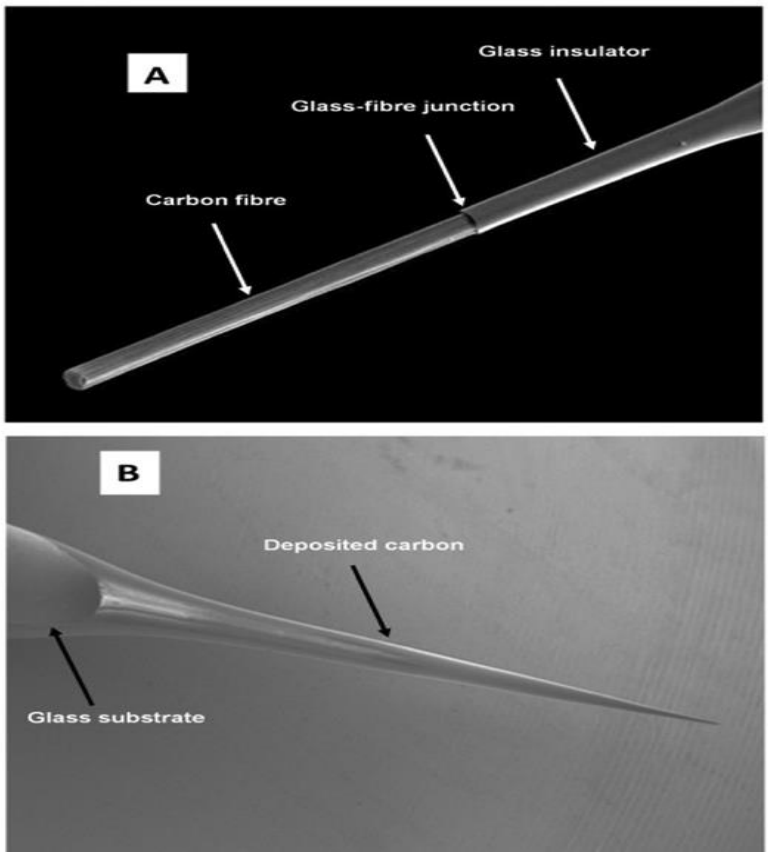

Figure 1.5. Scanning electron micrographs of a carbon fibre electrode (A) and a conical-tip carbon electrode (B).

1.6 Electrode fouling during electrochemical detection

Although most electrodes reported in literature so far have demonstrated effective and reliable neurotransmitter determination *in vitro*, their stability and sensitivity are often compromised when they are implanted *in vivo* in a complex biological medium.[42] Fouling of an electrode surface is such a phenomenon that is often a serious problem in some electrochemical analyses. Electrode fouling is a broad term generally describing the passivation of an electrode surface by a fouling agent that forms an increasingly impermeable layer on the electrode.[152,153,154] This occurs by a wide range of mechanisms predominantly depending on the identity of the responsible fouling agent. The fouling agent may be a component of the matrix, the analyte itself, or a product of the electrochemical reaction. Electrode fouling prevents an analyte of interest from making physical contact with the electrode for electron transfer to elicit an electrochemical response.[155,156,157,158] The fouling agent may specifically adhere to certain structural features present on the electrode surface, such as edges and grain boundaries.[159,160,161] The fouling agent tends to adhere to the electrode surface as a result of favourable interactions between the fouling agent and the electrode surface. This includes hydrophobic, hydrophilic, and electrostatic interactions depending on the particular chemistries of the fouling agent and the electrode surface.

Electrodes that tend to have hydrophobic surfaces, such as diamond, carbon nanotubes, and some other carbon-based electrodes,[160, 162] can promote hydrophobic-containing species such as aromatic compounds, saturated or aliphatic compounds, and proteins to adhere to and foul the electrode. The hydrophobic interactions are entropically favourable in an aqueous electrolyte because water molecules are released from the solvation shell around hydrophobic compounds or regions.[159, 163] These interactions are sufficiently favourable such that fouling by a hydrophobic mechanism is typically irreversible in an aqueous electrolyte under mild conditions.[163-164]

Fouling that occurs by hydrophilic interactions tends to be more reversible than fouling involving hydrophobic interactions.[159, 163-165] This greater reversibility in aqueous electrolytes containing a strong polar solvent, for example water, is because the

hydrophilic and electrostatic interactions are not exclusive to the fouling agent and the electrode surface, as water also has compatible hydrophilic (dipole-dipole interactions or hydrogen bonding) and electrostatic properties (ion-dipole interactions). In the case of electrostatic interactions, the electrode surface may possess ionisable functional groups, such as carboxylic acids, which will bind with a suitable fouling agent.[162a, 162c] Electrode fouling that occurs by a hydrophilic or electrostatic interaction is associated with polar, hydrophilic, or charged species, including proteins and other biological molecules.

Electrode fouling that occurs by the adsorption of biological macromolecules is frequently due to proteins as a result of their abundance in biological samples and tendency to cause fouling. The adsorption of other biological materials, such as cells, cell fragments, and DNA/RNA, can also foul an electrode. The binding of cells to an electrode surface is often mediated by proteins.[159] Soluble proteins are interesting fouling agents, as they are often hydrophilic on the surface to interact with an aqueous environment as well as hydrophobic on the inside to maintain protein folding or the binding of hydrophobic materials. As a result of the dual nature of most proteins, they can foul electrodes through both hydrophilic and hydrophobic interactions. To foul a hydrophobic electrode surface, many proteins will unfold to allow the hydrophobic residues to interact with the hydrophobic surface.[159,165b] Due to the greater strength of hydrophobic interactions in aqueous systems[159,165b], many antifouling strategies aimed at reducing fouling by biological materials involve increasing the hydrophilicity of the electrode surface.

Fouling agents discussed thus far have been monomeric species, where it is more energetically favourable for the fouling agent to adsorb to the electrode surface rather than be in solution. A fouling agent may also be a polymeric species that forms in the electrolyte, usually as a result of an electrochemical reaction. [155,157,166,167,168,169] The product of an electrochemical reaction may be reactive, such that it forms dimers or larger polymeric structures. These polymeric structures are often insoluble due to their large size and high molecular weight and will precipitate from solution on the nearest

surface, such as the electrode surface. Such adhesion of a polymer to the electrode surface obstructs the ability of the analyte to reach the electrode surface, thereby fouling the electrode.[155,166,167,168,169] The polymer may be a dense and closed structure that is impermeable, or it may be lighter and more open such that the polymer is permeable or semipermeable.[167,168,170] The permeability of the polymeric species will depend on the starting monomer and the electrochemical system conditions.[155,166] The important analytes of interest that foul electrodes by this route are phenols and neurotransmitters. In the case of phenols, following anodic oxidation, radicals are formed. Further reactions involving the radicals may produce soluble species, such as hydroquinone/benzoquinone or catechol, or may undergo coupling reactions to form dimers, then oligomers, and finally polymers.

1.7 Scope of the present study

As discussed in the preceding sections, an electrode may experience fouling during detection of neurotransmitter dopamine *in vivo* due to nonspecific adsorption of large biomolecules, which then prevents dopamine from reaching the electrode surface and participating in an electron transfer reaction. In addition, during electrochemical oxidation of dopamine, it forms a melanin-like polymer that tends to bind with electrode surface, leading to fouling. All these often lead to a compromised dopamine detection *in vivo*. Hence, there is a demand for developing fouling resistant sensing electrodes for use in *in vivo* detection. A number of initiatives was presented in work discussed above for developing strategies combating against fouling arisen from polymeric molecules that originate from the oxidation products of neurotransmitters. However, there has been very limited effort so far against biofouling during dopamine detection *in vitro* or *in vivo*. Therefore, this work is primarily aimed at developing fouling resistant physically small carbon electrodes modified by incorporating several antifouling layers on electrode surface. Further, the ability of the electrodes to withstand fouling effects and their suitability for use as an *in vivo* probe were also evaluated by performing dopamine detection in a synthetic fouling solution that mimics complex biological environment.

Initially, conical-tip carbon electrodes will be fabricated by following a procedure previously reported by our research group.[149] These electrodes will then be hydrogenated using an *n*-butylsilane reduction method to achieve an H-terminated carbon surface with extended butylsiloxane dendrimers. In Chapter 3, this method will demonstrate our finding that the *n*-butylsilane reduction method is also capable of reactivating non-functioning carbon microelectrodes. The hydrogenated electrodes will also be examined to assess their long term stability both in air and in a citrate/phosphate buffer. A significant outcome of this part of the work is that *n*-butylsilane reduction method would aid in improving the fabrication success rate of carbon microelectrodes to nearly 100%. Notably, hydrogenation by *n*-butylsilane is conducted under ambient laboratory conditions in the presence of a mild reducing agent. This method can therefore be readily adopted as an alternative to hydrogenation of carbon surface by plasma chemical vapour deposition that is often performed at very high temperature (~700°C) and pressure (~6 kPa).

Next, the antifouling capability of the *n*-butylsilane hydrogenated electrodes will be evaluated in a laboratory synthetic fouling solution in Chapter 4. The solution contains bovine serum albumin, cytochrome C, human fibrinopeptide and caproic acid that mimics complex biological environment. In this chapter, we will also demonstrate the capability of the modified surface in detecting dopamine at a defined concentration without any interference from its polymeric product originated during electrochemical oxidation. In this chapter, hydrogenated electrodes are further functionalised with 4-sulfobenzene in a controlled manner to enhance the electron transfer kinetics and sensitivity of the electrode towards dopamine. We also demonstrate that an improved fouling resistance can be achieved after grafting 4-sulfobenzene on a hydrogenated electrode surface.

In chapter 5, we systematically compare diethylsilane hydrogenation with *n*-butylsilane hydrogenation in terms of effectiveness of the modified carbon surface against fouling. More specifically, we are interested in examining the effects of longer chain and branched silane compounds on antifouling property. In this chapter, we will

demonstrate the remarkable property of diethylsilane in aiding dopamine detection. In addition, we immobilise 4-sulfobenzene on diethylsilane modified electrode similar to that performed on *n*-butylsilane modified electrode. Finally, this electrode was employed to achieve an improved fouling resistance due to combination effect of butylsiloxane and 4-sulfobenzene layers.

Several redox markers including $[Ru(NH_3)_6]^{3+}$, $[Fe(CN)_6]^{3-}$ anthraquinone-2,6-disulfonate and dopamine have been employed in this work to probe the surface characteristics of hydrogenated electrodes and are discussed in separate chapter where it is relevant. A range of spectroscopic analyses by X-ray photoelectron spectroscopy, Raman spectroscopy, electrochemical impedance spectroscopy and atomic force microscopy will be conducted to provide supporting results in characterising the surface modification.

Chapter 6 will be devoted to an overall summary and concluding remarks from work conducted in this thesis, followed by feasible future directions for this work.

1.8 References

1. Paul, D. W.; Stenken, J. A., A review of flux considerations for in vivo neurochemical measurements. *The Analyst* **2015,** *140* (11), 3709-3730.
2. Schultz, W., Updating dopamine reward signals. *Current Opinion in Neurobiology* **2013,** *23* (2), 229-238.
3. Alex, K. D.; Pehek, E. A., Pharmacologic mechanisms of serotonergic regulation of dopamine neurotransmission. *Pharmacology & Therapeutics* **2007,** *113* (2), 296-320.
4. Berke, J. D.; Hyman, S. E., Addiction, dopamine, and the molecular mechanisms of memory. *Neuron* **2000,** *25* (3), 515-532.
5. Amatore, C.; Delacotte, J.; Guille-Collignon, M.; Lemaître, F., Vesicular exocytosis and microdevices–microelectrode arrays. *The Analyst* **2015,** *140* (11), 3687-3695.
6. Xu, H.; Zuo, P.; Wang, S.; Zhou, L.; Sun, X.; Hu, M.; Liu, B.; Wu, Q.; Dou, H.; Liu, B., Striatal dopamine release in a schizophrenia mouse model measured by electrochemical amperometry in vivo. *The Analyst* **2015,** *140* (11), 3840-3845.
7. Lovinger, D. M., Neurotransmitter roles in synaptic modulation, plasticity and learning in the dorsal striatum. *Neuropharmacology* **2010,** *58* (7), 951-961.
8. Chen, K. H.; Reese, E. A.; Kim, H.-W.; Rapoport, S. I.; Rao, J. S., Disturbed neurotransmitter transporter expression in Alzheimer's disease brain. *Journal of Alzheimer's disease* **2011,** *26* (4), 755-766.
9. Kurian, M. A.; Gissen, P.; Smith, M.; Heales, S. J. R.; Clayton, P. T., The monoamine neurotransmitter disorders: an expanding range of neurological syndromes. *The Lancet Neurology* **2011,** *10* (8), 721-733.
10. Tritsch, Nicolas X.; Sabatini, Bernardo L., Dopaminergic Modulation of Synaptic Transmission in Cortex and Striatum. *Neuron* **2012,** *76* (1), 33-50.
11. Bäckman, L.; Lindenberger, U.; Li, S.-C.; Nyberg, L., Linking cognitive aging to alterations in dopamine neurotransmitter functioning: Recent data and future avenues. *Neuroscience & Biobehavioral Reviews* **2010,** *34* (5), 670-677.

12. Beaulieu, J.-M.; Gainetdinov, R. R., The physiology, signaling, and pharmacology of dopamine receptors. *Pharmacological reviews* **2011,** *63* (1), 182-217.

13. Chinta, S. J.; Andersen, J. K., Dopaminergic neurons. *The international journal of biochemistry & cell biology* **2005,** *37* (5), 942-946.

14. Wong, A.; Liu, F., Uncoupling the dopamine D1-D2 receptor complex: a novel target for antidepressant treatment. *Clinical pharmacology and therapeutics* **2012,** *91* (2), 298-302.

15. Budygin, E. A.; Park, J.; Bass, C. E.; Grinevich, V. P.; Bonin, K. D.; Wightman, R. M., Aversive stimulus differentially triggers subsecond dopamine release in reward regions. *Neuroscience* **2012,** *201* (0), 331-337.

16. Jacobs, C. B.; Peairs, M. J.; Venton, B. J., Review: Carbon nanotube based electrochemical sensors for biomolecules. *Analytica chimica acta* **2010,** *662* (2), 105-127.

17. Eriksson, B.-M.; Wikström, M., Determination of catecholamines in urine by liquid chromatography and electrochemical detection after online sample purification on immobilized boronic acid. *Journal of Chromatography A* **1992,** *593* (1), 185-190.

18. Gutiérrez, A.; Gasnier, A.; Pedano, M. L.; Gonzalez-Dominguez, J. M.; Ansón-Casaos, A.; Hernández-Ferrer, J.; Galicia, L.; Rubianes, M. D.; Martínez, M. T.; Rivas, G. A., Electrochemical Sensor for the Quantification of Dopamine Using Glassy Carbon Electrodes Modified with Single-Wall Carbon Nanotubes Covalently Functionalized with Polylysine. *Electroanalysis* **2015,** *27* (7), 1565-1571.

19. Gardner, D.; Shoback, D., Appendix: normal hormone reference ranges. *Greenspan's basic & clinical endocrinology. 9th ed. New York: McGraw-Hill* **2011**.

20. MOHAMMAD-ZADEH, L.; Moses, L.; GWALTNEY-BRANT, S., Serotonin: a review. *Journal of veterinary pharmacology and therapeutics* **2008,** *31* (3), 187-199.

21. Uher, R.; McGuffin, P., The moderation by the serotonin transporter gene of environmental adversity in the etiology of depression: 2009 update. *Molecular psychiatry* **2010,** *15* (1), 18-22.

22. Bertrand, P. P.; Bertrand, R. L., Serotonin release and uptake in the gastrointestinal tract. *Autonomic Neuroscience* **2010,** *153* (1–2), 47-57.

23. Geracioti Jr, T. D.; Baker, D. G.; Ekhator, N. N.; West, S. A.; Hill, K. K.; Bruce, A. B.; Schmidt, D.; Rounds-Kugler, B.; Yehuda, R.; Keck Jr, P. E., CSF norepinephrine concentrations in posttraumatic stress disorder. *American Journal of Psychiatry* **2001**.

24. Goddard, A. W.; Ball, S. G.; Martinez, J.; Robinson, M. J.; Yang, C. R.; Russell, J. M.; Shekhar, A., Current perspectives of the roles of the central norepinephrine system in anxiety and depression. *Depression and anxiety* **2010,** *27* (4), 339-350.

25. Heneka, M. T.; Nadrigny, F.; Regen, T.; Martinez-Hernandez, A.; Dumitrescu-Ozimek, L.; Terwel, D.; Jardanhazi-Kurutz, D.; Walter, J.; Kirchhoff, F.; Hanisch, U.-K.; Kummer, M. P., Locus ceruleus controls Alzheimer's disease pathology by modulating microglial functions through norepinephrine. *Proceedings of the National Academy of Sciences* **2010,** *107* (13), 6058-6063.

26. Taei, M.; Hadadzadeh, H.; Hasanpour, F.; Tavakkoli, N.; Dolatabadi, M. H., Simultaneous electrochemical determination of ascorbic acid, epinephrine, and uric acid using a polymer film-modified electrode based on Au nanoparticles/poly(3,3′,5,5′-tetrabromo-m-cresolsulfonphthalein). *Ionics* **2015,** *21* (12), 3267-3278.

27. Tavana, T.; Khalilzadeh, M. A.; Karimi-Maleh, H.; Ensafi, A. A.; Beitollahi, H.; Zareyee, D., Sensitive voltammetric determination of epinephrine in the presence of acetaminophen at a novel ionic liquid modified carbon nanotubes paste electrode. *Journal of Molecular Liquids* **2012,** *168* (0), 69-74.

28. Mazloum-Ardakani, M.; Beitollahi, H.; Mohseni, M. A. S.; Benvidi, A.; Naeimi, H.; Nejati-Barzoki, M.; Taghavinia, N., Simultaneous determination of epinephrine and acetaminophen concentrations using a novel carbon paste electrode prepared with 2,2′-[1,2 butanediylbis(nitriloethylidyne)]-bis-

hydroquinone and TiO2 nanoparticles. *Colloids and Surfaces B: Biointerfaces* **2010,** *76* (1), 82-87.

29. Michael, D. J.; Wightman, R. M., Electrochemical monitoring of biogenic amine neurotransmission in real time. *Journal of pharmaceutical and biomedical analysis* **1999,** *19* (1), 33-46.
30. Majdi, S.; Ren, L.; Fathali, H.; Li, X.; Ewing, A., Selected recent in vivo studies on chemical measurements in invertebrates. *The Analyst* **2015,** *140* (11), 3676-3686.
31. Paul, D. W.; Stenken, J. A., A review of flux considerations for in vivo neurochemical measurements. *The Analyst* **2015,** *140* (11), 3709-3730.
32. Syslová, K.; Rambousek, L.; Kuzma, M.; Najmanová, V.; Bubeníková-Valešová, V.; Šlamberová, R.; Kačer, P., Monitoring of dopamine and its metabolites in brain microdialysates: Method combining freeze-drying with liquid chromatography–tandem mass spectrometry. *Journal of Chromatography A* **2011,** *1218* (21), 3382-3391.
33. Navailles, S.; Lagiere, M.; Contini, A.; De Deurwaerdere, P., Multisite intracerebral microdialysis to study the mechanism of L-DOPA induced dopamine and serotonin release in the parkinsonian brain. *ACS chemical neuroscience* **2013,** *4* (5), 680-692.
34. Segovia, G.; Del Arco, A.; De Blas, M.; Garrido, P.; Mora, F., Environmental enrichment increases the in vivo extracellular concentration of dopamine in the nucleus accumbens: a microdialysis study. *Journal of neural transmission* **2010,** *117* (10), 1123-1130.
35. Cannazza, G.; Carrozzo, M. M.; Cazzato, A. S.; Bretis, I. M.; Troisi, L.; Parenti, C.; Braghiroli, D.; Guiducci, S.; Zoli, M., Simultaneous measurement of adenosine, dopamine, acetylcholine and 5-hydroxytryptamine in cerebral mice microdialysis samples by LC–ESI-MS/MS. *Journal of Pharmaceutical and Biomedical Analysis* **2012,** *71*, 183-186.
36. Suominen, T.; Uutela, P.; Ketola, R. A.; Bergquist, J.; Hillered, L.; Finel, M.; Zhang, H.; Laakso, A.; Kostiainen, R., Determination of serotonin and dopamine metabolites in human brain microdialysis and cerebrospinal fluid

samples by UPLC-MS/MS: discovery of intact glucuronide and sulfate conjugates. *PloS one* **2013,** *8* (6), e68007.

37. Mabrouk, O. S.; Li, Q.; Song, P.; Kennedy, R. T., Microdialysis and mass spectrometric monitoring of dopamine and enkephalins in the globus pallidus reveal reciprocal interactions that regulate movement. *Journal of neurochemistry* **2011,** *118* (1), 24-33.
38. Buck, K.; Voehringer, P.; Ferger, B., The α2 adrenoceptor antagonist idazoxan alleviates l-DOPA-induced dyskinesia by reduction of striatal dopamine levels: an in vivo microdialysis study in 6-hydroxydopamine-lesioned rats. *Journal of neurochemistry* **2010,** *112* (2), 444-452.
39. Ferry, B.; Gifu, E.-P.; Sandu, I.; Denoroy, L.; Parrot, S., Analysis of microdialysate monoamines, including noradrenaline, dopamine and serotonin, using capillary ultra-high performance liquid chromatography and electrochemical detection. *Journal of chromatography B* **2014,** *951*, 52-57.
40. Morelli, M.; Carboni, E.; Cozzolino, A.; Tanda, G.; Pinna, A.; Chiara, G., Combined Microdialysis and Fos Immunohistochemistry for the Estimation of Dopamine Neurotransmission in the Rat Caudate-Putamen. *Journal of neurochemistry* **1992,** *59* (3), 1158-1160.
41. Di Chiara, G.; Carboni, E.; Morelli, M.; Cozzolino, A.; Tanda, G.; Pinna, A.; Russi, G.; Consolo, S., Stimulation of dopamine transmission in the dorsal caudate nucleus by pargyline as demonstrated by dopamine and acetylcholine microdialysis and Fos immunohistochemistry. *Neuroscience* **1993,** *55* (2), 451-456.
42. Wilson, G. S.; Johnson, M. A., In-vivo electrochemistry: what can we learn about living systems? *Chemical reviews* **2008,** *108* (7), 2462-2481.
43. Jaquins-Gerstl, A.; Shu, Z.; Zhang, J.; Liu, Y.; Weber, S. G.; Michael, A. C., Effect of Dexamethasone on Gliosis, Ischemia, and Dopamine Extraction during Microdialysis Sampling in Brain Tissue. *Analytical Chemistry* **2011,** *83* (20), 7662-7667.

44. Wang, Y.; Michael, A. C., Microdialysis probes alter presynaptic regulation of dopamine terminals in rat striatum. *Journal of Neuroscience Methods* **2012,** *208* (1), 34-39.

45. Njagi, J.; Chernov, M. M.; Leiter, J.; Andreescu, S., Amperometric detection of dopamine in vivo with an enzyme based carbon fiber microbiosensor. *Analytical chemistry* **2010,** *82* (3), 989-996.

46. Shang, L.; Dong, S.; Nienhaus, G. U., Ultra-small fluorescent metal nanoclusters: Synthesis and biological applications. *Nano Today* **2011,** *6* (4), 401-418.

47. Wu, H.-P.; Cheng, T.-L.; Tseng, W.-L., Phosphate-modified TiO2 nanoparticles for selective detection of dopamine, levodopa, adrenaline, and catechol based on fluorescence quenching. *Langmuir* **2007,** *23* (14), 7880-7885.

48. Liu, S.; Shi, F.; Zhao, X.; Chen, L.; Su, X., 3-Aminophenyl boronic acid-functionalized CuInS2 quantum dots as a near-infrared fluorescence probe for the determination of dopamine. *Biosensors and Bioelectronics* **2013,** *47*, 379-384.

49. Xiangzhao, A.; Qiang, M.; Xingguang, S., Nanosensor for dopamine and glutathione based on the quenching and recovery of the fluorescence of silica-coated quantum dots. *Microchimica Acta* **2013,** *180* (3-4), 269-277.

50. Mu, Q.; Xu, H.; Li, Y.; Ma, S.; Zhong, X., Adenosine capped QDs based fluorescent sensor for detection of dopamine with high selectivity and sensitivity. *The Analyst* **2014,** *139* (1), 93-98.

51. Zhao, D.; Song, H.; Hao, L.; Liu, X.; Zhang, L.; Lv, Y., Luminescent ZnO quantum dots for sensitive and selective detection of dopamine. *Talanta* **2013,** *107*, 133-139.

52. Tao, Y.; Lin, Y.; Ren, J.; Qu, X., A dual fluorometric and colorimetric sensor for dopamine based on BSA-stabilized Aunanoclusters. *Biosensors and Bioelectronics* **2013,** *42*, 41-46.

53. Lin, Y.; Yin, M.; Pu, F.; Ren, J.; Qu, X., DNA-Templated Silver Nanoparticles as a Platform for Highly Sensitive and Selective Fluorescence Turn-On Detection of Dopamine. *Small* **2011,** *7* (11), 1557-1561.

54. Zhang, X.; Chen, X.; Kai, S.; Wang, H.-Y.; Yang, J.; Wu, F.-G.; Chen, Z., Highly Sensitive and Selective Detection of Dopamine Using One-Pot Synthesized Highly Photoluminescent Silicon Nanoparticles. *Analytical Chemistry* **2015,** *87* (6), 3360-3365.

55. Gaied, A.; Jaballah, N.; Tounsi, M.; Braiek, M.; Jaffrezic-Renault, N.; Majdoub, M., Selective Detection of Dopamine in Presence of Ascorbic Acid by Use of Glassy-Carbon Electrode Modified with Amino-β-Cyclodextrin and Carbon Nanotubes. *Electroanalysis* **2014,** *26* (12), 2747-2753.

56. Zhu, H.; Wu, W.; Zhang, H.; Fan, L.; Yang, S., Highly Selective and Sensitive Detection of Dopamine in the Presence of Excessive Ascorbic Acid Using Electrodes Modified with C60-Functionalized Multiwalled Carbon Nanotube Films. *Electroanalysis* **2009,** *21* (24), 2660-2666.

57. Brunetti, B.; Valdés-Ramírez, G.; Litvan, I.; Wang, J., A disposable electrochemical biosensor for l-DOPA determination in undiluted human serum. *Electrochemistry Communications* **2014,** *48*, 28-31.

58. Veerakumar, P.; Madhu, R.; Chen, S.-M.; Hung, C.-T.; Tang, P.-H.; Wang, C.-B.; Liu, S.-B., Porous carbon-modified electrodes as highly selective and sensitive sensors for detection of dopamine. *The Analyst* **2014,** *139* (19), 4994-5000.

59. Kemmegne-Mbouguen, J. C.; Angnes, L.; Mouafo-Tchinda, E.; Ngameni, E., Electrochemical Determination of Uric Acid, Dopamine and Tryptophan at Zinc Hexacyanoferrate Clay Modified Electrode. *Electroanalysis* **2015**, 27(10), 2387-2398.

60. Suresh, R.; Giribabu, K.; Manigandan, R.; Kumar, S. P.; Munusamy, S.; Muthamizh, S.; Stephen, A.; Narayanan, V., New electrochemical sensor based on Ni-doped V 2 O 5 nanoplates modified glassy carbon electrode for selective determination of dopamine at nanomolar level. *Sensors and Actuators B: Chemical* **2014,** *202*, 440-447.

61. Sun, H.; Chao, J.; Zuo, X.; Su, S.; Liu, X.-F.; Yuwen, L.; Fan, C.; Wang, L.-H., Gold nanoparticle-decorated MoS2 nanosheets for simultaneous detection of ascorbic acid, dopamine and uric acid. *RSC Advances* **2014**.

62. Cincotto, F. H.; Canevari, T. C.; de Campos, A. M.; Landers, R.; Machado, S. A., Simultaneous determination of epinephrine and dopamine by electrochemical reduction on the hybrid material SiO2/graphene oxide content Ag nanoparticles. *The Analyst* **2014**.

63. Tan, S. M.; Poh, H. L.; Sofer, Z.; Pumera, M., Boron-doped graphene and boron-doped diamond electrodes: detection of biomarkers and resistance to fouling. *The Analyst* **2013,** *138* (17), 4885-4891.

64. Silva, T. A.; Zanin, H.; May, P. W.; Corat, E. J.; Fatibello-Filho, O., Electrochemical Performance of Porous Diamond-like Carbon Electrodes for Sensing Hormones, Neurotransmitters, and Endocrine Disruptors. *ACS applied materials & interfaces* **2014,** *6* (23), 21086-21092.

65. Shalini, J.; Sankaran, K. J.; Dong, C.-L.; Lee, C.-Y.; Tai, N.-H.; Lin, I.-N., In situ detection of dopamine using nitrogen incorporated diamond nanowire electrode. *Nanoscale* **2013,** *5* (3), 1159-1167.

66. Zhuo, S.; Shao, M.; Lee, S.-T., Upconversion and downconversion fluorescent graphene quantum dots: ultrasonic preparation and photocatalysis. *ACS nano* **2012,** *6* (2), 1059-1064.

67. Wang, Y.; Li, Y.; Tang, L.; Lu, J.; Li, J., Application of graphene-modified electrode for selective detection of dopamine. *Electrochemistry Communications* **2009,** *11* (4), 889-892.

68. Ping, J.; Wu, J.; Wang, Y.; Ying, Y., Simultaneous determination of ascorbic acid, dopamine and uric acid using high-performance screen-printed graphene electrode. *Biosensors and Bioelectronics* **2012,** *34* (1), 70-76.

69. Yu, B.; Kuang, D.; Liu, S.; Liu, C.; Zhang, T., Template-assisted self-assembly method to prepare three-dimensional reduced graphene oxide for dopamine sensing. *Sensors and Actuators B: Chemical* **2014,** *205*, 120-126.

70. Yu, X.; Sheng, K.; Shi, G., A three-dimensional interpenetrating electrode of reduced graphene oxide for selective detection of dopamine. *The Analyst* **2014,** *139* (18), 4525-4531.

71. Han, H. S.; Seol, H.; Kang, D. H.; Ahmed, M. S.; You, J.-M.; Jeon, S., Electrochemical oxidation and determination of dopamine in the presence of

AA using ferulic acid functionalized electrochemically reduced graphene. *Sensors and Actuators B: Chemical* **2014,** *204*, 289-296.

72. Gutierrez, F.; Comba, F. N.; Gasnier, A.; Gutierrez, A.; Galicia, L.; Parrado, C.; Rubianes, M. D.; Rivas, G. A., Graphene Paste Electrode: Analytical Applications for the Quantification of Dopamine, Phenolic Compounds and Ethanol. *Electroanalysis* **2014**.

73. Sun, C.-L.; Lee, H.-H.; Yang, J.-M.; Wu, C.-C., The simultaneous electrochemical detection of ascorbic acid, dopamine, and uric acid using graphene/size-selected Pt nanocomposites. *Biosensors and Bioelectronics* **2011,** *26* (8), 3450-3455.

74. (a) Lian, Q.; He, Z.; He, Q.; Luo, A.; Yan, K.; Zhang, D.; Lu, X.; Zhou, X., Simultaneous determination of ascorbic acid, dopamine and uric acid based on tryptophan functionalized graphene. *Analytica chimica acta* **2014,** *823*, 32-39; (b) Wang, K.; Fishman, H. A.; Dai, H.; Harris, J. S., Neural stimulation with a carbon nanotube microelectrode array. *Nano letters* **2006,** *6* (9), 2043-2048.

75. Wightman, R. M., Probing cellular chemistry in biological systems with microelectrodes. *Science* **2006,** *311* (5767), 1570-1574.

76. Gosso, S.; Turturici, M.; Franchino, C.; Colombo, E.; Pasquarelli, A.; Carbone, E.; Carabelli, V., Heterogeneous distribution of exocytotic microdomains in adrenal chromaffin cells resolved by high-density diamond ultra-microelectrode arrays. *The Journal of physiology* **2014,** *592* (15), 3215-3230.

77. Meunier, A.; Bretou, M.; Darchen, F.; Collignon, M. G.; Lemaître, F.; Amatore, C., Amperometric detection of vesicular exocytosis from BON cells at carbon fiber microelectrodes. *Electrochimica Acta* **2014,** *126*, 74-80.

78. Hochstetler, S. E.; Puopolo, M.; Gustincich, S.; Raviola, E.; Wightman, R. M., Real-time amperometric measurements of zeptomole quantities of dopamine released from neurons. *Analytical chemistry* **2000,** *72* (3), 489-496.

79. Park, J.; Aragona, B. J.; Kile, B. M.; Carelli, R. M.; Wightman, R. M., In vivo voltammetric monitoring of catecholamine release in subterritories of the nucleus accumbens shell. *Neuroscience* **2010,** *169* (1), 132-142.

80. Bath, B. D.; Michael, D. J.; Trafton, B. J.; Joseph, J. D.; Runnels, P. L.; Wightman, R. M., Subsecond adsorption and desorption of dopamine at carbon-fiber microelectrodes. *Analytical chemistry* **2000,** *72* (24), 5994-6002.

81. Jacobs, C. B.; Ivanov, I. N.; Nguyen, M. D.; Zestos, A. G.; Venton, B. J., High temporal resolution measurements of dopamine with carbon nanotube yarn microelectrodes. *Analytical chemistry* **2014**.

82. Mo, J.-W.; Ogorevc, B., Simultaneous measurement of dopamine and ascorbate at their physiological levels using voltammetric microprobe based on overoxidized poly (1, 2-phenylenediamine)-coated carbon fiber. *Analytical chemistry* **2001,** *73* (6), 1196-1202.

83. Xiao, N.; Venton, B. J., Rapid, sensitive detection of neurotransmitters at microelectrodes modified with self-assembled SWCNT forests. *Analytical chemistry* **2012,** *84* (18), 7816-7822.

84. Özel, R. E.; Wallace, K. N.; Andreescu, S., Chitosan coated carbon fiber microelectrode for selective in vivo detection of neurotransmitters in live zebrafish embryos. *Analytica chimica acta* **2011,** *695* (1), 89-95.

85. Xiang, L.; Yu, P.; Hao, J.; Zhang, M.; Zhu, L.; Dai, L.; Mao, L., Vertically aligned carbon nanotube-sheathed carbon fibers as pristine microelectrodes for selective monitoring of ascorbate in vivo. *Analytical chemistry* **2014,** *86* (8), 3909-3914.

86. Revin, S. B.; John, S. A., Electrochemical sensor for neurotransmitters at physiological pH using a heterocyclic conducting polymer modified electrode. *The Analyst* **2012,** *137* (1), 209-215.

87. Keighron, J. D.; Wigström, J.; Kurczy, M. E.; Bergman, J.; Wang, Y.; Cans, A.-S., Amperometric Detection of Single Vesicle Acetylcholine Release Events from an Artificial Cell. *ACS chemical neuroscience* **2015,** *6* (1), 181-188.

88. Patel, B. A.; Bian, X.; Quaiserová-Mocko, V.; Galligan, J. J.; Swain, G. M., In vitro continuous amperometric monitoring of 5-hydroxytryptamine release from enterochromaffin cells of the guinea pig ileum. *The Analyst* **2006,** *132* (1), 41-47.

89. Macpherson, J. V., A practical guide to using boron doped diamond in electrochemical research. *Physical Chemistry Chemical Physics* **2015,** *17* (5), 2935-2949.

90. Suzuki, A.; Ivandini, T. A.; Yoshimi, K.; Fujishima, A.; Oyama, G.; Nakazato, T.; Hattori, N.; Kitazawa, S.; Einaga, Y., Fabrication, characterization, and application of boron-doped diamond microelectrodes for in vivo dopamine detection. *Analytical chemistry* **2007,** *79* (22), 8608-8615.

91. Arumugam, P. U.; Zeng, H.; Siddiqui, S.; Covey, D. P.; Carlisle, J. A.; Garris, P. A., Characterization of ultrananocrystalline diamond microsensors for in vivo dopamine detection. *Applied physics letters* **2013,** *102* (25), 253107.

92. Lin, Y.; Wang, K.; Xu, Y.; Li, L.; Luo, J.; Wang, C., Facile development of Au-ring microelectrode for in vivo analysis using non-toxic polydopamine as multifunctional material. *Biosensors and Bioelectronics* **2016,** *78*, 274-280.

93. Shi, B.-X.; Wang, Y.; Zhang, K.; Lam, T.-L.; Chan, H. L.-W., Monitoring of dopamine release in single cell using ultrasensitive ITO microsensors modified with carbon nanotubes. *Biosensors and Bioelectronics* **2011,** *26* (6), 2917-2921.

94. Abe, H.; Ino, K.; Li, C.-Z.; Kanno, Y.; Inoue, K. Y.; Suda, A.; Kunikata, R.; Matsudaira, M.; Takahashi, Y.; Shiku, H., Electrochemical imaging of dopamine release from three-dimensional-cultured PC12 cells using LSI-based amperometric sensors. *Analytical chemistry* **2015**.

95. Zachek, M. K.; Park, J.; Takmakov, P.; Wightman, R. M.; McCarty, G. S., Microfabricated FSCV-compatible microelectrode array for real-time monitoring of heterogeneous dopamine release. *The Analyst* **2010,** *135* (7), 1556-1563.

96. Sasso, L.; Heiskanen, A.; Diazzi, F.; Dimaki, M.; Castillo-León, J.; Vergani, M.; Landini, E.; Raiteri, R.; Ferrari, G.; Carminati, M., Doped overoxidized polypyrrole microelectrodes as sensors for the detection of dopamine released from cell populations. *The Analyst* **2013,** *138* (13), 3651-3659.

97. Patel, B. A.; Luk, C. C.; Leow, P. L.; Lee, A. J.; Zaidi, W.; Syed, N. I., A planar microelectrode array for simultaneous detection of electrically evoked dopamine

release from distinct locations of a single isolated neuron. *The Analyst* **2013,** *138* (10), 2833-2839.

98. Kim, L. T. T.; Escriou, V.; Griveau, S.; Girard, A.; Griscom, L.; Razan, F.; Bedioui, F., Array of ultramicroelectrodes for the simultaneous detection of nitric oxide and peroxynitrite in biological systems. *Electrochimica Acta* **2014,** *140*, 33-36.
99. Wang, J.; Trouillon, R. l.; Lin, Y.; Svensson, M. I.; Ewing, A. G., Individually addressable thin-film ultramicroelectrode array for spatial measurements of single vesicle release. *Analytical chemistry* **2013,** *85* (11), 5600-5608.
100. Lin, Y.; Trouillon, R. l.; Svensson, M. I.; Keighron, J. D.; Cans, A.-S.; Ewing, A. G., Carbon-ring microelectrode arrays for electrochemical imaging of single cell exocytosis: fabrication and characterization. *Analytical chemistry* **2012,** *84* (6), 2949-2954.
101. Wang, J.; Trouillon, R. l.; Dunevall, J.; Ewing, A. G., Spatial resolution of single-cell exocytosis by microwell-based individually addressable thin film ultramicroelectrode arrays. *Analytical chemistry* **2014,** *86* (9), 4515-4520.
102. Hascup, E. R.; Hascup, K. N.; Stephens, M.; Pomerleau, F.; Huettl, P.; Gratton, A.; Gerhardt, G. A., Rapid microelectrode measurements and the origin and regulation of extracellular glutamate in rat prefrontal cortex. *Journal of neurochemistry* **2010,** *115* (6), 1608-1620.
103. Gerwig, R.; Fuchsberger, K.; Schroeppel, B.; Link, G. S.; Heusel, G.; Kraushaar, U.; Schuhmann, W.; Stett, A.; Stelzle, M., PEDOT–CNT composite microelectrodes for recording and electrostimulation applications: fabrication, morphology, and electrical properties. *Frontiers in neuroengineering* **2012,** *5*.
104. Compton, R. G.; Wildgoose, G. G.; Rees, N. V.; Streeter, I.; Baron, R., Design, fabrication, characterisation and application of nanoelectrode arrays. *Chemical Physics Letters* **2008,** *459* (1), 1-17.
105. Rogers, M. L.; Boutelle, M. G., Real-time clinical monitoring of biomolecules. *Analytical Chemistry* **2013,** *6*.

106. Cans, A.-S.; Ewing, A. G., Highlights of 20 years of electrochemical measurements of exocytosis at cells and artificial cells. *Journal of Solid State Electrochemistry* **2011,** *15* (7-8), 1437-1450.

107. Tallman, D. E., Microelectrodes for voltammetry—a personal historical perspective. *Journal of Solid State Electrochemistry* **2011,** *15* (7-8), 1703-1710.

108. Hubel, D. H., Tungsten microelectrode for recording from single units. *Science* **1957,** *125* (3247), 549-550.

109. Clausmeyer, J.; Schuhmann, W., Nanoelectrodes: applications in electrocatalysis, single-cell analysis and high-resolution electrochemical imaging. *TrAC Trends in Analytical Chemistry*, **2016**, *79*, 46-59.

110. Yang, F.; Han, J.; Zhuo, Y.; Yang, Z.; Chai, Y.; Yuan, R., Highly sensitive impedimetric immunosensor based on single-walled carbon nanohorns as labels and bienzyme biocatalyzed precipitation as enhancer for cancer biomarker detection. *Biosensors and Bioelectronics* **2014,** *55*, 360-365.

111. Deng, L.; Young, R. J.; Kinloch, I. A.; Zhu, Y.; Eichhorn, S. J., Carbon nanofibres produced from electrospun cellulose nanofibres. *Carbon* **2013,** *58*, 66-75.

112. Lee, M.-S.; Lee, K.; Kim, S.-Y.; Lee, H.; Park, J.; Choi, K.-H.; Kim, H.-K.; Kim, D.-G.; Lee, D.-Y.; Nam, S.; Park, J.-U., High-Performance, Transparent, and Stretchable Electrodes Using Graphene–Metal Nanowire Hybrid Structures. *Nano Letters* **2013,** *13* (6), 2814-2821.

113. Zestos, A. G.; Yang, C.; Jacobs, C. B.; Hensley, D.; Venton, B. J., Carbon nanospikes grown on metal wires as microelectrode sensors for dopamine. *The Analyst* **2015,** *140* (21), 7283-7292.

114. Li, X.; Majdi, S.; Dunevall, J.; Fathali, H.; Ewing, A. G., Quantitative measurement of transmitters in individual vesicles in the cytoplasm of single cells with nanotip electrodes. *Angewandte Chemie International Edition* **2015,** *54* (41), 11978-11982.

115. Zhao, X.; Lu, X.; Tze, W. T. Y.; Wang, P., A single carbon fiber microelectrode with branching carbon nanotubes for bioelectrochemical processes. *Biosensors and Bioelectronics* **2010,** *25* (10), 2343-2350.

116. Tamiasso-Martinhon, P.; Cachet, H.; Deslouis, C.; Vivier, V., Amorphous carbon nitride a-CN x microelectrode: fabrication and characterization. *Electrochemistry Communications* **2010,** *12* (8), 1074-1076.

117. Cheng, H.; Wang, X.; Wei, H., Ratiometric Electrochemical Sensor for Effective and Reliable Detection of Ascorbic Acid in Living Brains. *Analytical Chemistry* **2015,** *87* (17), 8889-8895.

118. Amato, L.; Schulte, L.; Heiskanen, A.; Keller, S. S.; Ndoni, S.; Emnéus, J., Novel Nanostructured Electrodes Obtained by Pyrolysis of Composite Polymeric Materials. *Electroanalysis* **2015,** *27* (7), 1544-1549.

119. Cvačka, J.; Quaiserová, V.; Park, J.; Show, Y.; Muck, A.; Swain, G. M., Boron-Doped Diamond Microelectrodes for Use in Capillary Electrophoresis with Electrochemical Detection. *Analytical Chemistry* **2003,** *75* (11), 2678-2687.

120. Park, J.; Show, Y.; Quaiserova, V.; Galligan, J. J.; Fink, G. D.; Swain, G. M., Diamond microelectrodes for use in biological environments. *Journal of Electroanalytical Chemistry* **2005,** *583* (1), 56-68.

121. Park, J.; Quaiserová-Mocko, V.; Patel, B. A.; Novotný, M.; Liu, A.; Bian, X.; Galligan, J. J.; Swain, G. M., Diamond microelectrodes for in vitro electroanalytical measurements: current status and remaining challenges. *The Analyst* **2008,** *133* (1), 17-24.

122. Zhao, H.; Bian, X.; Galligan, J. J.; Swain, G. M., Electrochemical measurements of serotonin (5-HT) release from the guinea pig mucosa using continuous amperometry with a boron-doped diamond microelectrode. *Diamond and Related Materials* **2010,** *19* (2–3), 182-185.

123. Peteu, S. F.; Whitman, B. W.; Galligan, J. J.; Swain, G. M., Electrochemical detection of peroxynitrite using hemin-PEDOT functionalized boron-doped diamond microelectrode. *The Analyst* **2016,** *141* (5), 1796-1806.

124. Silva, E. L.; Bastos, A. C.; Neto, M. A.; Silva, R. F.; Ferreira, M. G. S.; Zheludkevich, M. L.; Oliveira, F. J., Novel diamond microelectrode for pH sensing. *Electrochemistry Communications* **2014,** *40*, 31-34.

125. Silva, E. L.; Gouvêa, C. P.; Quevedo, M. C.; Neto, M. A.; Archanjo, B. S.; Fernandes, A. n. J.; Achete, C. A.; Silva, R. F.; Zheludkevich, M. L.; Oliveira,

F. J., All-Diamond Microelectrodes as Solid State Probes for Localized Electrochemical Sensing. *Analytical chemistry* **2015,** *87* (13), 6487-6492.

126. Hutton, L. A.; Vidotti, M.; Iacobini, J. G.; Kelly, C.; Newton, M. E.; Unwin, P. R.; Macpherson, J. V., Fabrication and Characterization of an All-Diamond Tubular Flow Microelectrode for Electroanalysis. *Analytical Chemistry* **2011,** *83* (14), 5804-5808.
127. Wu, S.; Su, B., A simple approach for fabrication of microring electrodes. *Journal of Electroanalytical Chemistry* **2013,** *694*, 12-16.
128. Liu, Y.; Li, M.; Zhang, F.; Zhu, A.; Shi, G., Development of Au disk nanoelectrode down to 3 nm in radius for detection of dopamine release from a single cell. *Analytical chemistry* **2015,** *87* (11), 5531-5538.
129. Chen, S.-P.; Wu, J.; Yu, X.-D.; Xu, J.-J.; Chen, H.-Y., Preparation of metal nanoband microelectrode on poly(dimethylsiloxane) for chip-based amperometric detection. *Analytica chimica acta* **2010,** *665* (2), 152-159.
130. Jiang, J.; Wang, X., Fabrication of high-surface nanoporous gold microelectrode. *Electrochemistry Communications* **2012,** *20*, 157-159.
131. Chu, J.; Zhao, Y.; Li, S.-H.; Yu, H.-Q.; Liu, G.; Tian, Y.-C., An Integrated Solid-State pH Microelectrode Prepared Using Microfabrication. *Electrochimica Acta* **2015,** *152*, 6-12.
132. (a) Souza, A. P. R. d.; Lima, A. S.; Salles, M. O.; Nascimento, A. N.; Bertotti, M., The use of a gold disc microelectrode for the determination of copper in human sweat. *Talanta* **2010,** *83* (1), 167-170; (b) Mori, V.; Bertotti, M., Nitric oxide solutions: standardisation by chronoamperometry using a platinum disc microelectrode. *The Analyst* **2000,** *125* (9), 1629-1632.
133. Harvey, S. L. R.; Coxon, P.; Bates, D.; Parker, K. H.; O'Hare, D., Metallic ring-disc microelectrode fabrication using inverted hollow cylindrical sputter coater. *Sensors and Actuators B: Chemical* **2008,** *129* (2), 659-665.
134. Danis, L.; Snowden, M. E.; Tefashe, U. M.; Heinemann, C. N.; Mauzeroll, J., Development of Nano-Disc electrodes for Application as Shear Force Sensitive Electrochemical Probes. *Electrochimica Acta* **2014,** *136*, 121-129.

135. Laczka, O.; del Campo, F. J.; Muñoz-Pascual, F. X.; Baldrich, E., Electrochemical Detection of Testosterone by Use of Three-Dimensional Disc–Ring Microelectrode Sensing Platforms: Application to Doping Monitoring. *Analytical chemistry* **2011,** *83* (11), 4037-4044.

136. Xiao, L.; Streeter, I.; Wildgoose, G. G.; Compton, R. G., Fabricating random arrays of boron doped diamond nano-disc electrodes: Towards achieving maximum Faradaic current with minimum capacitive charging. *Sensors and Actuators B: Chemical* **2008,** *133* (1), 118-127.

137. Kim, L. T. T.; Girard, A.; Griscom, L.; Razan, F.; Griveau, S.; Bedioui, F., Micro-ring disc ultramicroelectrodes array for direct detection of NO-release from S-nitrosoglutathione. *Electrochemistry Communications* **2011,** *13* (7), 681-684.

138. Galceran, J.; Taylor, S. L.; Bartlett, P. N., Modelling the steady-state current at the inlaid disc microelectrode for homogeneous mediated enzyme catalysed reactions. *Journal of Electroanalytical Chemistry* **2001,** *506* (2), 65-81.

139. Ellison, J.; Eloul, S.; Batchelor-McAuley, C.; Tschulik, K.; Salter, C.; Compton, R. G., The effect of insulator nano-sheath thickness on the steady state current at a micro-disc electrode. *Journal of Electroanalytical Chemistry* **2015,** *745*, 66-71.

140. Daniele, S.; Ciani, I.; Battistel, D., Effect of the Insulating Shield Thickness on the Steady-State Diffusion-Limiting Current of Sphere Cap Microelectrodes. *Analytical Chemistry* **2008,** *80* (1), 253-259.

141. Dickinson, E. J. F.; Streeter, I.; Compton, R. G., Chronoamperometry and Cyclic Voltammetry at Conical Electrodes, Microelectrodes, and Electrode Arrays: Theory. *The Journal of Physical Chemistry B* **2008,** *112* (13), 4059-4066.

142. Hermans, A.; Wightman, R. M., Conical Tungsten Tips as Substrates for the Preparation of Ultramicroelectrodes†. *Langmuir* **2006,** *22* (25), 10348-10353.

143. Morton, K. C.; Morris, C. A.; Derylo, M. A.; Thakar, R.; Baker, L. A., Carbon Electrode Fabrication from Pyrolyzed Parylene C. *Analytical Chemistry* **2011,** *83* (13), 5447-5452.

144. Ha, J. G.; Park, J. H.; Bai, S. J.; Kim, Y. K.; Lee, S. K. In *Fabrication and measurements of high aspect ratio conductive microtip array with localized ultra-micro electrode at the tip end*, Micro Electro Mechanical Systems (MEMS), 2012 IEEE 25th International Conference on, Jan. 29 2012-Feb. 2 2012; 2012; pp 235-238.

145. Cao, X.-H.; Zhang, L.-X.; Cai, W.-P.; Li, Y.-Q., Amperometric sensing of dopamine using a single-walled carbon nanotube covalently attached to a conical glass micropore electrode. *Electrochemistry Communications* **2010,** *12* (4), 540-543.

146. Rees, H. R.; Anderson, S. E.; Privman, E.; Bau, H. H.; Venton, B. J., Carbon nanopipette electrodes for dopamine detection in Drosophila. *Analytical chemistry* **2015,** *87* (7), 3849-3855.

147. Bucher, E. S.; Wightman, R. M., Electrochemical Analysis of Neurotransmitters. *Annual Review of Analytical Chemistry* **2015,** *8*, 239 .

148. Huang, W.-H.; Pang, D.-W.; Tong, H.; Wang, Z.-L.; Cheng, J.-K., A method for the fabrication of low-noise carbon fiber nanoelectrodes. *Analytical chemistry* **2001,** *73* (5), 1048-1052.

149. McNally, M.; Wong, D. K., An in vivo probe based on mechanically strong but structurally small carbon electrodes with an appreciable surface area. *Analytical chemistry* **2001,** *73* (20), 4793-4800.

150. Chen, S.; Kucernak, A., Fabrication of carbon microelectrodes with an effective radius of 1 nm. *Electrochemistry communications* **2002,** *4* (1), 80-85.

151. Wong, D. K. Y.; Charles, D. B.; McNally, M., Amperometric detection of dopamine release. *Chemistry in Australia, Royal Australian Chemical Institute, Australia* **2003,** (12), 12-15.

152. Gao, F.; Guo, X.; Yin, J.; Zhao, D.; Li, M.; Wang, L., Electrocatalytic activity of carbon spheres towards NADH oxidation at low overpotential and its applications in biosensors and biofuel cells. *Rsc Advances* **2011,** *1* (7), 1301-1309.

153. Casella, I. G.; Contursi, M., Electrocatalytic Oxidation of Some Hydrazine Compounds at Glassy Carbon Electrode Modified with Co-Gluconate Complex. *Electroanalysis* **2012,** *24* (4), 752-758.

154. Gasnier, A.; Pedano, M. L.; Gutierrez, F.; Labbé, P.; Rivas, G. A.; Rubianes, M. D., Glassy carbon electrodes modified with a dispersion of multi-wall carbon nanotubes in dopamine-functionalized polyethylenimine: Characterization and analytical applications for nicotinamide adenine dinucleotide quantification. *Electrochimica Acta* **2012,** *71*, 73-81.

155. Narmadha, M.; Noel, M.; Suryanarayanan, V., Relative deactivation of boron-doped diamond (BDD) and glassy carbon (GC) electrodes in different electrolyte media containing substituted phenols–Voltammetric and surface morphologic studies. *Journal of electroanalytical chemistry* **2011,** *655* (2), 103-110.

156. Mudrinić, T.; Mojović, Z.; Milutinović-Nikolić, A.; Banković, P.; Dojčinović, B.; Vukelić, N.; Jovanović, D., Beneficial effect of Ni in pillared bentonite based electrodes on the electrochemical oxidation of phenol. *Electrochimica Acta* **2014,** *144*, 92-99.

157. Muna, G. W.; Partridge, M.; Sirhan, H.; VerVaet, B.; Guerra, N.; Garner, H., Electrochemical Detection of Steroid Hormones Using a Nickel-Modified Glassy Carbon Electrode. *Electroanalysis* **2014,** *26* (10), 2145-2151.

158. Stoytcheva, M.; Zlatev, R.; Gochev, V.; Velkova, Z.; Montero, G.; Beleño, M., Amperometric biosensors precision improvement. Application to phenolic pollutants determination. *Electrochimica Acta* **2014,** *147*, 25-30.

159. Wilson, C. J.; Clegg, R. E.; Leavesley, D. I.; Pearcy, M. J., Mediation of biomaterial-cell interactions by adsorbed proteins: a review. *Tissue engineering* **2005,** *11* (1-2), 1-18.

160. Goto, T.; Yasukawa, T.; Kanda, K.; Matsui, S.; Mizutani, F., Inhibition of electrochemical fouling against biomolecules on a diamond-like carbon electrode. *Analytical Sciences* **2011,** *27* (1), 91-94.

161. Zhuiykov, S.; Kalantar-zadeh, K., Development of antifouling of electrochemical solid-state dissolved oxygen sensors based on nanostructured

Cu 0.4 Ru 3.4 O 7+ RuO 2 sensing electrodes. *Electrochimica Acta* **2012,** *73*, 105-111.

162. (a) McCreery, R. L., Advanced carbon electrode materials for molecular electrochemistry. *Chemical Reviews* **2008,** *108* (7), 2646-2687; (b) Roeser, J.; Alting, N. F.; Permentier, H. P.; Bruins, A. P.; Bischoff, R., Boron-Doped Diamond Electrodes for the Electrochemical Oxidation and Cleavage of Peptides. *Analytical Chemistry* **2013,** *85* (14), 6626-6632; (c) Shin, D.; Tryk, D. A.; Fujishima, A.; Merkoçi, A.; Wang, J., Resistance to surfactant and protein fouling effects at conducting diamond electrodes. *Electroanalysis* **2005,** *17* (4), 305-311.

163. Malmsten, M., *Biopolymers at Interfaces, Second Edition*. Taylor & Francis: 2003; Vol. 110.

164. Grinnell, F.; Feld, M. K., Adsorption characteristics of plasma fibronectin in relationship to biological activity. *Journal of Biomedical Materials Research* **1981,** *15* (3), 363-381.

165. (a) Hess, H.; Vogel, V., Molecular shuttles based on motor proteins: active transport in synthetic environments. *Reviews in Molecular Biotechnology* **2001,** *82* (1), 67-85; (b) Thevenot, P.; Hu, W.; Tang, L., Surface chemistry influence implant biocompatibility. *Current topics in medicinal chemistry* **2008,** *8* (4), 270.

166. Anandhakumar, S.; Chandrasekaran, M.; Noel, M., Anodic oxidation of chlorophenols in micelles and microemulsions on glassy carbon electrode: the medium effect on electroanalysis and electrochemical detoxification. *Journal of applied electrochemistry* **2010,** *40* (2), 303-310.

167. Pirvu, C.; Manole, C. C., Electrochemical surface plasmon resonance for in situ investigation of antifouling effect of ultra thin hybrid polypyrrole/PSS films. *Electrochimica Acta* **2013,** *89*, 63-71.

168. Yang, X.; Kirsch, J.; Olsen, E. V.; Fergus, J. W.; Simonian, A. L., Anti-fouling PEDOT: PSS modification on glassy carbon electrodes for continuous monitoring of tricresyl phosphate. *Sensors and Actuators B: Chemical* **2013,** *177*, 659-667.

169. Quynh, B. T. P.; Byun, J. Y.; Kim, S. H., Nanoporous gold for amperometric detection of amino-containing compounds. *Sensors and Actuators B: Chemical* **2014,** *193*, 1-9.

170. Paul, D. W.; Prajapati, I.; Reed, M. L., Electropolymerized eugenol: Evaluation as a protective film for oxygen sensing. *Sensors and Actuators B: Chemical* **2013,** *183*, 129-135.

Chapter 2

Experimental

2.1 Introduction

The main aim of this work is to develop fouling resistant physically small electrode for effective determination of the neurotransmitter dopamine. Initially, a physically small conical tip carbon electrode was fabricated by depositing carbon on and in the fine tip of already pulled quartz capillary by pyrolysing C_2H_2 gas in the presence of a counter flowing stream of N_2. Then, the electrode was modified by introducing a hydrogenated layer on the bare electrode surface to achieve a more effective antifouling surface for the detection of dopamine in the presence of a laboratory synthetic fouling solution. In general, all bare and modified electrodes were characterised using different electroanalytical, spectroscopic and microscopic techniques to evaluate the degree of modification of the electrode surface. Successfully modified electrodes were employed for the detection of dopamine in a fouling solution that mimics complex biological environment. The present chapter is devoted to the detailed descriptions of the essential materials, reagents, instrumentation and adopted experimental procedure such that the electrodes can be modified systematically and the most reliable results can be obtained. More specific experimental techniques and reagents are described in the respective chapters devoted to specific aspects of work in this thesis.

2.2 Chemicals and Reagents

A list of chemicals and reagents used in this project is tabulated as below together with their sources.

Acetonitrile (HPLC grade)	Sigma Aldrich
Acetylene	BOC Australia
Anthraquinone 2,6-disulfonate	Sigma Aldrich
Bovine serum albumin	Sigma Aldrich
n-Butylsilane	Sigma Aldrich

Calcium chloride	Sigma Aldrich
Citric acid	Sigma Aldrich
Cytochrome c	Sigma Aldrich
Dichloromethane (anhydrous, ≥99.8%	Sigma Aldrich
Diethylsilane	Sigma Aldrich
Diethyl ether	Sigma Aldrich
Dopamine	Sigma Aldrich
Ethanol	Sigma Aldrich
Graphite powder	Sigma Aldrich
Hexanoic acid (Caproic acid)	Sigma Aldrich
Hexammine ruthenium (III) chloride	Sigma Aldrich
Human fibrinopeptide B	Sigma Aldrich
Methanol	Sigma Aldrich
Perchloric acid	Sigma Aldrich
Potassium chloride	Sigma Aldrich
Potassium ferricyanide	BDH
Sodium phosphate dibasic heptahydrate	Sigma Aldrich
Sodium tetrafluoroborate	Sigma Aldrich
Sodium nitrite	Sigma Aldrich
Sulfanilic acid	Sigma Aldrich
Tetrabutylammonium tetrafluoroborate	Sigma Aldrich
Tetrafluoroboric acid (48% w/v)	Sigma Aldrich
Tris(pentafluorophenyl)borane	Sigma Aldrich

2.3 Instrumentation and apparatus

Physically small conical-tip carbon electrodes were fabricated by initially pulling quartz capillaries (1 mm outside diameter × 0.5 mm inside diameter × 75 mm length; Sutter Instrument Company, Novato, CA, USA) using a laser based Model P-2000 Sutter micropipette puller (Sutter Instrument Co.). Similarly, carbon fibre microelectrodes

were fabricated by aspirating a single fibre of XAS grade (7 µm diameter, purchased from Goodfellow Cambridge Limited, UK) through a thin walled without-filament glass capillary (1.0 mm outside diameter × 0.78 mm inside diameter × 10.0 cm length) that was pulled by the same Sutter puller. Voltammetric measurements were carried out using a low current potentiostat (eDAQ Pty Ltd., Sydney, NSW, Australia) capable of measuring picoamperes of current. This potentiostat was operated using EChem version 2.1.2 software on a PC *via* an E-corder interface (eDAQ Pty Ltd.). The electrochemical cell was a conventional three electrode arrangement with a conical-tip carbon electrode or a carbon fibre microelectrode as the working electrode, a Ag|AgCl reference electrode (3 M KCl) and a platinum wire counter electrode. All measurements were carried out in an aluminium Faraday cage to avoid any possible noise and interruption from the main.

2.4 General methods and procedures

2.4.1 Fabrication of conical tip carbon electrode

Physically small conical tip carbon electrodes are routinely fabricated in our laboratory.[1,2] Initially, a quartz capillary was pulled down to a fine tapered end by a micropipette puller. This study requires electrodes with a conical tapered quartz tip that offers mechanical strength to facilitate easy penetration through a cell membrane in an *in vivo* experiment. Upon pulling, the capillary was left in the puller for 1 min to cool before it was visually examined under an optical microscope (Meiji, Industrial & Scientific Supply Company Pty Ltd, Australia, Model–VT-T-2) to ensure the diameter and tapered length are as desired.

The procedure adopted to fabricate a conical-tip carbon electrode is schematically shown in Figure 2.1. Initially, the pulled capillary was housed carefully in a nuclear magnetic resonance (NMR) sample tube (internal diameter 5 mm) through a $\frac{1}{16}\,\text{in} \times \frac{1}{16}\,\text{in} \times \frac{1}{16}\,\text{in}$ stainless steel union tee with the bolts intact (SGE Analytical Science). An acetylene flow of 65 kPa was delivered through the larger end of the pulled capillary using a rubber tubing, while a counter flow of ultrapure nitrogen gas

was supplied through the NMR tube at a flow rate of 20 mL min^{-1}. This setup was flushed by nitrogen gas for 5 min to generate an inert atmosphere in the NMR tube before acetylene was thermally pyrolysed using a Bunsen flame. In this way, the acetylene gas was blown backward as the acetylene effused from the pulled tip of the capillary and was reduced to carbon that eventually was deposited at the tip and on the shank of the capillary. (Caution: The union tee, NMR tube, and the rubber tubing must be set up such that there was no leakage of acetylene gas to the Bunsen flame during pyrolysis.) During pyrolysis, heating was initiated at the far end of the NMR tube away from the tip to avoid thermal shock that could lead to tip fracture. The flame was then slowly moved towards the shank followed by the tip of the capillary, where heating persisted for 3 min. Following pyrolysis, the capillary with carbon deposit was left in the NMR tube for another 30 s for cooling before it was carefully removed and rinsed with milli-Q water to remove any particulate matter prior to further use.

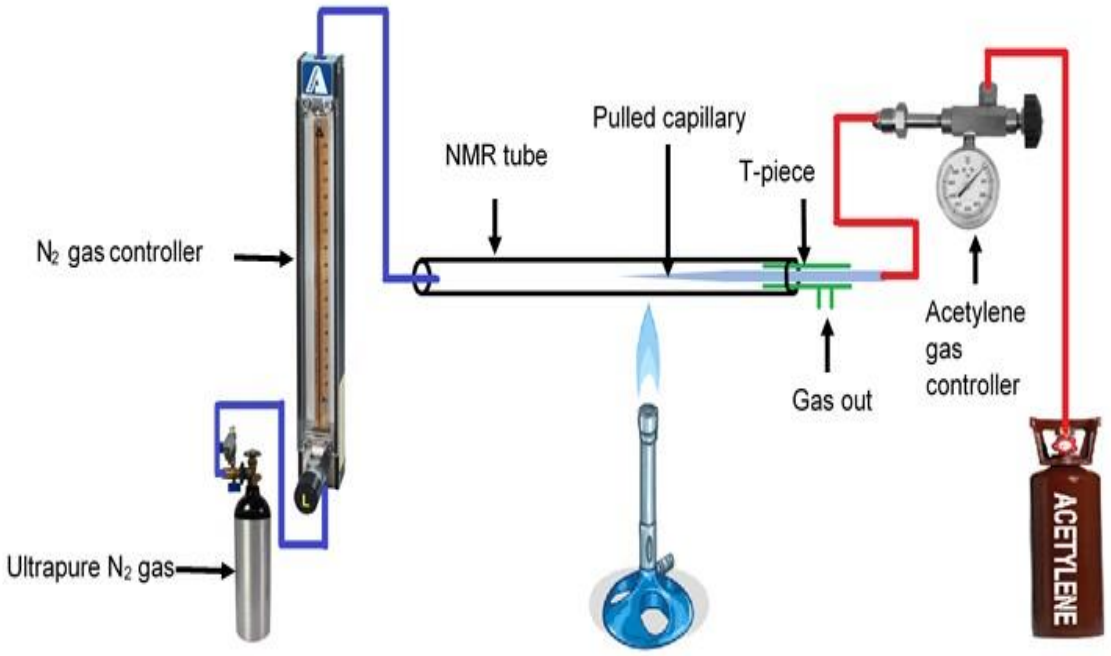

Figure 2.1 Fabrication of physically small conical-tip carbon electrode

2.4.2 Hydrogenation of conical-tip carbon electrode

All conical-tip carbon electrodes were hydrogenated using an *n*-butylsilane reduction method. A schematic diagram illustrating the procedure is shown in Figure 2.2. In this experiment, 5.0 mg of $B(C_6F_5)_3$ was dissolved in 5.0 mL anhydrous CH_2Cl_2 ($\geq$ 99.8%) by stirring for 10 min before 20 μL (0.156 mmol) of *n*-butylsilane (99% pure) was added. A conical-tip carbon electrode was placed in the reaction solution that was continuously purged by N_2, before the setup was sealed with parafilm. Hydrogenation at the electrode was continued for 2 h at room temperature. The hydrogenated electrodes were dried for at least 30 min before they were used for further analysis.

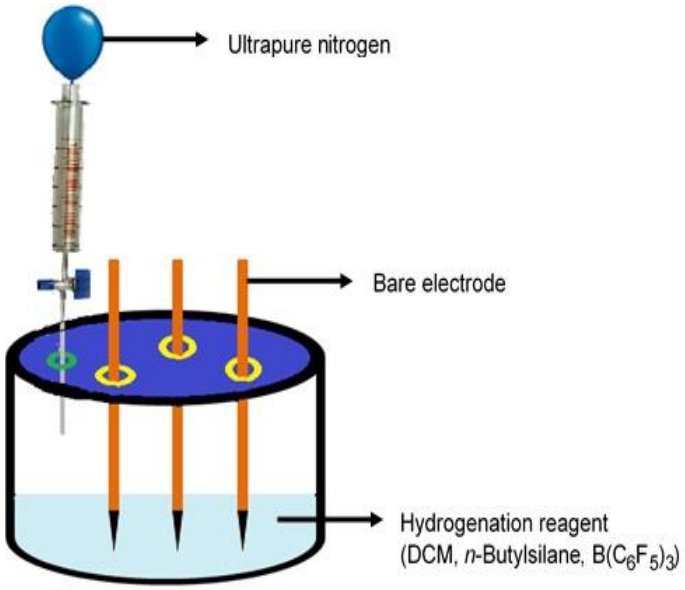

Figure 2.2 Hydrogenation of conical-tip carbon electrodes by *n*-butylsilane

2.4.3 Electrochemical experiments

Cyclic voltammetry was employed to assess all fabricated electrodes. In these experiments, several redox markers including $[Ru(NH_3)_6]^{3+}$, $[Fe(CN)_6]^{3-}$, anthraquinone-disulfonate and dopamine were used. Initially, the solution containing a redox marker was continuously purged by N_2 for 10 min. Then, a N_2 blanket was maintained over the solution during the experiment. In all experiments, a potential scan

rate of 100 mV s^{-1} was used. Conditions used in cyclic voltammetry of all redox markers are summarised in Table 2.1.

Redox Couple	Supporting Electrolyte	Potential Scan Range
1.0 mM $[Ru(NH_3)_6]^{3+}$	1.0 M KCl	+0.20 V to –0.40 V
1.0 mM $[Fe(CN)_6]^{3-}$	1.0 M KCl	+0.20 V to –0.60 V
1.0 mM AQDS	0.1 M $HClO_4$	+0.20 V to +1.00 V
1.0 mM Dopamine	citrate/phosphate buffer (pH 7.4)	+0.20 V to +0.60 V

Table 2.1 Redox markers used for electrochemical characterisation of bare and hydrogenated conical-tip carbon electrodes

2.4.4 Fouling Resistance Experiments

A laboratory synthetic fouling solution containing 1% (w/v) bovine serum album, 0.01% (w/v) cytochrome C (both are proteins), 1.0% (v/v) caproic acid (a lipid), and 0.002% (w/v) human fibrinopeptide B (a peptide) was prepared to mimic a complex biological environment *in vivo*.[3,4] The solution was homogenised by stirring before the electrodes were incubated in this solution. All fouling experiments were conducted in dopamine in citrate/phosphate buffer deliberately mixed with the laboratory synthetic fouling solution at laboratory room temperature. Notably, phosphate based buffer was chosen in these experiments to obtain higher electrode sensitivity to dopamine in citrate/phosphate buffer compared to that in bicarbonate-based buffer. Previously, it was also investigated by Kume-Kick and Rice (1998) in their work where they observed 2-3 fold higher sensitivity of carbon fibre microelectrode to dopamine in phosphate or HEPES buffer compared to that in a bicarbonate buffer.[5]

2.4.5 Data Analysis

In this study, the statistical significance of all correlation coefficients at the 95% confidence level was tested using Student's *t*-test and the linearity of all straight line plots assessed using the Wald-Wolfowitz runs test.[6] The uncertainties associated with the slope and ordinate intercept of a linear plot were expressed as confidence intervals at the 95% level.

2.5 References

1. McNally, M.; Wong, D. K., An in vivo probe based on mechanically strong but structurally small carbon electrodes with an appreciable surface area. *Analytical chemistry* **2001,** *73* (20), 4793-4800.
2. Chandra, S.; Miller, A. D.; Wong, D. K. Y., Evaluation of physically small p-phenylacetate-modified carbon electrodes against fouling during dopamine detection in vivo. *Electrochimica Acta* **2013,** *101*, 225-231.
3. Shin, D.; Tryk, D. A.; Fujishima, A.; Merkoçi, A.; Wang, J., Resistance to surfactant and protein fouling effects at conducting diamond electrodes. *Electroanalysis* **2005,** *17* (4), 305-311.
4. Aluise, C. D.; Sowell, R. A.; Butterfield, D. A., Peptides and proteins in plasma and cerebrospinal fluid as biomarkers for the prediction, diagnosis, and monitoring of therapeutic efficacy of Alzheimer's disease. *Biochimica et Biophysica Acta (BBA)-Molecular Basis of Disease* **2008,** *1782* (10), 549-558.
5. Kume-Kick, J.; Rice, M. E., Dependence of dopamine calibration factors on media Ca2+ and Mg2+ at carbon-fiber microelectrodes used with fast-scan cyclic voltammetry. *Journal of Neuroscience Methods* **1998,** *84* (1–2), 55-62.
6. Miller, J. N.; Miller, J. C., *Statistics and Chemometrics for Analytical Chemistry*. Sixth ed.; Pearson Education: 2010; p 45, 162.

Chapter 3

Activation of conical-tip carbon electrodes by *n*-butylsilane reduction

3.1 General Introduction on Microelectrodes

Microelectrodes are electrodes with ≤100 μm in at least one dimension.[1] They are of general interest owing to their capability in spatially resolved measurements in a small volume of a highly resistant analyte, and in investigating the chemistry of an analyte at a submicrosecond time scale.[2,3] For example, microelectrodes are particularly useful for applications in biological micro-environments. Recently, diamond microelectrodes were used to measure norepinephrine release from the mesenteric artery of a rat[4] and serotonin uptake at lymphocytes extracted in monkey's blood.[5] These diamond microelectrodes exhibit high temporal and spatial resolutions with improved sensitivity, reproducibility and response stability required to monitor small changes of analyte concentration during the analytical detection of neurotransmitters. Similarly, a microelectrode allows the selection of the recording site in single cells with minimal damage during implantation through the cell membrane. All these features have continued to stimulate and demand advancements in microelectrode fabrication technology.

3.2 Applications of microelectrodes to bioanalytical chemistry

Developments in the area of microelectrodes have partly emerged due to basic needs for fundamental studies in small biological cells. In this respect, microelectrodes are used in electrophysiology for recording biochemical events occurring or the concentration of biomolecules released from cells. For example, a carbon fibre microelectrode was employed to investigate serotonin exocytosis in mast cells of 10–20 μm diameters in varying cell culture conditions.[6,7] For secretion, the cells were initially stimulated by a secretagogue solution through a micropipette placed 20–100 μm away from cells. Then, the exocytosis events were monitored by applying +700 mV (versus a Ag|AgCl

reference electrode) to an electrode placed in contact with the mast cell membrane. Similarly, a carbon fibre microelectrode with a 7-µm diameter and 300 µm in length was implanted in the striatum of a rat to measure striatal dopamine release in a schizophrenia mouse model.[8] In this work, dopamine release, reuptake and vesicle pool recycling in striatal dopmaminergic terminals of the mouse model was systematically analysed. The authors observed that the striatal dopamine signal was not altered in a schizophrenia model. In other work, single adrenal chromaffin vesicles of 60 nm diameter were adsorbed and spread over a disc-shaped carbon microelectrode of 33 µm diameter such that the vesicular contents were trapped against the electrode surface.[9] Subsequently, the contents were quantitatively detected at the electrode. The same group developed a conical tip carbon-fibre microelectrode of 50-100 nm diameter.[10] They demonstrated the detection of total electroactive neurotransmitters including dopamine in individual nano-scale vesicles of single PC12 cells without any significant damage. Samba *et al*.[11] employed PEDOT-CNT modified microelectrodes of 25 µm diameter for sensing dopamine in B27, a typical culture media for primary neurons. The initial signal of dopamine was attenuated as proteins including bovine serum albumin, insulin and other smaller molecules (*e.g*. biotin) present in B27 clogged the pores of PEDOT-CNTs. A permselective poly(phenylene diamine)-L-glutamate oxidase modified platinum microelectrode was implanted in Xenopus embryos for real time measurement of adenosine triphosphate without interferences during L-glutamate detection in rat brain.[12,13] In a separate work, a cytochrome c entrapped terthiophene-3′-carboxylic acid (a conducting polymer) modified platinum microelectrode of 100 µm diameter was positioned at 1 mm anterior to bregma, 2.5 mm right to midline, and 4 mm below the skull surface of adult male Sprague-Dawley rat to investigate NO secretion after administering cocaine.[14] The modified electrode showed high sensitivity towards NO and the electrode was capable to determine as low as micormolar level of NO *in vivo* in an intact brain. Further applications of microelectrodes to bioanalytical chemistry have already been discussed in Chapter 1.

3.3 Problems encountered during microelectrode fabrication

In many microelectrode fabrication techniques, inadequate insulation or the need for sealing the junction between the electroactive surface area and the insulating substrate contributes to substantial charging current in a cyclic voltammogram. For example, in Zhang *et al.*'s work[15], a small charging current in the cyclic voltammogram of 5 mM $[Fe(CN)_6]^{3-}$ at a scan rate of 10 mV s^{-1} was used to indicate good insulation and sealing of carbon fibre and glass capillary during fabrication of carbon fibre microelectrodes. Similarly, fabrication of nanometer-sized carbon fibre cone electrodes by flame etching at high temperature often produced a rough carbon surface that limits the utility of the electrode.[16] To overcome this problem, an ion beam etching method was developed to obtain a smooth carbon surface on a fabricated electrode. A relatively small background current was then achieved during characterisation of these electrodes by the cyclic voltammetry of 1 mM $[Fe(CN)_6]^{3-}$ over a scan rate range of 10-500 mV s^{-1}. The use of a thin layer of silicon dioxide also effectively reduced capacitive current during fabrication of a carbon nanotube modified microelectrode array employed for neural stimulation.[17] Swain and co-workers[18] reported that capacitance at a hydrogenated glassy carbon electrode decreased by 50% following hydrogenation using a hydrogen microwave plasma method. Hydrogen terminated diamond ultramicroelectrode arrays showed a lower background current compared to those that were electrochemically oxidised.[19] A nitrogen-doped cap layer was grown on a single crystal boron-doped diamond electrode using nitrogen gas in a chemical vapour deposition method to obtain less charging current.[20] Metals were electroplated on tungsten substrate to fabricate gold and platinum ultramicroelectrodes. A complete and smooth surface coverage was attained by optimising deposition variables such as temperature, plating time and plating potential.[21] However, the oxides present on electrode surface were found to produce a large background current that interfered with the Faradaic current from species in solution.[21]

Upon fabrication of microelectrodes, cyclic voltammetry of well-behaved redox systems is commonly performed at the electrodes to assess their integrity. For example, the outer-sphere complex ion $[Ru(NH_3)_6]^{3+}$ is often used to characterise carbon

surfaces because of its independence on the type of carbon surface.[22] Similar to microelectrodes with other geometries, a typical response of $[Ru(NH_3)_6]^{3+}$ in KCl supporting electrolyte showing (1) a sigmoidal shaped cyclic voltammogram (CV) and, (2) a small capacitive charging current between the forward and backward scans, is used to indicate a functioning conical-tip carbon microelectrode. Owing to the small electrode surface area, in addition to linear diffusion, edge diffusion of $[Ru(NH_3)_6]^{3+}$ becomes more prominent in the vicinity of the electrode, which maintains a constant supply of $[Ru(NH_3)_6]^{3+}$ to the electrode for reduction. This constant supply of $[Ru(NH_3)_6]^{3+}$ results in a steady-state diffusion current, giving rise to a sigmoidal shaped CV. Moreover, a good seal between the carbon film and the quartz substrate with minimal cracks and crevices on the carbon surface yields a small capacitive charging current between the forward and backward cyclic voltammetric scan. In many cases, pinholes, cracks or crevices arising from carbon surface imperfections and/or poor epoxy sealing, for example, between a fibre and the glass substrate in carbon fibre microelectrodes, will yield non-sigmoidal CVs with appreciable charging current between the forward and backward scans. When non-sigmoidal CVs were obtained at Pt and Au microdisc electrodes, they were often mechanically polished to minimise the imperfections, which could sometimes aid in subsequently achieving a sigmoidal-shape CV.[23] Laczka *et al.*[24] developed a three dimensional disc-ring microelectrode array of a trilayer metals consisting of Ti, Ni, and Au deposited on silicon wafer. The electrode array was activated electrochemically by applying a series of potential pulses from 0 to - 2 V versus Ag|AgCl (3 M KCl) in 0.1 M KNO_3 supporting electrolyte. After activation, if less than 80% of electrodes in the array were not active, they were simply discarded. Alternatively, a pre-treatment involving scanning the potential from −0.2 V to 1.8 V and back to −0.2 V (against a sodium saturated calomel reference electrode) at 200 mV s^{-1} was previously used to activate physically small, fragile carbon electrodes.[25] However, this pre-treatment was not known to yield a long-lasting improved characteristic. In the event of unsuccessful activation of these microelectrodes, they were simply discarded.

3.4 Scope of the present study

Previously, Nimmagadda and McRae[26,27] reported a one-pot reaction involving *n*-butylsilane reduction capable of reducing carbon–oxygen functionalities to chemically modify an analyte for chromatographic separation. As shown in Scheme 3.1, in the *n*-butylsilane reduction method catalysed by $B(C_6F_5)_3$, carbon–oxygen functionalities present on carbon materials, e.g. aldehydes, ketones and primary, secondary and tertiary alcohols, polycarboxylic acid group were converted to their corresponding alkyl functionalities, leaving carbon–carbon double bonds and the graphitic structure undisturbed. Phenolic hydroxyl groups are, however not reduced but are instead silanised to form a dendrimeric butylsiloxane.[26] This work aims at investigating the feasibility of activating non-functional conical-tip carbon electrodes by hydrogenating the electrodes using the *n*-butylsilane reduction method. X-ray photoelectron spectroscopy will be used to characterise the surface of the hydrogenated carbon electrodes. We will also study the electrochemistry of $[Ru(NH_3)_6]^{3+}$ and anthraquinone-2,6-disulfonate (AQDS) at the hydrogenated carbon electrodes.

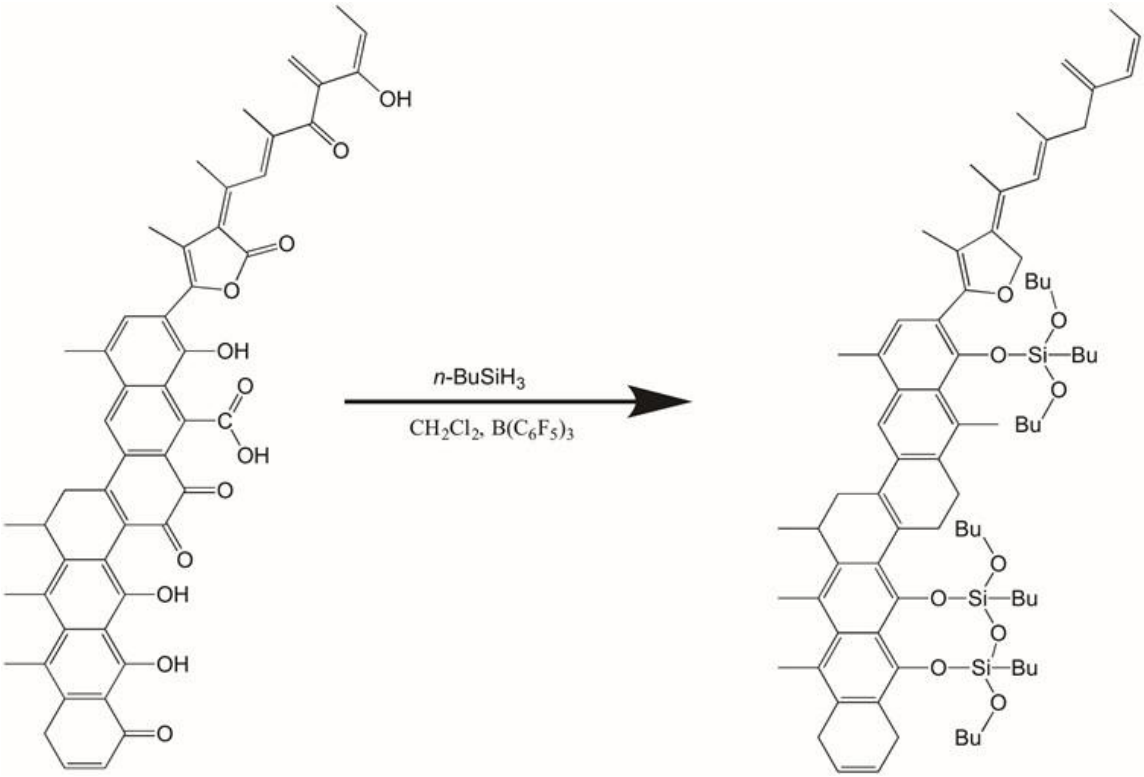

Scheme 3.1 Hydrogenation of carbon electrodes by *n*-butylsilane reduction method.

3.5 Experimental

3.5.1 Reagents and Materials

The list of chemicals and reagents used in this work is as tabulated in Section 2.2.

3.5.2 Fabrication of conical-tip carbon electrodes

Physically small conical-tip carbon electrodes were fabricated using the procedure described in Section 2.4.1.

3.5.3 Determination of electrode dimensions

According to work reported by our group[28], the chronoamperometric current (i) at a conical-tip electrode can be approximated by the expression

$$i = \frac{nFADC}{r}\left[0.5 + \frac{r}{\sqrt{Dt}}\right] \qquad \text{Equation 1}$$

where n denotes the number of electrons transferred, F the Faraday constant (96,485 C mol^{-1}), A is the electrochemical area (cm^2), D is the diffusion coefficient (5.3×10^{-6} cm^2s^{-1})[28], C the concentration of the redox species (mol cm^{-3}) and r is the radius of the disc at the electrode tip (cm). Accordingly, a linear plot of i versus $t^{-1/2}$ will yield a slope that estimates A, which will in turn allow the use of the ordinate intercept to estimate r. In this way, we will be able to determine the tip diameter and the axial length of the carbon deposit on the electrode shank. In such an experiment, a constant potential in the reduction limiting current region in the cyclic votalmmogram of 1.0 mM $[Ru(NH_3)_6]^{3+}$ was applied to a conical-tip carbon electrode in 1.0 M KCl for 10 s, and the corresponding current decay was then measured as a function of time. The corresponding current decay was chosen in a steady state region of the chronoamperomogram. The results were then processed as described to estimate the tip diameter and the axial length of the carbon electrode.

3.5.4 Scanning electron microscopy

Carbon deposited on the shank and at the tip of an electrode was visualised using scanning electron microscopy. This also permits the examination of electrode integrity, geometry, shape and size. In our study, bare electrodes were initially deposited with gold before being examined using a JEOL–JSM 6480–LA variable pressure scanning electron microscope at the Microscopy Unit, Department of Biological Sciences, Macquarie University.

3.5.5 Hydrogenation of conical-tip carbon electrodes

The fabricated conical-tip carbon electrodes were hydrogenated by an *n*-butylsilane reduction as described in Section 2.4.2.

3.5.6 Electrochemistry at bare and hydrogenated electrodes

Fabricated electrodes were next characterised by cyclic voltammetry of 1.0 mM $[Ru(NH_3)_6]^{3+}$in 1.0 M KCl supporting electrolyte between +0.2 V to -0.4 V, and 1.0 mM AQDS in 0.1 M $HClO_4$ supporting electrolyte between +1.0 V to -1.2 V, both at 100 mV s^{-1}, using a low-current potentiostat (eDAQ Pty Ltd., Sydney, Australia) operated by EChem version 2.1.2 software on a PC via an E-corder interface (eDAQ Pty Ltd.). A single compartment, three-electrode cell accommodating a Ag|AgCl reference electrode and a platinum wire counter electrode was used for electrochemical measurement. All measurements were performed at room temperature in a Faraday cage to minimise any noise interference.

3.5.7 X-ray photoelectron spectroscopy

XPS was conducted using an ESCALAB250Xi spectrometer (Thermo Scientific, Loughborough, UK) interfaced to a computer with data acquisition and processing software (Avantage; Thermo Scientific). Samples were irradiated with a monochromatic Al Kα X-ray source of 1486.68 eV energy. A vacuum system at 2 ×

10^{-9} mbar was operating at 73 W (13.8 kV × 5.25 mA) power. A sample of ~320 µm spot size was used. The photoelectron takeoff angle was 90° with pass energy of 100 eV for survey scans or 20 eV for region scans.

3.6 Results and Discussion

3.6.1 Characterising bare conical-tip electrodes in 1.0 mM $[Ru(NH_3)_6]^{3+}$

After assembling a conical-tip carbon electrode together, cyclic voltammetry of 1.0 mM $[Ru(NH_3)_6]^{3+}$ in 1.0 M KCl is always conducted. A typical sigmoidal-shaped voltammogram with a small charging current between the forward and the reverse scan, shown in Figure 3.1, is used to indicate a functioning electrode. As discussed earlier, the features shown in the voltammogram were attributed to a radial diffusion profile of $[Ru(NH_3)_6]^{3+}$ towards the conical-tip carbon electrode with minimal holes, cracks and crevices.

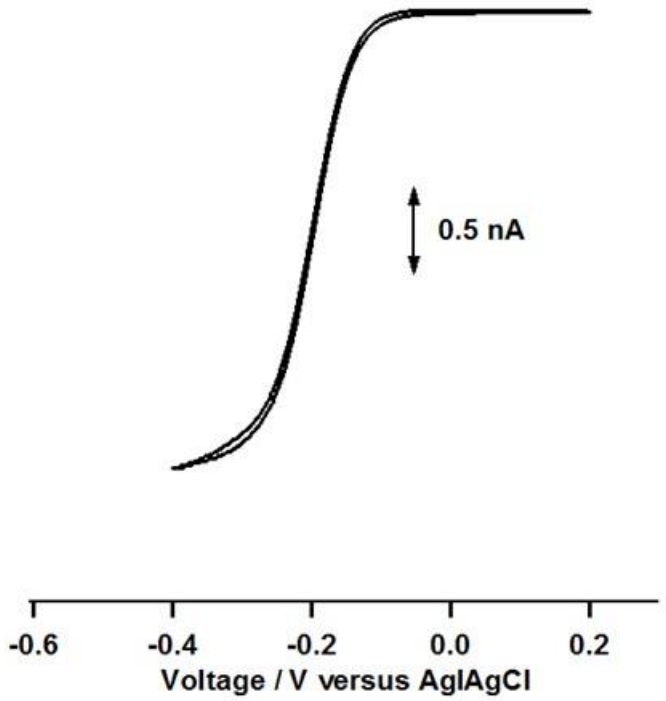

Figure 3.1 Cyclic voltammetry of 1.0 mM $[Ru(NH_3)_6]^{3+}$ at a functioning conical-tip carbon electrode in 1.0 M KCl. Scan rate: 100 mV s^{-1}.

3.6.2 Determination of electrode dimensions

Previous work[28] in our group has shown that Equation 1 can be used to estimate the tip diameter and the axial length of the carbon deposit on the shank of the conical-tip carbon electrode. Figure 3.2 shows an example of a chronoamperomogram of 1.0 mM $[Ru(NH_3)_6]^{3+}$ obtained at a conical-tip carbon electrode in a 1.0 M KCl supporting electrolyte.

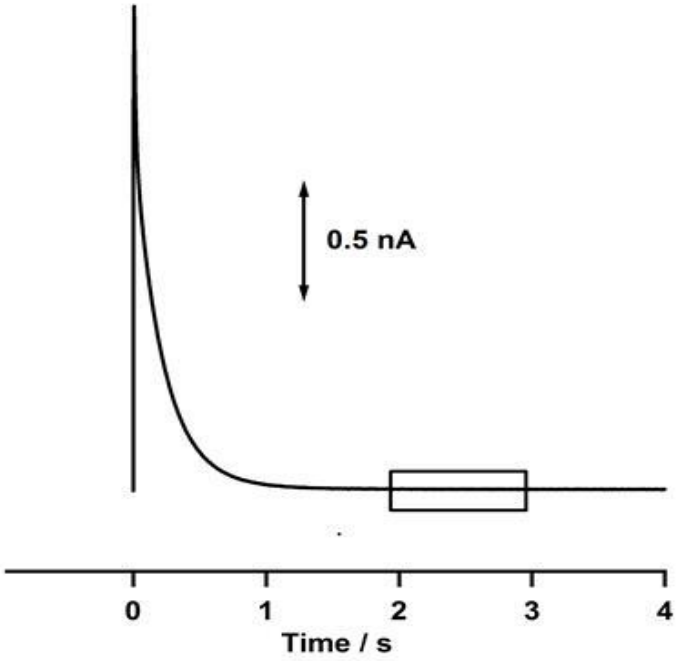

Figure 3.2 Chronoamperomogram of 1.0 mM $[Ru(NH_3)_6]^{3+}$ in 1.0 M KCl at a carbon electrode (-0.4 V pulse of 10 s duration).

As highlighted in Section 3.5.3, the steady state current between 2.0 and 3.0 s in the chronoamperomogram above was substituted into Equation 1 to estimate the tip diameter and the axial length of the carbon deposit. Typically, the mean tip diameter of these electrodes was estimated to be 2 µm (standard deviation (SD) 1 µm; N=7) and the mean axial length of deposited carbon was 15 µm (SD 10 µm; N=7). We have next attempted to estimate the geometric electrode dimensions from the scanning electron micrograph of the electrode in Figure 3.3. A uniform carbon deposit is clearly visible in this figure and a geometric tip diameter of ~1.2 µm was estimated. Unfortunately, the boundary of the upper end of the carbon deposit is not readily visible, making it

difficult to estimate the axial length of the carbon deposit. Nonetheless, both the electroactive tip diameter estimated using Equation 1 is in good agreement with the geometric tip diameter. We have also performed a similar chronoamperometric experiment using an electrode with a much larger dimension and the results are shown in Figure 3.4.

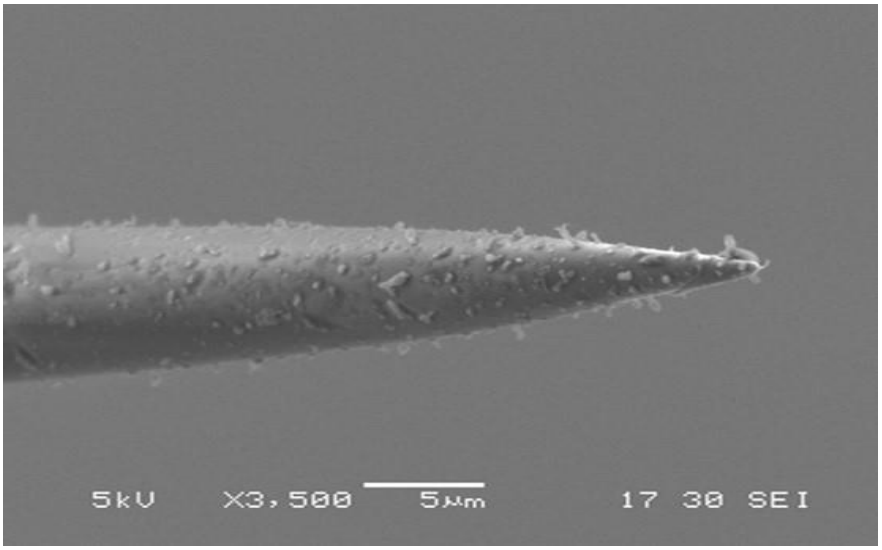

Figure 3.3 Scanning electron micrograph of a bare conical-tip carbon electrode

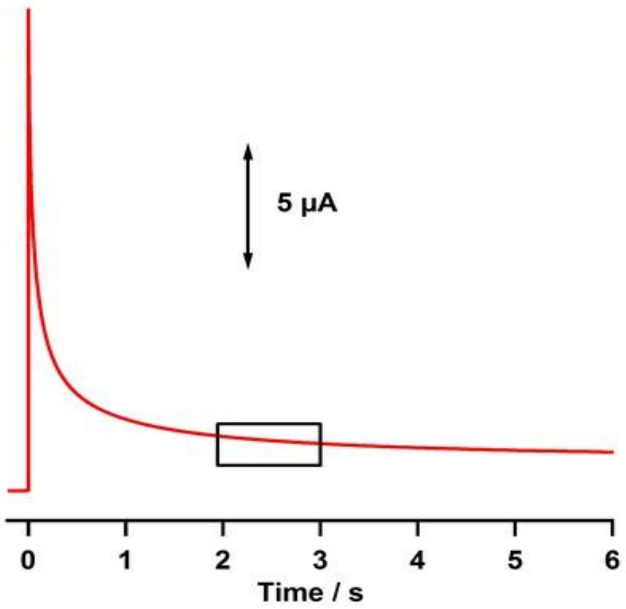

Figure 3.4 Chronoamperomogram of 1.0 mM $[Ru(NH_3)_6]^{3+}$ in 1.0 M KCl at a conical-tip carbon electrode with larger dimension (-0.4 V pulse of 10 s duration).

Similarly, the steady state current between 2.0 and 3.0 s was substituted into Equation 1 to estimate the tip diameter and the axial length of the carbon deposit. Here, the corresponding tip diameter was estimated to be 7 µm (SD 3 µm; N=5) and the axial length was 2290 µm (SD 102 µm; N=5). These results are again in good agreement with the geometric tip diameter of ~2700 µm and geometric axial length of ~5 µm estimated from the corresponding scanning electron micrograph in Figure 3.5(a) and (b).

(a)

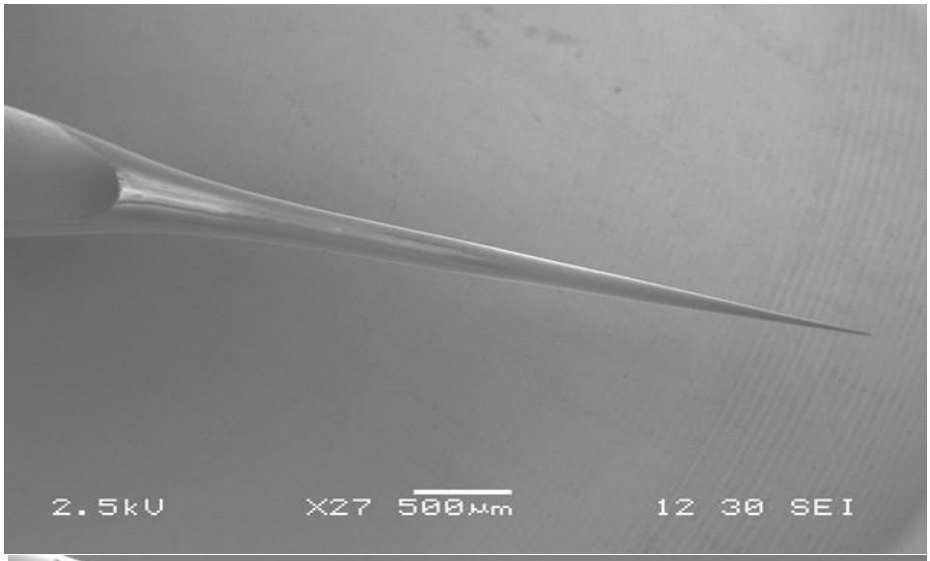

(b)

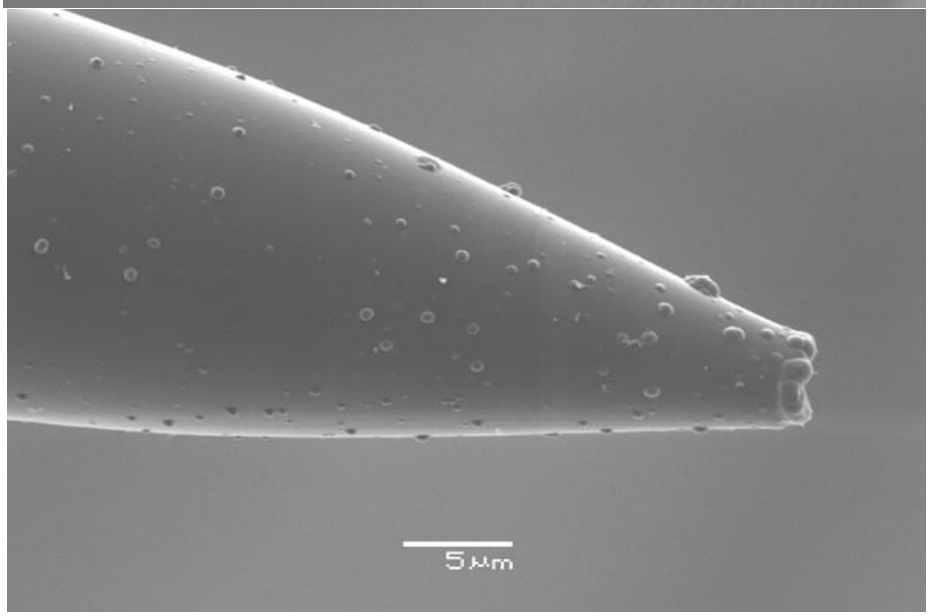

Figure 3.5 Scanning electron micrograph of a bare conical-tip carbon electrode to determine the (a) axial length and (b) diameter.

3.6.3 Characterising hydrogenated conical-tip electrodes in 1.0 mM $[Ru(NH_3)_6]^{3+}$

In contrast to the results shown in Figure 3.1, trace i in Figure 3.6 shows an example of a non-sigmoidal shaped CV with an appreciable charging current occasionally obtained at a conical-tip carbon electrode. At these electrodes, non-uniform deposition of electroactive carbon on the quartz surface during pyrolysis would have resulted in cracks and crevices on the electrode surface, allowing $[Ru(NH_3)_6]^{3+}$ to travel through by capillary action. Such "leaky" electrodes would exhibit a large charging current. On a carbon electrode, edge planes resulting from cracks and crevices on the electrode surface contain many oxygen functionalities, which would contribute to a large background current.[29] Similarly, oxygen functionalities present on hexagonal rings of sp^2 carbon atoms on an electrode surface[22] will also contribute to a significant charging current. This feature becomes undesirable when microelectrodes are used in detecting low concentration analytes with the small detection signal masked by a large background current. Similar to other microelectrodes, conical-tip carbon electrodes that produced such non-sigmoidal-shaped CVs were just discarded, contributing to their unsuccessful fabrication rate.

After hydrogenating the bare conical-tip carbon electrode that yielded trace i in Figure 3.6 by *n*-butylsilane reduction, the CV of 1.0 mM $[Ru(NH_3)_6]^{3+}$ at the electrode (trace ii) in 1.0 M KCl appears sigmoidal in shape with negligible charging current, indicating a characteristic functioning microelectrode.

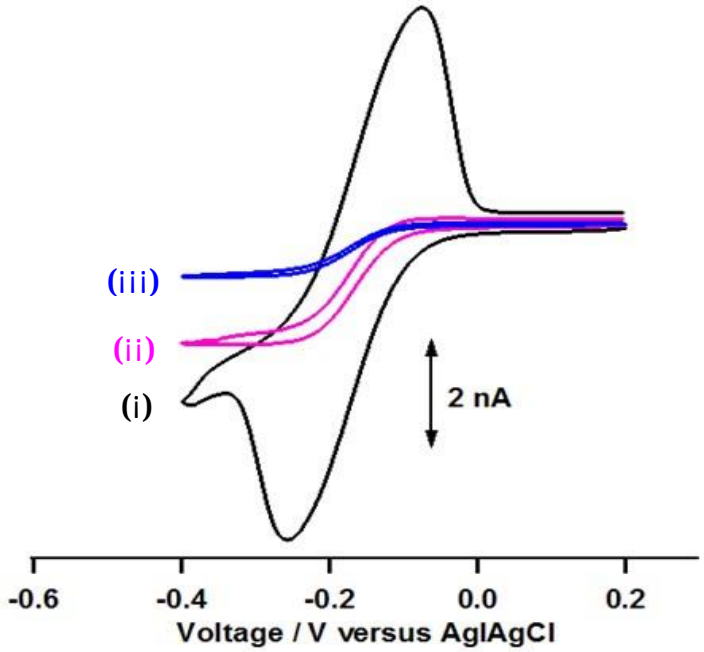

Figure 3.6. Cyclic voltammetry of 1.0 mM $[Ru(NH_3)_6]^{3+}$ at (i) a non-functioning conical-tip carbon electrode that was (ii) hydrogenated and (iii) twice hydrogenated in 1.0 M KCl. Scan rate: 100 mV s^{-1}.

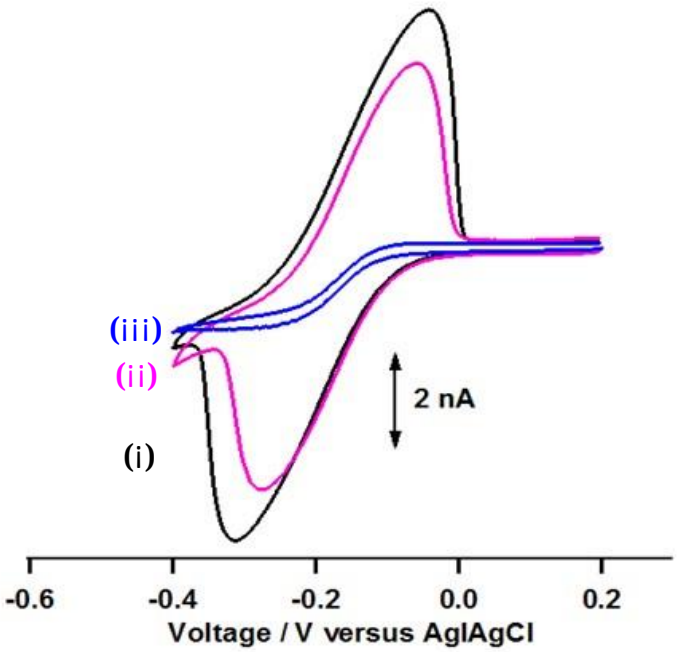

Figure 3.7 Cyclic voltammetry of 1.0 mM $[Ru(NH_3)_6]^{3+}$ at (i) a non-functioning conical-tip carbon electrode that was (ii) hydrogenated and (iii) twice hydrogenated in 1.0 M KCl. Scan rate: 100 mV s^{-1}.

In some experiments, hydrogenation of a non-functioning carbon electrode, represented by trace i in Figure 3.7, still produced a peak-shaped CV for $[Ru(NH_3)_6]^{3+}$, as denoted by trace ii in Figure 3.7, indicating unsuccessful modification in single hydrogenation. In this case, after repeating an identical hydrogenation step at such an electrode, a similarly sigmoidal shaped CV to that depicted in trace iii in Figure 3.7 was obtained. In trace ii of Figure 3.6, the half-wave potential (E½) and waveslope (0.0592/n) were estimated (based on the equation[30], $E=E_{½}+(0.0592/n)\log_{10}[(I_{lim}- I)/I]$, where E denotes potential, n the number of electrons transferred, I_{lim} the limiting current and I the current) to be -171 mV (standard deviation (SD) 15 mV; N=10) and 60.2 mV decade^{-1} (SD 4.2 mV decade^{-1}; N=10), respectively. After a repeated hydrogenation at the same electrode used to acquire trace ii in Figure 3.6, the $E_{½}$ and waveslope of the corresponding CV (trace iii) in Figure 3.6 were -177 mV (SD 12 mV; N=10) and 63.9 mV decade^{-1} (SD 5.6 mV decade^{-1}; N=10). Therefore, no discernible $E_{½}$ and waveslope shift was observed after repeated hydrogenation, which supports the insensitivity of $[Ru(NH_3)_6]^{3+}$ to the electrode surface chemistry. Moreover, the good agreement in waveslope to the expected 59 mV decade^{-1} for a one-electron transfer at hydrogenated electrodes indicates a reversible electron transfer reaction of $[Ru(NH_3)_6]^{3+}$. Further, the charging current in the sigmoidal-shaped CV became almost negligible after repeated hydrogenation. In their work involving the activation of glassy carbon electrodes by vacuum heat-treatment, Fagan *et al.*[31] suggested the reduced charging current is due to removed surface redox species and microscopic surface structure changes. Notably, the limiting current diminished by ~30-50% after repeated hydrogenation, which is attributable to the silanisation of phenolic hydroxyl groups on the electrode surface, leading to an increased electron tunnelling distance.[22] Therefore, this clearly demonstrates the ability of *n*-butylsilane reduction to activate electrodes by potentially filling in microfractures on the electrode surface. As the electrochemistry of $[Ru(NH_3)_6]^{3+}$ is independent of surface chemistry, the transformation of a peak-shaped voltammogram to a sigmoidal shape can be attributed to a range of physical changes on the electrode surface. For example, the hydrogenation process can result in the bonding of the silicon atom in a butylsiloxane

group to the carbon structure and this might function as a mechanical support for carbons on the electrode surface, as described by Amato *et al*.[32]

3.6.4 Voltammetry of anthraquinone-2,6-disulfonate at a bare and a hydrogenated electrode

In our work, cyclic voltammetry of 1.0 mM AQDS in 0.1 M $HClO_4$, often used to show the presence of carbon-oxygen functionalities at edge plane of highly ordered pyrolytic graphite and other carbon surfaces[18,33], was also conducted. As shown by Figure 3.8 (a),

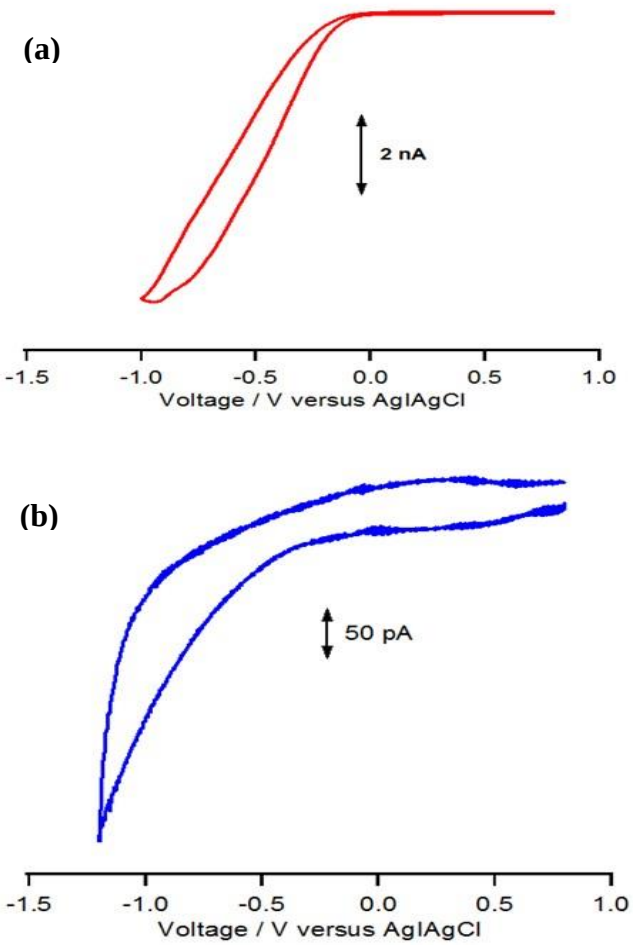

Figure 3.8 Cyclic voltammetry of 1.0 mM AQDS in 0.1 M $HClO_4$ at (a) a carbon electrode and (b) a hydrogenated carbon electrode. Scan rate: 100 mV s^{-1}.

the CV obtained depicts a reduction current arising from physisorbed AQDS on carbon-oxygen functionalities at carbon electrodes. However, a featureless, highly magnified CV (Figure 3.8 (b)) at the corresponding hydrogenated electrode has provided strong evidence for the removal of the functionalities from the electrode surface.

3.6.5 Characterising bare and hydrogenated electrode by X-ray photoelectron spectroscopy

XPS was next conducted to further probe the characteristics of the hydrogenated carbon surface. Both the survey XPS spectra and Gaussian-fitted results obtained using bare and hydrogenated carbon electrodes are presented in the following sections. In Figure 3.9, the survey XPS spectrum of a bare carbon electrode shows distinct C1s and O1s peaks. However, in Figure 3.10, after hydrogenation, an additional Si2p peak was also observed.

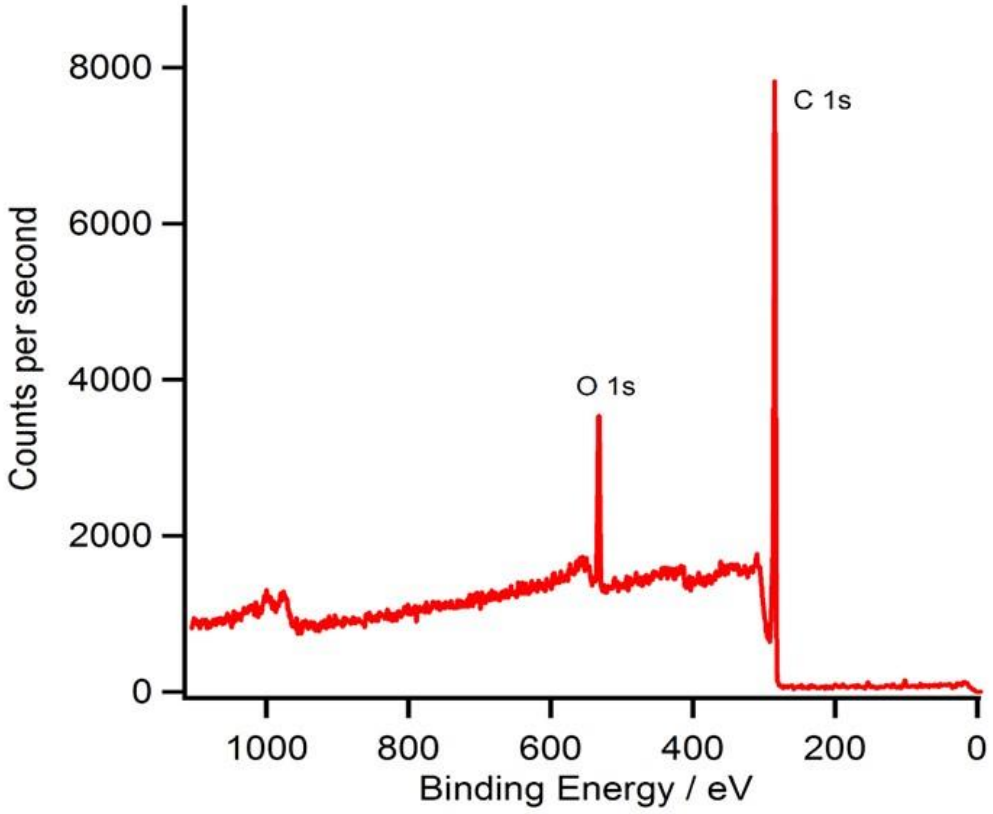

Figure 3.9 XPS survey spectrum of a bare carbon electrode.

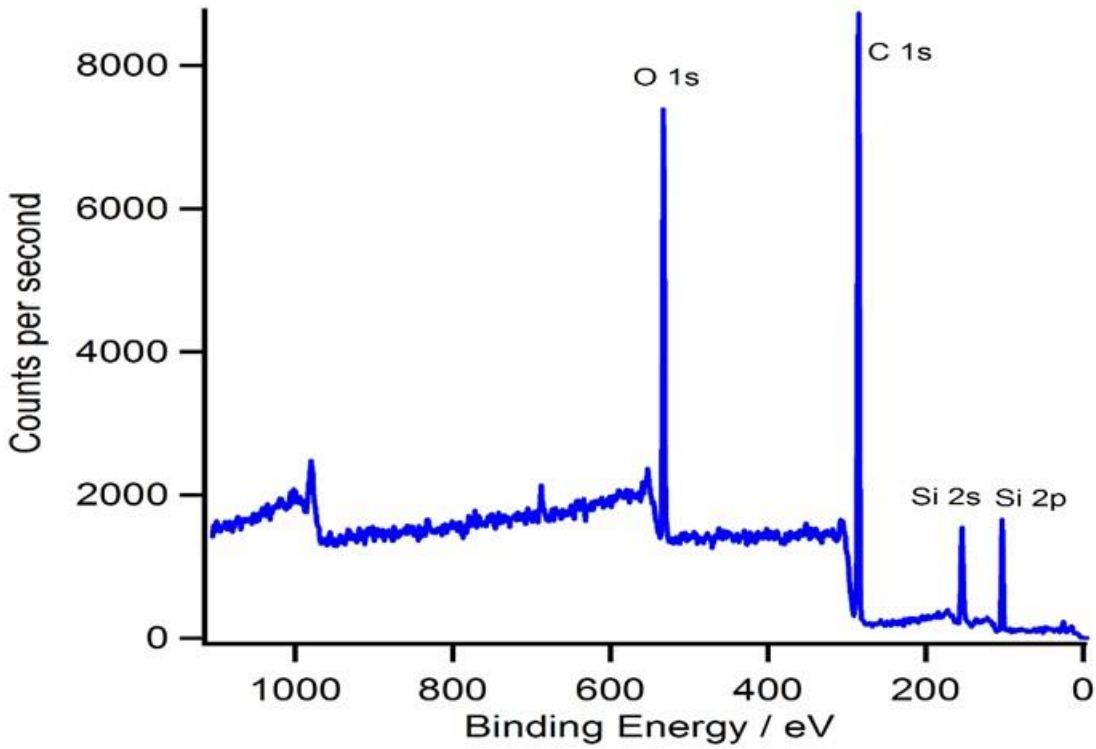

Figure 3.10 XPS survey spectrum of a hydrogenated carbon electrode.

By deconvolution, the corresponding high-resolution spectra obtained at these electrodes are displayed in Figure 3.11, 3.12, 3.13, 3.14, and 3.15. In Figure 3.11, 5 peaks were identified in the C1s spectrum of a bare carbon electrode. It is therefore apparent that the carbon obtained from the pyrolysis of C_2H_2 contributed several peaks under C1s including sp^2-like graphitic carbon and sp^3-hybridised diamond-like carbon. Among the fitted results in Figure 3.11, the most intense peak at ~285.0 eV is attributable to aliphatic, sp^3-like carbon (explicitly, quaternary C in long aliphatic chain) by comparing to a peak at the same binding energy obtained using an electrochemically and thermally oxidised boron-doped diamond film on a silicon substrate.[34] The peak at 284.5 eV is assigned to the presence of sp^2 graphitised carbon as this is analogous to that obtained using amorphous carbon films deposited by plasma on a single crystal silicon substrate.[35] Notably, the carbon film was exposed to air while being deposited during pyrolysis, giving rise to oxidation products on the electrode, which may account for carbon binding energies at 286.6, 288.0, 289.2 eV.

According to Zhou *et al.*[36], who examined chemically and thermally functionalised carbon nanofibres, the 286.6 eV peak represents carbon in the form of phenols, alcohols or ether groups, the 288.0 eV peak represents carbon in carbonyl or quinone groups, and the 289.2 eV peak indicates the presence of carbon as carboxyl groups on the electrode surface.

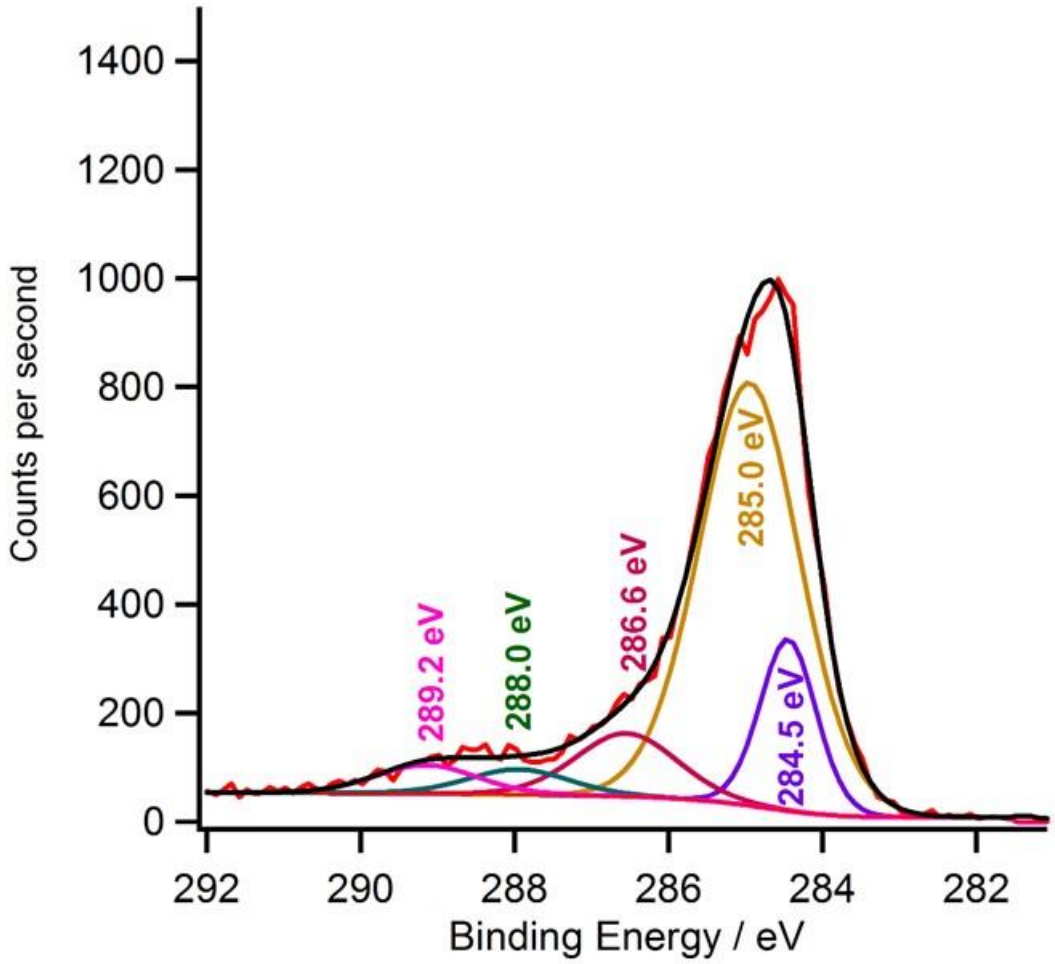

Figure 3.11 C1s peak fitting of spectrum of a bare carbon electrode.

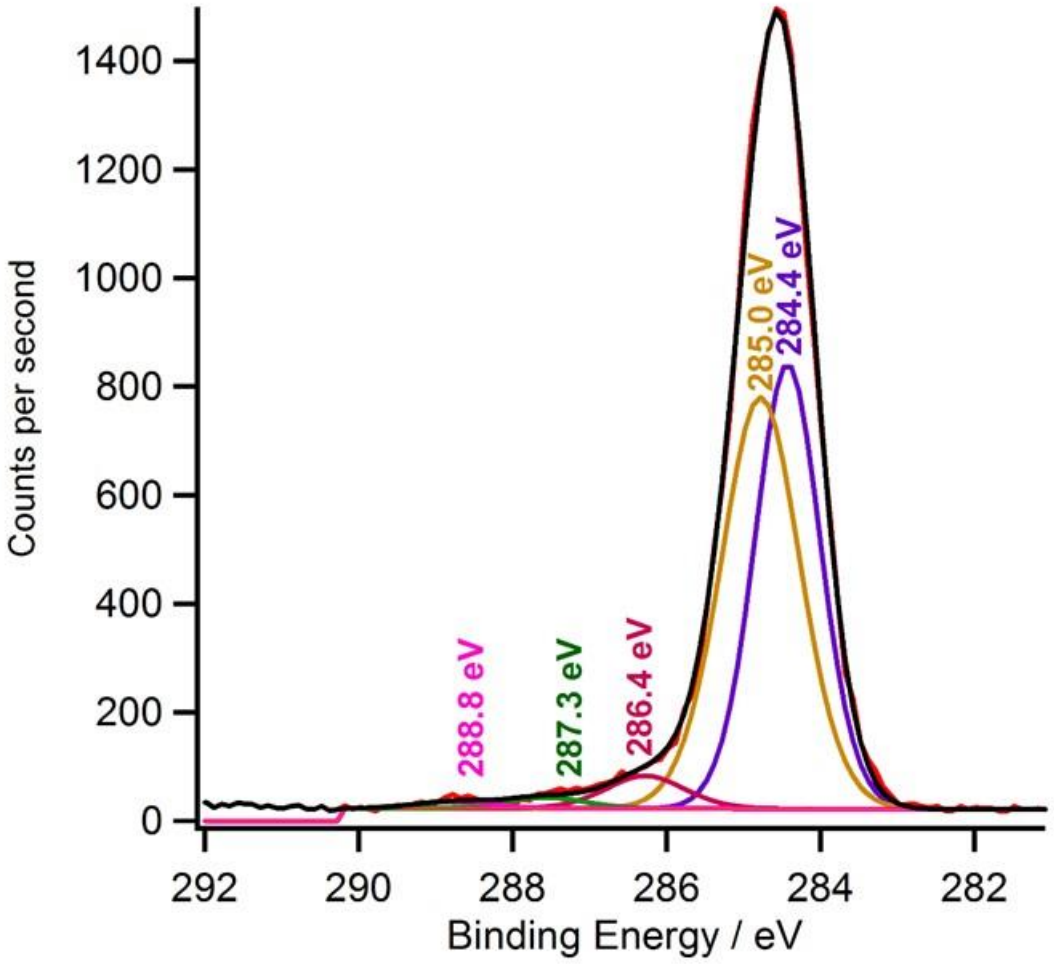

Figure 3.12 C1s peak fitting of spectrum of a hydrogenated electrode.

As shown in Figure 3.12, the deconvoluted results at a hydrogenated carbon electrode also yielded 5 peaks under C1s. Compared to Figure 3.11, a peak of similar intensity is observable at 285.0 eV. However, the 284.5 eV peak in Figure 3.11 has slightly shifted to 284.4 eV after hydrogenation due to an altered chemical environment on the electrode surface.[35] Moreover, at the hydrogenated carbon electrode, the 284.4 eV peak becomes ~60% more intense than that obtained at the bare electrode. This is attributed to the composition of carbon films with mixed sp^2 carbon as graphite and silane-like carbon (–C-Si-O–) formed after hydrogenation, as illustrated in Scheme 3.1. This is further supported by the presence of both the Si2p and O1s signals obtained at the hydrogenated electrode surface, in agreement with Ferro *et al.*'s work involving a boron-doped diamond film electrode grown on a single-crystal, p-silicon wafer.[34] However, as expected, the intensity of the remaining three peaks is significantly lower

after hydrogenation and these peaks have correspondingly shifted to 286.4, 287.3 and 288.8 eV due to different chemical environment after hydrogenation.[35]

Most functional oxygen groups would reportedly yield O1s binding energies within a narrow 531-535 eV range.[35,37] In this work, the deconvolution of the O1s spectrum at a bare electrode yielded two peaks at 532.25 and 533.7 eV, as shown in Figure 3.13, with

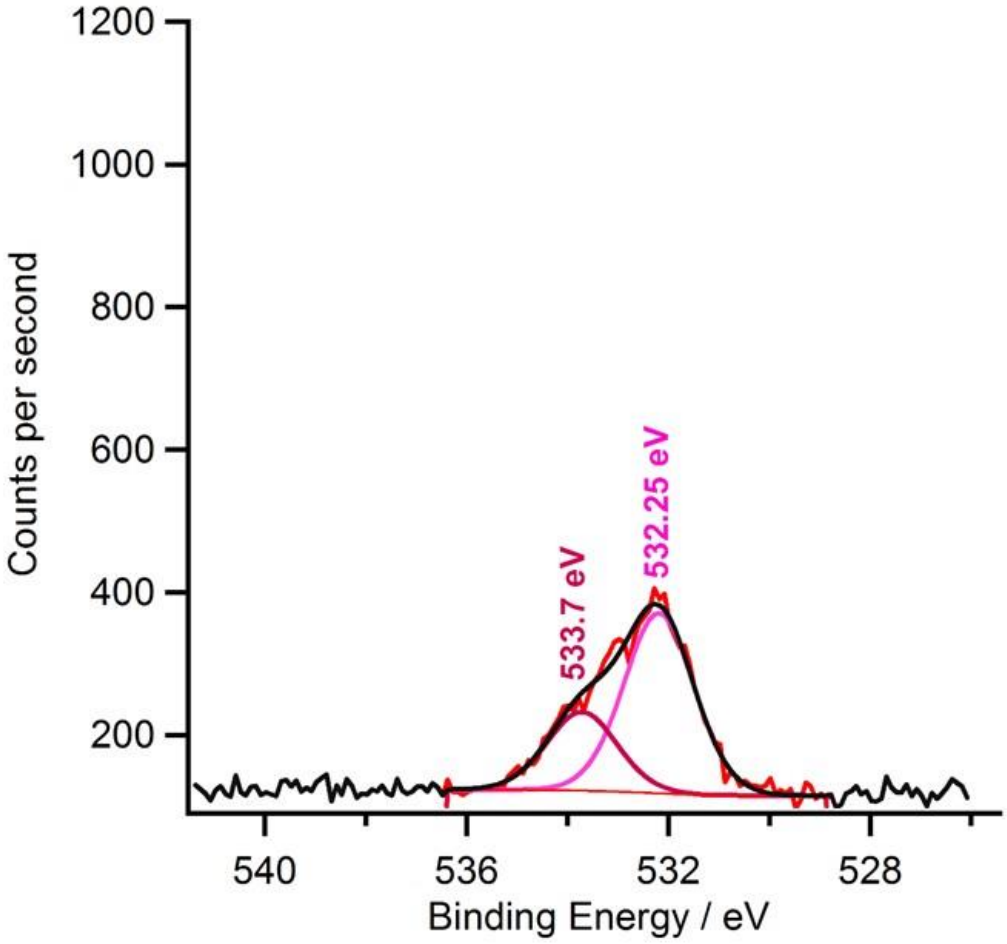

Figure 3.13 O1s peak fitting of spectrum of a bare electrode.

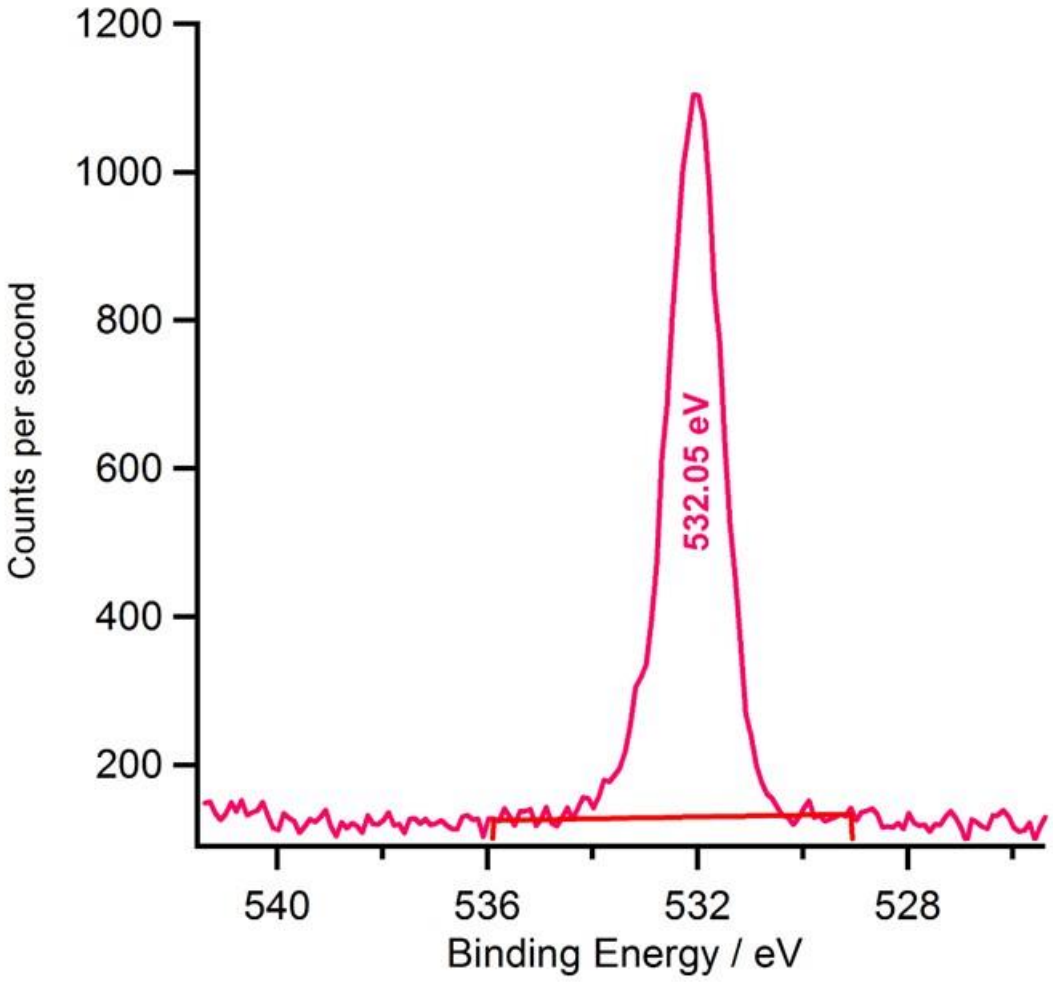

Figure 3.14 O1s peak fitting of spectrum of a hydrogenated electrode.

a relative abundance of ~7.13% and 3.10%, respectively. Using Ferro *et al.*'s work[34] as a guide, the 532.25 eV peak is assigned to etheric/alcoholic aliphatic functions and, to a lesser extent, to carbonylic aliphatic groups, most likely originating from dangling bonds on the sp^3-carbon skeleton. On the other hand, the 533.7 eV peak is assigned to oxygen present as ethers, alcohols, and esters in aromatic frames.[34,36] After hydrogenation, binding energies arising from oxygen-bearing functionalities (carbonyl, carboxyl, epoxy, etc) associated with carbon on an electrode surface, except phenolic hydroxyl, have diminished when hydrogen atoms replaced these functionalities. However, we observed a separate intense oxygen peak at 532.05 eV in Figure 3.14, possibly arising from a large number of oxygen present in the dendrimeric butylsiloxane derivative formed during hydrogenation shown in Scheme 3.1. Ferro *et*

al.[34] also obtained a sharp oxygen peak at 532.8 eV that was assigned as oxygen present in aliphatic –C–O-Si– group when a boron-doped diamond film was deposited on a single-crystal *p*-silicon wafer.

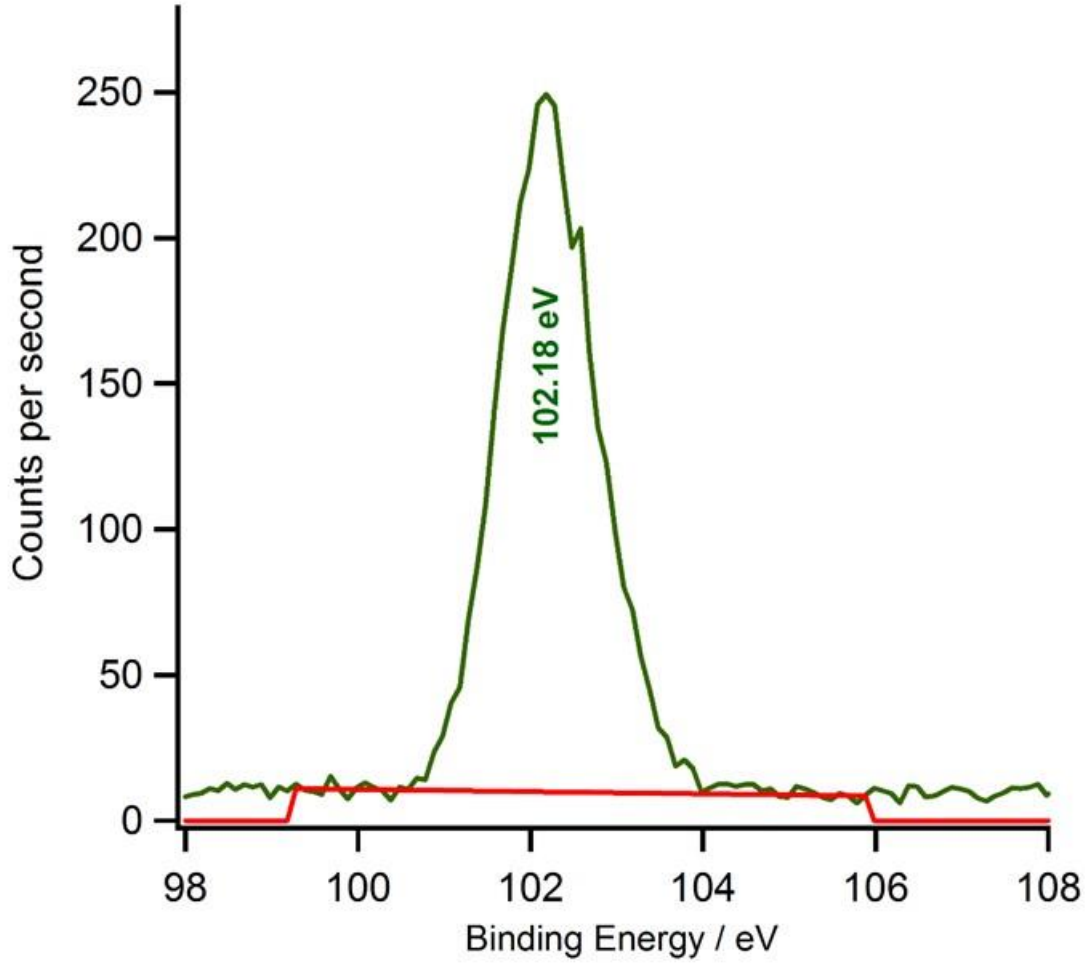

Figure 3.15 Si2p peak fitting of a spectrum of a hydrogenated electrode. The red trace denotes the baseline of the spectrum.

On the other hand, a characteristic Si2p peak at 102.18 eV is notably observable in Figure 3.15, which was absent in the spectrum of the bare electrode. According to Ferro *et al*.[34], Si in aliphatic and aromatic species is expected to appear respectively at 102.1 and 102.0 eV, while the Si peak originated from the quartz substrate (SiO_2) is expected to be located between 103.21 and 103.9 eV. Therefore, the Si2p signal at the hydrogenated electrodes could be confidently assigned to aliphatic bonded silicon, indicating the formation of a butylsiloxane group on electrode surface by hydrogenation

shown in Scheme 3.1. All XPS data above provided strong support for the proposed electrode surface structure obtained by *n*-butylsilane reduction in Scheme 3.1.

3.6.6 Stability of hydrogenated electrodes

In the next experiment, 20 cyclic voltammetric scans of 1.0 mM $[Ru(NH_3)_6]^{3+}$ in 1.0 M KCl were conducted at hydrogenated electrodes. The results obtained, depicted in Figure 3.16, show repeatable sigmoidal-shaped voltammograms with negligible changes in charging current obtained at a hydrogenated electrode, compared to a peak-shaped voltammogram with high charging at non-hydrogenated electrodes. These results demonstrate the stability of hydrogenated electrode surface. To further establish the integrity of modified electrodes, cyclic voltammetry of $[Ru(NH_3)_6]^{3+}$ was conducted at both bare and hydrogenated electrodes that were separately stored in air and in a pH 7.4 citrate/phosphate buffer.

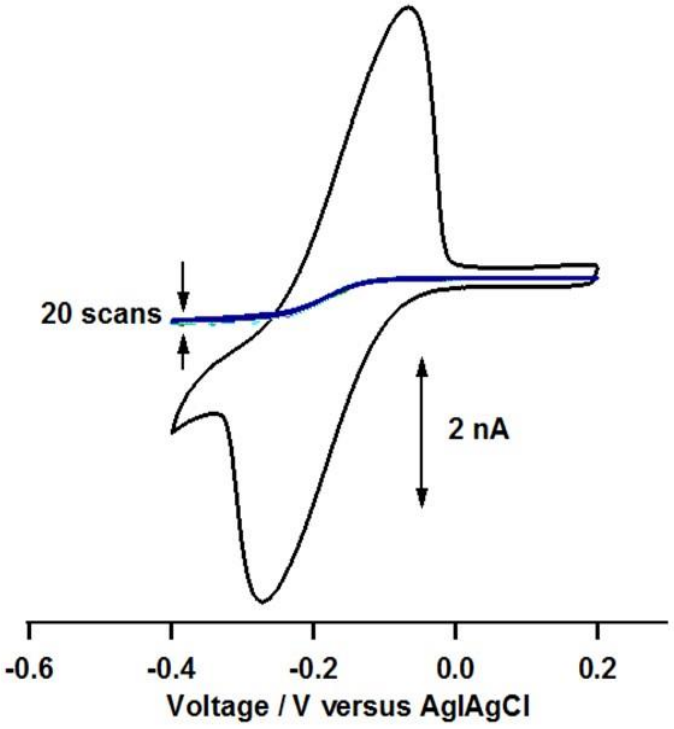

Figure 3.16 Cyclic voltammograms of 1.0 mM $[Ru(NH_3)_6]^{3+}$ at non-functioning (peak shaped) and functioning (sigmoidal shaped) conical-tip carbon electrodes in 1.0 M KCl. Scan rate: 100 mV s^{-1}. Time between scans: 8 s.

The changes in the $[Ru(NH_3)_6]^{3+}$ reduction signal obtained at these electrodes after a week of storage are shown in Figure 3.17 and 3.18. The changes of the reduction signal of $[Ru(NH_3)_6]^{3+}$ was calculated using the mathematical expression $((I - Io) \times 100)/Io$, where I denotes final reduction limiting current, I_o initial reduction limiting current. After storage, the reduction current at bare electrodes stored in air increased by 25% (SD 27%; N=9).

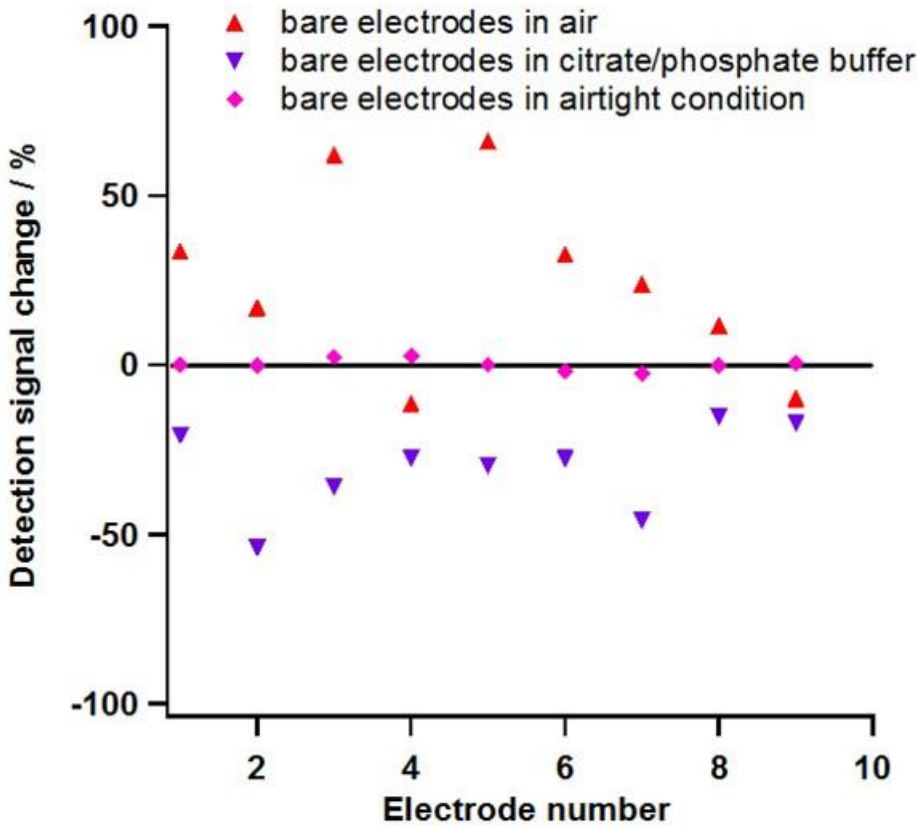

Figure 3.17 $[Ru(NH_3)_6]^{3+}$ detection signal change at bare carbon electrodes in air and in pH 7.4 citrate/phosphate buffer.

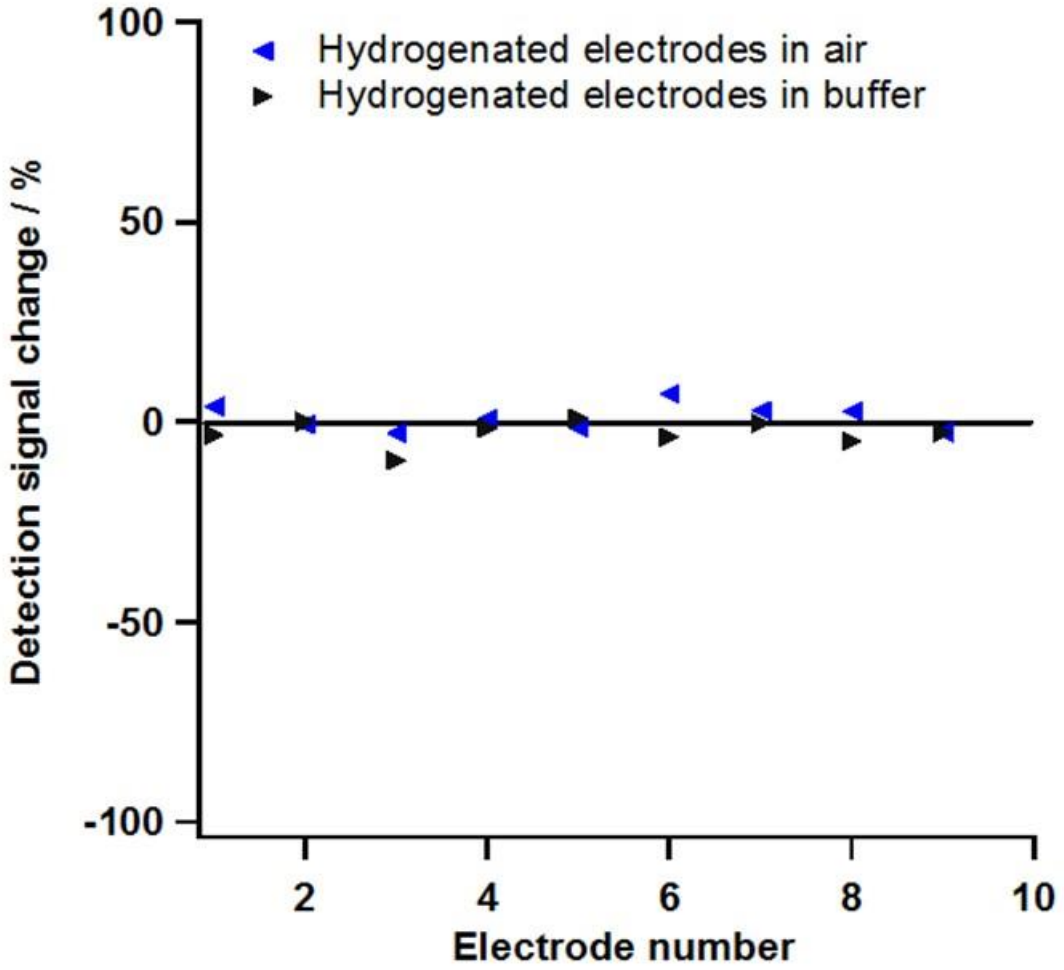

Figure 3.18 $[Ru(NH_3)_6]^{3+}$ detection signal change at hydrogenated carbon electrodes in air and in pH 7.4 citrate/phosphate buffer.

In this experiment, exposure of carbon surface to air might have increased the specific surface area by surface fragmentation, roughening and channels originated through the deposited carbon, leading to the formation of surface oxides, as reported by Toebes *et al.*[38]. According to Lee *et al.*[39], upon exposure to air, the number of functional groups substantially increased on a carbon fibre surface, which would in turn enlarge the surface area of a carbon fibre and thus the enhanced detection signal. In addition, the charging current increased between the forward and backward scan in the voltammogram after storage (data not shown). This may serve as evidence for surface oxide formation after exposure to air.[40] Similarly, the bare electrodes were also stored in an airtight condition as a control and their detection signal remained almost unchanged at 0.11% (SD 1.6%; N=9) with a small charging current over the same

period. In contrast, the bare electrodes stored in buffer showed a diminished detection signal by 30% (SD 13%; N=9). Wang *et al*.[41] also observed a gradual decrease in detection signal and up to 50% loss of the detection signal after storing iridium and glucose oxidase modified carbon fibre microelectrodes in phosphate buffer for one week. Previously, polar functional groups (e.g. –OH) on a carbon surface reportedly provide coordination sites for phosphate to bind onto a carbon surface.[42] Anions can bind on a polar functional group-containing carbon surface by electrostatic interaction or ligand exchange mechanism and therefore, carbon was previously used as an adsorbent for removal of phosphate from aqueous waste.[43] In our work, we assume citrate/phosphate ions in buffer can bind to the electrode surface and block the active surface area that ultimately causes diminishing detection signal at the electrodes. Hydrogenated electrodes were similarly stored in both air and buffer for 1 week. As shown in Figure 3.18, very minimal detection signal change was observed at the hydrogenated electrodes in air (1.1% (SD 3.3%; N=9)) and the buffer (2.8% (SD 3.2%; N=9)). These results clearly indicated that hydrogenated electrodes were less prone to both air and buffer exposure because of the formation of an H-terminated hydrophobic surface in *n*-butylsilane reduction. Previously, H-terminated glassy carbon electrodes showed long-term surface stability towards air oxidation and also demonstrated weaker adsorption to polar compounds compared to bare glassy carbon electrodes. The absence of surface oxide might have enhanced the stability of H-terminated glassy carbon, which would otherwise increase adsorption to carbon promoted by local electron withdrawal by oxygen and the possibility of ionic and covalent bonding of adsorbates.[44]

3.7 Conclusion

As illustrated in Scheme 3.1, during *n*-butylsilane hydrogenation, carbon-oxygen functional groups on electrode surface are eliminated, except phenolic hydroxyl groups, and are replaced by sp^3 carbon-hydrogen. We attribute the reduction of charging current at the hydrogenated carbon electrodes to the removal of carbon-oxygen functionalities from the electrode surface, followed by terminating defect sites with carbon-hydrogen, as described by Xu *et al.*[18] for glassy carbon electrodes hydrogenated by microwave plasma. Similarly, H-terminated diamond electrodes also show low background current due to a lack of detectable electroactive surface carbon-oxygen functionalities.[4] In this way, we postulate that hydrogenated conical tip carbon electrodes surface behave similarly to a diamond electrode surface and produced CVs with minimal charging current.

In summary, this work has demonstrated the application of the *n*-butylsilane reduction as an effective activation of non-functional carbon microelectrodes to obtain sigmoidal-shaped voltammograms with minimal charging current at these electrodes. Chemical modification of these microelectrodes was confirmed by electrochemistry and XPS. In this way, the fabrication success rate of carbon microelectrodes has been improved to nearly 100%. Equally significant, these activated carbon electrodes have shown long-term stability in air and in citrate/phosphate buffer.

3.5 References

1. Compton, R. G.; Wildgoose, G. G.; Rees, N. V.; Streeter, I.; Baron, R., Design, fabrication, characterisation and application of nanoelectrode arrays. *Chemical Physics Letters* **2008,** *459* (1), 1-17.
2. Koudelka-Hep, M.; van der Wal, P. D., Microelectrode sensors for biomedical and environmental applications. *Electrochimica Acta* **2000,** *45* (15), 2437-2441.
3. Wightman, R. M., Probing cellular chemistry in biological systems with microelectrodes. *Science* **2006,** *311* (5767), 1570-1574.
4. Park, J.; Show, Y.; Quaiserova, V.; Galligan, J. J.; Fink, G. D.; Swain, G. M., Diamond microelectrodes for use in biological environments. *Journal of Electroanalytical Chemistry* **2005,** *583* (1), 56-68.
5. Singh, Y. S.; Sawarynski, L. E.; Michael, H. M.; Ferrell, R. E.; Murphey-Corb, M. A.; Swain, G. M.; Patel, B. A.; Andrews, A. M., Boron-doped diamond microelectrodes reveal reduced serotonin uptake rates in lymphocytes from adult rhesus monkeys carrying the short allele of the 5-HTTLPR. *ACS chemical neuroscience* **2009,** *1* (1), 49-64.
6. Marquis, B. J.; McFarland, A. D.; Braun, K. L.; Haynes, C. L., Dynamic Measurement of Altered Chemical Messenger Secretion after Cellular Uptake of Nanoparticles Using Carbon-Fiber Microelectrode Amperometry. *Analytical Chemistry* **2008,** *80* (9), 3431-3437.
7. Marquis, B. J.; Haynes, C. L., The effects of co-culture of fibroblasts on mast cell exocytotic release characteristics as evaluated by carbon-fiber microelectrode amperometry. *Biophysical Chemistry* **2008,** *137* (1), 63-69.
8. Xu, H.; Zuo, P.; Wang, S.; Zhou, L.; Sun, X.; Hu, M.; Liu, B.; Wu, Q.; Dou, H.; Liu, B., Striatal dopamine release in a schizophrenia mouse model measured by electrochemical amperometry in vivo. *The Analyst* **2015,** *140* (11), 3840-3845.
9. Dunevall, J.; Fathali, H.; Najafinobar, N.; Lovric, J.; Wigström, J.; Cans, A.-S.; Ewing, A. G., Characterizing the Catecholamine Content of Single Mammalian Vesicles by Collision–Adsorption Events at an Electrode. *Journal of the American Chemical Society* **2015,** *137* (13), 4344-4346.

10. Li, X.; Majdi, S.; Dunevall, J.; Fathali, H.; Ewing, A. G., Quantitative Measurement of Transmitters in Individual Vesicles in the Cytoplasm of Single Cells with Nanotip Electrodes. *Angewandte Chemie International Edition* **2015,** *54* (41), 11978-11982.
11. Samba, R.; Fuchsberger, K.; Matiychyn, I.; Epple, S.; Kiesel, L.; Stett, A.; Schuhmann, W.; Stelzle, M., Application of PEDOT-CNT Microelectrodes for Neurotransmitter Sensing. *Electroanalysis* **2014,** *26* (3), 548-555.
12. Llaudet, E.; Hatz, S.; Droniou, M.; Dale, N., Microelectrode biosensor for real-time measurement of ATP in biological tissue. *Analytical chemistry* **2005,** *77* (10), 3267-3273.
13. Tian, F.; Gourine, A. V.; Huckstepp, R. T. R.; Dale, N., A microelectrode biosensor for real time monitoring of l-glutamate release. *Analytica chimica acta* **2009,** *645* (1–2), 86-91.
14. Alvin Koh, W. C.; Rahman, M. A.; Choe, E. S.; Lee, D. K.; Shim, Y.-B., A cytochrome c modified-conducting polymer microelectrode for monitoring in vivo changes in nitric oxide. *Biosensors and Bioelectronics* **2008,** *23* (9), 1374-1381.
15. Zhang, M.; Liu, K.; Xiang, L.; Lin, Y.; Su, L.; Mao, L., Carbon nanotube-modified carbon fiber microelectrodes for in vivo voltammetric measurement of ascorbic acid in rat brain. *Analytical chemistry* **2007,** *79* (17), 6559-6565.
16. Zhang, X.; Zhang, W.; Zhou, X.; Ogorevc, B., Fabrication, characterization, and potential application of carbon fiber cone nanometer-size electrodes. *Analytical chemistry* **1996,** *68* (19), 3338-3343.
17. Wang, K.; Fishman, H. A.; Dai, H.; Harris, J. S., Neural stimulation with a carbon nanotube microelectrode array. *Nano letters* **2006,** *6* (9), 2043-2048.
18. Xu, J.; Chen, Q.; Swain, G. M., Anthraquinonedisulfonate electrochemistry: A comparison of glassy carbon, hydrogenated glassy carbon, highly oriented pyrolytic graphite, and diamond electrodes. *Analytical chemistry* **1998,** *70* (15), 3146-3154.
19. Yang, N.; Smirnov, W.; Hees, J.; Hoffmann, R.; Kriele, A.; Obloh, H.; Müller-Sebert, W.; Nebel, C. E., Diamond ultra-microelectrode arrays for achieving

maximum Faradaic current with minimum capacitive charging. *physica status solidi (a)* **2011,** *208* (9), 2087-2092.

20. Pietzka, C.; Denisenko, A.; Kibler, L. A.; Scharpf, J.; Men, Y.; Kohn, E., Surface modification of single-crystal boron-doped diamond electrodes for low background current. *Diamond and Related Materials* **2009,** *18* (5–8), 816-819.
21. Hermans, A.; Wightman, R. M., Conical Tungsten Tips as Substrates for the Preparation of Ultramicroelectrodes†. *Langmuir* **2006,** *22* (25), 10348-10353.
22. Chen, P.; McCreery, R. L., Control of electron transfer kinetics at glassy carbon electrodes by specific surface modification. *Analytical Chemistry* **1996,** *68* (22), 3958-3965.
23. Zoski, C. G., Ultramicroelectrodes: design, fabrication, and characterization. *Electroanalysis* **2002,** *14* (15-16), 1041-1051.
24. Laczka, O.; del Campo, F. J.; Muñoz-Pascual, F. X.; Baldrich, E., Electrochemical Detection of Testosterone by Use of Three-Dimensional Disc–Ring Microelectrode Sensing Platforms: Application to Doping Monitoring. *Analytical Chemistry* **2011,** *83* (11), 4037-4044.
25. Chien, J. B.; Saraceno, R. A.; Ewing, A. G., Intracellular voltammetry with ultrasmall carbon ring electrodes. In *Redox Chemistry and Interfacial Behavior of Biological Molecules*, Springer US: 1988; pp 417-424.
26. Nimmagadda, R. D.; McRae, C., Characterisation of the backbone structures of several fulvic acids using a novel selective chemical reduction method. *Organic geochemistry* **2007,** *38* (7), 1061-1072.
27. Nimmagadda, R. D.; McRae, C., A novel reduction reaction for the conversion of aldehydes, ketones and primary, secondary and tertiary alcohols into their corresponding alkanes. *Tetrahedron letters* **2006,** *47* (32), 5755-5758.
28. McNally, M.; Wong, D. K., An in vivo probe based on mechanically strong but structurally small carbon electrodes with an appreciable surface area. *Analytical chemistry* **2001,** *73* (20), 4793-4800.
29. Swamy, B. K.; Venton, B. J., Carbon nanotube-modified microelectrodes for simultaneous detection of dopamine and serotonin in vivo. *The Analyst* **2007,** *132* (9), 876-884.

30. Wang, J., *Analytical electrochemistry*. third ed. ed.; John Wiley & Sons: 2006.
31. Fagan, D. T.; Hu, I. F.; Kuwana, T., Vacuum heat-treatment for activation of glassy carbon electrodes. *Analytical chemistry* **1985,** *57* (14), 2759-2763.
32. Amato, L.; Schulte, L.; Heiskanen, A.; Keller, S. S.; Ndoni, S.; Emnéus, J., Novel Nanostructured Electrodes Obtained by Pyrolysis of Composite Polymeric Materials. *Electroanalysis* **2015,** *27* (7), 1544-1549.
33. Kneten, K. R.; McCreery, R. L., Effects of redox system structure on electron-transfer kinetics at ordered graphite and glassy carbon electrodes. *Analytical Chemistry* **1992,** *64* (21), 2518-2524.
34. Ferro, S.; Dal Colle, M.; De Battisti, A., Chemical surface characterization of electrochemically and thermally oxidized boron-doped diamond film electrodes. *Carbon* **2005,** *43* (6), 1191-1203.
35. Filik, J.; May, P.; Pearce, S.; Wild, R.; Hallam, K., XPS and laser Raman analysis of hydrogenated amorphous carbon films. *Diamond and related Materials* **2003,** *12* (3), 974-978.
36. Zhou, J.-H.; Sui, Z.-J.; Zhu, J.; Li, P.; Chen, D.; Dai, Y.-C.; Yuan, W.-K., Characterization of surface oxygen complexes on carbon nanofibers by TPD, XPS and FT-IR. *Carbon* **2007,** *45* (4), 785-796.
37. Goeting, C. H.; Marken, F.; Gutiérrez-Sosa, A.; Compton, R. G.; Foord, J. S., Electrochemically induced surface modifications of boron-doped diamond electrodes: an X-ray photoelectron spectroscopy study. *Diamond and Related Materials* **2000,** *9* (3), 390-396.
38. Toebes, M. L.; van Heeswijk, J. M.; Bitter, J. H.; Van Dillen, A. J.; de Jong, K. P., The influence of oxidation on the texture and the number of oxygen-containing surface groups of carbon nanofibers. *Carbon* **2004,** *42* (2), 307-315.
39. Lee, J.-S.; Kang, T.-J., Changes in physico-chemical and morphological properties of carbon fiber by surface treatment. *Carbon* **1997,** *35* (2), 209-216.
40. Bleda-Martínez, M. J.; Maciá-Agulló, J. A.; Lozano-Castelló, D.; Morallón, E.; Cazorla-Amorós, D.; Linares-Solano, A., Role of surface chemistry on electric double layer capacitance of carbon materials. *Carbon* **2005,** *43* (13), 2677-2684.

41. Wang, J.; Rivas, G.; Chicharro, M., Glucose microsensor based on electrochemical deposition of iridium and glucose oxidase onto carbon fiber electrodes. *Journal of Electroanalytical Chemistry* **1997,** *439* (1), 55-61.

42. Zhang, L.; Zhou, Q.; Liu, J.; Chang, N.; Wan, L.; Chen, J., Phosphate adsorption on lanthanum hydroxide-doped activated carbon fiber. *Chemical Engineering Journal* **2012,** *185*, 160-167.

43. Wang, Z.; Nie, E.; Li, J.; Yang, M.; Zhao, Y.; Luo, X.; Zheng, Z., Equilibrium and kinetics of adsorption of phosphate onto iron-doped activated carbon. *Environmental Science and Pollution Research* **2012,** *19* (7), 2908-2917.

44. Kuo, T.-C.; McCreery, R. L., Surface chemistry and electron-transfer kinetics of hydrogen-modified glassy carbon electrodes. *Analytical Chemistry* **1999,** *71* (8), 1553-1560.

Chapter 4

Development of Antifouling Electrodes by Hydrogenating Conical-tip Carbon Electrodes using *n*-Butylsilane Reduction

4.1 Introduction

Dopamine is a neurotransmitter released in the forebrain well known for responding to rewards, non-reward and positive motivation. It is also involved in brain networks for seeking, evaluating, and value learning. In some cases, it is also implicated with supporting brain network for orienting, cognition, and general motivation.[1] The development of obesity is linked with the deficit in neural reward responses related to dopamine concentration in the central nervous system.[2] Dopamine serves important physiologic functions in organs such as the kidney. Deficiency of intrarenal dopamine may lead to hypertension and decreased longevity.[3] Disruption of dopamine in brain is associated with common neurological disorders such as Parkinson's and Alzheimer's diseases. Diabetes may cause a reduction in retinal dopamine and could cause early visual defects.[4] Therefore, determination of dopamine is of interest to neuroscientists studying the factors influencing neurotransmitter actions and the roles neurotransmitters play in neuronal signalling.

4.2 Dopamine

Dopamine release in the central nervous system is involved with reward, and, to some extent, risk as well, whereas punishment and salience have only limited effects on dopamine activation.[5] Neurons in the central nervous system accumulate the information, process and relay them within the brain. Such information moves through the central nervous system as electrical impulses called action potentials. The action potential propagates by travelling from the cell body to the axon and dendrites of a

dopaminergic neuron as shown in Figure 4.1.[6] However, the action potential is unable to pass from a neuron to an adjacent neuron because of a synaptic gap of ~300 nm by ~15 nm between the neurons.[7] Instead, the arrival of an action potential to the dopaminergic nerve terminal evokes vesicular release of dopamine into the cleft, wherein it crosses the gap to activate postsynaptic receptors to initiate the postsynaptic neuron to fire its own action potential. Reuptake clears dopamine from the synaptic cleft (gap) via presynaptic dopamine transporters (DAT). Thus, neurotransmission processes these signals throughout the entire body. However, dopaminergic neurons are only located in a limited discrete region of the brain. The cell bodies of the neurons are embedded in the substantia nigra or ventral tegmental area and the axons are projected to the caudate-putamen or the nucleus accumbens. A dopaminergic metabolic pathway showing its synthesis in this part of the brain is presented in Figure 4.2. In the first step, tyrosine (Tyr) is converted to L-DOPA in the presence of tyrosine hydroxylase (TH). In the next step, in the presence of L-amino acid decarboxylase (AADC), L-DOPA is transformed to dopamine, which can also be dissociated by catechol-*O*-methyltransferase (COMT) and monoamine oxidase (MAO), resulting in 3-methoxytyramine (3-MT) and 3,4-dihydroxyphenylacetic acid (DOPAC), respectively. In the final step, both of them are further metabolised by MAO and COMT to homovanillic acid (HVA) as a final product. Alternatively, dopamine is converted to norepinephrine (NE) by dopamine beta-hydroxylase (DBH), then norepinephrine is converted to epinephrine (E) by N-methyltransferase.[8]

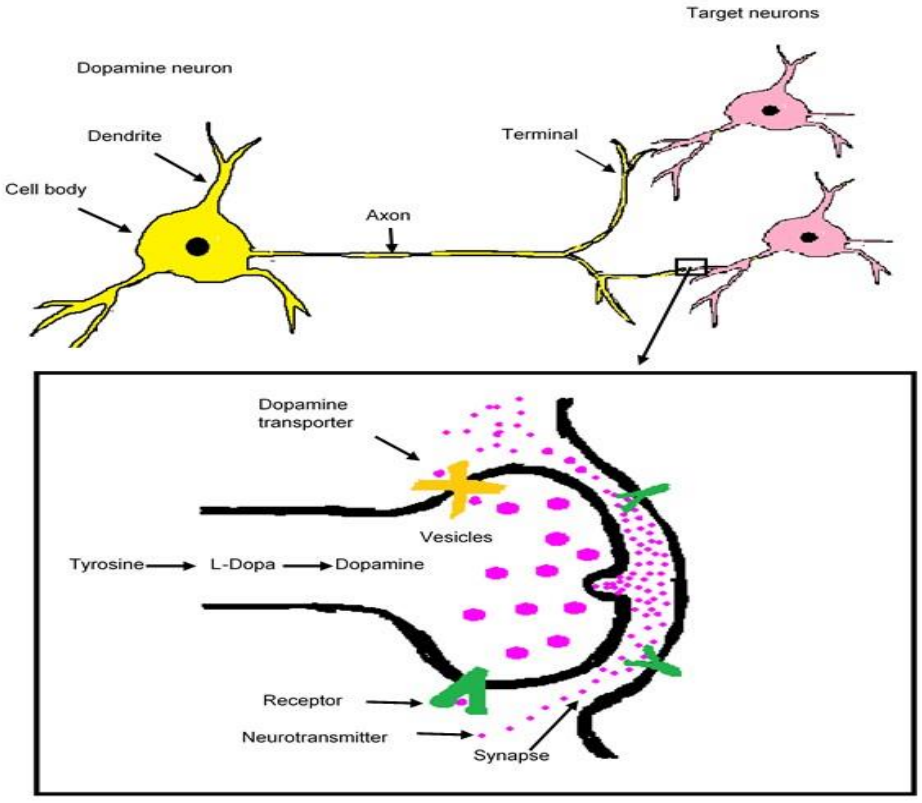

Figure 4.1 Schematic of a dopaminergic cell. Adapted from reference 6. [6]

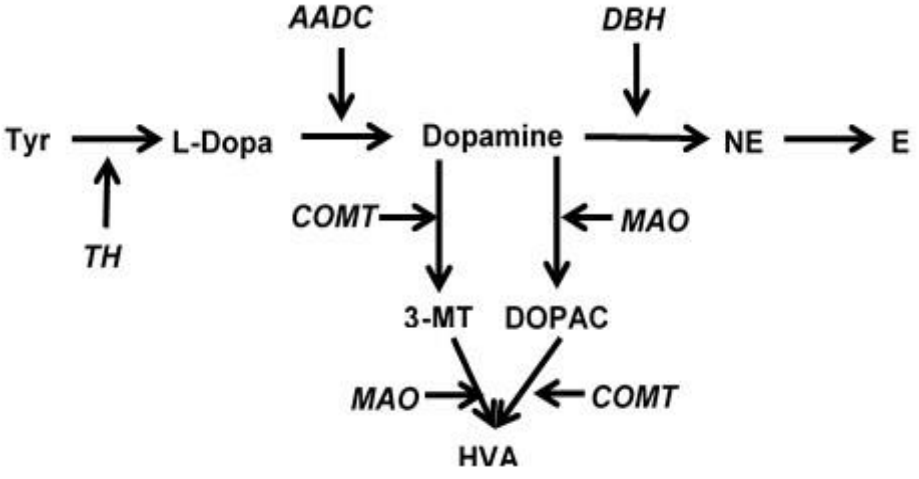

Figure 4.2 Dopaminergic metabolic pathway. Adapted from reference 8. [8]

4.3 Chemistry of dopamine

Dopamine is one of the major neurotransmitters in the catecholamine group present in the central nervous system. Understanding the chemistry involved with dopamine is important not only in biomedical research, but also in diagnostic and pathological research. In terms of electrochemistry, dopamine can easily be oxidised by applying a potential and it undergoes a two-electron oxidation to produce dopamine o-quinone, as shown in Scheme 4.1.

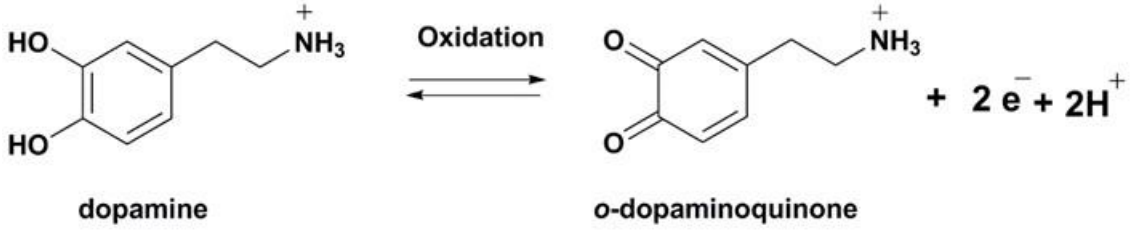

Scheme 4.1. Oxidation of dopamine

However, the oxidation product of dopamine is very reactive and it can undergo a series of cyclisation reaction to form a melanin-like polymeric compound as depicted in Scheme 4.2. Initially, dopaminoquinone cyclises to leukodopaminochrome, which then undergoes a two-electron oxidation to form dopaminochrome. Subsequently, dopaminochrome polymerises to yield a melanin-like compound.[9,10] Alternatively, dopaminoquinone can also be polymerised to form polydopamine and polydopaminoquinone as shown in Scheme 4.3.[11,12]

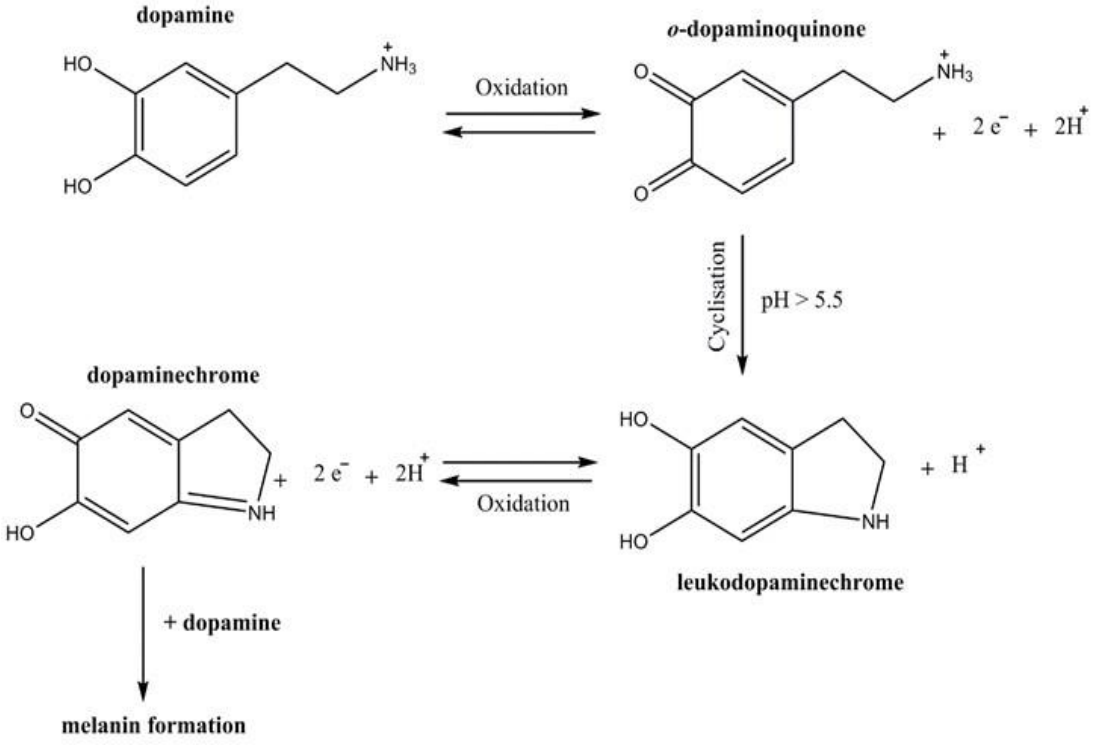

Scheme 4.2. A mechanism for the electrochemical oxidation of dopamine in aqueous solutions. Adapted from reference 10. [10]

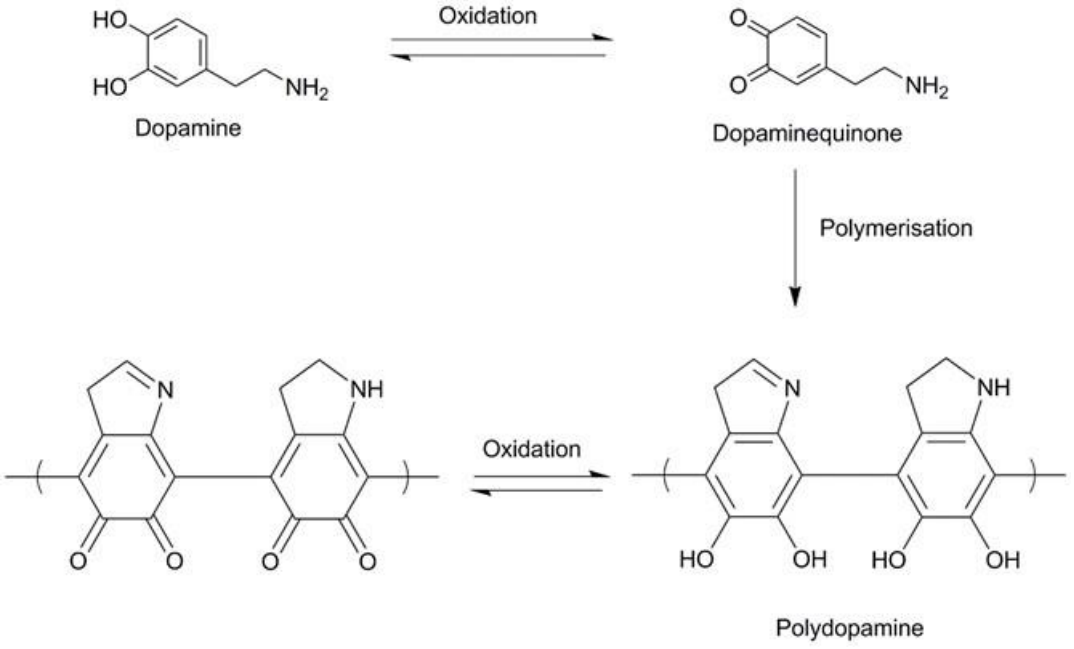

Scheme 4.3 Mechanism of dopamine polymerisation. Adapted from reference 12. [12]

Next, owing to the presence of a catechol and an amine group in dopamine, it may polymerise to form a compound that mimics a protein (Mefp-5) of blue mussel (*Mytilus edulis*), as shown in Scheme 4.4, which can spontaneously deposit as a thin polymer film on a bulk material surface.[13]

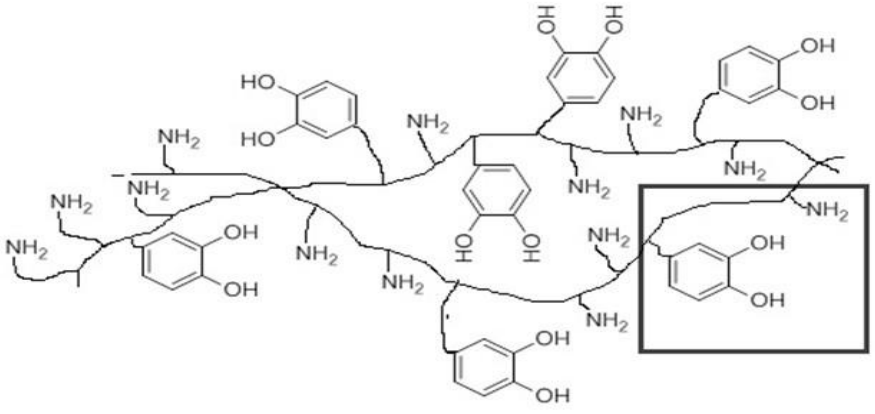

Scheme 4.4 A schematic illustration of the interfacial location of Mefp-5 and a simplified molecular representation of characteristic amine and catechol groups; Adapted from reference 13. [13]

4.4 Challenges to dopamine detection *in vivo*

A challenge in dopamine detection *in vivo* is to identify the target dopamine neurons located in the substantia nigra pars compacta (SNC) and ventral tegmental area (VTA) in the midbrain. Due to the presence of a minority population of non-dopamine neurons (*e.g.*, GABAergic neurons, glutamatergic neurons) in the same location that are not readily distinguishable from dopamine neurons, selection of dopamine neurons using an electrode implanted through several millimetres into the brain is a complicated process and this may compromise the reliability of detection.[14] Although the majority (70%) of

neurons in SNC and VTA are dopaminergic neurons, it is crucial to identify the specific neurons for reliable recording of dendritic release of dopamine. Another challenge in detecting such neurotransmitters *in vivo* as dopamine or serotonin is that they are present for a very short time (milliseconds) in the synaptic gap, while presynaptic and postsynaptic events are taking place. However, microelectrodes give unprecedented spatial and temporal resolution overcoming many aspects of the problems these days.[15]

With their similar chemical structures and properties, dopamine, ascorbic acid, and uric acid coexist in extracellular fluids of the central nervous system, human blood plasma, and urine. As a result of overlapping oxidation potentials, it is always challenging to detect them individually and/or simultaneously by electroanalytical methods.[16,17] In order to overcome this problem, modification of the electrode surface is required to obtain high selectivity to dopamine. However, while not perfect, selective detection of dopamine at carbon fibre microelectrodes using fast-scan cyclic voltammetry does not always require surface modification.[18]

Another common challenge in detecting dopamine *in vivo* is electrode fouling. High-molecular weight amphiphilic proteins, peptides, lipids or other biomolecules present in extracellular fluid, can irreversibly adsorb on oxygenated sp^2 carbon electrodes through dipole-dipole interaction, hydrogen bonding or ion dipole interaction. All these then form a barrier on the electrode surface that deters dopamine from making direct contact with the electrode surface for electron transfer reaction, leading to a transient attenuated dopamine response, as illustrated in Figure 4.3.[19] On the other hand, a non-polar, H-terminated surface with no extended π electron system is reportedly less prone to fouling.[20] Meanwhile, other properties including stability and charging current at a H-terminated surface are also expected to be much improved compared to an O-terminated electrode surface. [19]

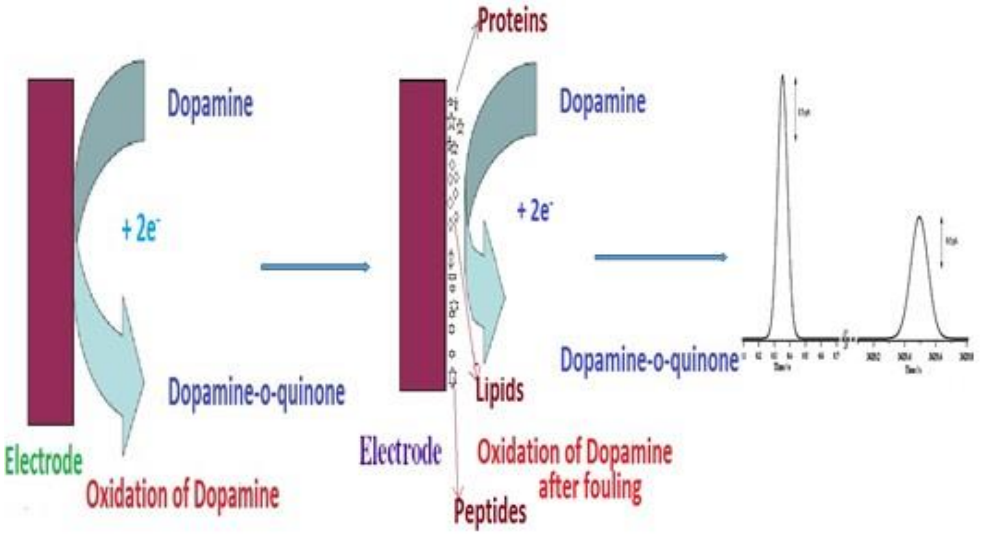

Figure 4.3 Effect of fouling on a bare carbon electrode during dopamine oxidation.

In addition, the polymeric compound, polydopamine or melanin, originating from dopamine oxidation during electrochemical detection, may also yield an insulating film via strong covalent bonds with organic moieties and noncovalent bonds with inorganic species present on the electrode surface. All the above will therefore jeopardise the long-term stability of the electrode and compromise the detection process.[10,13,20]

4.5 Hydrogenation of Electrode surface

H-terminated electrode surfaces have recently received much attention due to their potential use as a biosensing platform. One way to fabricate a H-terminated surface is to reduce graphene oxide on a quartz glass using a flow of hydrogen in the presence of argon in an autoclave at 500°C and 75×10^3 torr pressure.[21] Graphene oxide can also be chemically reduced using hydrazine.[22] Similarly, polycrystalline diamond was grown on a silicon wafer by microwave chemical vapour deposition at 700-900°C from a mixture of 0.7% methane in 100 standard cm^3 min^{-1} hydrogen.[23] After growing diamond, the methane flow was stopped while a hydrogen plasma at 25 torr reactor

pressure with 600 W microwave power at 700°C was maintained for an additional 30 min to obtain a H-terminated diamond surface. Kanazawa *et al.*[24] deposited a polycrystalline diamond film on a silicon substrate by microwave-plasma-assisted chemical vapour deposition at 700 W and 50 torr, with a hydrogen and methane gas flow of 198 and 2 standard cm^3 min^{-1}, respectively. To obtain a H-terminated surface, the deposited film was exposed to a hydrogen plasma for 10 min. By using a similar strategy to form a diamond layer of 0.2 –1.0 μm thick, Rezek *et al.*[25] then hydrogenated the diamond surface by maintaining only a hydrogen plasma for 5 min. Vanhove *et al.*[26] treated a diamond film of 500 nm thick for 2 h in hydrogen delivered into a microwave plasma enhanced chemical vapour deposition reactor. Alternatively, the oxide layer on a silicon wafer substrate was removed before the diamond film was deposited. For example, Biswas *et al.*[27] initially hydrogenated a silicon wafer for 15 min in a hydrogen plasma at 500 standard cm^3 min^{-1}, at a pressure of 0.193 torr in 30 W radio frequency power. In other work[28], a similar diamond of 200 μm thick was hydrogenated in a microwave plasma for 5 min at 500°C. Undoped diamond of 60-80 nm thickness was grown in a chemical vapour deposition reactor where the deposited diamond was exposed *in situ* to a hydrogen plasma at 650°C for 10-30 min.[29] Hoffmann *et al.*[30] reduced a boron doped diamond electrode in a microwave induced hydrogen plasma of 2500 W, while 75 torr hydrogen was fed into the reactor at a rate of 300 standard cm^3 min^{-1}. In the same work[30], the electrode was cathodically treated at -35 V in 2 M HCl for 1-5 min to obtain a clean hydrogenated surface. Salazar-Banda *et al.*[31] reduced a boron doped diamond electrode in 0.5 M H_2SO_4 by applying a potential of +3 V to -3 V (versus a hydrogen reference electrode) at 0.1 V s^{-1} scan rate for 30 min. In a separate work, graphene oxide was reduced at a glassy carbon electrode by applying a potential of -1.1 V for 300 s and palladium nanoparticles were incorporated in the reduced graphene.[32] The modified sensor was applied to measure dopamine in commercially available dopamine injection at a lower oxidation potential (0.234 V

versus Ag|AgCl) than electrodes modified with reduced graphene or palladium nanoparticles only.

4.6 Strategies to minimise fouling

In Section 1.6, we have briefly discussed about antifouling strategies. Due to the diversity of the fouling agents and antifouling strategies, the evaluation or comparison of one strategy over another for a particular application is not straightforward. In this section, we will discuss antifouling strategies that are categorised according to the types of electrode modification. These modification strategies are commonly conducted by immobilising/developing antifouling film on bare electrodes. Films that have hitherto been reported include carbon nanotubes, graphene, diamond or diamond-like and polymeric materials.

4.6.1 Carbon nanotubes and graphene

Carbon nanotubes are commonly used due to their large surface area, electrical conductivity, and electrocatalytic properties.[33,34] Carbon nanotube-modified electrodes exhibit antifouling properties in electrochemical analysis *in vivo*, where proteins of all sizes could potentially foul the electrode surface. In an *in vivo* analysis, Xiang *et al*.[35] immobilised vertically aligned carbon nanotubes on SiO_2 passivated carbon fibres. Such an electrode was prepared by the pyrolysis of iron phthalocyanine under an Ar/H_2 atmosphere in which the temperature was increased from 800^{o}C to 1100^{o}C. In applying the electrode to selectively monitor ascorbate in cerebrospinal fluid *in vivo*, the authors reported a 2% loss of sensitivity in a 30-min experiment. A corresponding 21% loss was observed at an unmodified carbon fibre microelectrode. The modified electrode was also used to successively detect ascorbate in the striatum of an anesthetised rat brain every 5 min.[35] Excellent reproducibility (relative standard deviation (RSD) 6.4%)

and durability (after six consecutive scans with a 5-min time interval), along with well-defined sigmoidal voltammograms of ascorbate in the rat brain, supported an antifouling capability of the carbon nanotube-modified electrode in real time analysis. The antifouling properties of carbon nanotubes may be due to their electrocatalytic activity that arises from various defects at the ends of the nanotubes or on the cylindrical walls.[33,34, 36] These defects often undergo oxidation or other reactions producing a variety of functional groups.

Zestos *et al*.[37] also developed a carbon nanotube fibre electrode by pumping a suspension of single-walled carbon nanotubes in water and sodium dodecylbenzenesulfonic acid into a rotating polyethylenimine solution in a custom-built rotating stage. The polyethylenimine-carbon nanotube fibre modified electrode showed higher conductivity than that at a poly(vinyl alcohol)-carbon nanotube fibre modified electrode developed by the same group and a 6-fold greater oxidation current for 1 μM dopamine was obtained at the former electrode. The fouling resistance of the polyethylenimine-carbon nanotube fibre electrodes was examined by measuring serotonin in the presence of its metabolite, 5-hydroxyindolacetic acid, which is also known to cause electrode fouling during the detection of serotonin. Electrode fouling from 5-hydroxyindolacetic acid is particularly important because its physiological concentration is often 10 times higher than that of serotonin. The serotonin oxidation peak at the polyethylenimine-carbon nanotube electrode was reported to remain almost constant upon incubation in 5-hydroxyindolacetic acid for 2 h. The polyethylenimine-carbon nanotube fibre electrode has also exhibited antifouling properties towards the oxidation product of dopamine, as no significant change in dopamine oxidation current was observed when a bolus of dopamine was injected every 2 h over a 10 h period.[37] When the polyethylenimine-carbon nanotube fibre electrode was applied to measure exogenous serotonin concentration in rat brain slices of the caudate putamen for 10 min, the peak-shaped cyclic voltammograms and the dopamine oxidation peak current

remained unchanged. The authors proposed that the antifouling properties of the electrode were due to the presence of additional edge plane sites arising from carbon nanotubes. Similarly, Harreither *et al.*[10] developed a 35 μm diameter carbon nanotube fibre electrode by continuously spinning single-walled carbon nanotubes dispersed in sodium dodecyl sulfate in a co-flowing stream of aqueous poly(vinyl alcohol). Based on a steady-state amperometric measurement of 1 mM and 100 μM dopamine at the fabricated electrode, the electrode exhibited a loss of half of its initial steady-state current in 15 min at the 1 mM concentration.[10] However, the steady-state current obtained in 100 μM dopamine was unchanged for 2 h. The results of these experiments indicated the potential application of carbon nanotube fibres in the brain, although the extracellular concentration of dopamine (0.01–1 μM) is much lower than that used in this experiment. These results also indicated that fouling of dopamine is concentration dependent and a lower concentration of dopamine may lead to decreased chemical fouling. The authors also reported a slow growth of insulating patches on carbon nanotube modified fibres compared to conventional carbon fibres.

Graphene is a two-dimensional single layer of sp^2 carbon atoms with very high electrical conductivity, surface area, and mechanical strength.[22,38] It can be considered as an individual layer of graphite or an unrolled carbon nanotube and has been shown to reduce electrode fouling. The most common graphene preparation involves oxidation of graphite that is then separated into single layers of graphene oxide. The latter is then chemically or electrochemically transformed to reduced graphene oxide. For example, Alwarappan *et al.*[39] studied the direct electrochemical activity of cytochrome c at a chemically reduced graphene-modified glassy carbon electrode. In addition to improving electron transfer kinetics, the current at the modified electrode was found to have reduced by only 7.5±0.3% after 50 repetitive cycles.[39] The presence of graphene protected the electrode from fouling by preventing cytochrome c from reaching the

glassy carbon electrode surface and provided electrocatalytic sites for the efficient detection of the protein.

4.6.2 Diamond and other carbon-based materials

Diamond has a very low electrical conductivity due to a completely sp^3 structure, but doping with boron sufficiently increases the conductivity for use as an electrode material.[36] The extensive sp^3 structure of a boron-doped diamond, together with the typically low surface polar functional groups, results in a dramatic decrease in the adsorption of fouling agents such as proteins.[36,40] However, the electrode surface that contains polar functional groups e.g. carbonyl, hydroxyl has reported offered high sensitivity to catecholamine through improved adsorptivity of the compounds.[41] Thus, the surface chemistry of an electrode has a major effect on the electrochemical performance and antifouling characteristics. Indeed, Trouillon *et al.*[42] demonstrated that the boron doping level affects the antifouling properties of boron-doped diamond electrodes. They investigated a range of boron doping levels (0.1, 1, and 5%, v/v) to investigate the stability of electrodes employed for dopamine detection in the presence of bovine serum albumin as a biological fouling agent. Albumin is commonly used to assess the antifouling properties of electrodes and sensors because it is often considered a biological fouling standard.[43,44,45] A non-significant decrease of dopamine oxidation current was observed at the 0.1% and 1% doping levels. However, a corresponding 25% decrease was observed when the doping level was increased to 5%. These results indicate that high-density boron-doped diamond electrodes are more prone to fouling. A high level of boron doping would facilitate the formation of a high density of defect sites that are electrocatalytically active. Consequently, the inactivation of these defect sites by fouling agents would result in diminished electrochemical detection of the analyte. Therefore, low-level boron-doped diamond electrodes should limit the adsorption of fouling agents on an electrode surface. For example, Zhao *et al.*[46]

fabricated a conical-tip boron-doped diamond microelectrode with a low doping level. No significant attenuation in the oxidation signal was observed during the amperometric detection of serotonin in guinea pig mucosa *in vitro* for 100 min. As well as the doping level, the surface termination and roughness affect the fouling resistance of boron-doped diamond electrodes. The effect of electrode fouling was also investigated at H- and O-terminated electrodes, which have low and high proportions of surface oxygen functionalities, respectively. For the analysis of serotonin, Güell *et al.*[47] observed that O-terminated boron-doped diamond electrodes exhibited superior antifouling properties compared to a carbon nanotube network electrode after 10 consecutive scans. Similarly, Patel *et al.*[48] compared a boron-doped diamond electrode to several other carbon-based electrodes in the analysis of dopamine. The O-terminated polycrystalline boron-doped diamond electrode was considered the least susceptible to fouling even in a high concentration of 1 mM dopamine compared to other electrode materials including glassy carbon, edge plane pyrolytic graphite, basal plane pyrolytic graphite, and basal plane highly oriented pyrolytic graphite.

Similar to boron-doped diamond electrodes, diamond-like carbon electrodes are amorphous carbon with a high proportion of diamond-like bonds (sp^3), which provides good resistance to electrode fouling.[49] The fouling resistance of a diamond-like carbon electrode treated with oxygen plasma to increase hydrophilicity has been investigated using bovine serum albumin, DNA, and human serum.[49] There was a negligible change in the current response to ferricyanide/ferrocyanide after incubation in solutions of bovine serum albumin, DNA, and human serum for up to 24 h. The very strong resistance to fouling at the electrode is likely the result of the generally inert sp^3 diamond-like structure that reduces adsorption. On the contrary, Chandra *et al.*[50] reported physically small conical-tip carbon electrodes (~2–5 μm diameter and ~4 μm axial length) that were hydrogenated by plasma-enhanced chemical vapour deposition to achieve an H-terminated diamond-like sp^3 electrode surface. These electrodes

retained 65% of dopamine oxidation current after they were incubated in a laboratory synthetic fouling solution containing caproic acid (a lipid), bovine serum albumin (a protein), cytochrome c (a protein), and human fibrinopeptide B (a peptide) for 7 days. By implanting the electrode in the left striatum of a male Sprague-Dawley rat during 60-min *in vivo* experiments, more than 70% of the dopamine oxidation current remained after the first 30 min and 50% remained over the next half period of the experiment. Although these results can be attributed to the H-terminated hydrophobic surface, the hydrophilic oxygen plasma-treated diamond-like electrode appeared to have a greater resistance to fouling.

An electron cyclotron resonance-sputtered nano-carbon film is a carbon electrode with similar properties to diamond-like carbon electrodes and it has both sp^2 and sp^3 characteristics.[51,52] Kato *et al*.[51] and Xue *et al*.[52] both prepared oxidised electron cyclotron resonance-sputtered nanocarbon films to resist fouling by bovine serum albumin. The electrode used by Kato *et al*.[51] was anodically pretreated to oxidise the electrode surface. Coupled with flow injection analysis, there was a negligible decrease in the current at this electrode after 12 injections (RSD 0.75%). At a bare glassy carbon electrode, the current was highly variable, fluctuating over the 12 injections (RSD 9.28%). The authors suggested that the greater fouling resistance of the pretreated nano-carbon film electrode was due to the increased hydrophilicity from oxidation. To oxidise their nanocarbon film, Xue *et al*.[52] treated the electrode with oxygen plasma to partially oxidise the electrode surface. After a 30-min incubation in bovine serum albumin, the peak separation of ferricyanide/ferrocyanide increased from 80 to 120 mV and the peak current decreased to 92.0% of the initial value. On the contrary, for a pristine electron cyclotron resonance-sputtered nanocarbon film electrode without the oxygen plasma treatment, the peak separation increased from 217 to 620 mV and the peak current decreased to 71.7% of the initial value, which illustrated the requirement of a partially oxidised surface for antifouling properties. Compared to glassy carbon

electrodes, the treated nanocarbon film electrode also demonstrated superior fouling resistance and was slightly improved compared to diamond-like carbon electrodes. The nanocarbon film electrode treated with oxygen plasma remained relatively hydrophobic compared to glassy carbon electrodes and diamond-like carbon electrodes, which suggests that, in addition to hydrophilicity, there are other important factors influencing the antifouling properties.[52] For example, surface flatness is also believed to contribute to the observed fouling resistance, as the nanocarbon films were much smoother than diamond-like carbon electrodes.[51,52]

The surface chemistry of electrodes can be altered to produce either H- or O-termination. There is some disagreement as to which type of termination has superior resistance to fouling, with some studies indicating O-termination[47,53] and another suggesting H-termination[54]. Although H- or O-termination can have a significant impact on the fouling resistance of boron-doped diamond electrodes, few studies have investigated the use of oxidised carbon nanotubes or other oxidised carbon-based materials. Oxidation increases the number of oxygen functionalities on the electrode surface and thus hydrophilicity. It is debatable whether surface hydrophilicity or hydrophobicity increase fouling resistance, as it tends to depend on the analyte and fouling agents. Surface roughness has also been identified as a possible cause of electrode fouling.[52,53,55]

4.6.3 Polymeric films

The formation or presence of a polymeric film on an electrode surface can be detrimental to the electrode performance during the analysis of neurotransmitters. However, conductive polymers have been demonstrated to show antifouling properties. For example, a polystyrene sulfonate-doped polypyrrole film modified interdigitated gold microelectrode used for the detection of dopamine released from

pheochromocytoma (PC12) cells has demonstrated stability under cell culture conditions in long-term amperometric experiments.[56] In this work, the three-dimensional polypyrrole structure was speculated to decrease the freedom of movement of the positively charged protonated amino group tail of dopamine and hence reduce polydopamine fouling. There could also be a combination of steric and electrostatic hindrance, limiting the intermolecular cyclisation, which is the prerequisite for the polymerisation of dopamine on an electrode surface.

In addition to conductive polymers, non-conducting polymers may also be useful provided they are porous, allowing the analyte to reach the electrode surface while restricting the access of larger fouling agents, or mediate the electrochemical reaction on the polymer rather than the electrode surface. The polymer formed from the electropolymerisation of eugenol is known to be a nonconducting, porous polymer.[57] The application of this polyeugenol coating to a gold electrode preserved the electrode from fouling while it was incubated in bovine serum albumin for 16 h.[57] The pores in the polyeugenol film were too small to allow bovine serum albumin to reach the electrode surface, but oxygen was sufficiently small to travel through the pores. Another nonconducting, porous polymer, chitosan, was immobilised on an electrode simply by incubating carbon fibre microelectrodes in a chitosan solution for 15 s.[58] The fabricated electrodes showed no decrease in signal after four consecutive measurements of serotonin. These modified electrodes were also satisfactorily used in four repeated determinations of serotonin in a live embryonic zebrafish intestine with minimum interference, while brief electrochemical reconditioning was performed between determinations. The authors observed similar current response after the four consecutive determinations. As chitosan has excellent sieving properties, the chitosan layer was likely acting as a protective barrier against the direct adsorption of biological molecules or large polymeric molecules formed during the oxidation of serotonin.

Individual polymer chains, such as poly(ethylene glycol), can be attached to an electrode surface to provide a dense polymeric film that resists fouling by a diversity of fouling agents. To protect against protein fouling, various poly(ethylene glycol) monomethyl ether moieties were grafted on a hydrogenated silicon surface by Perez *et al*.[59] to investigate the adsorption of bovine serum albumin. The modified electrode exhibited excellent anti-fouling properties toward bovine serum albumin after being incubated in a solution for 1 h. With grafted moieties, the chain length, rather than the number of ethylene oxide monomers, was reportedly related to the antifouling behaviour. Similarly, Zhang *et al*.[60] investigated the use of oligo(ethylene glycol) thiols as an electrode coating for an electrochemiluminescent sequence-specific DNA sensor. The use of oligo(ethylene glycol) thiols was found to reduce the nonspecific adsorption of the glucose oxidase enzyme label. After incubating an oligo(ethylene glycol) thiol-modified electrode in glucose oxidase for 30 min, there was only a minimal increase in the electrochemiluminescent signal compared to the signal before enzyme incubation. On the contrary, there was a 10-fold increase in signal at a comparable electrode modified with the commonly used antifouling agent, 6-mercaptohexanol, indicating significant nonspecific adsorption of glucose oxidase.[60] In addition to neutrally charged polymer chains such as poly(ethylene glycol), charged chains can be attached to an electrode to provide fouling resistance. Li *et al*.[61] have used surface-initiated photoiniferter-mediated polymerisation to guide the growth of the amino acid-based zwitterionic polymers, poly[*N*4-(2-methacrylamidoethyl)asparagine] and poly[*N*5-(2-methacrylamidoethyl) glutamine], on gold surfaces. Using surface plasmon resonance, the authors reported the effective resistance to nonspecific protein adsorption from human blood serum and plasma when the polymer thickness was <11 nm. Moreover, the surface was also resistant to cell adhesion after incubating these polymer-coated electrodes in a culture medium with a concentration of 105 cells ml^{-1}.[61] These polymers could be resistant to fouling due to the net balanced charge, which increases hydrophilicity without placing a net charge on the electrode surface.

4.7 Scope of this study

Most hitherto reported antifouling strategies in neurotransmitter detection involved electrode surface modification. For example, carbon nanotubes[10,33,37] or graphene[39,62] have been used to develop an antifouling surface and to obtain enhanced electrocatalytic properties. A range of polymeric films including polypyrrole[56], poly(ethylene glycol)[63], and poly(vinyl chloride)[64] was immobilised on bare electrode surfaces to act as a barrier that prevented fouling agents from making direct contact with the electrode surface, thus allowing dopamine to undergo electron transfer at the electrode surface. Alternatively, the extensive sp^3 structure together with low surface polar functional groups of diamond materials, *e.g.*, microcrystalline boron-doped diamond, diamond powder, and detonation nanodiamond powder offered a significant improvement in fabricating antifouling electrodes owing to the benefit of less adsorption on a relatively inert surface.[42,46,48,53] In the last two decades, diamond-like carbon electrodes have replaced diamond electrodes as an alternative that not only provides good resistance to fouling,[49] but also acts as a good platform for cell culture with an excellent survival rate.[65] In our laboratory, we previously developed a diamond-like surface on conical-tip carbon electrode using radio frequency plasma enhanced chemical vapour deposition, where a stream of hydrogen atoms interacted with a carbon electrode surface to produce a diamond-like C-H surface with diminished C-O functionalities.[50,66] However, a <50% success rate of fabricating diamond like surface was achieved.[50,66] This was mainly caused by the damage of the fragile tips of these electrodes by the high radio frequency radiation (13.56 MHz).

In this work, we report a method that effectively introduces an antifouling layer on a carbon electrode surface in a relatively mild chemical environment and at laboratory room temperature involving an *n*-butylsilane hydrogenation. In Chapter 3, we reported the formation of an H-terminated carbon surface with dendrimeric butylsiloxane by *n*-butylsilane hydrogenation in the presence of the catalyst, tris(pentafluorophenyl)borane.

We demonstrated that the *n*-butylsilane hydrogenation successfully activated non-functioning conical-tip carbon electrodes. These hydrogenated electrodes also exhibited superb stability while being stored in air or a citrate/phosphate buffer for one week. The present chapter is aimed at

1. characterising the *n*-butylsilane modified electrodes using electrochemistry, spectroscopy and microscopy;
2. investigating the fouling resistance of the hydrogenated electrodes;
3. detecting dopamine selectively in the presence of ascorbic acid at the hydrogenated electrodes.

4.8 Experimental

4.8.1 Chemicals and Reagents

The list of chemicals and reagents used in this work is similar to that presented in Section 2.2.

4.8.2 Instrumentation and apparatus

Instrumentation required for electrochemical measurement is as described in Section 2.3.

4.8.3 Differential pulse voltammetry

For differential pulse voltammetry, a pulse width of 0.05 s, an amplitude of 0.1 V, a sampling period of 0.01 s and a pulse period of 0.25 s were used.

4.8.4 Fabrication of hydrogenated conical-tip carbon and carbon fibre electrodes

Physically small conical-tip carbon electrodes were fabricated as described in Section 2.4.1.

Carbon fibre microelectrodes were fabricated by adopting the procedure described by Armstrong-James *et al.*[67]. Initially, a bundle of carbon fibres of XAS grade (7 μm diameter of a single fibre), purchased from Goodfellow Cambridge Limited, UK, was cut at a length of 1.25 times the length of a borosilicate glass capillary (outside diameter 1.0 mm, inside diameter 0.78 mm, length 10.0 cm). The fibre was cleaned in 100 mL of boiling acetone, followed by 50-100 mL fresh acetone to remove any possible particulate materials. Then the fibres were air dried overnight. A single dried fibre was aspirated into a borosilicate glass capillary before the capillary was pulled. Graphite powder and a copper wire were used as described in Section 2.4.1 to accomplish electrical connection. Epoxy was applied to the fibre-capillary junction to secure the carbon fibre in the capillary. Finally, the carbon fibre was cut to achieve a length of ~100 μm protruding from the glass capillary.

The fabricated conical-tip carbon and carbon fibre electrodes were next hydrogenated by *n*-butyl silane reduction as described in Section 2.4.2.

4.8.5 Raman Spectroscopic Analysis

Raman spectra were acquired using a Renishaw 1000 model confocal microscopy Raman spectrometer with a Peltier cooled charge-coupled detector and a holographic notch filter. For excitation, a 50 mW diode pumped solid-state laser operating at 532 nm (Renishaw model RL532C50) was used. The microscope attachment was based on a Leica DMLM system, and a 50 × objective was used to focus the laser beam on a

~1μm diameter spot. The spectral resolution was ~0.7 cm^{-1}. Multiple peak Gaussian fittings of Raman peaks were performed using Origin (Pro) 2016 statistical software and the intensity was evaluated based on the peak area.

4.8.6 Atomic Force Microscopy

An atomic force microscope (Ntegra; NT-MDT, Moscow) equipped with a gold-coated silicon tip (NSG 01, curvature radius 6-10 nm; NT-MDT) was used for imaging a section of the shank of electrodes. Scanning was performed in a semi-contact mode while the electrodes were anchored on a stage with two screwable clamps (NT-MDT). A scanning cantilever was used to scan the shank area and an OPTEM ZOOM 125 positioning camera (Brook Anco Corporation, Rochester, New York) was used to acquire images.

4.8.7 Electrochemical impedance spectroscopy

Electrochemical impedance spectroscopy was conducted using an Autolab PGStat12 potentiostat (MEP Instruments Pty Ltd, Australia), interfaced with a Frequency Response Analysis v4.9.007 software (MEP Instruments Pty Ltd, Australia) and a desktop computer. Electrochemical impedance spectroscopy measurements of 1.0 mM $[Ru(NH_3)_6]^{3+}$ were performed at bare and hydrogenated conical-tip carbon electrodes in a 1.0 M KCl supporting electrolyte. An alternating potential of 10 mV peak-to-peak amplitude over the 10 kHz – 0.1 Hz frequency range, spaced logarithmically, was superimposed on an applied DC potential corresponding to the half-wave potential independently determined by cyclic voltammetry. A Frequency Response Analysis v4.9.007 software was used to fit simulated results to experimental results in all Nyquist plots obtained based on a Randles circuit/modified Randles circuit model.

4.9 Result and discussion

In this work, we are assessing the antifouling resistance of hydrogenated conical-tip carbon electrodes in a laboratory synthetic fouling solution. Bare carbon electrodes were fabricated by pyrolysing C_2H_2 at the tip and on the shank of pulled capillaries. All electrodes used here displayed a sigmoidal-shaped cyclic voltammogram for 1.0 mM $[Ru(NH_3)_6]^{3+}$ in 1.0 M KCl with a small charging current between the forward and reverse scan. Using chronoamperometry (see Section 3.6.2), the mean tip diameter of these electrodes was estimated to be 2 µm (standard deviation (SD) 1 µm; N=7) and the mean axial length of deposited carbon was ~15 µm (SD 10 µm; N=7). The bare carbon surface was then hydrogenated by subjecting the carbon electrodes to *n*-butylsilane reduction. We have previously described in Section 3.6.5 that, based on X-ray photoelectron spectroscopic results, the bare carbon surface obtained from the pyrolysis of C_2H_2 consisted of different types of carbons including sp^2–like graphitic carbon and sp^3–hybridised diamond-like carbon. The surface also contained a range of carbon oxidation products in the form of carbonyl, quinone, carboxyl, phenols, alcohols or ether groups when the deposited carbon film was exposed to air. After hydrogenation, the C–O bonds were converted to C–H bonds, but phenolic groups were converted to butylsiloxane dendrimers.

4.9.1 Electrochemical characterisation of hydrogenated carbon electrodes

In addition to cyclic voltammetry of 1.0 mM $[Ru(NH_3)_6]^{3+}$ in 1.0 M KCl reported in Section 3.6.3, we have also performed cyclic voltammetry of 1.0 mM $[Fe(CN)_6]^{3-}$ in 1.0 M KCl, and 1.0 mM dopamine in pH 7.4 citrate/phosphate buffer at hydrogenated conical-tip carbon electrodes in this chapter. The results obtained were then compared to those obtained at bare electrodes to probe the characteristics of the hydrogenated electrode surface. Based on the cyclic voltammograms obtained, we estimated the half

wave potential ($E_{1/2}$), waveslope as described in Section 3.6.3. In addition, the Tomes criterion (E_T) for the three redox markers at all electrodes was also estimated using the equation $E_T = | E_{3/4} - E_{1/4} | = (56.4 / n)$ mV at 25ºC, where $E_{3/4}$ and $E_{1/4}$ correspond to potentials at 75% and 25% of the diffusion current, respectively.[68] The results obtained for all three redox markers are presented in Table 4.1.

4.9.1.1 Characterisation of modified electrodes in $[Ru(NH_3)_6]^{3+}$

A sigmoidal-shaped cyclic voltammogram of 1.0 mM $[Ru(NH_3)_6]^{3+}$ in 1.0 M KCl was obtained at a different bare (trace i) and a different hydrogenated conical-tip carbon electrode (trace ii) from those used in Section 3.6.3 at a scan rate 100 mV s^{-1} is presented in Figure 4.4(a). The electrochemical parameters I_{lim}, $E_{1/2}$, waveslope determined from these cyclic voltammograms are already described in Section 3.6.3. For completeness, these parameters are tabulated in Table 4.1 for comparison. Additionally, the respective cyclic voltammograms obtained at bare and hydrogenated carbon fibre electrodes are presented in Figure 4.4(b) and the three estimated electrochemical parameters are included in Table 4.1.

Notably, the two sets of results ($E_{1/2}$, waveslope and E_T) obtained at the bare / hydrogenated conical-tip carbon electrodes and carbon fibre electrodes are comparable to each other, indicating a similar diffusion profile of $[Ru(NH_3)_6]^{3+}$ around these electrodes. Also, hydrogenation exhibited minimal effect on the diffusion profile.[10] Meanwhile, we observed a 16% decrease in the reduction limiting current at carbon fibre microelectrodes after hydrogenation, compared to 20% at conical-tip carbon electrodes after hydrogenation.

	Redox markers								
	$[Ru(NH_3)_6]^{3+}$			$[Fe(CN)_6]^{3-}$			Dopamine		
Electrodes	$E_{1/2}$ / mV	Waveslope / mV decade^{-1}	E_T / mV	$E_{1/2}$ / mV	Waveslope / mV decade^{-1}	E_T / mV	$E_{1/2}$ / mV	Waveslope / mV decade^{-1}	E_T / mV
Bare conical-tip carbon	-171 (15)	60.2 (4.2)	57 (1.8)	160 (11)	153 (39)	198 (29)	237 (30)	136 (22)	140 (20)
Hydrogenated conical-tip	-177 (12)	63.9 (5.6)	63 (3.9)	99.5 (14)	210 (37)	208 (28)	337 (51)	182 (32)	193 (42)
Bare carbon fibre	-160 (20)	49.0 (4.5)	52 (3.9)	250 (14)	52 (6.3)	52 (6.9)	137 (12)	41 (9)	38.8 (9)
Hydrogenated carbon fibre	-164 (20)	46.0 (4.4)	46 (3.8)	251 (17)	60 (9.7)	57 (11)	165 (16)	60 (11)	53.6 (10)

Table 4.1. Summary of electrochemical parameters obtained for the three redox markers at bare and hydrogenated conical-tip carbon and carbon fibre electrodes.

All values in parentheses are standard deviations estimated from seven electrodes.

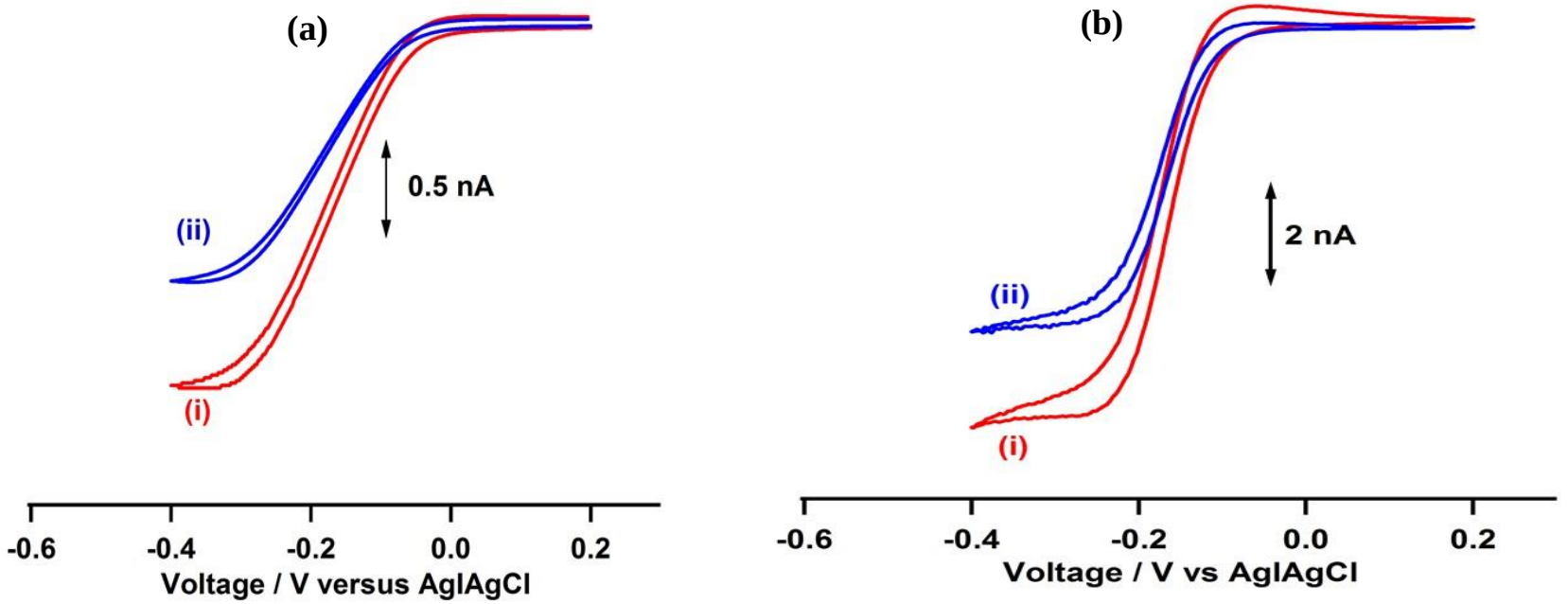

Figure 4.4 Cyclic voltammetry of 1.0 mM $[Ru(NH_3)_6]^{3+}$ at (a) a bare (i) and hydrogenated (ii) conical-tip carbon electrode and (b) a bare (i) and hydrogenated (ii) carbon fibre electrode in 1.0 M KCl. Scan rate: 100 mV s^{-1}.

4.9.1.2 Characterisation of modified electrodes in $[Fe(CN)_6]^{3-}$

Hydrogenated electrodes were next characterised in 1.0 mM $[Fe(CN)_6]^{3-}$ in 1.0 M KCl. In Figure 4.5(a), trace i and trace ii represent the corresponding cyclic voltammogram obtained at a bare and a hydrogenated conical-tip carbon electrode. In contrast to $[Ru(NH_3)_6]^{3+}$, $[Fe(CN)_6]^{3-}$ is an inner sphere complex ion, the reduction of which is very sensitive to monolayer adsorption.[69] As shown in Table 4.1, there is a 60.5 mV negative $E_{1/2}$ shift in the voltammograms obtained at hydrogenated conical-tip carbon electrodes compared to those obtained at the bare counterparts, indicating sluggish kinetics at the former. The measured waveslope also indicates quasi-reversible electron-transfer kinetics for the one electron transfer of $[Fe(CN)_6]^{3-}$ at both bare and hydrogenated electrodes, in agreement with kinetics observed at a diamond electrode surface.[70] The measured E_T also supports quasi-reversible $[Fe(CN)_6]^{3-}$ electron transfer kinetics at both bare and hydrogenated electrodes. However, by examining the corresponding cyclic voltammograms obtained at a carbon fibre electrode in Figure 4.5(b), there was no significant difference in $E_{1/2}$ and waveslope at the carbon fibre electrode before and after hydrogenation. In fact, both the waveslope and E_T support a reversible $[Fe(CN)_6]^{3-}$ reaction at carbon fibre electrodes before and after hydrogenation. Additionally, the electron transfer kinetics of $[Fe(CN)_6]^{3-}$ were reportedly reversible at hydrogen-terminated diamond surface with a redox peak potential separation (ΔE_p) of 64 mV, which is almost half of that obtained at an oxygen-terminated diamond surface.[71] After electrochemical hydrogenation of diamond electrodes, Yang *et al.*[72] also found accelerated electron transfer kinetics of $[Fe(CN)_6]^{3-}$ as indicated by a ΔE_p of 90 mV, compared to 480 mV at oxygenated electrodes, indicating that $[Fe(CN)_6]^{3-}$ is not catalysed by surface oxides on an electrode and the reduction of O/C ratio has also minor effects on the reduction potential of $[Fe(CN)_6]^{3-}$.[69] Ji *et al.*[73] demonstrated that oxygenated species at edge plane sites may decrease the electron transfer kinetics of $[Fe(CN)_6]^{3-}$ at the electrodes. As the oxide functional groups were removed from the electrode surface after hydrogenation in our work, the

C-H surface termination might not exhibit any effect on $[Fe(CN)_6]^{3-}$ kinetics. Instead, as the kinetics of $[Fe(CN)_6]^{3-}$ are sensitive to monolayer adsorption[69], we propose that the butylsiloxane layer formed on electrode surface has predominantly affected the process and therefore the resultant hydrophobic surface may not be suitable for electron transfer reaction for such a polar analyte as $[Fe(CN)_6]^{3-}$. The reduction limiting current of 1.0 mM $[Fe(CN)_6]^{3-}$ at hydrogenated conical-tip carbon electrodes was diminished by 39% relative to bare electrodes, compared to 24% at carbon fibre electrodes. Previously, plasma hydrogenated conical-tip carbon electrodes demonstrated a 39% reduction limiting current of 1.0 mM $[Fe(CN)_6]^{3-}$.[50]

4.9.1.3 Characterisation of modified electrodes in dopamine

Next, all electrodes were characterised in 1.0 mM of dopamine, a surface sensitive/inner sphere redox marker, in pH 7.4 citrate/phosphate buffer. The results obtained at conical-tip electrodes and carbon fibre electrodes are shown in Figure 4.6(a) and Figure 4.6(b), respectively. As tabulated in Table 4.1, the $E_{1/2}$ of dopamine voltammograms at bare and hydrogenated conical-tip carbon electrodes are comparable to those at carbon fibre electrodes. These results are also in good agreement with 421 mV obtained at diamond microelectrodes at a scan rate of 20 mV s^{-1}.[74] $E_{1/2}$ of dopamine oxidation has positively shifted by 100 mV at hydrogenated conical tip carbon electrodes, and by 28 mV at hydrogenated carbon fibre electrodes. The waveslopes in Table 4.1 indicate that the reaction of dopamine at both bare and hydrogenated conical tip carbon electrodes is irreversible. E_T at bare and hydrogenated electrodes also supports an irreversible dopamine oxidation at these electrodes. Previously, Wang *et al.*[71] reported that dopamine redox system was electrochemically more irreversible at nanocrystalline diamond thin-film electrodes (500 mV ΔE_p) than at carbon electrodes (125-175 mV ΔE_p). However, the waveslope and E_T at bare and hydrogenated carbon fibre electrodes suggest a quasi-reversible dopamine electron transfer reaction. A 15%

decrease in oxidation current and also the reduced electron transfer kinetics of dopamine were attributed to the absence of ionisable carbon-oxygen functional groups on a hydrogenated surface that facilitate dopamine oxidation at the electrode surface.[70] We also observed a similar trend at plasma hydrogenated electrodes that exhibited an 18% loss in oxidation current.[50] Moreover, the alkyl chain of butylsilyl group formed during hydrogenation might also contribute to reducing the electron transfer kinetics due to the hindrance of carbon chains on an electrode surface, as described by Chen *et al*[75]. In their work, the oxidation peak potential of dopamine shifted positively from 170 mV to 300 mV after modifying gold electrodes by 3-marcaptopropylphosphonic acid accompanied by a ~20% decrease in the dopamine oxidation peak current, attributable to a hindrance by the carbon chains of the organic acid. Kuo *et al.*[76] also reported the decelerated kinetics of dopamine in the presence of a nitrophenyl monolayer on a glassy carbon electrode surface.

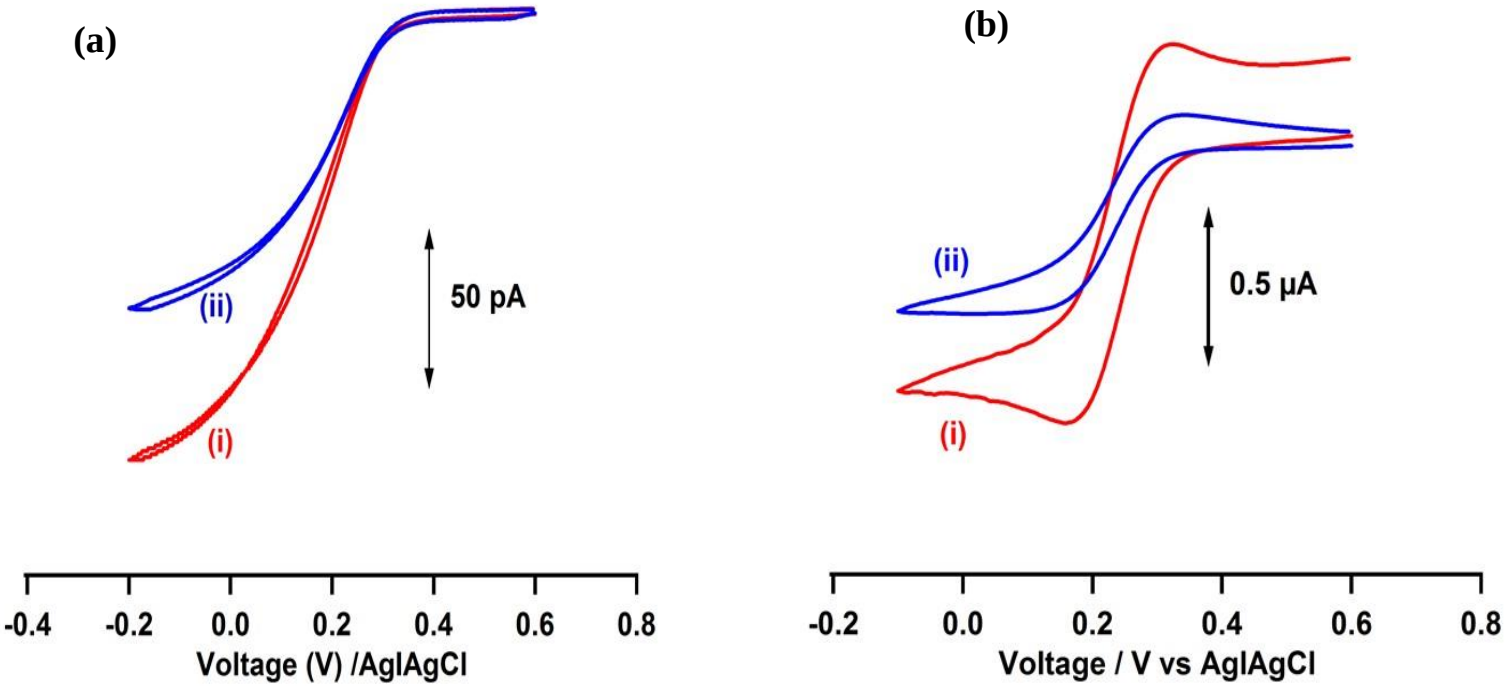

Figure 4.5 Cyclic voltammetry of 1.0 mM $[Fe(CN)_6]^{3-}$ at (a) a bare (i) and a hydrogenated (ii) conical-tip carbon electrode and (b) a bare (i) and a hydrogenated (ii) carbon fibre electrode in 1.0 M KCl. Scan rate: 100 mV s^{-1}.

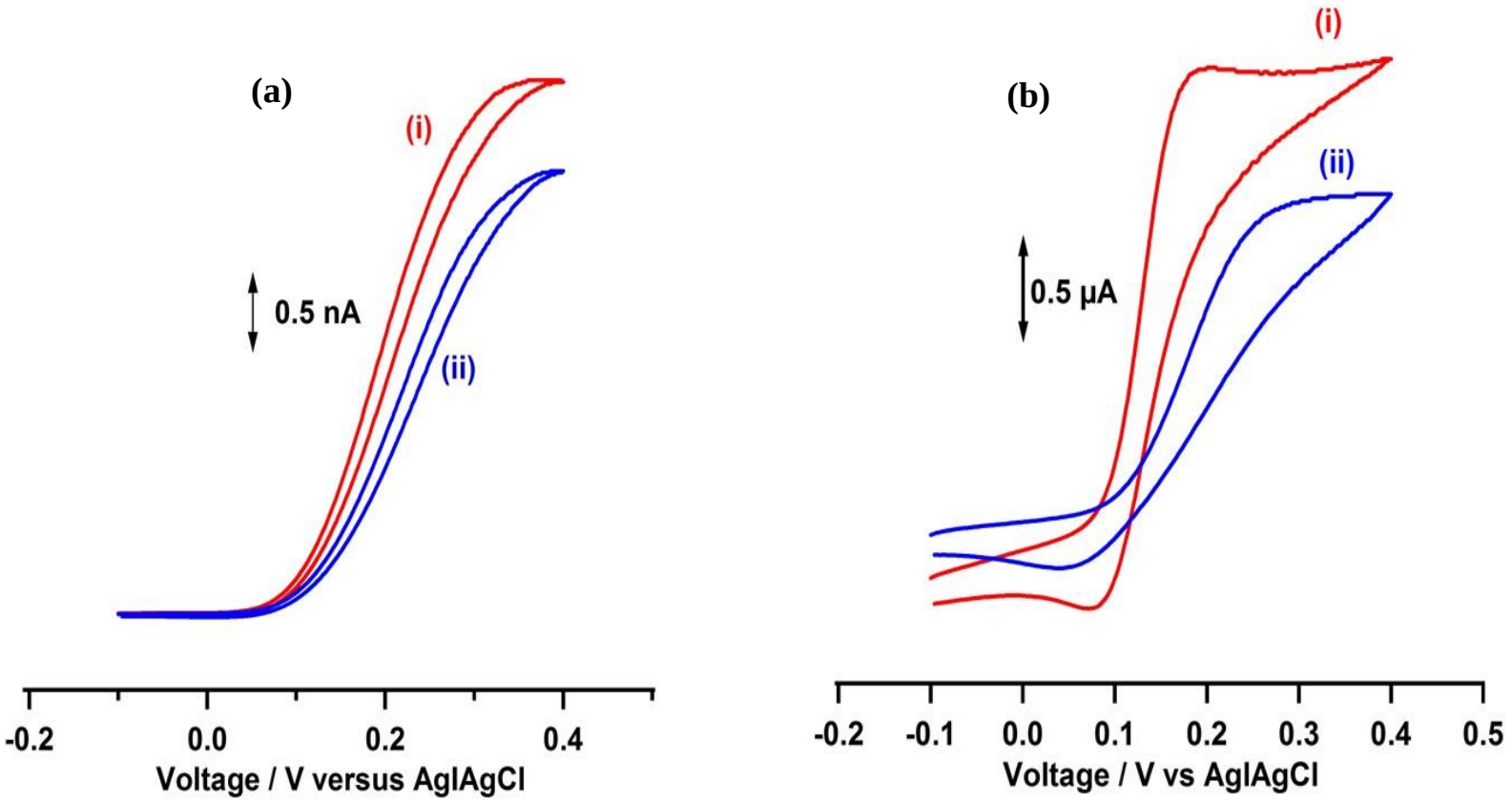

Figure 4.6 Cyclic voltammetry of 1.0 mM dopamine at (a) a bare (i) and a hydrogenated (ii) conical-tip carbon electrode and (b) a bare (i) and a hydrogenated (ii) carbon fibre electrode in pH 7.4 citrate/phosphate buffer. Scan rate: 100 mV s^{-1}.

4.9.1.4 Characterisation of hydrogenated electrodes by electrochemical impedance spectroscopy

Electrochemical impedance spectroscopy of $[Ru(NH_3)_6]^{3+}$ at bare and hydrogenated conical-tip carbon electrodes was employed to investigate the interfacial impedance changes at the electrodes. A representative Nyquist plot of 1.0 mM $[Ru(NH_3)_6]^{3+}$ obtained at $E_{1/2}$ of +0.2 V at a bare electrode is shown in Figure 4.7(a), where a semicircle in the high frequency region and a linear segment in the low frequency region are observed. The diameter of the semicircle corresponds to the electron transfer resistance (R_{ct}) of $[Ru(NH_3)_6]^{3+}$ at the electrode interface, while the linear segment corresponds to the capacitive behaviour of the finite thickness diffusion process.[77,78] Very often, the electrical property of an electrode/solution interface is represented by a Randles equivalent circuit shown in the inset of Figure 4.7(a). This equivalent circuit consists of an electrolyte solution resistance (R_s) in a series arrangement with a constant phase element (CPE; which incorporates the Helmholtz double layer and surface roughness or heterogeneity of the electrode), which is in turn in a parallel arrangement with R_{ct} of the redox probe and a Warburg impedance (Z_w). Z_w generally arises from the diffusion of ions from the bulk of the electrolyte to the interface. Notably, both R_s and Z_w are independent of the electrode surface modification[79]. In general, theoretically generated Nyquist plots produced by manipulating R_{ct} and CPE of such an equivalent circuit are repeatedly compared to an experimental Nyquist plot until a satisfactory fit (estimated error <10%) is obtained. The equivalent circuit can then be used to describe the electrode/solution interface. In this way, the R_{ct}, R_s, Z_w and C_{dl} were estimated at the bare carbon electrode and their values are tabulated in Table 4.2.

At the hydrogenated conical-tip carbon electrodes, two semicircles were observed in the Nyquist plot, as shown in Figure 4.7(b). A corresponding equivalent circuit, consisting of similar elements present in the inset of Figure 4.7(a) and an additional resistance (R_c) in parallel with a double layer capacitance (C_{dl}), was found to be necessary to generate

the most satisfactory Nyquist plot compared to the experimental Nyquist plot, as depicted in Figure 4.7(b).[80,81] In this circuit, R_c denotes the resistance of a film on an electrode, such as the butysiloxane polymer film on a hydrogenated conical-tip carbon electrode. Accordingly, the diameter of the first semicircle in Figure 4.7(b) represents the coating resistance originated from butylsiloxane group and that of the second semicircle represents R_{ct}.[81,82,83] The fitted parameters are presented in Table 4.2. In this study, we observed a three-fold increase in R_{ct} at the hydrogenated electrode relative to that at the bare electrode due to reduced electron transfer kinetics caused by H-termination and butylsiloxane layer formed on the modified electrode surface during hydrogenation. Notably, compared to that at a bare electrode, we found it necessary to include an R_c of 0.62 kΩ in fitting the Nyquist plot obtained at the hydrogenated electrode.

As expected, R_s in the Nyquist plot obtained at the bare electrode remained unchanged after hydrogenation. However, the Warburg element at the hydrogenated electrode was halved compared to that obtained at the bare electrode. Similar trend was also observed at an electrochemically or a photocatalytically reduced graphene modified glassy carbon electrode compared to a graphene oxide modified glassy carbon electrode when C-OH, C-O, C=O, and O-C=O functional groups were absent on the reduced electrode surface.[84] The double layer capacitance at a hydrogenated electrode was found to be half of that at a bare electrode. A significant reduction of capacitance after *n*-butylsilane hydrogenation was also observed, as explained in Section 3.6.3.

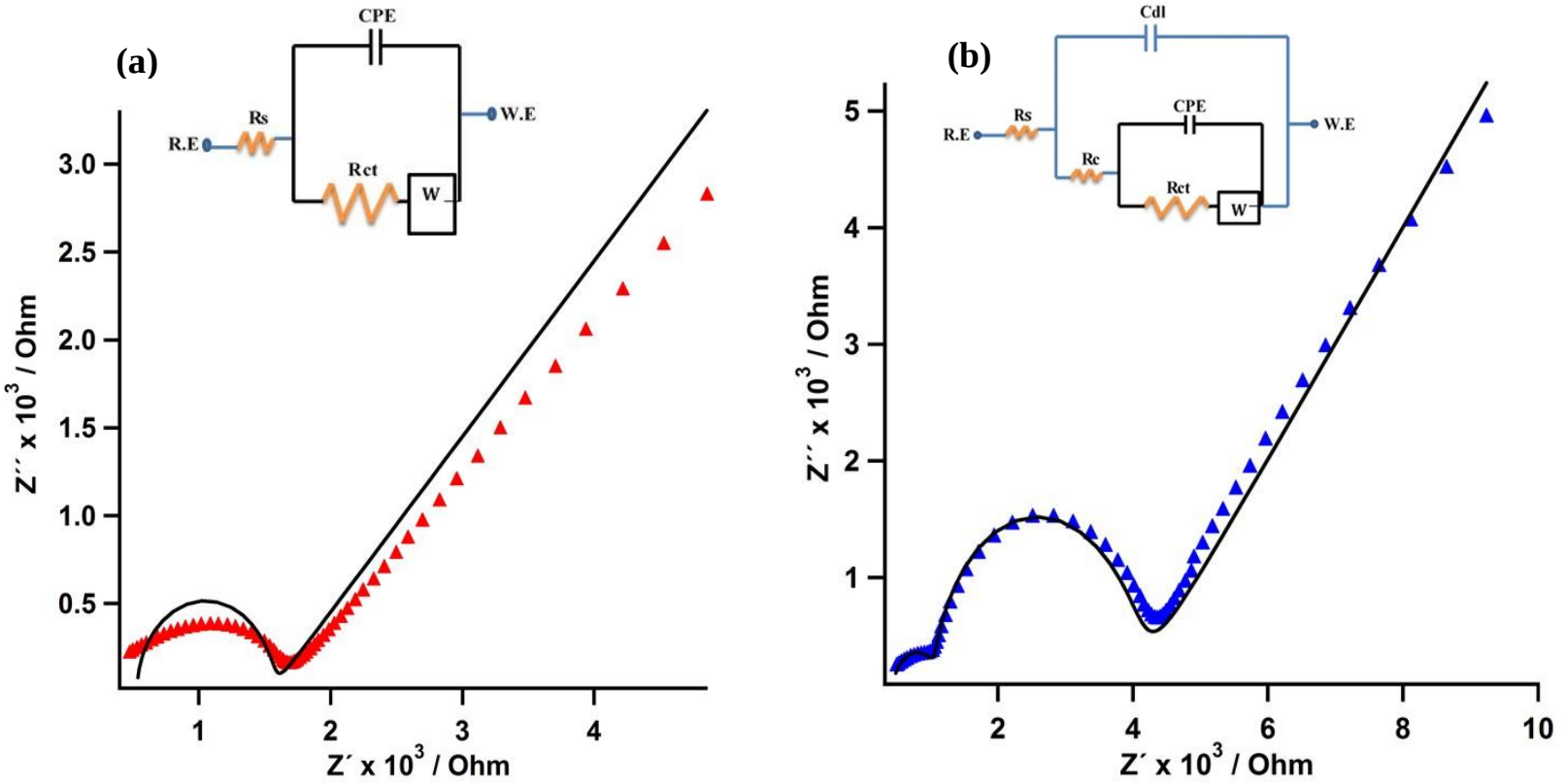

Figure 4.7 (a) Nyquist plot for 1.0 mM $[Ru(NH_3)_6]^{3+}$ obtained at 0.2 V at a bare and (b) a hydrogenated conical-tip carbon electrode in 1.0 M KCl supporting electrolyte. Frequency range is 100 kHz – 0.1 Hz with 10 mV wave potential amplitude. Inset (a) A Randles equivalent circuit model representing a bare carbon electrode-solution interface, (b) A modified Randles equivalent circuit model representing a hydrogenated carbon electrode-solution interface. Solid lines (–) correspond to the fittings of the experimental data.

Electrode	R_{ct} / kΩ	R_c / kΩ	R_s / kΩ	Z_w / kΩ	C_{dl} / nF
Bare carbon	0.985	—	0.622	2.69×10^{-4}	19.4
	(0.50)		(0.16)	(0.98×10^{-4})	(6.2)
Hydrogenated carbon	2.90	0.615	0.651	1.30×10^{-4}	9.33
	(1.20)	(0.31)	(0.25)	(0.60×10^{-4})	(2.6)

Table 4.2 EIS parameters estimated from Nyquist plots of $[Ru(NH_3)_6]^{3+}$at a bare and a hydrogenated electrode.

All values in parentheses are standard deviations estimated from seven electrodes for EIS parameters.

4.9.2 Characterisation of electrodes by atomic force microscopy

Surface flatness has previously been reported to contribute to electrode surface resistance against adsorption of biomolecules[51-52]. A smooth hydrophobic nano-carbon film surface was reported to be more resistant to fouling compared to a diamond-like carbon electrode[52]. In our work, the surface morphology of bare and hydrogenated electrodes was investigated using atomic force microscopy and the micrographs obtained are depicted in Figure 4.8. Based on the feature heights of the carbon formations on the quartz surface shown in Figure 4.8(a), the roughness of the carbon deposit, was estimated to be 500 nm[50]. After hydrogenating the same electrode, the feature heights in Figure 4.8(b) were estimated to be 300 nm, indicating a ~50% decrease in surface roughness (N=5). This compared to a corresponding 90% decrease in surface roughness at electrodes hydrogenated by plasma chemical vapour deposition previously reported by our group. This indicates a flatter electrode surface after hydrogenation relative to bare electrodes. This observation can be explained by the presence of coarse hillocks in Figure 4.8(a), which became fine and smoother after hydrogenation as observed in Figure 4.8(b), in agreement with observation reported by

Rezek and Nevel[85] on a plasma hydrogenated diamond surface. A strip developed on the surface is an indication of morphological distortion at edge plane sites of electrode by hydrogen chemisorption, as suggested by Chen and Swain[86] who hydrogenated a glassy carbon electrode using hydrogen microwave plasma. Similarly, an organosilane modified silicon substrate was also found to be smoother compared to that before modification[87] and hydrogenated diamond-like carbon films were described as smooth and compact[88]. In our work, butylsiloxanes probably formed a monolayer that filled the cracks on electrode surface and yielded a smoother electrode surface.

4.9.3 Raman spectroscopy

Raman spectroscopy is a useful, non-destructive tool for examining carbonaceous materials, particularly in distinguishing ordered and disordered carbon structures. In the Raman spectrum of a carbon material, two peaks are commonly observed, (i) a commonly known D peak that arises from sp^3-hybridised carbon and is associated with the structural defects or partially disordered structures of graphite domains, and (ii) a G peak representing the E_{2g} zone centre mode of the crystalline graphite.[89,90,91] For amorphous carbon, the peak widths of the D and G peaks are generally broader and the relative intensity of the sp^3 peak to the sp^2 G peak is often used as a qualitative assessment of the diamond material.[92] In addition, the relative intensity of the D peak to G peak (I_D / I_G) is proportional to the number of defective sites in graphite.[93]

The *n*-butylsilane hydrogenation is known for its capability in converting sp^2 C–O functionalities to sp^3 C–H and derivatising phenolic hydroxyl groups to butylsiloxane dendrimers, as illustrated in Scheme 3.1. Accordingly, after hydrogenation a higher sp^3-to-sp^2 content is expected. In this work, Raman spectroscopy was conducted using both bare and hydrogenated electrodes and the results obtained are shown in Figure 4.9(a) and 4.9(b), respectively. As expected, both the D and G bands are clearly

identified in the spectrum obtained at the bare electrode at 1368 cm^{-1} and 1592 cm^{-1}, respectively. In the corresponding spectrum obtained at the hydrogenated electrode, both peaks were still present but they have shifted to 1349 cm^{-1} and 1582 cm^{-1}, respectively. Indeed, a hydrogenated amorphous carbon film was previously reported to cause a slight downshift in the wavenumber of the D and G bands and this downward shift in the D band was proportional to the increase in the sp^3 / sp^2 ratio in the films.[94]

In our work, the peak area under each peak was evaluated to determine the corresponding intensity, I_D and I_G, and hence the I_D / I_G ratio for the electrodes. As tabulated in Table 4.3, the Gaussian-fitted I_D / I_G ratio at a bare electrode was estimated to be 3.82, but this ratio was improved to 4.72 at the hydrogenated electrode. Similarly, Lian *et. al*.[95] obtained an I_D / I_G ratio of 0.982 at a graphene surface and 1.13 at tryptophan modified graphene. They attributed this to an increase in the number of sp^3 carbon on the tryptophan modified graphene. In work reported by Yu *et al*.[90], the I_D / I_G was determined to be 0.72 at a graphene oxide surface, which increased to 1.28 at the corresponding electrochemically reduced graphene oxide surface. These authors explained that the oxidised areas of a graphene sheet were partly restored upon reduction to form small conjugated domains. Accordingly, the spectra and the associated results in Table 4.3 strongly indicate a change in the surface characteristic of the conical-tip carbon electrodes after hydrogenation, and the increased I_D / I_G and downshifting of the peaks supported the enrichment of sp^3 carbon at the hydrogenated surface.

Electrode type	Peak position / cm^{-1}	I_D / I_G
Bare carbon	1368 (D) 1592 (G)	3.82
Hydrogenated carbon	1349 (D) 1582 (G)	4.72

Table 4.3 I_D / I_G ratio estimated based on Gaussian fitted Raman spectra shown in Figure 4.9(a) and Figure 4.9(b).

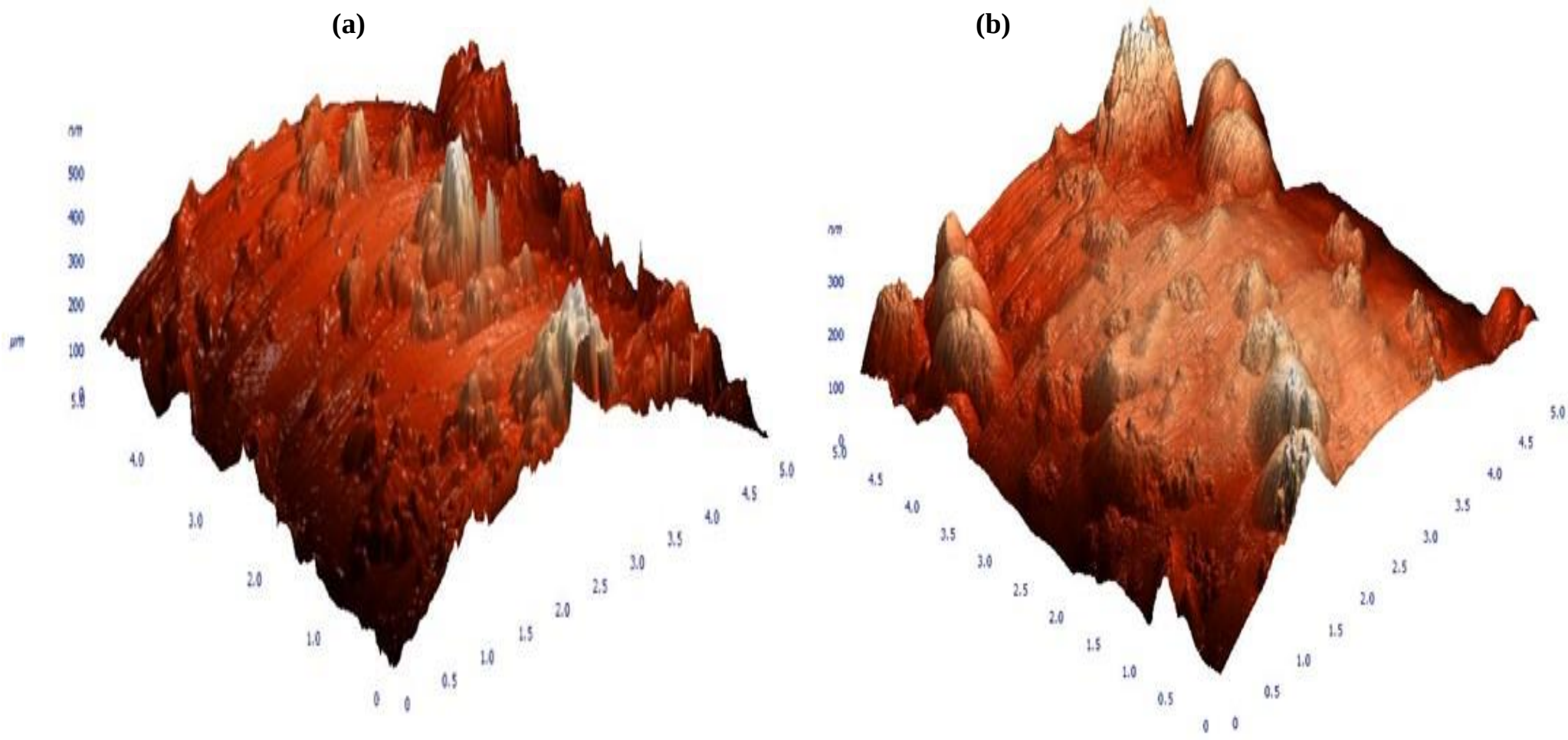

Figure 4.8 Atomic force micrographs of (a) a bare and (b) a hydrogenated conical-tip carbon electrode.

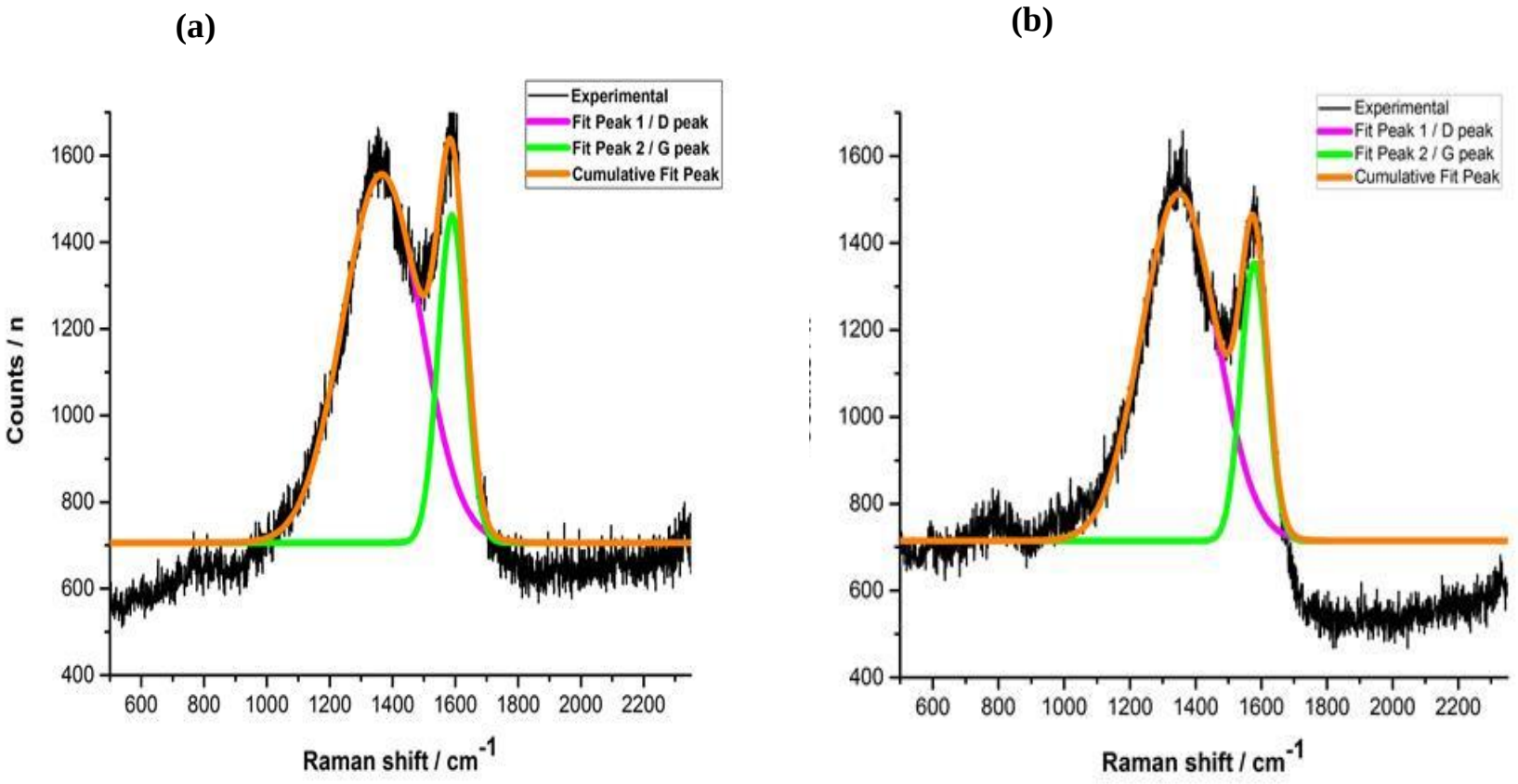

Figure 4.9 Raman spectra of (a) a bare conical-tip carbon and (b) a hydrogenated conical-tip carbon electrode.

4.9.4 Detection of dopamine and ascorbic acid at bare and hydrogenated carbon electrodes

Ascorbic acid is a well-known interfering species in dopamine detection owing to their co-existence in the central nervous system with a relatively high concentration of ascorbic acid at 100-500 μM[96] compared to dopamine at 0.01-1 μM dopamine[97]. Their similar oxidation potentials at ~0.198 V for dopamine and ~0.172 V for ascorbic acid and comparable sensitivity make the selective detection of dopamine in the presence of ascorbic acid at bare carbon electrodes very challenging. Thus, there have been a lot of attempts in modifying bare carbon electrodes to selectively determine dopamine in the presence of ascorbic acid.

In this study, we have conducted differential pulse voltammetry of 20 μM dopamine and 500 μM ascorbic acid in pH 7.4 citrate/phosphate buffer at a bare conical-tip carbon electrode and a corresponding hydrogenated electrode. Notably, the ascorbic acid concentration represents the typical ascorbic acid concentration found in extracellular fluid. 20 μM of dopamine concentration was chosen to obtain a reasonable dopamine oxidation peak at bare electrode with minimum noise so that the peak can be easily compared to that at electrode after hydrogenation. The results are shown in Figure 4.10(a) and 4.10(b). At the bare electrode, the voltammogram of dopamine (trace i, Figure 4.10(a)) displayed a peak at 0.120 V, while that of ascorbic acid (trace i, Figure 4.10(b)) displayed a peak at 0.185 V. As expected, at the hydrogenated carbon electrode, the dopamine oxidation peak current was reduced by 50% compared to that observed at the bare electrode due to reduced electrostatic attraction of dopamine as described in Section 4.9.1.3. Meanwhile, the hydrogenated electrode surface blocked ascorbic acid and completely suppressed the ascorbic acid oxidation, as shown by trace ii in Figure 4.10(b). At physiological pH of 7.4, with a pKa of 4.10, ascorbic acid exists as a negatively charged compound in extracellular fluid.[98] This suggests that the anionic ascorbate might not be favourable at the H-terminated hydrophobic surface for

electron transfer reaction. On the other hand, with its phenyl moiety, dopamine may have relied on hydrophobic-hydrophobic interaction for participating in an electron transfer reaction.

In another experiment, the dopamine concentration was kept constant at 100 μM, while the ascorbate-to-dopamine concentration ratio was either increased from 1 to 5 (*i.e.*, the ascorbate concentration > the dopamine concentration) or decreased from 1 to 0 (*i.e.*, the ascorbate concentration < the dopamine concentration). The corresponding differential pulse voltammograms obtained at a bare and a hydrogenated conical-tip carbon electrode are depicted in Figure 4.11 and 4.12. At the bare carbon electrode, the voltammograms in Figure 4.11(A) and Figure 4.11(B) showed that the dopamine oxidation peak increased with concentration of ascorbate in either option of the concentration ratio. However, the voltammograms obtained at the hydrogenated carbon electrode, depicted in Figure 4.12, showed that the dopamine oxidation peak increased when the ascorbate concentration was less than that of dopamine (Figure 4.12(A)) but there was no noticeable change in the dopamine oxidation peak when the ascorbate concentration was higher than dopamine concentration (Figure 4.12(B)). We have also plotted the relationship between the dopamine oxidation peak current and ascorbate concentration at both the bare and hydrogenated electrodes in Figure 4.11(C) and 4.12(C). The results indicate that the dopamine oxidation peak current increased with ascorbate concentration at the bare carbon electrode (Figure 4.11(C)). On the other hand, the voltammograms obtained at the hydrogenated electrode showed that the dopamine oxidation peak current increased with ascorbate concentration, which then plateaued off when equal dopamine and ascorbate concentration was reached (Figure 4.12(C)).

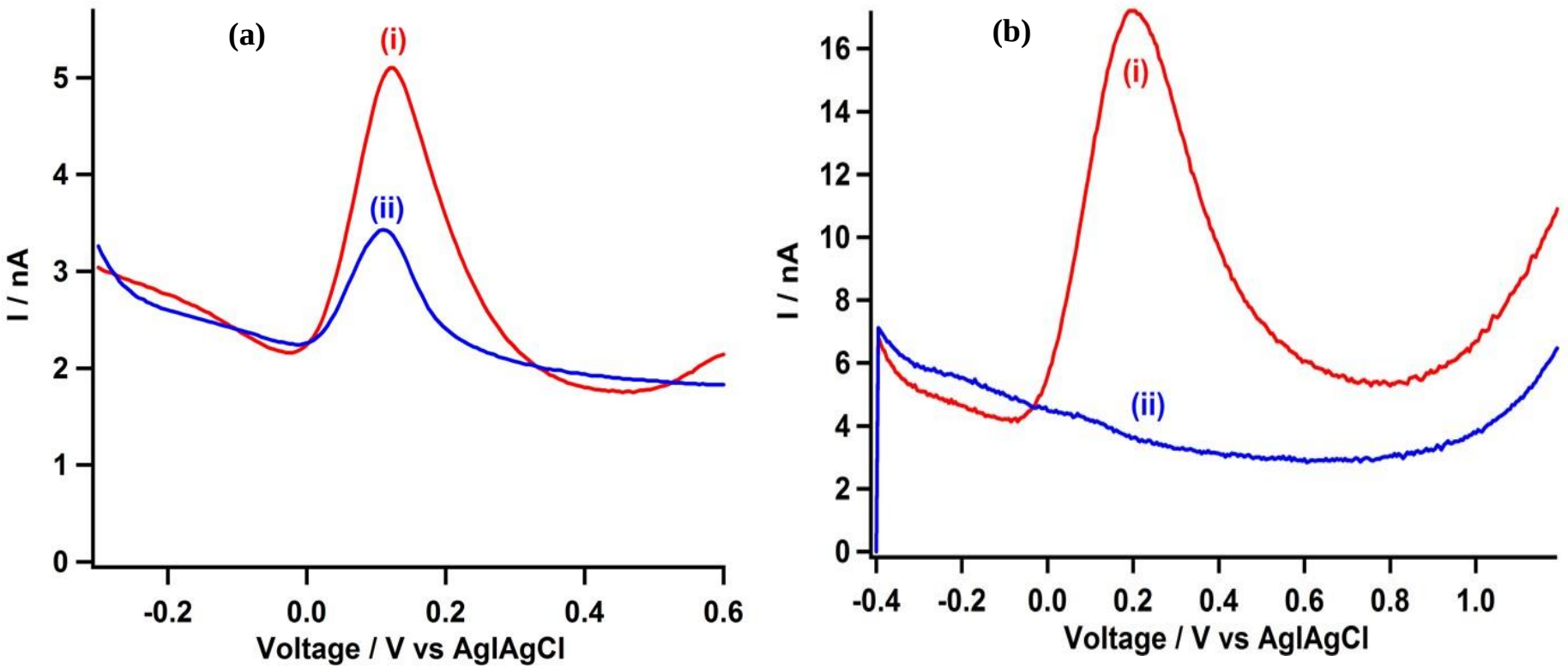

Figure 4.10. Differential pulse voltammogram of 20 µM dopamine (a) and 500 µM ascorbate (b) at a bare (i) and a hydrogenated electrode (ii). Scan rate: 20 mV s^{-1}.

In these experiments, ascorbate was not expected to be capable of penetrating through the butylsiloxane layer. In addition, the H–terminated electrode would have also discouraged the access of ascorbate to the electrode surface. However, ascorbate would still be able to chemically reduce the dopamine oxidation product, dopamine-*o*-quinone, back to dopamine outside the butylsiloxane film, leading to additional dopamine readily available for oxidation in close proximity of the electrode and yielded increased dopamine oxidation current than expected.[99,100] The electro-reduction of dopamine-*o*-quinone by ascorbate back to dopamine only occurred up to a certain 1:1 concentration can be attributed to the diffusion pattern of dopamine-*o*-quinone and ascorbate to the electrode surface and/or near to the butylsiloxane layer. When the ascorbate concentration was lower than that of dopamine or dopamine-*o*-quinone, the limiting current was controlled by the diffusion of ascorbate. This explains the fact that the dopamine oxidation peak current increased as a function of ascorbate concentration when the ascorbate concentration was lower than that of dopamine. However, when the ascorbate concentration was higher than that of dopamine, the quantity of dopamine-*o*-quinone produced would be lower than the ascorbate concentration and the electrocatalytic current was then limited by dopamine. Hence, the electrocatalytic current reached a plateau at a unity ascorbate-to-dopamine concentration ratio as shown in our results. Similar findings were previously demonstrated by Xiao *et al.*,[100] who modified a gold electrode by 11-mercaptoundecanoic acid, further derivatised by polyethylene glycol and was employed for detection of dopamine in the presence of ascorbate.

From the above results, we have concluded that *n*-butylsilane hydrogenated conical-tip carbon electrodes are capable of detecting dopamine while they completely blocked the ascorbate oxidation. We have also demonstrated that there was no change in dopamine oxidation current detected in the presence of ascorbate when the latter concentration was higher than that of dopamine.

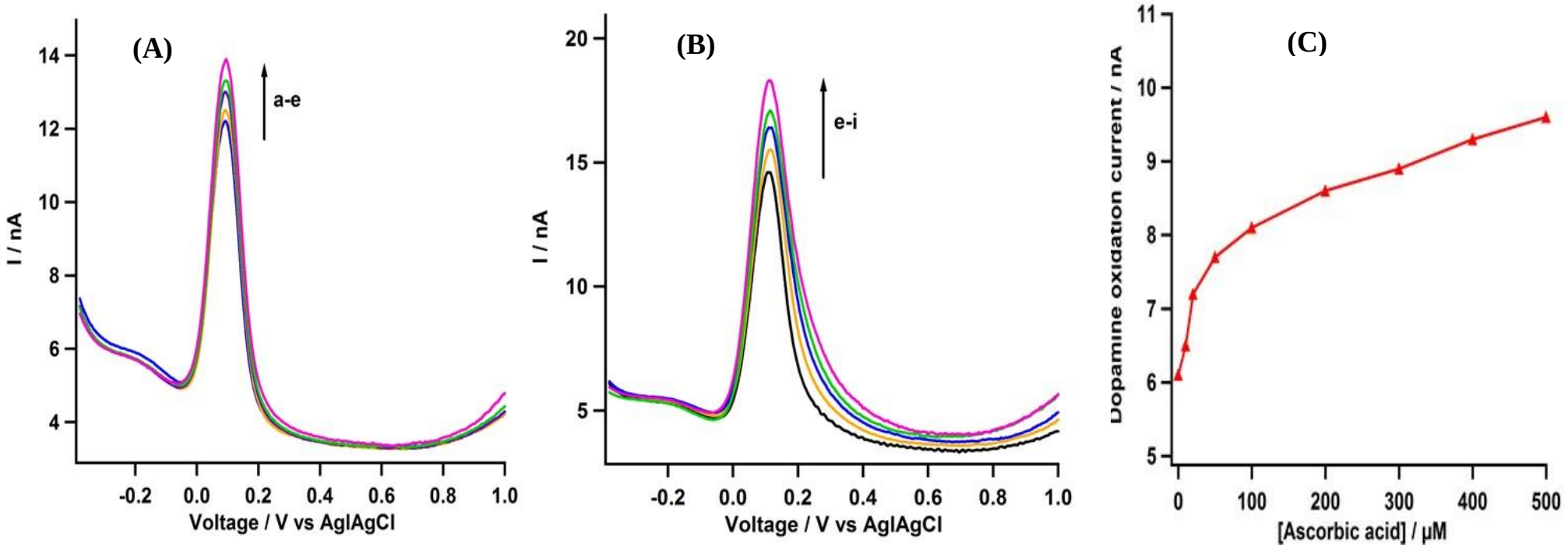

Figure 4.11 Differential pulse voltammogram of dopamine at bare electrode in citrate/phosphate buffer with different ascorbate:dopamine ratio of (A) (a) 0:1; (b) 0.1:1; (c) 0.2:1; (d) 0.5:1; (e) 1:1, and (B) (e) 1:1; (f) 2:1; (g) 3:1; (h) 4:1; (i) 5:1. Dopamine concentration was kept constant at 100 µM in (A) and (B). (C) A plot of dopamine oxidation peak current against ascorbate concentration. Scan rate: 20 mV s^{-1}.

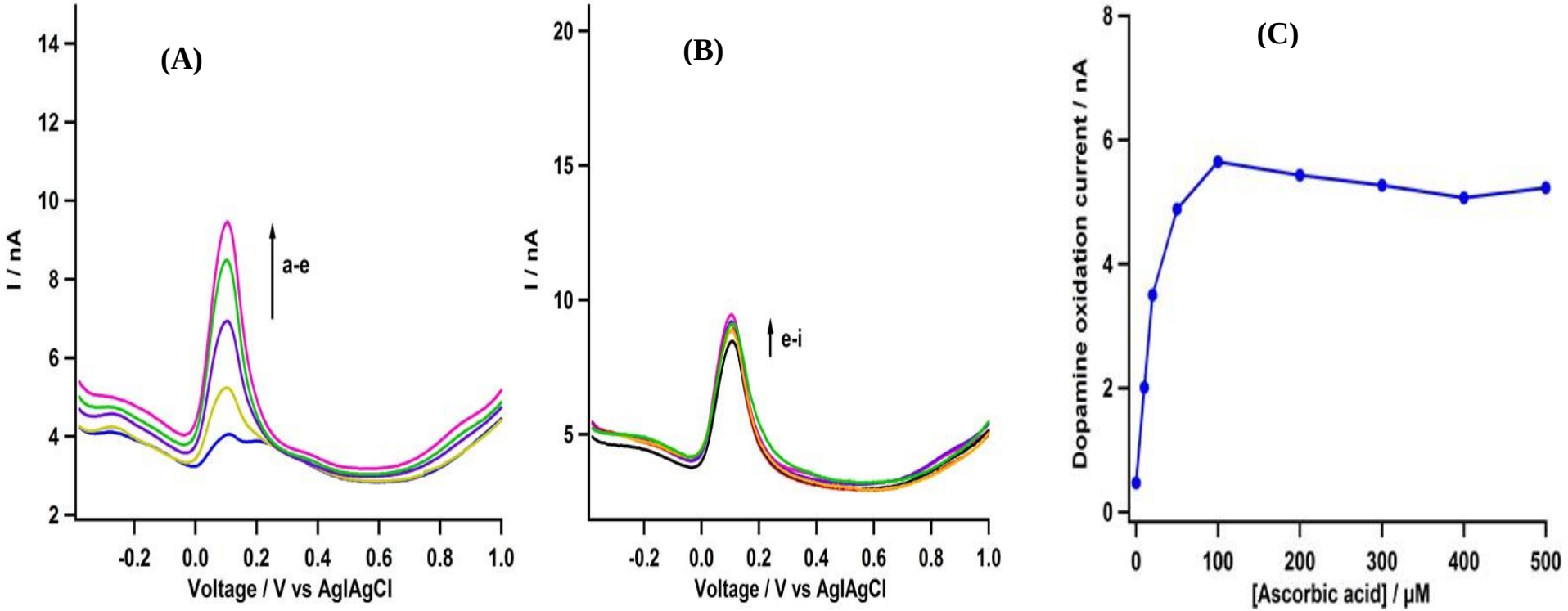

Figure 4.12 Differential pulse voltammogram of dopamine at hydrogenated electrode in citrate/phosphate buffer with different ascorbate:dopamine ratio of (A) (a) 0:1; (b) 0.1:1; (c) 0.2:1; (d) 0.5:1; (e) 1:1, and (B) (e) 1:1; (f) 2:1; (g) 3:1; (h) 4:1; (i) 5:1. Dopamine concentration was kept constant at 100 µM in (A) and (B). (C) A plot of dopamine oxidation peak current against ascorbate concentration. Scan rate: 20 mV s^{-1}.

4.9.5 Electrode Performance in Solutions Containing Fouling Agents

As discussed in Section 4.4, amphiphilic, high-molecular-weight entities present in extracellular fluid can often adsorb on the surface of an implanted sensor and severely affect the analytical characteristics of a technique or a sensor and thus compromise its sensitivity, detection limit, reproducibility, and overall reliability. In general, proteins are known[101] to occupy ~0.05% (maximum 45 mg/dL) of the cerebrospinal fluid, which is in direct communication with the extracellular fluid. Therefore, protein is the most common agent responsible for electrode fouling. In this work, a laboratory synthetic solution consisting of 4% (w/v) bovine serum albumin, 0.01% (w/v) cytochrome *c* (both are proteins), 1.0% (v/v) caproic acid (a lipid), and 0.002% (w/v) human fibrinopeptide B (a peptide) was prepared to mimic a solution with several major bio-fouling components. The two proteins were chosen as bovine serum albumin (isoelectric point of 4.8) exist as an anion and cytochrome *c* (isoelectric point of 10.0) as a cation at physiological pH 7.4.[102] In addition to large proteins with numerous residues, the short peptide caproic acid with only a few residues was also included in the fouling solution as such a peptide is also known to significantly foul an electrode surface[103]. The lipid fibrinopeptide B is added as it is known to be an integral part of cells.

All cyclic voltammograms of 1.0 mM dopamine obtained in the experiment involving the laboratory synthetic fouling solution are shown in Figure 4.13. Here, trace (i), Figure 4.13(a) represents the cyclic voltammogram at a hydrogenated conical-tip carbon electrode. During cyclic voltammetric detection of 1.0 mM dopamine at hydrogenated electrodes in the presence of laboratory synthetic fouling solution is shown in trace (ii), Figure 4.13(a), the dopamine oxidation limiting current decreased by ~35% (SD 12%, N=8).

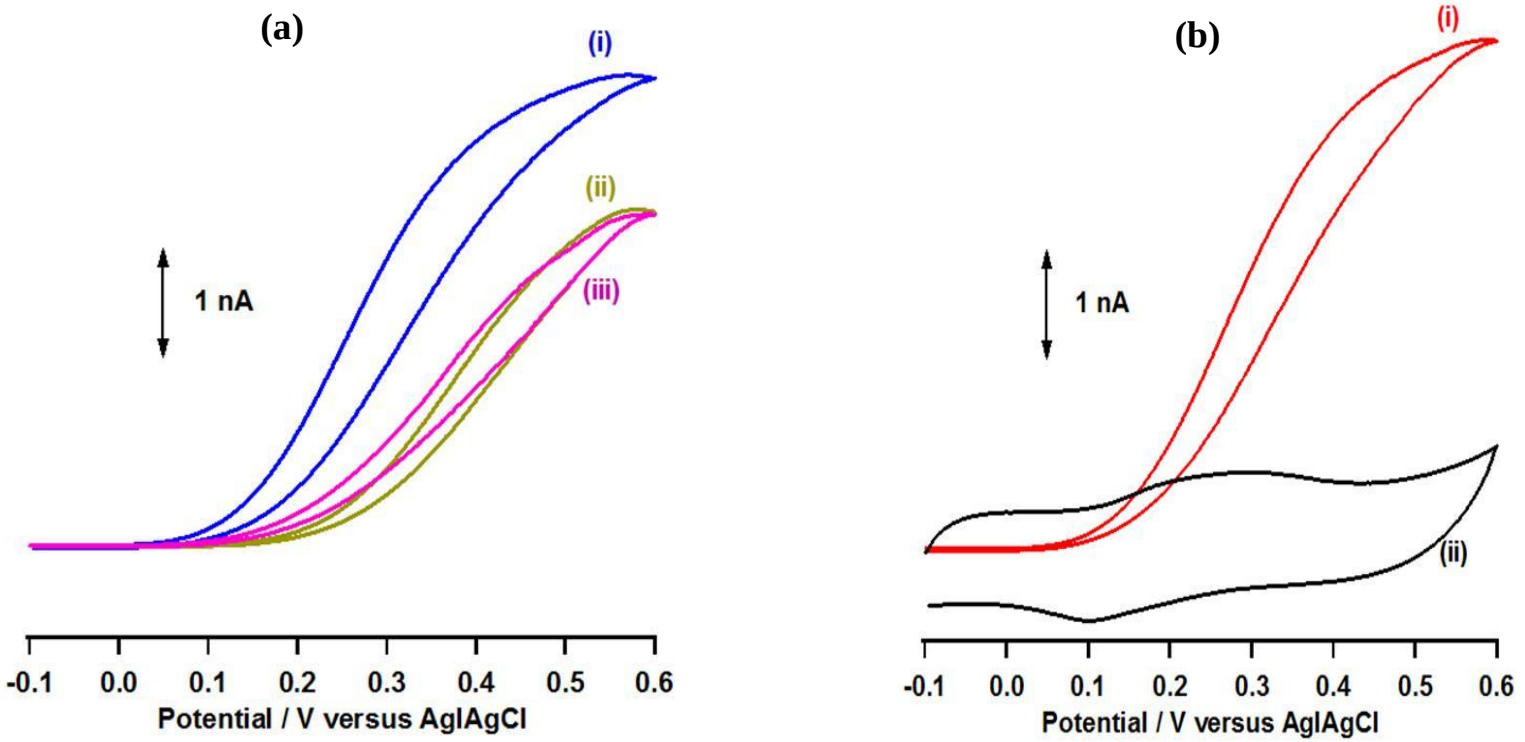

Figure 4.13 Cyclic voltammetry of 1 mM dopamine at (a) trace (i) a hydrogenated electrode; trace (ii) a hydrogenated electrode after incubation in the fouling solution for 30 min; (iii) a hydrogenated electrode after incubation in the fouling solution for 1 week; and (b) trace (i) a bare electrode; trace (ii) a bare electrode after incubation in the fouling solution for 30 min. Scan rate: 100 mV s^{-1}.

The positive $E_{1/2}$ shift of dopamine oxidation from 0.27 V at the hydrogenated carbon electrode (trace i, Figure 4.13(a)) to 0.39 V at the corresponding hydrogenated carbon electrode (trace (ii), Figure 4.13(a)) incubated in fouling solution also indicates more sluggish dopamine electrode kinetics, most likely arisen from a range of electrode fouling after they were incubated in the fouling solution for 30 min. However, based on cyclic voltammograms of dopamine (trace (iii), Figure 4.13(a)) obtained after incubating these electrodes for one week, there was no noticeable change in $E_{1/2}$ and the limiting current measured. In contrast, a featureless dopamine oxidation cyclic voltammogram with high charging current, shown in trace (ii), Figure 4.13(b), was obtained at the bare carbon electrode trace (i), Figure 4.13(b), indicating severe fouling at the electrode.

Electrochemical impedance spectroscopy was also performed to gain an understanding of the interfacial characteristics of the electrode surface during the fouling process. These experiments were conducted at both bare and hydrogenated conical-tip carbon electrodes in the presence of 1.0 mM $[Ru(NH_3)_6]^{3+}$ in 1.0 M KCl. All Nyquist plots were recorded at a DC potential of - 0.2 V, which corresponds to the $E_{1/2}$ of the reduction of $[Ru(NH_3)_6]^{3+}$ in the corresponding cyclic voltammograms. In Figure 4.14(a), trace (i) shows the typical Nyquist plot of a hydrogenated electrode, consisting of two semicircles in the high frequency region, and a linear Warburg impedance in the low frequency region. First semicircle represents *Rc*, the resistance of butylsiloxane film on an electrode, and the second semicircle represents R_{ct}, the charge transfer resistance of the electrode. Trace (ii), Figure 4.14(a) was then recorded after incubating the same hydrogenated electrode in the fouling solution for 30 min. Here, based on the diameter of the semicircle, an R_{ct} of 2.2 kΩ was estimated compared to 1.6 kΩ measured at in trace (i). This increase in R_{ct} is not significantly different compared to that at the hydrogenated electrode before fouling. Trace (iii) shows the Nyquist plot obtained at a hydrogenated carbon electrode that has been incubated in the fouling

solution for 1 week. In this Nyquist plot, R_{ct} remained almost unchanged at 2.2 kΩ. This result also complements the cyclic voltammograms in trace (ii) and (iii) in Figure 4.13(a), where the dopamine oxidation signal initially decreased by 35% after 30 min incubation and remained almost unchanged after 1 week of incubation. In contrast, from the corresponding Nyquist plot shown in Figure 4.14(b), the R_{ct} of $[Ru(NH_3)_6]^{3+}$ at the bare electrode (trace i) has increased 15 times after a 30-min incubation (trace ii) and continued to increase by 45 times after a 1-week incubation (trace iii). We attribute all these results to the formation of an insulating adsorbed layer by the fouling agents that hindered the electron transfer. Similar increase in R_{ct} was observed by Gui *et al.*[102] after incubating a bare glassy carbon electrode and a bare gold electrode in bovine serum albumin for 1 hr.

In other work, Singh *et al.*[104] reported no difference in fouling rate at Nafion coated carbon fibre electrodes that were incubated in bovine serum albumin or implanted in brain tissues for 2 h and overnight, suggesting the majority of fouling occured early in the time course of electrode implantation. Our results above are also in agreement with the suggestion of an initial rapid fouling rate at electrodes as the fouling agents in the solution adsorbed on the surface, followed by a characteristic fouling resistance property. These electrodes then became fouling resistant after the initial rapid fouling period. Notably, the Nyquist plots in Figure 4.14(a) showed similar capacitances were measured at a hydrogenated carbon electrode before (694 nF cm^{-2}) and after (662 nF cm^{-2}) being incubated in the fouling solution for 1 week, indicating non-significant adsorption of fouling agent at the electrode surface[105]. Trouillon *et al.*[105] also measured similarly low capacitances at a boron doped diamond electrode before (452 nF cm^{-2}) and after (551 nF cm^{-2}) incubation in albumin. In contrast, capacitance at bare electrode (trace (i) in Figure 4.13(b)) increased significantly, as can be observed qualitatively in trace (ii) in Figure 4.13(b), due to non-specific adsorption of fouling agents.

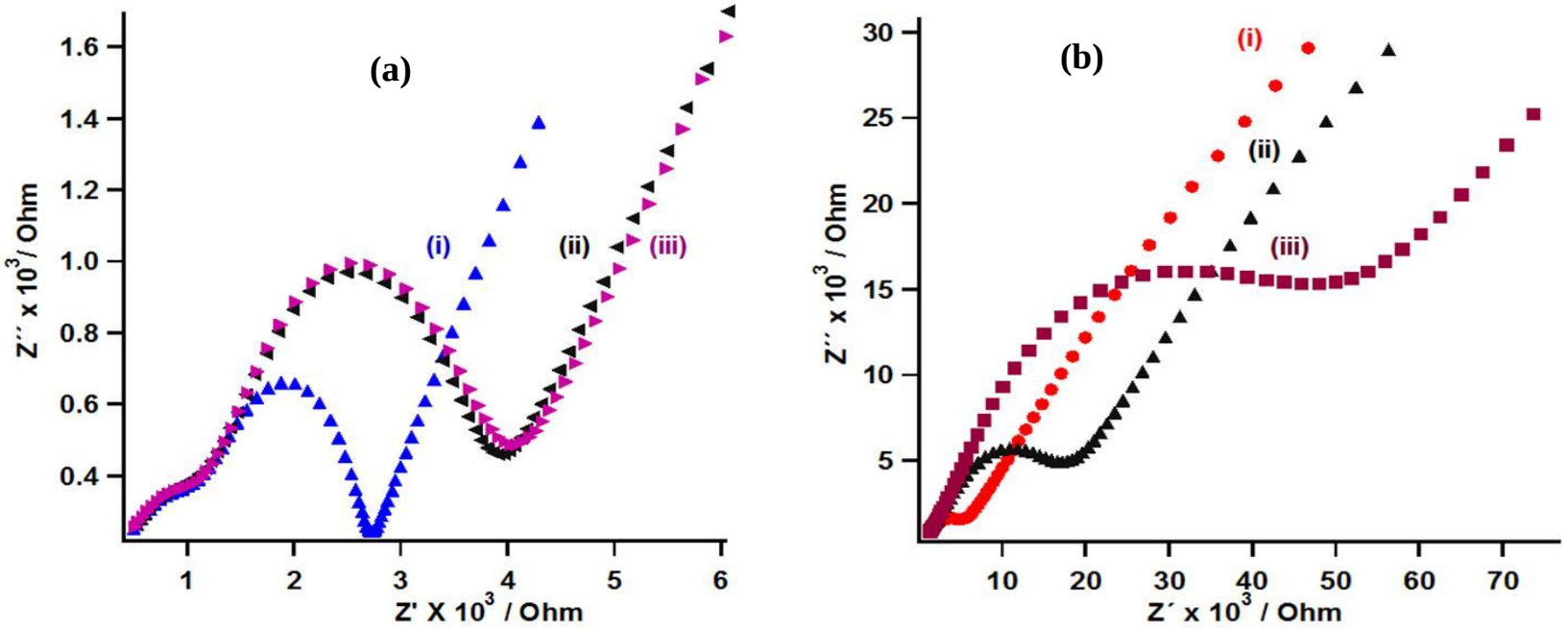

Figure 4.14 (a) Nyquist plots of 1.0 mM $[Ru(NH_3)_6]^{3+}$ at a hydrogenated electrode (trace i), a hydrogenated electrode after a 30-min incubation (trace ii) and a 1-week incubation (trace iii) in the fouling solution containing 1.0 M KCl supporting electrolyte; (b) Nyquist plots of 1.0 mM $[Ru(NH_3)_6]^{3+}$ at a bare electrode (trace i), a bare electrode after a 30-min (trace ii) and a 1-week (trace iii) incubation in the fouling solution containing 1.0 M KCl supporting electrolyte. Frequency range is 100 kHz – 0.1 Hz with 10 mV peak-to-peak potential amplitude at the formal $E_{1/2}$ of 0.2 V.

The antifouling property of the hydrogenated electrode can be attributed to the several aspects. The antifouling mechanism at the hydrogenated electrode is illustrated in Figure 4.15. Firstly, the surface flatness or smoothness of hydrogenated electrodes, as shown in Figure 4.15(a), also evident in atomic force micrographs shown in Figure 4.8, may contribute to the adsorption resistance of biomolecules on an electrode surface. According to Zhuiykov *et al.*,[106] fouling agents may specifically adhere to certain structural features present on an electrode surface, such as edges and grain boundaries that contain exposed carbon-oxygen functionalities as shown in Figure 4.15(b). During hydrogenation of our conical-tip carbon electrodes, oxygen-containing groups on their edge planes have been terminated by C-H bonds, as confirmed by the AQDS experiment reported in Section 3.6.4. Therefore, we similarly postulate that the modified edge sites of our electrodes are neither readily available nor favourable for the adsorption of fouling agents. In addition, the butylsiloxane dendrimers (see discussion in Section 3.4) may have also restricted structurally large fouling molecules to approach the electrode surface, while dopamine was able to penetrate the butylsiloxane layer to participate in electron transfer reaction at the electrode surface (Figure 4.15(a)).

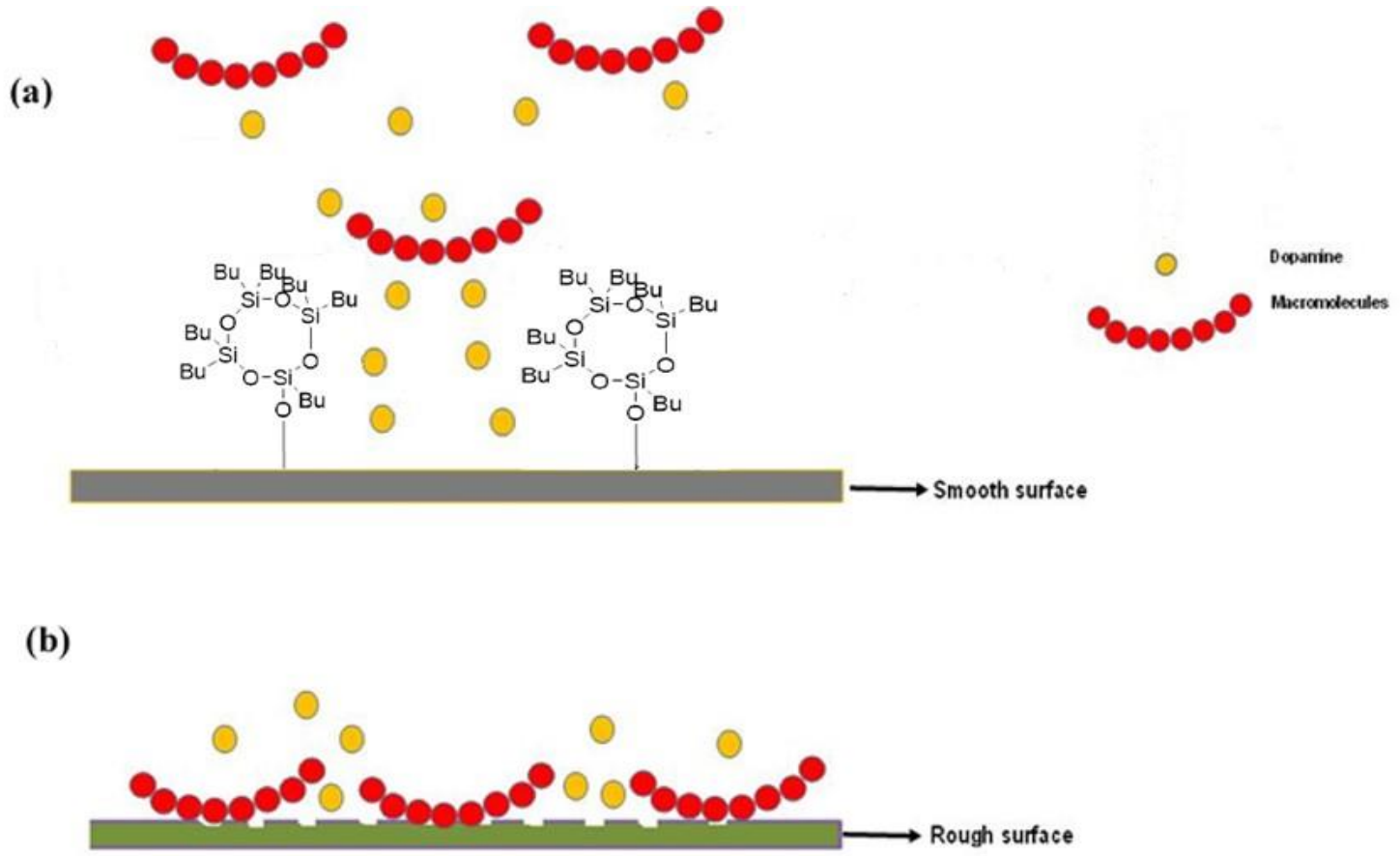

Figure 4.15 (a) Fouling resistance mechanism of a hydrogenated electrode surface and (b) fouling of a bare electrode surface.

Electrode fouling will not only compromise the quantitative detection of an analyte, but will also suppress the integrity and deteriorate the long-term application of the electrode. It is therefore required to evaluate the limit of detection and sensitivity of hydrogenated conical-tip carbon electrodes in a fouling experiment. Accordingly, we have calibrated hydrogenated conical-tip carbon electrodes based on their cyclic voltammetric responses of dopamine in a pH 7.4 citrate/phosphate buffer. To mimic biological fouling at these hydrogenated electrodes, they were incubated in the fouling solution for 1 week before they were used in the cyclic voltammetry of dopamine. A plot of the dopamine oxidation limiting current at hydrogenated carbon electrodes before incubation in the fouling solution and dopamine concentration is presented as trace i in Figure 4.16. Based on a Student's *t*-test, the correlation coefficient of 0.9938 (N = 7) of the plot was found to be statistically significant at the 95% confidence level. Moreover, the Wald-Wolfowitz runs test was used to confirm a random sequence of the positive and negative residuals of the ordinate values in trace i. All these support a linear calibration plot, which may be expressed as

$$\text{Current / pA} = 23.7 \pm 1.2 \times [\text{dopamine}] / \mu\text{M} + 0.0752 \pm 0.65 \quad \text{Equation 4.1}$$

where the uncertainties associated with the slope and the ordinate intercept denote the 95% confidence intervals. Using Equation 4.1, the limit of detection based on a signal-to-noise ratio of 3 was estimated to be 138 ± 12 nM. Similarly, we have performed cyclic voltammetry of dopamine at a hydrogenated electrode that has been incubated in the fouling solution for 1 week. The corresponding calibration plot based on the dopamine oxidation limiting current is shown in trace ii of Figure 4.16. Accordingly, a statistically significant linear calibration plot can be represented by the expression

$$\text{Current / pA} = 14.5 \pm 0.83 \times [\text{dopamine}] / \mu\text{M} + 0.389 \pm 0.45 \quad \text{Equation 4.2}$$

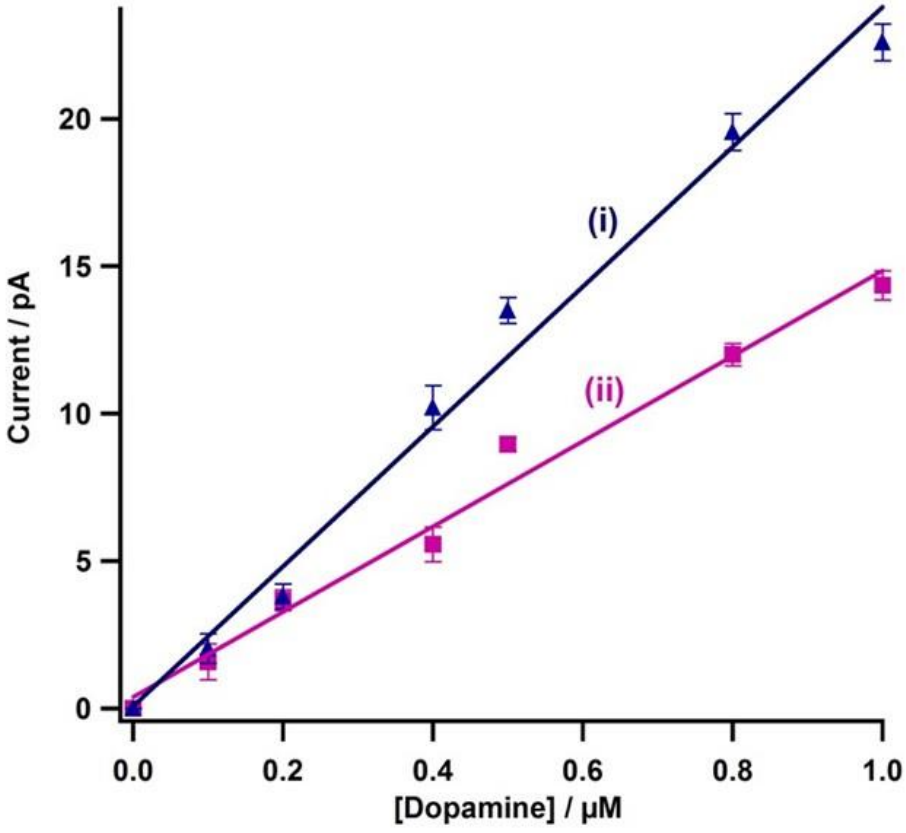

Figure 4.16. Calibration plots based on I_{lim} of dopamine cyclic voltammograms in pH 7.4 cittrate / phosphate buffer at a hydrogenated electrode (trace i) and after (trace ii) incubation for 1 week in 1.0% (v/v) caproic acid (a lipid), 4% (w/v) bovine serum albumin and 0.01% (w/v) cytochrome C (both are proteins), and 0.002% (w/v) human fibrinopeptide B (a peptide). Scan rate: 100 mV s^{-1} in all voltammograms.

Using this calibration plot, the limit of detection of dopamine at the hydrogenated electrode as 154 ± 10 nM after being incubated in fouling solution for 1 week. The limit of detection of dopamine at the electrodes was determined as 138 nM, which is favourably comparable with those previously reported at other electrodes, as tabulated in Table 4.4. Thus, our hydrogenated electrodes are expected to be able to detect low dopamine concentrations approaching 0.2-2.0 µM generally encountered *in vivo*[107].

Electrode type	Limit of detection / μM	References
Porous diamond-like carbon electrode	2.9	[91]
PEDOT-CNT microelectrode	1.0	[108]
Nitrogen doped graphene	0.25	[109]
Nanocrystalline BDD nanoelectrode array	0.10	[110]
Carbon nanotubes modified tantalum microelectrode	0.091	108
Carbon nanotubes modified carbon fibre microelectrode	0.046	[111]
Carbon nanopipette electrode	0.025	[112]
Hydrogenated conical-tip carbon electrode	0.14 – 0.15	This work

Table 4.4 Limits of detection at different electrode types.

The detection sensitivity (based on the slope of the linear calibration plot) was estimated to be 23.7 and 14.5 pA μM^{-1} for hydrogenated electrode and hydrogenated electrode after incubation, respectively. However, the sensitivity decreased by 38% when fouling experiment was performed at hydrogenated conical-tip carbon electrodes after they were incubated for 30 min. In our previous study involving conical-tip carbon electrodes hydrogenated by plasma vapour deposition[50], the detection sensitivity decreased by 35% at electrodes that were incubated in a fouling solution of slightly different composition (1.0% (v/v) caproic acid (a lipid), 0.1% (w/v) bovine serum

albumin, 0.01% (w/v) cytochrome C (both are proteins), and 0.002% (w/v) human fibrinopeptide B (a peptide)) for one week. In contrast, widely scattered dopamine oxidation signals were obtained at a bare electrode that was incubated in the fouling solution for 30 min and the corresponding calibration plot exhibited a statistically non-significant correlation coefficient at the 95% confidence level, in agreement with our previously obtained results[50,113]. Accordingly, the limit of detection and sensitivity could not confidently be determined. We attribute this to extreme surface degradation, leading to almost non-observable sensitivity to dopamine at the bare electrodes. These results show that the hydrogenated electrodes exhibited a degree of fouling resistance in the laboratory synthetic fouling solution compared to bare electrodes.

4.9.6 Electrode fouling during voltammetric cycling of dopamine

Next, we investigated electrode fouling caused by the oxidation products of dopamine during electrochemical detection of dopamine. As described in Section 4.3, dopamine is electrochemically oxidised to *o*-dopaminoquinone that is subsequently cyclised to form leukodopaminechrome. In the next step, leukodopaminechrome is further oxidised to yield dopaminechrome that may polymerise into melanin-like molecules. These molecules of ~3.8 Å in size[114] can form strong covalent bonds with organic moieties and non-covalent bonds with inorganic groups present on an electrode surface, leading to electrode fouling and thus compromising the detection of dopamine *in situ*. Previously, the sp^3 structure of boron-doped diamond electrodes bearing low surface polar functionalities was reportedly not favourable for adsorption of fouling agents.[36] In other report, a diamond electrode was cathodically pre-treated to remove oxygen functionalities that demonstrated antifouling properties in 1 mM dopamine.[20] On this basis, our sp^3 enriched hydrophobic electrode surface and butylsiloxane dendrimers are expected to repel the polar melanin-like polymers formed during dopamine oxidation. In this work, we have studied the extent to which the response of hydrogenated conical-

tip carbon electrodes changed during dopamine electro-oxidation by recording consecutive cyclic voltammograms (typically 8 at 100 mV s^{-1}). The voltammograms of 1.0 mM and 20 μM dopamine obtained at hydrogenated electrodes are displayed in Figure 4.17(a) and (b). As expected, the electrode response deteriorated on subsequent cycles, but these results were found to depend on dopamine concentration. More specifically, after 8 consecutive scans at these hydrogenated carbon electrodes in the presence of 1.0 mM and 20 μM dopamine, the oxidation signal decreased by 42% and 14%, respectively. It is noted that, after the 1st scan, the oxidation signal decreased only by 5.2% and 2.5%, respectively. Although many studies on dopamine fouling seemed to have focussed on millimolar levels of dopamine[10,20,115], detection at a lower level is much more relevant to practical applications. Therefore, we have next considered cyclic voltammetry for the oxidation of 1.0 μM dopamine and the results obtained are shown in Figure 4.17(c). Most significantly, the oxidation signals in these voltammograms remained stable without any obvious change even after 20 consecutive scans, demonstrating the effectiveness of hydrogenated electrodes in determining up to 1.0 μM dopamine, which is much more concentrated than the generally known concentration of 10 nM present in a mammalian brain[116]. Similar results were reported in the oxidation of 1.0 μM dopamine at the basal plane of a highly ordered pyrolytic graphite electrode containing low oxygen functionalities, which was thus expected to be inert toward adsorption of dopamine fouling products.[48] However, at the same electrode, a 45% oxidation signal loss was observed after 8 consecutive voltammetric scans in 1.0 mM dopamine[48]. Figure 4.18 shows a typical plot of the peak current ratio of the n^{th} cycle ($I_{l(n)}$) to that of cycle 1 ($I_{l(initial)}$) obtained at a hydrogenated conical-tip electrode. In this figure, the hydrogenated conical-tip carbon electrode was clearly unable to prevent the adsorption of dopaminergic products on the electrode. However, the electrode showed improved resistance to dopamine fouling in the presence of 20 μM of dopamine and 1.0 μM of dopamine. A similar result trend was obtained when

these experiments were repeated using other independently constructed conical-tip carbon electrodes (N=5).

In summary, the results of this experiment support a dopamine concentration dependent fouling taking place at the hydrogenated conical-tip carbon electrodes and low dopamine concentration leads to less severe chemical fouling at the electrodes.[10]

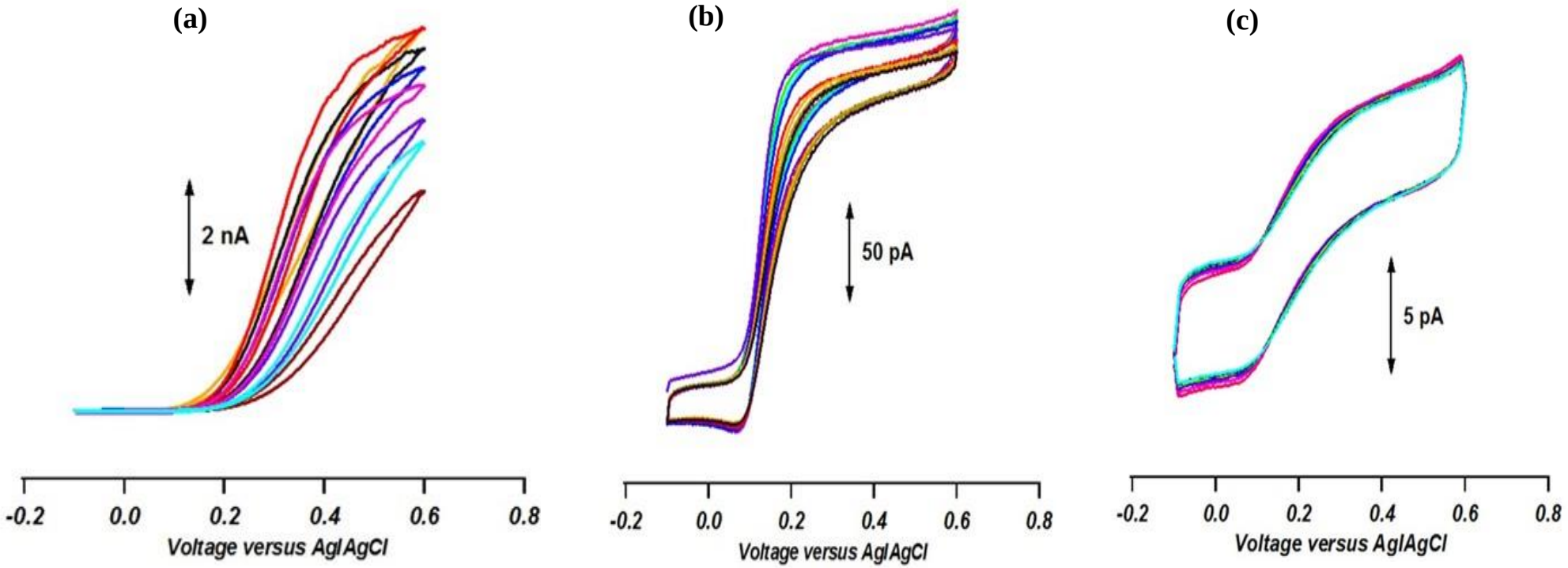

Figure 4.17 Consecutive cyclic voltammograms for the oxidation of dopamine at concentrations of (a) 1.0 mM, (b) 20 µM and (c) 1 µM at hydrogenated conical-tip carbon electrodes in pH 7.4 citrate / phosphate buffer. Scan rate: 100 mV s^{-1} in all voltammograms.

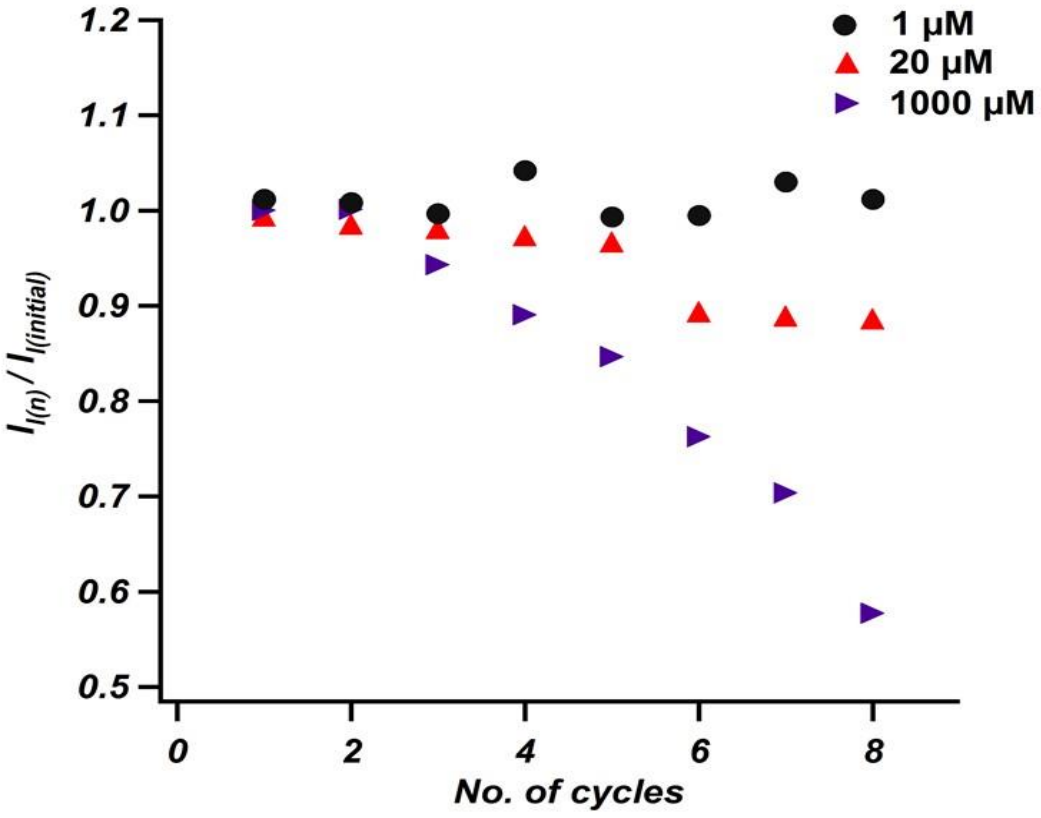

Figure 4.18 A plot of $I_l(n)/ I_l(i)$ versus the number of cycles, *n*, for the electro-oxidation of dopamine (data in Figure 4.17) at hydrogenated electrode: 1 mM, 20 µM, 1 µM.

4.10 Concluding remarks

A major aim of this study was to develop physically small carbon electrodes with antifouling property so that meaningful results could be achieved during the detection of dopamine *in vivo*. In this respect, an *n*-butylsilane reduction strategy was adopted to hydrogenate conical tip carbon electrodes to achieve an H–terminated electrode surface with butylsiloxane dendrimers. These electrodes demonstrated antifouling property during detection of dopamine in the presence a laboratory synthetic fouling solution containing proteins, a peptide, and a lipid, all generally present in an extracellular fluid. The surface property of these electrodes discouraged adsorption of melanin-like

polymers originated from the oxidation products of dopamine. The hydrogenated carbon electrodes were characterised using several redox markers including $[Ru(NH_3)_6]^{3+}$, $[Fe(CN)_6]^{3-}$, and dopamine and the results were compared to those obtained using the corresponding bare carbon electrodes. Hydrogenated carbon electrodes were found to exhibit reduced electron transfer reaction due to the absence of polar C–O functionalities or tunnelling distance generated by butylsiloxanes as described in Section 3.6.3. For comparison, carbon fibre microelectrodes were also hydrogenated by *n*-butylsilane reduction. The electrochemical behaviour of the same three redox markers at hydrogenated carbon fibre electrodes also indicated comparable kinetics to those observed at hydrogenated conical tip carbon electrodes.

In addition to conventional cyclic voltammetry, electrodes hydrogenated by *n*-butylsilane reduction were also assessed by electrochemical impedance spectroscopy. The results obtained supported the formation of a butylsiloxane film on a hydrogenated carbon electrode surface. A three-fold increase in R_{ct} observed at hydrogenated carbon electrodes, relative to that at bare carbon electrodes, also supported reduced kinetics. The reduced kinetics was attributed to the removal of negatively charged oxygen moieties from the edge planes of a carbon film at the bare carbon electrode after being hydrogenated by *n*-butylsilane reduction. This has led to a surface smoothing effect, giving rise to quasi-reversible reaction kinetics in all three redox systems. Using atomic force microscopy, a relatively defect free surface was visualised at a hydrogenated carbon electrode, which would be less favourable for adsorption of large biomolecules that could cause electrode fouling. As a result, the physical surface changes of hydrogenated carbon electrodes were expected to contribute substantial antifouling properties at these electrodes.

Raman spectroscopy was employed to confirm a larger proportion of sp^3 hybridised carbon at hydrogenated carbon electrodes, compared to the corresponding carbon

electrodes before hydrogenation. These sp^3 hybridised moities of the carbon film would cause hydrophobicity on the electrode surface to repel polar ascorbate. In this way, we have demonstrated the feasibility of selectively determining dopamine in the presence of ascorbate under physiological pH at hydrogenated carbon electrodes. Moreover, there was minimal interference in the detection of dopamine even in the presence of ascorbate at concentration as high as 500 μM generally expected in extracellular fluid.

Finally, hydrogenated conical-tip carbon electrodes that have been incubated in a laboratory synthetic solution containing 1.0% (v/v) caproic acid (a lipid), 4% (w/v) bovine serum albumin and 0.01% (w/v) cytochrome C (both are proteins), and 0.002% (w/v) human fibrinopeptide B (a peptide) for 30 min were applied to the detection of dopamine. By assessing the dopamine oxidation limiting current at these hydrogenated carbon electrodes, a 35% signal reduction was estimated. However, there was no discernable change of dopamine signal and detection sensitivity observed at hydrogenated carbon electrodes that were incubated in the same fouling solution for one week. In investigating possible fouling caused by dopamine oxidation products, there was no observable interference at hydrogenated carbon electrodes when the dopamine concentration was kept below of 1.0 μM, which is a 100 fold higher concentration than that generally expected in central nervous system.

4.11 References

1. Bromberg-Martin, E. S.; Matsumoto, M.; Hikosaka, O., Dopamine in Motivational Control: Rewarding, Aversive, and Alerting. *Neuron* **2010,** *68* (5), 815-834.
2. Johnson, P. M.; Kenny, P. J., Dopamine D2 receptors in addiction-like reward dysfunction and compulsive eating in obese rats. *Nature neuroscience* **2010,** *13* (5), 635-641.
3. Zhang, M.-Z.; Yao, B.; Wang, S.; Fan, X.; Wu, G.; Yang, H.; Yin, H.; Yang, S.; Harris, R. C., Intrarenal dopamine deficiency leads to hypertension and decreased longevity in mice. *The Journal of clinical investigation* **2011,** *121* (7), 2845-2854.
4. Aung, M. H.; na Park, H.; Han, M. K.; Obertone, T. S.; Abey, J.; Aseem, F.; Thule, P. M.; Iuvone, P. M.; Pardue, M. T., Dopamine deficiency contributes to early visual dysfunction in a rodent model of type 1 diabetes. *The Journal of Neuroscience* **2014,** *34* (3), 726-736.
5. Schultz, W., Updating dopamine reward signals. *Current Opinion in Neurobiology* **2013,** *23* (2), 229-238.
6. Venton, B. J.; Wightman, R. M., Psychoanalytical electrochemistry: dopamine and behavior. *Analytical Chemistry* **2003,** *75* (19), 414 A-421 A.
7. Cahill, P. S.; Walker, Q. D.; Finnegan, J. M.; Mickelson, G. E.; Travis, E. R.; Wightman, R. M., Microelectrodes for the measurement of catecholamines in biological systems. *Analytical chemistry* **1996,** *68* (18), 3180-3186.
8. Marín-Valencia, I.; Serrano, M.; Ormazabal, A.; Pérez-Dueñas, B.; García-Cazorla, A.; Campistol, J.; Artuch, R., Biochemical diagnosis of dopaminergic disturbances in paediatric patients: Analysis of cerebrospinal fluid homovanillic acid and other biogenic amines. *Clinical Biochemistry* **2008,** *41* (16–17), 1306-1315.

9. Lv, X.; Hu, B.; Wang, Z.; Peng, J.; Weng, J., Two-Electron Oxidation of Dopamine Controlled by Surface Modification of Few-Layer Graphene. *Electrochimica Acta* **2015,** *180*, 43-52.
10. Harreither, W.; Trouillon, R.; Poulin, P.; Neri, W.; Ewing, A. G.; Safina, G., Carbon Nanotube Fiber Microelectrodes Show a Higher Resistance to Dopamine Fouling. *Analytical chemistry* **2013,** *85* (15), 7447-7453.
11. Wei, Q.; Zhang, F.; Li, J.; Li, B.; Zhao, C., Oxidant-induced dopamine polymerization for multifunctional coatings. *Polymer Chemistry* **2010,** *1* (9), 1430-1433.
12. Mazario, E.; Sánchez-Marcos, J.; Menéndez, N.; Herrasti, P.; García-Hernández, M.; Muñoz-Bonilla, A., One-pot electrochemical synthesis of polydopamine coated magnetite nanoparticles. *RSC Advances* **2014,** *4* (89), 48353-48361.
13. Lee, H.; Dellatore, S. M.; Miller, W. M.; Messersmith, P. B., Mussel-inspired surface chemistry for multifunctional coatings. *Science* **2007,** *318* (5849), 426-430.
14. Ungless, M. A.; Grace, A. A., Are you or aren't you? Challenges associated with physiologically identifying dopamine neurons. *Trends in Neurosciences* **2012,** *35* (7), 422-430.
15. Dale, N.; Hatz, S.; Tian, F.; Llaudet, E., Listening to the brain: microelectrode biosensors for neurochemicals. *Trends in Biotechnology* **2005,** *23* (8), 420-428.
16. Hu, H.; Song, Y.; Feng, M.; Zhan, H., Carbon nanomaterials for simultaneous determination of dopamine and uric acid in the presence of ascorbic acid: from one-dimensional to the quasi one-dimensional. *Electrochimica Acta* **2016,** *190*, 40-48.
17. Wang, C.; Li, J.; Shi, K.; Wang, Q.; Zhao, X.; Xiong, Z.; Zou, X.; Wang, Y., Graphene coated by polydopamine/multi-walled carbon nanotubes modified electrode for highly selective detection of dopamine and uric acid in the

presence of ascorbic acid. *Journal of Electroanalytical Chemistry* **2016,** *770*, 56-61.

18. Robinson, D. L.; Venton, B. J.; Heien, M. L.; Wightman, R. M., Detecting subsecond dopamine release with fast-scan cyclic voltammetry in vivo. *Clinical chemistry* **2003,** *49* (10), 1763-1773.
19. Park, J.; Show, Y.; Quaiserova, V.; Galligan, J. J.; Fink, G. D.; Swain, G. M., Diamond microelectrodes for use in biological environments. *Journal of Electroanalytical Chemistry* **2005,** *583* (1), 56-68.
20. Trouillon, R.; Einaga, Y.; Gijs, M. A. M., Cathodic pretreatment improves the resistance of boron-doped diamond electrodes to dopamine fouling. *Electrochemistry Communications* **2014,** *47* (0), 92-95.
21. Tan, S. M.; Sofer, Z.; Pumera, M., Biomarkers detection on hydrogenated graphene surfaces: towards applications of graphane in biosensing. *Electroanalysis* **2013,** *25* (3), 703-705.
22. Zhou, M.; Zhai, Y.; Dong, S., Electrochemical sensing and biosensing platform based on chemically reduced graphene oxide. *Analytical Chemistry* **2009,** *81* (14), 5603-5613.
23. Szunerits, S.; Jama, C.; Coffinier, Y.; Marcus, B.; Delabouglise, D.; Boukherroub, R., Direct amination of hydrogen-terminated boron doped diamond surfaces. *Electrochemistry communications* **2006,** *8* (7), 1185-1190.
24. Kanazawa, H.; Song, K.-S.; Sakai, T.; Nakamura, Y.; Umezawa, H.; Tachiki, M.; Kawarada, H., Effect of iodide ions on the hydrogen-terminated and partially oxygen-terminated diamond surface. *Diamond and related materials* **2003,** *12* (3), 618-622.
25. Rezek, B.; Shin, D.; Watanabe, H.; Nebel, C., Intrinsic hydrogen-terminated diamond as ion-sensitive field effect transistor. *Sensors and Actuators B: Chemical* **2007,** *122* (2), 596-599.

26. Vanhove, E.; De Sanoit, J.; Arnault, J.; Saada, S.; Mer, C.; Mailley, P.; Bergonzo, P.; Nesladek, M., Stability of H-terminated BDD electrodes: an insight into the influence of the surface preparation. *physica status solidi (a)* **2007,** *204* (9), 2931-2939.

27. Biswas, H. S.; Datta, J.; Chowdhury, D.; Reddy, A.; Ghosh, U. C.; Srivastava, A. K.; Ray, N. R., Covalent immobilization of protein onto a functionalized hydrogenated diamond-like carbon substrate. *Langmuir* **2010,** *26* (22), 17413-17418.

28. Garrido, J. A.; Härtl, A.; Kuch, S.; Stutzmann, M.; Williams, O. A.; Jackmann, R., pH sensors based on hydrogenated diamond surfaces. *Applied Physics Letters* **2005,** *86* (7), 073504.

29. Kubovic, A.; Denisenko, A.; Ebert, W.; Kasu, M.; Kallfass, I.; Kohn, E., Electronic surface barrier characteristics of H-terminated and surface conductive diamond. *Diamond and related materials* **2004,** *13* (4), 755-760.

30. Hoffmann, R.; Kriele, A.; Obloh, H.; Hees, J.; Wolfer, M.; Smirnov, W.; Yang, N.; Nebel, C. E., Electrochemical hydrogen termination of boron-doped diamond. *Applied Physics Letters* **2010,** *97* (5), 052103.

31. Salazar-Banda, G. R.; Andrade, L. S.; Nascente, P. A.; Pizani, P. S.; Rocha-Filho, R. C.; Avaca, L. A., On the changing electrochemical behaviour of boron-doped diamond surfaces with time after cathodic pre-treatments. *Electrochimica Acta* **2006,** *51* (22), 4612-4619.

32. Palanisamy, S.; Ku, S.; Chen, S.-M., Dopamine sensor based on a glassy carbon electrode modified with a reduced graphene oxide and palladium nanoparticles composite. *Microchimica Acta* **2013,** *180* (11-12), 1037-1042.

33. Gasnier, A.; Pedano, M. L.; Gutierrez, F.; Labbé, P.; Rivas, G. A.; Rubianes, M. D., Glassy carbon electrodes modified with a dispersion of multi-wall carbon nanotubes in dopamine-functionalized polyethylenimine: Characterization and

analytical applications for nicotinamide adenine dinucleotide quantification. *Electrochimica Acta* **2012,** *71*, 73-81.

34. Teymourian, H.; Salimi, A.; Hallaj, R., Electrocatalytic oxidation of NADH at electrogenerated NAD+ oxidation product immobilized onto multiwalled carbon nanotubes/ionic liquid nanocomposite: application to ethanol biosensing. *Talanta* **2012,** *90*, 91-98.
35. Xiang, L.; Yu, P.; Hao, J.; Zhang, M.; Zhu, L.; Dai, L.; Mao, L., Vertically aligned carbon nanotube-sheathed carbon fibers as pristine microelectrodes for selective monitoring of ascorbate in vivo. *Analytical chemistry* **2014,** *86* (8), 3909-3914.
36. McCreery, R. L., Advanced carbon electrode materials for molecular electrochemistry. *Chemical reviews* **2008,** *108* (7), 2646-2687.
37. Zestos, A. G.; Jacobs, C. B.; Trikantzopoulos, E.; Ross, A. E.; Venton, B. J., Polyethylenimine Carbon Nanotube Fiber Electrodes for Enhanced Detection of Neurotransmitters. *Analytical chemistry* **2014,** *86* (17), 8568-8575.
38. Shan, C.; Yang, H.; Song, J.; Han, D.; Ivaska, A.; Niu, L., Direct electrochemistry of glucose oxidase and biosensing for glucose based on graphene. *Analytical Chemistry* **2009,** *81* (6), 2378-2382.
39. Alwarappan, S.; Joshi, R. K.; Ram, M. K.; Kumar, A., Electron transfer mechanism of cytochrome c at graphene electrode. *Applied Physics Letters* **2010,** *96* (26), 263702.
40. Shin, D.; Tryk, D. A.; Fujishima, A.; Merkoçi, A.; Wang, J., Resistance to surfactant and protein fouling effects at conducting diamond electrodes. *Electroanalysis* **2005,** *17* (4), 305-311.
41. Roberts, J. G.; Moody, B. P.; McCarty, G. S.; Sombers, L. A., Specific Oxygen-Containing Functional Groups on the Carbon Surface Underlie an Enhanced Sensitivity to Dopamine at Electrochemically Pretreated Carbon Fiber Microelectrodes. *Langmuir* **2010,** *26* (11), 9116-9122.

42. Trouillon, R.; O'Hare, D.; Einaga, Y., Effect of the doping level on the biological stability of hydrogenated boron doped diamond electrodes. *Physical chemistry chemical physics : PCCP* **2011,** *13* (12), 5422-9.

43. Wilson, C. J.; Clegg, R. E.; Leavesley, D. I.; Pearcy, M. J., Mediation of biomaterial-cell interactions by adsorbed proteins: a review. *Tissue engineering* **2005,** *11* (1-2), 1-18.

44. Thevenot, P.; Hu, W.; Tang, L., Surface chemistry influence implant biocompatibility. *Current topics in medicinal chemistry* **2008,** *8* (4), 270.

45. Trouillon, R.; Combs, Z.; Patel, B. A.; O'Hare, D., Comparative study of the effect of various electrode membranes on biofouling and electrochemical measurements. *Electrochemistry Communications* **2009,** *11* (7), 1409-1413.

46. Zhao, H.; Bian, X.; Galligan, J. J.; Swain, G. M., Electrochemical measurements of serotonin (5-HT) release from the guinea pig mucosa using continuous amperometry with a boron-doped diamond microelectrode. *Diamond and Related Materials* **2010,** *19* (2–3), 182-185.

47. Güell, A. G.; Meadows, K. E.; Unwin, P. R.; Macpherson, J. V., Trace voltammetric detection of serotonin at carbon electrodes: comparison of glassy carbon, boron doped diamond and carbon nanotube network electrodes. *Physical Chemistry Chemical Physics* **2010,** *12* (34), 10108-10114.

48. Patel, A. N.; Tan, S.-y.; Miller, T. S.; Macpherson, J. V.; Unwin, P. R., Comparison and reappraisal of carbon electrodes for the voltammetric detection of dopamine. *Analytical chemistry* **2013,** *85* (24), 11755-11764.

49. Goto, T.; Yasukawa, T.; Kanda, K.; Matsui, S.; Mizutani, F., Inhibition of electrochemical fouling against biomolecules on a diamond-like carbon electrode. *Analytical Sciences* **2011,** *27* (1), 91-94.

50. Chandra, S.; Miller, A. D.; Bendavid, A.; Martin, P. J.; Wong, D. K., Minimizing fouling at hydrogenated conical-tip carbon electrodes during dopamine detection in vivo. *Analytical chemistry* **2014,** *86* (5), 2443-2450.

51. Kato, D.; Komoriya, M.; Nakamoto, K.; Kurita, R.; Hirono, S.; Niwa, O., Electrochemical determination of oxidative damaged DNA with high sensitivity and stability using a nanocarbon film. *Analytical Sciences* **2011,** *27* (7), 703.

52. Xue, Q.; Kato, D.; Kamata, T.; Umemura, S.; Hirono, S.; Niwa, O., Electron Cyclotron Resonance-Sputtered Nanocarbon Film Electrode Compared with Diamond-Like Carbon and Glassy Carbon Electrodes as Regards Electrochemical Properties and Biomolecule Adsorption. *Japanese Journal of Applied Physics* **2012,** *51* (9R), 090124.

53. Shpilevaya, I.; Foord, J. S., Electrochemistry of methyl viologen and anthraquinonedisulfonate at diamond and diamond powder electrodes: The influence of surface chemistry. *Electroanalysis* **2014,** *26* (10), 2088-2099.

54. Brocenschi, R. F.; Rocha-Filho, R. C.; Duran, B.; Swain, G. M., The analysis of estrogenic compounds by flow injection analysis with amperometric detection using a boron-doped diamond electrode. *Talanta* **2014,** *126*, 12-19.

55. Zhuiykov, S.; Kalantar-zadeh, K., Development of antifouling of electrochemical solid-state dissolved oxygen sensors based on nanostructured Cu 0.4 Ru 3.4 O 7+ RuO 2 sensing electrodes. *Electrochimica Acta* **2012,** *73*, 105-111.

56. Sasso, L.; Heiskanen, A.; Diazzi, F.; Dimaki, M.; Castillo-León, J.; Vergani, M.; Landini, E.; Raiteri, R.; Ferrari, G.; Carminati, M., Doped overoxidized polypyrrole microelectrodes as sensors for the detection of dopamine released from cell populations. *The Analyst* **2013,** *138* (13), 3651-3659.

57. Paul, D. W.; Prajapati, I.; Reed, M. L., Electropolymerized eugenol: Evaluation as a protective film for oxygen sensing. *Sensors and Actuators B: Chemical* **2013,** *183*, 129-135.

58. Özel, R. E.; Wallace, K. N.; Andreescu, S., Chitosan coated carbon fiber microelectrode for selective in vivo detection of neurotransmitters in live zebrafish embryos. *Analytica chimica acta* **2011,** *695* (1), 89-95.

59. Perez, E.; Lahlil, K.; Rougeau, C.; Moraillon, A.; Chazalviel, J.-N. l.; Ozanam, F. o.; Gouget-Laemmel, A. C., Influence of the molecular design on the antifouling performance of poly (ethylene glycol) monolayers grafted on (111) Si. *Langmuir* **2012,** *28* (41), 14654-14664.

60. Zhang, L.; Li, D.; Meng, W.; Huang, Q.; Su, Y.; Wang, L.; Song, S.; Fan, C., Sequence-specific DNA detection by using biocatalyzed electrochemiluminescence and non-fouling surfaces. *Biosensors and Bioelectronics* **2009,** *25* (2), 368-372.

61. Li, W.; Liu, Q.; Liu, L., Antifouling Gold Surfaces Grafted with Aspartic Acid and Glutamic Acid-Based Zwitterionic Polymer Brushes. *Langmuir* **2014,** *30(42)***,** 12619-12626.

62. Keeley, G. P.; O'Neill, A.; Holzinger, M.; Cosnier, S.; Coleman, J. N.; Duesberg, G. S., DMF-exfoliated graphene for electrochemical NADH detection. *Physical Chemistry Chemical Physics* **2011,** *13* (17), 7747-7750.

63. Liu, X.; Barizuddin, S.; Shin, W.; Mathai, C. J.; Gangopadhyay, S.; Gillis, K. D., Microwell device for targeting single cells to electrochemical microelectrodes for high-throughput amperometric detection of quantal exocytosis. *Analytical chemistry* **2011,** *83* (7), 2445-2451.

64. Kivlehan, F.; Garay, F.; Guo, J.; Chaum, E.; Lindner, E., Toward Feedback-Controlled Anesthesia: Voltammetric Measurement of Propofol (2, 6-Diisopropylphenol) in Serum-Like Electrolyte Solutions. *Analytical chemistry* **2012,** *84* (18), 7670-7676.

65. Nistor, P. A.; May, P. W.; Tamagnini, F.; Randall, A. D.; Caldwell, M. A., Long-term culture of pluripotent stem-cell-derived human neurons on diamond–A substrate for neurodegeneration research and therapy. *Biomaterials* **2015,** *61*, 139-149.

66. Chandra, S. S. Development of Fouling-resistant Physically Small Carbon Electrodes for in Vivo Dopamine Detection. Macquarie University, 2011.

67. Armstrong-James, M.; Millar, J., Carbon fibre microelectrodes. *Journal of neuroscience methods* **1979,** *1* (3), 279-287.

68. Tomeš, J., Polarographic studies with the dropping mercury kathode. LXVII. Equation of the polarographic wave in the electrodeposition of hydrogen from strong and weak acids. *Collection of Czechoslovak Chemical Communications* **1937,** *9*, 150-167.

69. Chen, P.; McCreery, R. L., Control of electron transfer kinetics at glassy carbon electrodes by specific surface modification. *Analytical Chemistry* **1996,** *68* (22), 3958-3965.

70. Xu, J.; Chen, Q.; Swain, G. M., Anthraquinonedisulfonate electrochemistry: A comparison of glassy carbon, hydrogenated glassy carbon, highly oriented pyrolytic graphite, and diamond electrodes. *Analytical chemistry* **1998,** *70* (15), 3146-3154.

71. Wang, S.; Swope, V. M.; Butler, J. E.; Feygelson, T.; Swain, G. M., The structural and electrochemical properties of boron-doped nanocrystalline diamond thin-film electrodes grown from Ar-rich and H2-rich source gases. *Diamond and Related Materials* **2009,** *18* (4), 669-677.

72. Yang, N.; Smirnov, W.; Hees, J.; Hoffmann, R.; Kriele, A.; Obloh, H.; Müller-Sebert, W.; Nebel, C. E., Diamond ultra-microelectrode arrays for achieving maximum Faradaic current with minimum capacitive charging. *physica status solidi (a)* **2011,** *208* (9), 2087-2092.

73. Ji, X.; Banks, C. E.; Crossley, A.; Compton, R. G., Oxygenated edge plane sites slow the electron transfer of the ferro-/ferricyanide redox couple at graphite electrodes. *Chemphyschem : a European journal of chemical physics and physical chemistry* **2006,** *7* (6), 1337-44.

74. Park, J.; Quaiserová-Mocko, V.; Patel, B. A.; Novotný, M.; Liu, A.; Bian, X.; Galligan, J. J.; Swain, G. M., Diamond microelectrodes for in vitro

electroanalytical measurements: current status and remaining challenges. *The Analyst* **2008,** *133* (1), 17-24.

75. Chen, Y.; Guo, L.-R.; Chen, W.; Yang, X.-J.; Jin, B.; Zheng, L.-M.; Xia, X.-H., 3-mercaptopropylphosphonic acid modified gold electrode for electrochemical detection of dopamine. *Bioelectrochemistry* **2009,** *75* (1), 26-31.
76. Kuo, T.-C.; McCreery, R. L., Surface chemistry and electron-transfer kinetics of hydrogen-modified glassy carbon electrodes. *Analytical Chemistry* **1999,** *71* (8), 1553-1560.
77. Zhao, D.; Wang, T.; Han, D.; Rusinek, C.; Steckl, A. J.; Heineman, W. R., Electrospun Carbon Nanofiber Modified Electrodes for Stripping Voltammetry. *Analytical chemistry* **2015,** *87* (18), 9315-9321.
78. Pan, S.; Rothberg, L., Chemical control of electrode functionalization for detection of DNA hybridization by electrochemical impedance spectroscopy. *Langmuir* **2005,** *21* (3), 1022-1027.
79. Chen, H.; Heng, C. K.; Puiu, P. D.; Zhou, X. D.; Lee, A. C.; Lim, T. M.; Tan, S. N., Detection of Saccharomyces cerevisiae immobilized on self-assembled monolayer (SAM) of alkanethiolate using electrochemical impedance spectroscopy. *Analytica chimica acta* **2005,** *554* (1), 52-59.
80. Uzun, D.; Gündüzalp, A. B.; Hasdemir, E., Selective determination of dopamine in the presence of uric acid and ascorbic acid by N, N′-bis (indole-3-carboxaldimine)-1, 2-diaminocyclohexane thin film modified glassy carbon electrode by differential pulse voltammetry. *Journal of Electroanalytical Chemistry* **2015,** *747*, 68-76.
81. Ghosh, T.; Sarkar, P., Isolation of a novel uric-acid-degrading microbe Comamonas sp. BT UA and rapid biosensing of uric acid from extracted uricase enzyme. *Journal of biosciences* **2014,** *39* (5), 805-819.
82. Zen, J.-M.; Ilangovan, G.; Jou, J.-J., Square-wave voltammetric determination and ac impedance study of dopamine on preanodized perfluorosulfonated

ionomer-coated glassy carbon electrodes. *Analytical Chemistry* **1999,** *71* (14), 2797-2805.

83. Sarac, A. S.; Sezgin, S.; Ates, M.; Turhan, C. M., Electrochemical impedance spectroscopy and morphological analyses of pyrrole, phenylpyrrole and methoxyphenylpyrrole on carbon fiber microelectrodes. *Surface and Coatings Technology* **2008,** *202* (16), 3997-4005.

84. Casero, E.; Parra-Alfambra, A.; Petit-Domínguez, M.; Pariente, F.; Lorenzo, E.; Alonso, C., Differentiation between graphene oxide and reduced graphene by electrochemical impedance spectroscopy (EIS). *Electrochemistry Communications* **2012,** *20*, 63-66.

85. Rezek, B.; Nebel, C., Electronic properties of plasma hydrogenated diamond surfaces: a microscopic study. *Diamond and related materials* **2006,** *15* (9), 1374-1377.

86. Chen, Q.; Swain, G. M., Structural characterization, electrochemical reactivity, and response stability of hydrogenated glassy carbon electrodes. *Langmuir* **1998,** *14* (24), 7017-7026.

87. Hozumi, A.; Ushiyama, K.; Sugimura, H.; Takai, O., Fluoroalkylsilane monolayers formed by chemical vapor surface modification on hydroxylated oxide surfaces. *Langmuir* **1999,** *15* (22), 7600-7604.

88. Yan, X.; Xu, T.; Yang, S.; Liu, H.; Xue, Q., Characterization of hydrogenated diamond-like carbon films electrochemically deposited on a silicon substrate. *Journal of Physics D: Applied Physics* **2004,** *37* (17), 2416.

89. Huang, K.-J.; Wang, L.; Liu, Y.-J.; Gan, T.; Liu, Y.-M.; Wang, L.-L.; Fan, Y., Synthesis and electrochemical performances of layered tungsten sulfide-graphene nanocomposite as a sensing platform for catechol, resorcinol and hydroquinone. *Electrochimica Acta* **2013,** *107*, 379-387.

90. Yu, X.; Sheng, K.; Shi, G., A three-dimensional interpenetrating electrode of reduced graphene oxide for selective detection of dopamine. *The Analyst* **2014,** *139* (18), 4525-4531.

91. Silva, T. A.; Zanin, H.; May, P. W.; Corat, E. J.; Fatibello-Filho, O., Electrochemical Performance of Porous Diamond-like Carbon Electrodes for Sensing Hormones, Neurotransmitters, and Endocrine Disruptors. *ACS applied materials & interfaces* **2014,** *6* (23), 21086-21092.

92. Macpherson, J. V., A practical guide to using boron doped diamond in electrochemical research. *Physical Chemistry Chemical Physics* **2015,** *17* (5), 2935-2949.

93. Li, S.-J.; Qian, C.; Wang, K.; Hua, B.-Y.; Wang, F.-B.; Sheng, Z.-H.; Xia, X.-H., Application of thermally reduced graphene oxide modified electrode in simultaneous determination of dihydroxybenzene isomers. *Sensors and Actuators B: Chemical* **2012,** *174*, 441-448.

94. Yan, X. B.; Xu, T.; Chen, G.; Liu, H. W.; Yang, S. R., Effect of deposition voltage on the microstructure of electrochemically deposited hydrogenated amorphous carbon films. *Carbon* **2004,** *42* (15), 3103-3108.

95. Lian, Q.; He, Z.; He, Q.; Luo, A.; Yan, K.; Zhang, D.; Lu, X.; Zhou, X., Simultaneous determination of ascorbic acid, dopamine and uric acid based on tryptophan functionalized graphene. *Analytica chimica acta* **2014,** *823*, 32-39.

96. O'Neill, R. D., Microvoltammetric techniques and sensors for monitoring neurochemical dynamics in vivo. A review. *The Analyst* **1994,** *119* (5), 767-779.

97. Capella, P.; Ghasemzadeh, B.; Mitchell, K.; Adams, R. N., Nafion-coated carbon fiber electrodes for neurochemical studies in brain tissue. *Electroanalysis* **1990,** *2* (3), 175-182.

98. Wang, C.; Yuan, R.; Chai, Y.; Chen, S.; Hu, F.; Zhang, M., Simultaneous determination of ascorbic acid, dopamine, uric acid and tryptophan on gold

nanoparticles/overoxidized-polyimidazole composite modified glassy carbon electrode. *Analytica chimica acta* **2012,** *741*, 15-20.

99. McNally, M.; Wong, D. K., An in vivo probe based on mechanically strong but structurally small carbon electrodes with an appreciable surface area. *Analytical chemistry* **2001,** *73* (20), 4793-4800.

100. Xiao, Y.; Guo, C.; Li, C. M.; Li, Y.; Zhang, J.; Xue, R.; Zhang, S., Highly sensitive and selective method to detect dopamine in the presence of ascorbic acid by a new polymeric composite film. *Analytical biochemistry* **2007,** *371* (2), 229-237.

101. Mo, J.-W.; Ogorevc, B., Simultaneous measurement of dopamine and ascorbate at their physiological levels using voltammetric microprobe based on overoxidized poly (1, 2-phenylenediamine)-coated carbon fiber. *Analytical chemistry* **2001,** *73* (6), 1196-1202.

102. Gui, A. L.; Luais, E.; Peterson, J. R.; Gooding, J. J., Zwitterionic Phenyl Layers: Finally, Stable, Anti-Biofouling Coatings that Do Not Passivate Electrodes. *ACS applied materials & interfaces* **2013,** *5* (11), 4827-4835.

103. Roeser, J.; Alting, N. F.; Permentier, H. P.; Bruins, A. P.; Bischoff, R., Boron-doped diamond electrodes for the electrochemical oxidation and cleavage of peptides. *Analytical chemistry* **2013,** *85* (14), 6626-6632.

104. Singh, Y. S.; Sawarynski, L. E.; Dabiri, P. D.; Choi, W. R.; Andrews, A. M., Head-to-Head Comparisons of Carbon Fiber Microelectrode Coatings for Sensitive and Selective Neurotransmitter Detection by Voltammetry. *Analytical Chemistry* **2011,** *83* (17), 6658-6666.

105. Trouillon, R.; O'Hare, D., Comparison of glassy carbon and boron doped diamond electrodes: Resistance to biofouling. *Electrochimica Acta* **2010,** *55* (22), 6586-6595.

106. Zhuiykov, S.; Kalantar-zadeh, K., Development of antifouling of electrochemical solid-state dissolved oxygen sensors based on nanostructured

Cu0.4Ru3.4O7 + RuO2 sensing electrodes. *Electrochimica Acta* **2012,** *73*, 105-111.

107. Schenk, J. O.; Miller, E.; Rice, M. E.; Adams, R. N., Chronoamperometry in brain slices: quantitative evaluations of in vivo electrochemistry. *Brain research* **1983,** *277* (1), 1-8.
108. Samba, R.; Fuchsberger, K.; Matiychyn, I.; Epple, S.; Kiesel, L.; Stett, A.; Schuhmann, W.; Stelzle, M., Application of PEDOT-CNT Microelectrodes for Neurotransmitter Sensing. *Electroanalysis* **2014,** *26* (3), 548-555.
109. Sheng, Z.-H.; Zheng, X.-Q.; Xu, J.-Y.; Bao, W.-J.; Wang, F.-B.; Xia, X.-H., Electrochemical sensor based on nitrogen doped graphene: simultaneous determination of ascorbic acid, dopamine and uric acid. *Biosensors and Bioelectronics* **2012,** *34* (1), 125-131.
110. Dincer, C.; Ktaich, R.; Laubender, E.; Hees, J. J.; Kieninger, J.; Nebel, C. E.; Heinze, J.; Urban, G. A., Nanocrystalline boron-doped diamond nanoelectrode arrays for ultrasensitive dopamine detection. *Electrochimica Acta* **2015,** *185*, 101-106.
111. Yang, C.; Jacobs, C. B.; Nguyen, M. D.; Ganesana, M.; Zestos, A. G.; Ivanov, I. N.; Puretzky, A. A.; Rouleau, C. M.; Geohegan, D. B.; Venton, B. J., Carbon Nanotubes Grown on Metal Microelectrodes for the Detection of Dopamine. *Analytical Chemistry* **2016,** *88* (1), 645-652.
112. Rees, H. R.; Anderson, S. E.; Privman, E.; Bau, H. H.; Venton, B. J., Carbon nanopipette electrodes for dopamine detection in Drosophila. *Analytical chemistry* **2015,** *87* (7), 3849-3855.
113. Chandra, S.; Miller, A. D.; Wong, D. K. Y., Evaluation of physically small p-phenylacetate-modified carbon electrodes against fouling during dopamine detection in vivo. *Electrochimica Acta* **2013,** *101*, 225-231.

114. Liu, L.; Shao, B.; Yang, F., Polydopamine coating – Surface modification of polyester filter and fouling reduction. *Separation and Purification Technology* **2013,** *118* (0), 226-233.

115. Takmakov, P.; Zachek, M. K.; Keithley, R. B.; Walsh, P. L.; Donley, C.; McCarty, G. S.; Wightman, R. M., Carbon microelectrodes with a renewable surface. *Analytical chemistry* **2010,** *82* (5), 2020-2028.

116. Jacobs, C. B.; Peairs, M. J.; Venton, B. J., Review: Carbon nanotube based electrochemical sensors for biomolecules. *Analytica chimica acta* **2010,** *662* (2), 105-127.

Chapter 5

A Comparative Study of the Antifouling Characteristics between *n*-Butylsilane and Diethylsilane Hydrogenated Conical-tip Carbon Electrodes that were Subsequently Modified by 4-Sulfobenzene for Enhanced Dopamine Detection

5.1 Hydrogenation of carbon-oxygen functionalities by silane compounds

The reduction of functional groups in an organic compound, *e.g.*, carboxyl, ketones and aldehydes using such common methods as hydrazine reduction and electrocatalytic reduction is typically a multi-step process. For example, ketones and aldehydes are converted to the corresponding alkanes through a multistep reduction procedure in which amalgamated zinc in a hydroxylic solvent containing HCl was used as a reducing agent.[1] "One-pot" procedures of converting functional groups in a single step to the corresponding alkanes have been reported that resolved the problems involving multistep reactions to a great extent.[2] Among such work, Nimmagadda and McRae[3,4] reported on a silane reduction method, which can reduce carbon-oxygen functionalities including primary, secondary and tertiary alcohols, aldehydes, ketones, carboxyls and quinones to their corresponding alkanes on both aliphatic and aromatic systems. In their work[5], alkyl silanes, including triethylsilane, dimethylethylsilane, diethylsilane and *n*-butylsilane were used to study the one-pot reduction of different functional groups on aliphatic and aromatic compounds. The ability of various silanes to reduce the functional groups was found to be dependent upon steric hindrance, thus the less sterically hindered silanes (e.g., *n*-butylsilane and diethylsilane) proved to be more efficient than sterically hindered silanes (e.g., dimethylethylsilane and triethylsilane). Similarly, the duration of a reaction with less sterically hindered / less bulky

substituents silanes was found to be shorter than that involving sterically hindered silanes. This has prompted the use of *n*-butylsilane (long chained) and diethylsilane (only two alkyl substituents) as reducing agents in their work. Although diethylsilane was reportedly also capable of reducing the carbon-oxygen functional groups to the corresponding alkane, the reaction did not yield the same alkane products as those by *n*-butylsilane, as shown in Table 5.1, because of steric hindrance.

5.2 Functionalisation of electrode surface and dopamine detection

During electrochemical detection of neurotransmitters, improving the sensitivity and selectivity of the working electrodes towards a specific species is a major goal of many research efforts. In general, selective attraction of electroactive molecules towards the electrode surface promotes the detection sensitivity. As an example, owing to its sulfonic acid terminated side chains, Nafion offers selectivity and electrostatic attraction towards such cationic species as dopamine in physiological conditions.[6] Therefore, a Nafion-nano-TiO_2 composite immobilised glassy carbon electrode was demonstrated to measure dopamine without interference even in the presence of 500 μM ascorbic acid.[7] At the modified electrode surface, the cationic dopamine was selectively exchanged with Na^+ in the Nafion film, but the anionic ascorbic acid was repelled and hence unable to participate in electron transfer reaction at the electrode surface. More specifically, the bulky sulfonate (SO_3^-) terminated polymeric film was able to electrostatically attract dopamine towards the electrode for oxidation, while the porous and compact nano-TiO_2 facilitated fast electron transfer kinetics for dopamine. All these were strategically designed to enhance the dopamine detection response. However, Nafion is not completely impermeable to ascorbic acid that some ascorbic acid would still undergo an electron transfer reaction.[8] Compared to a Nafion modified electrode, sulfonated graphene sheets demonstrated superiority in terms of flexible film thickness and a unique distribution of sulfonate on graphene sheet. Based on diazonium chemistry, Li *et al*.[8] modified graphene sheets with sulfonate groups to exploit the synergistic advantages arising from high conductivity of graphene and electrostatic attraction from SO_3^- towards dopamine to attain limit of detection as low as 20 nM.

Substrate	Product	Percentage yield / %	
		n-Butylsilane	Diethylsilane
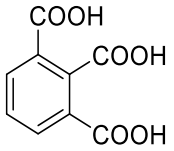	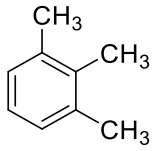	71	34
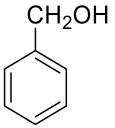	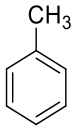	97	41
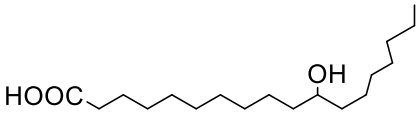	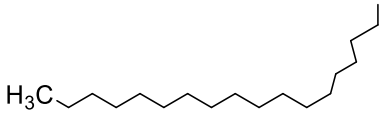	91	27
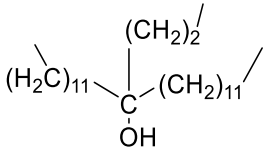	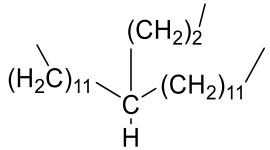	72	17
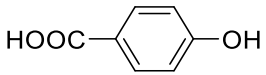	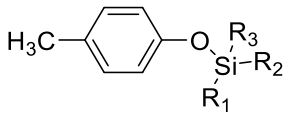	67	48
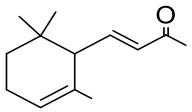	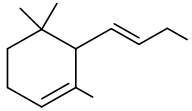	93	64
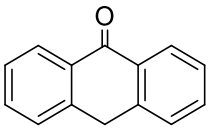	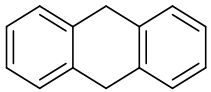	93	56

Table 5.1. Reduction of carbon-oxygen functionalities using either *n*-butylsilane or diethylsilane. Adapted from reference 3 and 5.

The sulfonated graphene also selectively detected dopamine in the presence of ascorbic acid and uric acid with three well resolved oxidation potentials for the three analytes. However, graphene can agglomerate and be precipitated out in an aqueous solution. By exploiting the capability of carbon dots in preventing the agglomeration of graphene, a graphene oxide/carbon dot composite film modified glassy carbon electrode was used to enhance dopamine determination.[9] In such work, carboxyl groups present in carbon dots electrostatically attracted dopamine and the π-π stacking force between graphene and dopamine further strengthened the attraction. These features have aided in achieving an excellent limit of detection of 1.5 nM dopamine. However, Zen *et al.*[10] reported a ten-time higher double-layer charging current at a pre-anodised Nafion-coated glassy carbon electrode, compared to an unmodified glassy carbon electrode, for dopamine detection. Similarly, a carboxyl group functionalised single-wall carbon nanotube modified glassy carbon electrode was developed to achieve an enhanced sensitivity of 0.073 μA μM^{-1} for dopamine.[11] The modified surface demonstrated high selectivity to dopamine in the presence of uric acid and ascorbic acid. Silica mesochannels were developed on an indium tin oxide coated glass electrode for selective and enhanced detection of ascorbic acid and dopamine.[12] In such work, pores of 2-3 nm in size were functionalised with ammonium groups to obtain electrostatic and steric effects towards the analyte. The permselectivity of electrode surface towards ascorbic acid and dopamine was controlled by monitoring the ionic strength of buffer.

5.3 Polymeric materials as antifouling agents

Nafion is a porous membrane that contains sulfonic acid functional groups, making the membrane a negatively charged film. As an electrode coating, Nafion has demonstrated some antifouling properties when it not only acts as a physical barrier, but also electrostatically repels negatively charged fouling agents.[13] Jolly *et al.*[14] demonstrated that a thiol-terminated sulfobetaine modified sensor yielded a <1% R_{ct} after the sensor was incubated in human serum albumin. Trouillon *et al.*[15] investigated the performance of many polymeric membrane coatings including Nafion, cellulose acetate, chitosan, fibronectin, and polystyrene sulfonate/poly(l-lysine) for a gold electrode in resisting

fouling by bovine serum albumin. Their ability to resist fouling was evaluated by performing cyclic voltammetry of $[Ru(NH_3)_6]^{2+/3+}$ and dissolved oxygen in the presence and absence of bovine serum albumin. Based on the peak potential, peak width, peak current, and capacitance, the $[Ru(NH_3)_6]^{2+/3+}$ detection results obtained at a fibronectin coated electrode was the only membrane that was not significantly different in the presence of bovine serum albumin from a pristine bare gold electrode.[15] All other coated electrodes showed some significant difference from a pristine bare gold electrode in the presence of bovine serum albumin, suggesting that the other membrane coatings provided less fouling protection. However, all of the tested membrane coatings provided some protection from fouling by bovine serum albumin compared to a bare gold electrode. Singh *et al.*[16] also investigated the effectiveness of several different polymeric film coated carbon fibre electrodes in resisting fouling during dopamine detection in brain tissues. Polymers used included Nafion, base-hydrolysed cellulose acetate, and fibronectin. While some 70%–80% dopamine oxidation current was retained at all electrodes even after incubating these electrodes in bovine serum albumin and then brain tissue for 2 h, base-hydrolysed cellulose acetate-modified electrodes were found to be most resistant to fouling. The authors attributed this finding to a steric barrier of cellulose film (with porosity easily manipulated by controlled hydrolysis) that has prevented macromolecules from diffusing to the surface.[17]

5.4 Grafting antifouling films on electrodes by diazonium chemistry

There are several challenges associated with polymer modified electrodes including film thickness control, poor reproducibility, slow response due to the low diffusion coefficient of the analyte through the film, and memory effect due to the strong affinity between a cationic analyte and the film. A feasible solution to these problems is to functionalise compounds with suitable functional groups on a carbon electrode by diazonium reduction so that the modified electrode will exhibit antifouling property against large fouling materials, but allow the small analyte to participate in electron

transfer reaction at the electrode surface. For example, Chira *et al.*[18] exploited diazonium chemistry to covalently attach 1-[(4-nitrophenyl)methyl]-4,4-bipyridinium to a glassy carbon electrode surface, yielding a stable 1-phenylmethyl-4,4´-bipyridine film. After incubating this electrode in bovine serum albumin for 20 min, the change in R_{ct} before and after incubation was estimated to be <2.5 kΩ. However, a corresponding change in R_{ct} of ~30 kΩ was observed at a bare glassy carbon electrode. The authors suggested that the antifouling property of the modified electrode was due to the reduction of surface hydrophobicity, masking of functional groups on the electrode by the immobilised film, and steric repulsion of fouling agents by the 1-phenylmethyl-4,4´-bipyridine. Similarly, Chandra *et al.*[19] electrochemically deposited a *p*-phenylacetate film on conical-tip carbon electrodes using diazonium chemistry to enhance the antifouling properties of the electrodes. Their modified electrodes offered a degree of protection for carbon electrodes against fouling during dopamine detection, as the modified electrodes were found to retain 75% of the initial detection signal after being incubated for 7 days in a simulated fouling solution containing caproic acid (a lipid), bovine serum albumin (a protein), cytochrome c (a protein), and human fibrinopeptide B (a peptide) that partially mimics the environment of extracellular fluid. During their *in vivo* experiments involving Sprague-Dawley rats, 70% to 95% of the dopamine oxidation current remained after the first 40 min and 50% remained over the next 20 min, indicating that the electrodes were not as fouling resistant as in the *in vitro* experiments. Therefore, the complex environment *in vivo* may need to be taken into consideration in the development of electrodes for *in vivo* detection. Notably, a polymer layer that passivates an electrode surface will tend to increase the impedance. Therefore, the compromise between impedance and fouling resistance must be assessed in considering the use of such films. As an alternative, Gui *et al.*[20] (2013) reported a low impedance phenyl phosphorylcholine based zwitterionic layer immobilised glassy carbon electrode. Owing to the influence of the charge of proteins on fouling, the adsorption of anionic bovine serum albumin and cationic cytochrome c was monitored at this modified electrode by fluorescence microscopy. Although the phenyl phosphorylcholine modified electrode demonstrated a greater or similar resistance to fouling by the two proteins compared to oligo(ethylene glycol)-modified glassy carbon

or gold electrodes, the impedance was much lower than that at the oligo(ethylene glycol)-modified electrodes. The results of this work suggest that complete charge balancing and packing of the charged groups of phophorylcholine zwitterions provided resistance to electrode fouling without producing a high impedance.

5.5 Antifouling and catalytic capability of the SO_3^- functional group

Gui *et al*.[20] investigated the resistance of a Ph-SO_3^- alone and a Ph-SO_3^- and Ph-$N^+(Me)_3$ modified glassy carbon electrodes towards nonspecific adsorption of bovine serum albumin and cytochrome c. They found less adsorption (almost 0%) of bovine serum albumin at the former electrode compared to the latter electrode, but the opposite was observed in cytochrome c. Although cytochrome c is cationic at physiological pH, it is also repelled by negatively charged Ph-SO_3^- and the reason was attributed to the similarity of Ph-SO_3^- coated surface to the kosmotrope-based protein resistant SO_4^{2-} kosmotropic anion. The term 'kosmotrope' refers to a group of salts of anions such as SO_4^{2-}, Cl^-, Br^- that can interact with the charged group of the proteins through electrostatic interaction. In addition, they may either affect protein folding or interact with structurally bound water molecules in the proteins.[21] Holmlin *et al*.[22] also reported antifouling behaviour at a *N*,*N*-dimethyl-amino-propane-1-sulfonic acid (-$N^+(CH_3)_2(CH_2)_3SO_3^-$) terminated self-assembled monolayer of thiol on a gold surface in fibrinogen and lysozyme proteins. Trouillon *et al*.[23] found that a poly(styrene-sulfonate)/poly(L-lysine) coated gold electrode exhibited fouling resistance against 4%(w/v) bovine serum albumin in a physiological concentration. In another work, Herman *et al*.[24] demonstrated a four-fold enhanced dopamine signal at a Ph-SO_3^- modified carbon fibre microelectrode compared to a bare carbon fibre microelectrode. Similarly, Jin *et al*.[25] observed an enhanced interaction between a negatively charged *p*-aminebenzene sulfonic acid (*p*-$NH_2PhSO_3^-$) film on a glassy carbon electrode and positively charged dopamine. They have also observed electrocatalytic activity of the film during oxidation of dopamine.

5.6 Scope of the present study

Based on the unique antifouling and catalytic capability of the $-SO_3^-$ functional group, we have further attached a 4-sulfophenyl group (Ph-SO_3^-) to a conical-tip carbon electrode already hydrogenated by *n*-butylsilane reduction to obtain a 4-sulfobenzene modified electrode. For comparison, we have also attached a 4-sulfophenyl group (Ph-SO_3^-) to a bare conical-tip carbon electrode. We will hereafter refer to a bare conical-tip carbon electrode as Electrode I, a bare conical-tip carbon electrode modified with 4-sulfobenzene as Electrode II (see classification tabulated in Table 5.2). We will also hereafter refer to a conical-tip carbon electrode hydrogenated by *n*-butylsilane reduction as Electrode III and the corresponding 4-sulfobenzene modified electrode as Electrode IV. Electrode IV will be achieved by the electrochemical reduction of 4-sulfobenzenediazonium tetrafluoroborate (4-SBD) to enhance the antifouling property already achieved at Electrode III. Additionally, as reported in Section 4.9.1.3, there was still a ~15% decrease in the dopamine oxidation signal at Electrode III. We aim at achieving enhanced dopamine detection signal at Electrode IV arising from the electrostatic attraction between the negatively charged surface and the positively charged dopamine.

In this chapter, we will also compare the antifouling property of diethylsilane hydrogenated carbon electrodes to that of *n*-butylsilane hydrogenated carbon electrodes. We will also hereafter collectively refer to conical-tip carbon electrodes hydrogenated by diethylsilane reduction as Electrode V. This experiment has been performed to investigate the difference between branched and straight alkyl-chain silane compounds on antifouling property. A 4-sulfobenzene was then immobilised on Electrode V (denoted as Electrode VI) to maximise antifouling property during dopamine detection in the presence of fouling agents. Finally, Electrode III, Electrode IV, Electrode V and Electrode VI were used to determine dopamine spiked in human serum to demonstrate their applicability to routine dopamine analysis in biological samples.

Electrode Name	Electrode type
Electrode I	Bare conical-tip carbon electrode
Electrode II	Bare conical-tip carbon electrode modified with 4-sulfobenzene
Electrode III	Conical-tip carbon electrode hydrogenated by *n*-butylsilane
Electrode IV	*n*-Butylsilane hydrogenated conical-tip carbon electrode further modified by 4-sulfobenzene
Electrode V	Conical-tip carbon electrode hydrogenated by diethylsilane
Electrode VI	Diethylsilane hydrogenated conical-tip carbon electrode further modified by 4-sulfobenzene

Table 5.2. Summary of different types of electrodes investigated.

5.7 Experimental

5.7.1 Chemicals and Reagents

Tetrabutylammoniumtetrafluoroborate, sodium tetrafluoroborate, sulfanilic acid, sodium nitrite, tetrafluoroboric acid (48%), acetonitrile (HPLC grade), diethylether, ethanol, methanol, calcium chloride and human serum were purchased from Sigma-Aldrich (Sydney, Australia). All reagents were used without further purification.

5.7.2 Hydrogenation of conical-tip carbon electrodes by diethylsilane

Bare conical-tip carbon electrodes were fabricated and then hydrogenated by *n*-butylsilane reduction (Electrode III) as described in Section 2.4.1 and 2.4.2. In this

chapter, bare carbon electrodes were also hydrogenated by diethylsilane (Electrode V) in a similar procedure adopted in the *n*-butylsilane reduction method with diethylsilane replacing *n*-butylsilane.

5.7.3 Synthesis and characterisation of 4-sulfobenzenediazonium tetrafluoroborate (4-SBD)

4-SBD was synthesised according to the method proposed by Herman *et al*.[24] Briefly, sulfanilic acid (17.3 g, 0.1 mol) was dissolved in tetrafluoroboric acid (48%(v/v), 37 mL, 0.2 mol). The solution was cooled in an ice-salt bath to –5 °C. Sodium nitrite (6.9 g, 0.1 mol) was then completely dissolved in water before it was added dropwise to sulfanilic acid over a 30-min period with mechanical stirring. The resulting suspension was vacuum filtered, and the white precipitate was washed with an ice cold ether/methanol mixture (4:1), purified by washing with small amounts of ice cold ethanol, and dried over calcium chloride in a desiccator. The compound was then stored at 4°C. For characterisation, Fourier Transform Infrared (FT-IR) spectrum of 4-SBD was recorded on a Thermo Scientific Nicolet iS10 ATR FTIR spectrometer.

5.7.4 Construction of Electrode IV and Electrode VI

Cyclic voltammetry[26] of 1.0 μM 4-SBD was carried out at Electrode III and Electrode V in 0.1 M tetrafluoroboric acid (48%) (HBF_4; prepared in 1:9 water-acetonitrile mixture) between +0.5 V and −1.2 V to graft 4-SB on to these electrodes to obtain Electrode IV and Electrode VI, respectively. The 4-SBD solution was deaerated with nitrogen for at least 10 min prior to use. Electrode IV and Electrode VI were rinsed with copious volumes of acetonitrile, followed by Mili-Q water and dried under a stream of nitrogen before further use.

5.7.5 XPS Analysis

XPS was performed as described in Section 3.5.7.

5.7.6 Electrochemical measurements and electrochemical impedance spectroscopy

All electrochemical measurements were carried out as described in Section 3.5.6 and Section 4.8.7. Differential pulse voltammetry was performed as described in Section 4.8.3.

5.8 Results and Discussion

5.8.1 Controlled grafting of a 4-SB film on Electrode III

In this work, we have deposited a 4-SB film on Electrode III by electrochemical reduction of 4-SBD. Before electrochemical reduction, the synthesised 4-SBD was characterised by FT-IR. A strong band at 2298 cm^{-1} in the FT-IR spectrum shown in Figure 5.1 indicates the presence of diazonium group. We have used this as an evidence for the successful synthesis of 4-SBD.

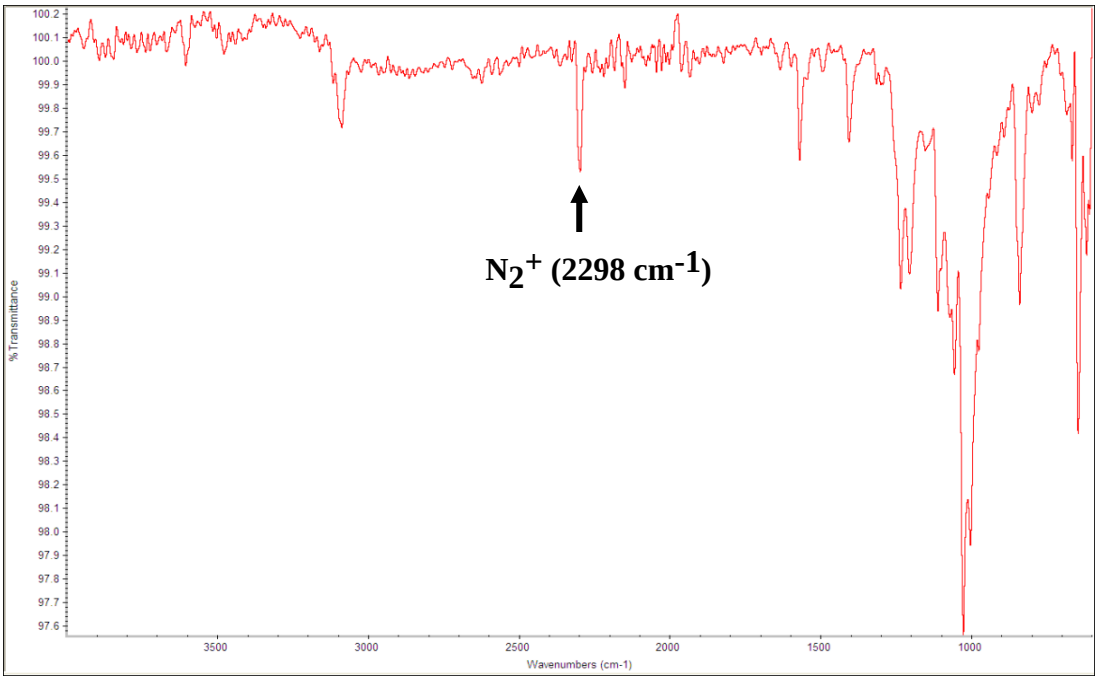

Figure 5.1 An FT-IR spectrum of the 4-SBD salt.

For comparison, we have initially deposited 4-SB on a bare conical-tip carbon electrode to obtain Electrode II and Figure 5.2(a) shows a cyclic voltammogram for the reduction of 1.0 µM 4-SBD at Electrode I. In this voltammogram, we observed a reduction peak at ~ - 0.78 V in the first scan, which then gradually became attenuated starting from the second scan and the electrode was eventually passivated by 4-SB, in agreement with observation reported by Gui *et al.*[26] involving grafting of 4-SB on a glassy carbon electrode. Herman *et al.*[24] also modified a carbon fibre microelectrode by reducing 1.0 mM 4-SBD and they observed a completely attenuated reduction signal even just after one scan. Therefore, our observation above was attributed to the formation of 4-SB-derived Electrode I. We have further illustrated a possible mechanism for this reduction process in Scheme 5.1(a). As shown, a covalent bond between Electrode I and the 4-SB organic layer originates from the reduction of the diazonium salt 4-SBD. In the next step, this same radical attacks the first grafted aryl group to yield a polyaryl layer nanometre to micrometre in thickness. As a result, monolayers can not be obtained by this method.[27] The absence of the 4-SBD reduction wave in the second scan also indicated that the electrode was already passivated by the molecular layer formed on the surface during the first scan. Liu *et al.* proposed that a propagating multilayer could form a poorly defined molecular-level structure on electrode surface[28], which may not favour electron transfer reaction. Kariuki *et al.*[29, 30] described the nucleation and growth of functionalised aryl films on ordered graphite. Repetitive cycling has caused continual deposition of aryl group multilayers through the formation of electrochemically generated free radicals and polymerisation reaction. Notably, a thick aryl film passivated the electrode and rendered it useless for redox process involving the analyte. The effect of multilayer formation in our work is further discussed in Section 5.8.2.1 – 5.8.2.3.

As a first option, the attachment of aryl groups and the thickness of the film through electrochemical reduction of the corresponding diazonium salt can be controlled by potential cycling or through diazonium concentration and electrolysis time.[31] Alternatively, a strategy to suppress the growth of multilayers is to use bulky diazonium salts to prevent formation of bonds between the *in situ* generated radicals and the aryl

groups already grafted on the surface, by way of steric repulsion between substituents on the reagent. Previously, trimethylammonio[32], and very recently, triisopropylsilyl[28] attached with diazonium moieties were used to obtain steric hindrance and sterically controlled functionalisation of an electrode surface.

In our work, we observed complete passivation of bare electrodes after adopting the first option, making these electrodes useless for further application. Hence, we have decided to apply the alternative option involving steric hindrance during grafting of 4-SB. In these experiments, we have sequentially prepared Electrode III, and then grafted 4-SB on these electrodes to obtain Electrode IV. As shown in Figure 5.2(b), the reduction of 4-SBD signal at Electrode III was attenuated slowly and the electrode was only passivated after 10 cyclic voltammetric scans. As shown in Scheme 5.1(b), on Electrode III, the bulky butylsiloxane group was ideal to cause steric hindrance that in turn prevented the free radicals from propagating multi/close packed layers of 4-SB, and hence a slow passivation process during reductive adsorption. A similar pattern was observed by Allongue *et al.*[31] at a 4-nitrobenze diazonium tetrafluoroborate grafted highly ordered pyrolytic graphite electrode. These authors also found that the aryl groups grafted on the electrode surface were closely packed and exhibited a self-inhibition phenomenon during cyclic voltammetric reduction. This supported a slower grafting rate of 4-SB at Electrode III compared to Electrode I. Gui *et al.*[32] also observed that multiple scans required when bulky 4-(trimethylammonio)-phenyl diazonium salt was reduced at a glassy carbon electrode. Although the edge planes on an electrode are generally more reactive than the basal planes, the edge planes on Electrode III were terminated to C-H with diminished C-O functionalities responsible for fast electron transfer, giving rise to a lower rate of reduction of diazonium at Electrode III compared to that at Electrode I.

Randriamahazaka *et al.*[33] extensively reviewed the electrografting of different functionalities on an electrode by diazonium chemistry in a controlled manner. They described that a drawback of diazonium chemistry is the possible formation of multilayers from high radical intermediates when a diazonium salt was reduced,

rendering it difficult to obtain a well-controlled interface for electrochemical analysis. It was also found that 4-nitrobenzenediazonium tetrafluoroborate reduction produced a broad, irreversible reduction peak on the first scan that then disappeared in the second scan[33]. Combellas *et al*.[34] also reported the formation of aryl multilayers formed on a nitrobenzene modified glassy carbon electrode using diazonium reaction. As a result, large diazonium salts that facilitated steric hindrance on an electrode surface were suggested for use in preventing the formation of multilayers. In an analogous manner, the bulky butylsiloxane formed on Electrode III was expected to cause steric hindrance, which then prevented the formation of 4-SB multilayers, facilitating a controlled grafting of 4-SB on Electrode III.

5.8.2 Electrochemical characterisation of Electrode IV

Similar to work reported in Section 4.9.1, we have characterised Electrode II and Electrode IV using three redox systems: (i) 1.0 mM $[Ru(NH_3)_6]^{3+}$ in 1.0 M KCl, (ii) 1.0 mM $[Fe(CN)_6]^{3-}$ in 1.0 M KCl and (iii) 1.0 mM dopamine in pH 7.4 citrate/phosphate buffer. In this section, all carbon electrodes were hydrogenated by the *n*-butylsilane reduction method.

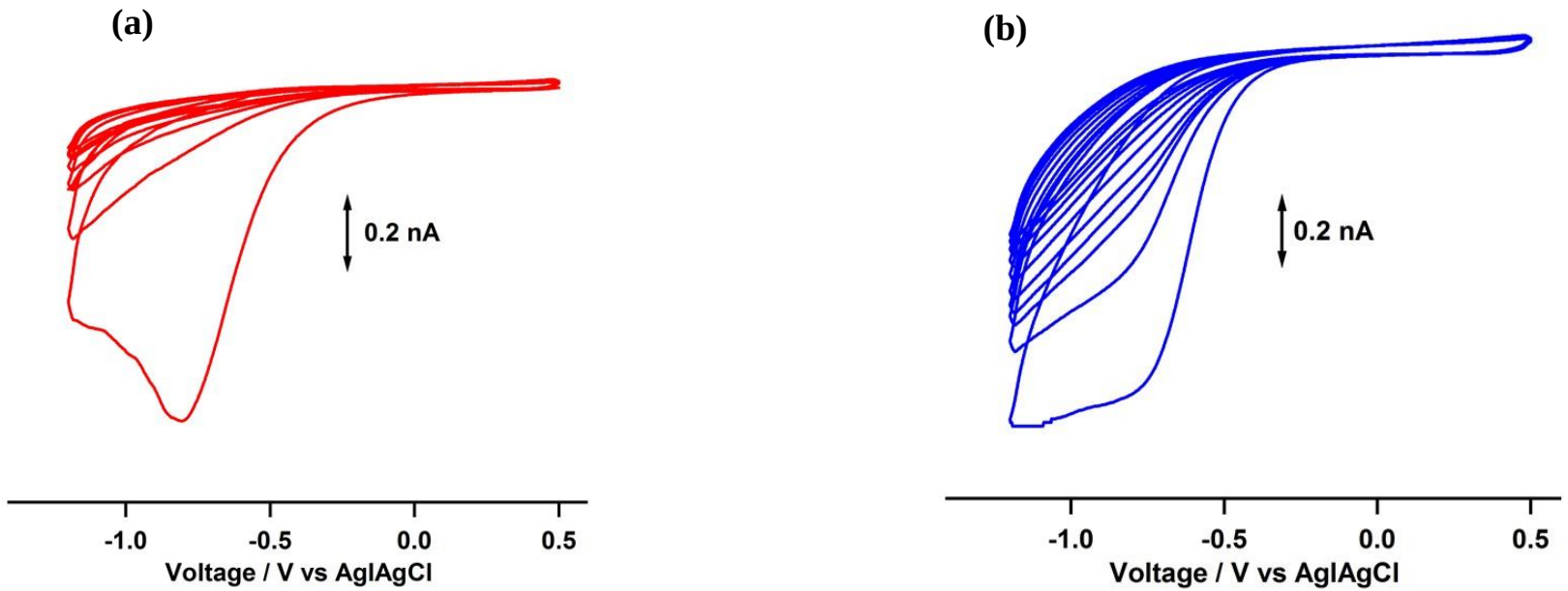

Figure 5.2. Cyclic voltammetry of 1.0 μM 4-SBD in 0.1 M HBF_4 / (1:9 water-acetonitrile), at (a) Electrode I and (b) Electrode III; scan rate: 100 mV s^{-1}.

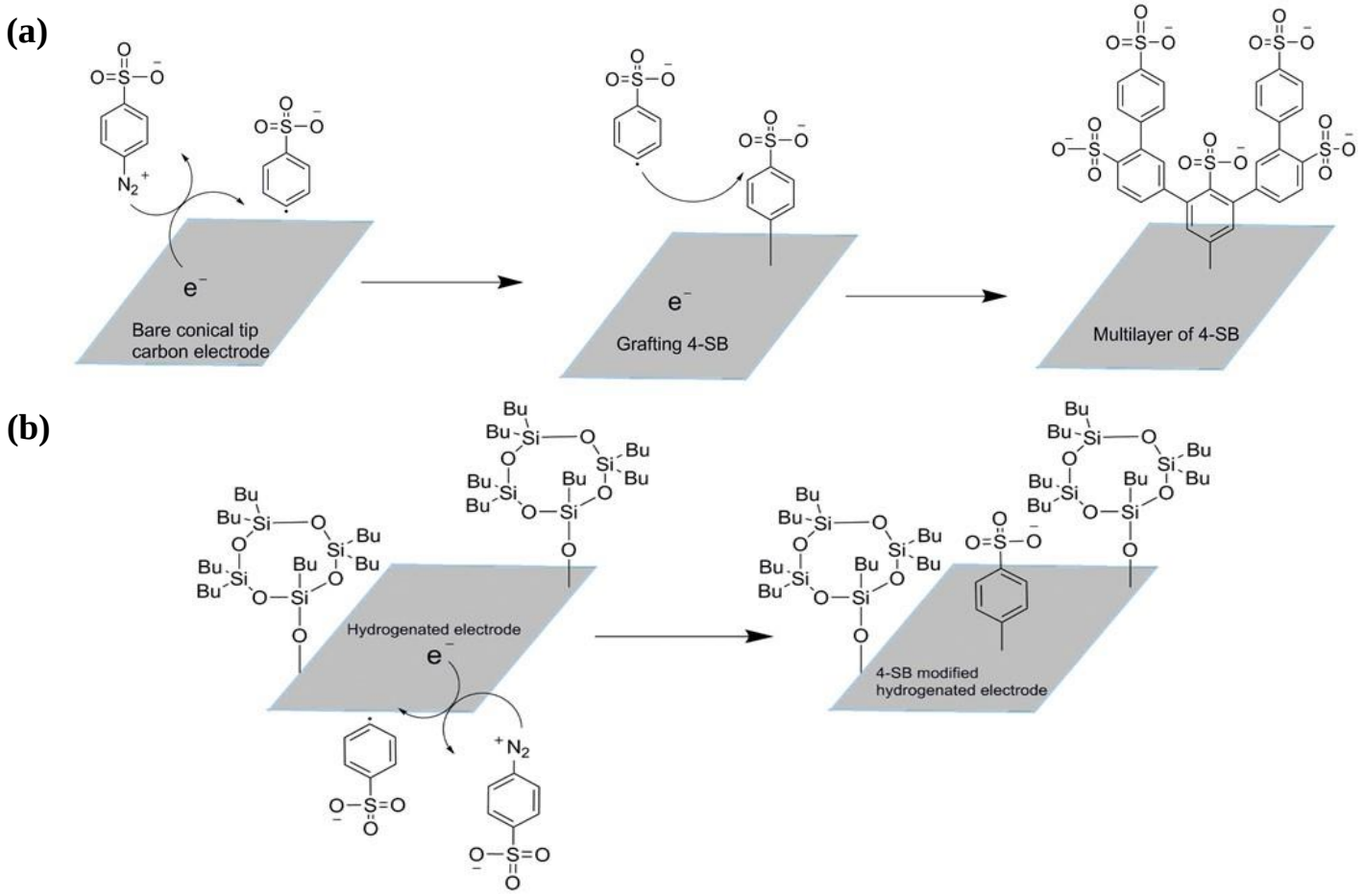

Scheme 5.1. Formation of (a) thick, dendritic polyphenyl multilayers on Electrode I and (b) a thin, isolated 4-sulfobenzene monolayer with an *n*-butylsiloxane film on Electrode III, while 4-SB was immobilised through diazonium reduction.

5.8.2.1 Characterisation of Electrode IV in $[Ru(NH_3)_6]^{3+}$

Cyclic voltammograms of 1.0 mM $[Ru(NH_3)_6]^{3+}$ in 1.0 M KCl at Electrode II and Electrode IV are shown in Figure 5.3. In Figure 5.3(a), a familiar wave (trace i) was obtained for the reduction of $[Ru(NH_3)_6]^{3+}$ at Electrode I. This experiment was then repeated at Electrode II and the voltammogram obtained is shown in trace ii. $[Ru(NH_3)_6]^{3+}$ is generally known as an outer sphere redox marker and its electrochemistry is not expected to be influenced by the type of carbon electrode surface. However, we observed a 50% decrease of the $[Ru(NH_3)_6]^{3+}$ limiting current in trace ii, compared to trace i. We attribute this to the formation of a closely packed, thick aryl film functionalised with sulfonate groups (see Scheme 5.1(a)), causing the electrode to lose its conductivity. Previously, Gui *et al.*[32] also reported the complete suppression of $[Ru(NH_3)_6]^{3+}$ reduction signal at a 4-(trimethylammonio)-phenyl group modified glassy carbon electrode. The cyclic voltammogram of $[Ru(NH_3)_6]^{3+}$ obtained at Electrode III is displayed in trace i of Figure 5.3(b), and the corresponding voltammogram at Electrode IV is shown in trace ii. We observed a ~4% increase in the $[Ru(NH_3)_6]^{3+}$ reduction limiting current in trace ii relative to that in trace i. This was most likely caused by an electrostatic attraction of positively charged $[Ru(NH_3)_6]^{3+}$ by the negatively charged 4-SB on the electrode surface. This would have in turn enhanced the electron transfer rate, suggesting that the 4-SB layer was not sufficiently closely packed on the hydrogenated electrode surface compared to that on the bare electrode. Similarly, ~7% increase in the $[Ru(NH_3)_6]^{3+}$ reduction signal was also reported at a 4-sulfophenyl diazonium tetrafluoroborate modified glassy carbon electrode.[26] Electrochemical parameters including $E_{1/2}$, waveslope, and E_T estimated from the cyclic voltammograms obtained at Electrode III and Electrode IV are tabulated in Table 5.2. All these parameters appear to be very similar at Electrode III and Electrode IV, which is expected for such an outersphere redox marker as $[Ru(NH_3)_6]^{3+}$.

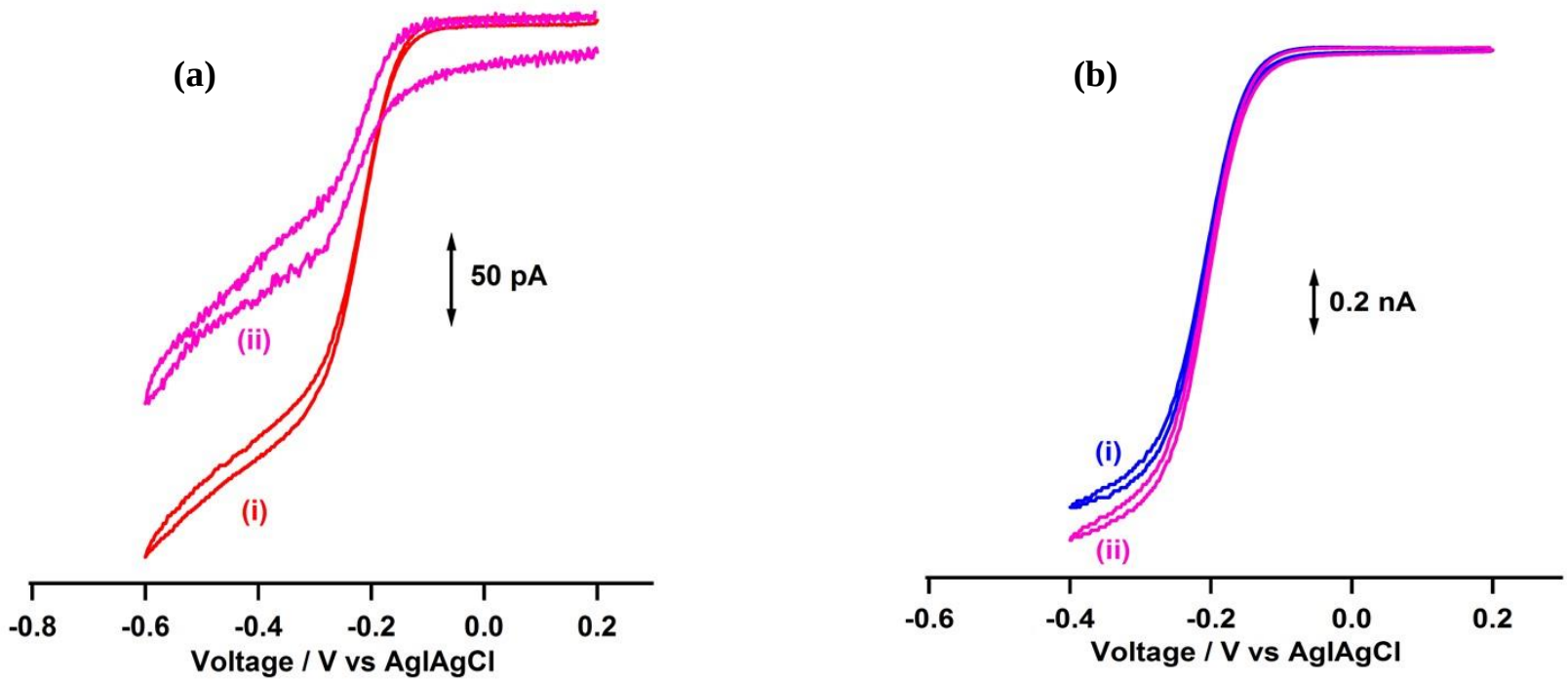

Figure 5.3. Cyclic voltammetry of 1.0 mM $[Ru(NH_3)_6]^{3+}$ at (a) Electrode I (trace i) and (trace ii) Electrode II (b) Electrode III (trace i) and (trace ii) Electrode IV in 1.0 M KCl. Scan rate: 100 mV s^{-1}.

5.8.2.2 Characterisation of Electrode IV in $[Fe(CN)_6]^{3-}$

In general, the heterogeneous electron-transfer reaction of an inner-sphere redox-active molecule on a modified electrode requires permeation of the redox marker through pinholes in the molecular layer to the electrode surface. In this way, such work may therefore help elucidate the presence and size of void spaces in the layer.[35] Initially, we conducted cyclic voltammetry of 1.0 mM $[Fe(CN)_6]^{3-}$ at Electrode I and the result obtained is shown by trace i of Figure 5.4(a). The corresponding voltammogram obtained at Electrode II is shown by trace ii. In trace ii, the $[Fe(CN)_6]^{3-}$ reduction signal was completely suppressed, yielding a featureless cyclic voltammogram. This result indicates a severe electrode passivation by multilayers of 4-SB. Similarly, Gui *et al*.[26] reported a featureless cyclic voltammogram of $[Fe(CN)_6]^{3-}$ at a 4-SB modified glassy carbon electrode, attributable to the barrier effect of the 4-SB layer to $[Fe(CN)_6]^{3-}$. However, the cyclic voltammogram of $[Fe(CN)_6]^{3-}$ at a 4-SB modified gold electrode showed only a 20% decrease in the redox current suggesting the layer was not as compact as that on a glassy carbon electrode.[26]

The above experiment was then repeated at Electrode III and Electrode IV. The cyclic voltammograms obtained are shown in trace i and trace ii of Figure 5.4(b), respectively. In these experiments, a sigmoidal shaped cyclic voltammogram with ~22% reduction of limiting current was estimated in trace ii compared to that in trace i. This indicates that void spaces remaining between the grafted 4-SB and the butylsiloxane layer, permitting $[Fe(CN)_6]^{3-}$ to pass through and reach the electrode surface. The $E_{1/2}$ at Electrode IV has shifted negatively by 166 mV compared to that at Electrode III, supporting slower kinetics of $[Fe(CN)_6]^{3-}$ at the former electrodes. As demonstrated in Section 4.9.1.2, a hydrogenated electrode surface is not favourable for the electron transfer reaction of $[Fe(CN)_6]^{3-}$ and the electron transfer process was found to be irreversible. At Electrode IV, the process became even more irreversible as shown by the changes in waveslope and E_T compared to those at hydrogenated electrodes, as tabulated in Table 5.2.

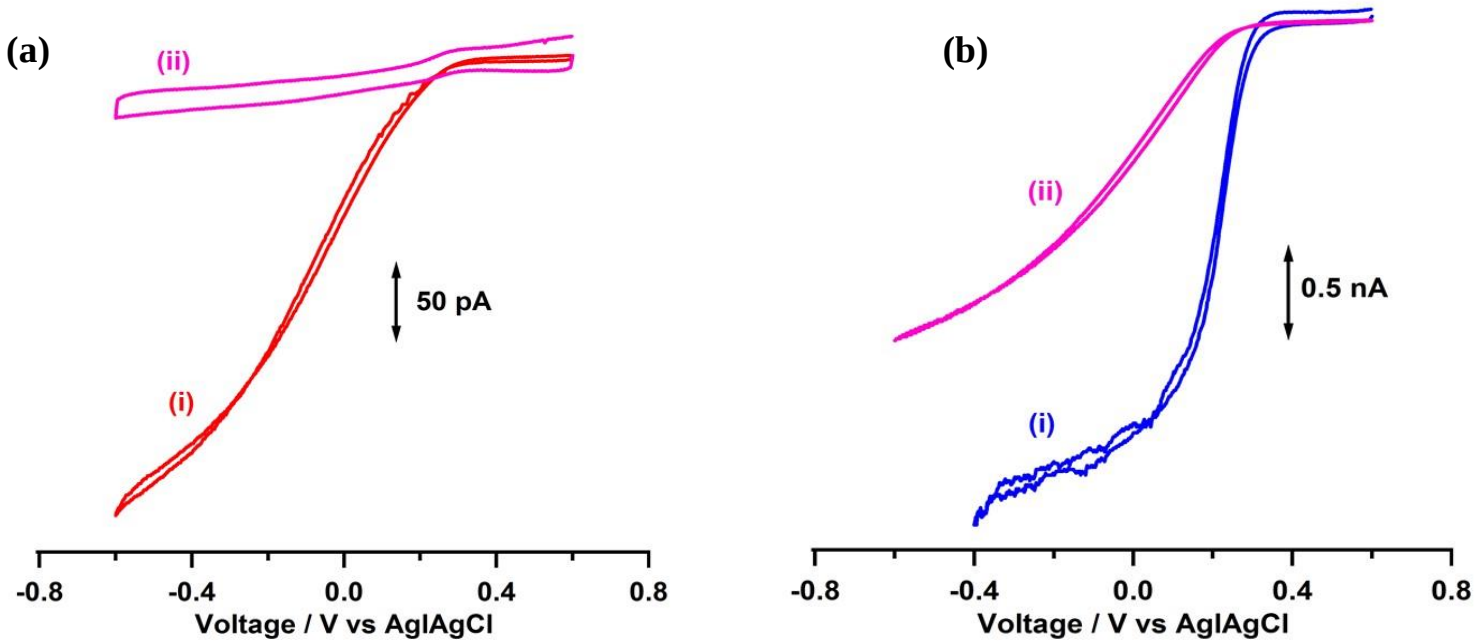

Figure 5.4 Cyclic voltammetry of 1.0 mM $[Fe(CN)_6]^{3-}$ at (a) Electrode I (trace i) and (trace ii) Electrode II; (b) Electrode III (trace i) and Electrode IV (trace ii) in 1.0 M KCl. Scan rate: 100 mV s^{-1}.

5.8.2.3 Characterisation of Electrode IV in 1.0 mM dopamine

In this work, Electrode IV were also characterised using the inner-sphere redox marker dopamine and the corresponding cyclic voltammograms are presented in Figure 5.5(a) and (b). Trace i in Figure 5.5(a) shows an expected sigmoidal-shape cyclic voltammogram of 1.0 mM dopamine at Electrode I in a pH 7.4 citrate/phosphate buffer. However, the corresponding cyclic voltammogram obtained at Electrode II, displayed in trace ii, has lost the sigmoidal-shape feature and the charging current has significantly increased. As discussed earlier, this is attributed to hindered electron transfer of dopamine at an electrode passivated by a thick layer of 4-SB. Such an electrode has therefore become useless in the analytical detection of dopamine. In comparison, Liu *et al*.[28] also observed a featureless cyclic voltammogram of ferrocene at a multi polyphenylene layer modified glassy carbon electrode that was achieved by the reduction of benzyl alcohol. However, these authors subsequently reported a quasi-reversible ferrocene response at a separate electrode modified by a controlled grafting of benzyl alcohol involving a bulky triisopropylsilyl group.[28] In contrast, Herman *et al*.[24] were able to achieve enhanced dopamine oxidation signal at a 4-SB grafted carbon fibre electrode based on the electrostatic attraction between cationic dopamine and the negatively charged 4-SB. Similarly, by doping negatively charged polystyrene sulfonate as a counterion in an electrochemically polymerised pyrrole film on interdigitated gold microelectrodes, Sasso *et al*.[36] were able to achieved a 2-fold enhanced dopamine signal compared to that at a corresponding unmodified bare gold electrode. However, by comparing the cyclic voltammograms of dopamine at Electrode III (trace i of Figure 5.5(b)) and at Electrode IV (trace ii of Figure 5.5(b)), a 10% enhanced dopamine signal was estimated at the latter electrode. In addition, there was a 35% negative shift of $E_{1/2}$ at Electrode IV compared to Electrode III, indicating faster electron transfer kinetics at modified electrodes. As tabulated in Table 5.2, there is a 58% decrease in the waveslope and a 61% decrease in E_T at Electrode IV, compared to Electrode III, also supporting a more electrochemically reversible dopamine electron reaction at Electrode IV.

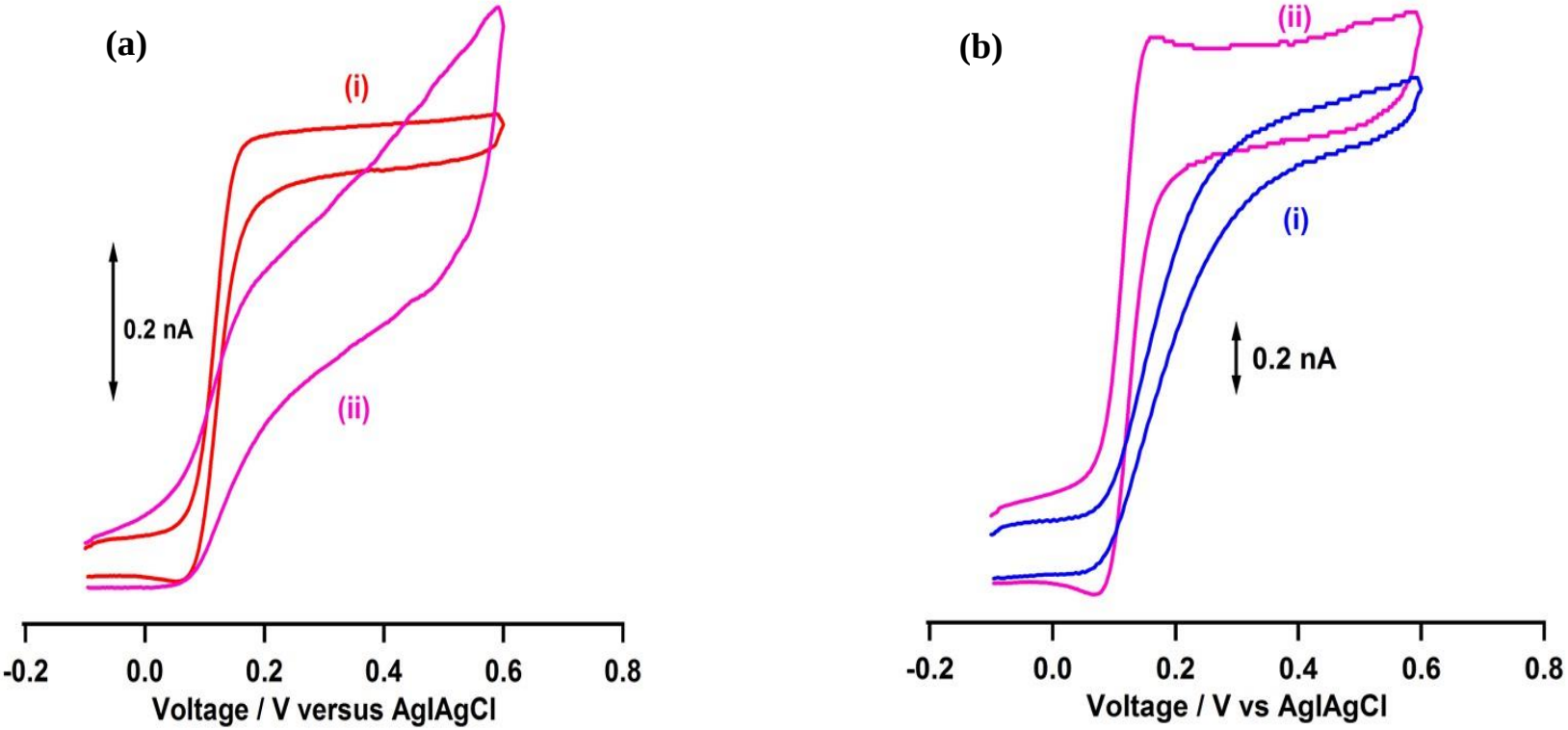

Figure 5.5 Cyclic voltammetry of 1.0 mM dopamine at (a) Electrode I (trace i) and (trace ii) Electrode II; (b) Electrode III (trace i) and Electrode IV (trace ii) in citrate/phosphate buffer. Scan rate: 100 mV s^{-1}.

	Redox markers								
	$[Ru(NH_3)_6]^{3+}$			$[Fe(CN)_6]^{3-}$			Dopamine		
Electrodes	$E_{1/2}$ / mV	Waveslope / mV decade^{-1}	E_T / mV	$E_{1/2}$ / mV	Waveslope / mV decade^{-1}	E_T / mV	$E_{1/2}$ / mV	Waveslope / mV decade^{-1}	E_T / mV
Electrode III	-206 (8)	65 (6)	64 (1.8)	130 (8)	125 (40)	174 (43)	186 (36)	92 (28)	100 (34)
Electrode IV	-212 (11)	69 (9)	63 (0.9)	-33 (78)	236 (33)	264 (59)	121 (12)	38 (8)	39 (11)

Table 5.2. Summary of electrochemical parameters obtained for the three redox markers at Electrode III and Electrode IV.

All values in parentheses are standard deviations estimated from seven electrodes.

5.8.2.4 Electrochemical impedance spectroscopic studies of modified electrode surfaces

We have previously reported an electrochemical impedance spectroscopic investigation of Electrode I and Electrode III in Section 4.9.1.4. In this chapter, we will focus on the R_{ct} obtained in the electrochemical impedance spectroscopic study of Electrode IV to examine the effect of 4-SB on the electron transfer kinetics of $[Ru(NH_3)_6]^{3+}$ at the corresponding Electrode II and Electrode IV. By comparing the Nyquist plot (trace i, Figure 5.6(a)) obtained at Electrode I to that (trace ii) obtained at Electrode II, we observed that the R_{ct} at Electrode II was ~5 times larger than that at Electrode I. In addition, as shown in Figure 5.6(b), the Nyquist plots obtained at Electrode III and Electrode IV displayed two semicircles in the high frequency region. Based on the diameter of the first semicircle, the R_c has most likely originated from the butylsiloxane film as described in Section 4.9.1.4, and this was observed to remain almost unchanged after 4-SB modification. However, the R_{ct} from the second semicircle in trace ii was half of that in trace i. This is most likely due to the electrostatic attraction of $[Ru(NH_3)_6]^{3+}$ to the electrode by the negatively charged 4-SB for electron transfer reaction.

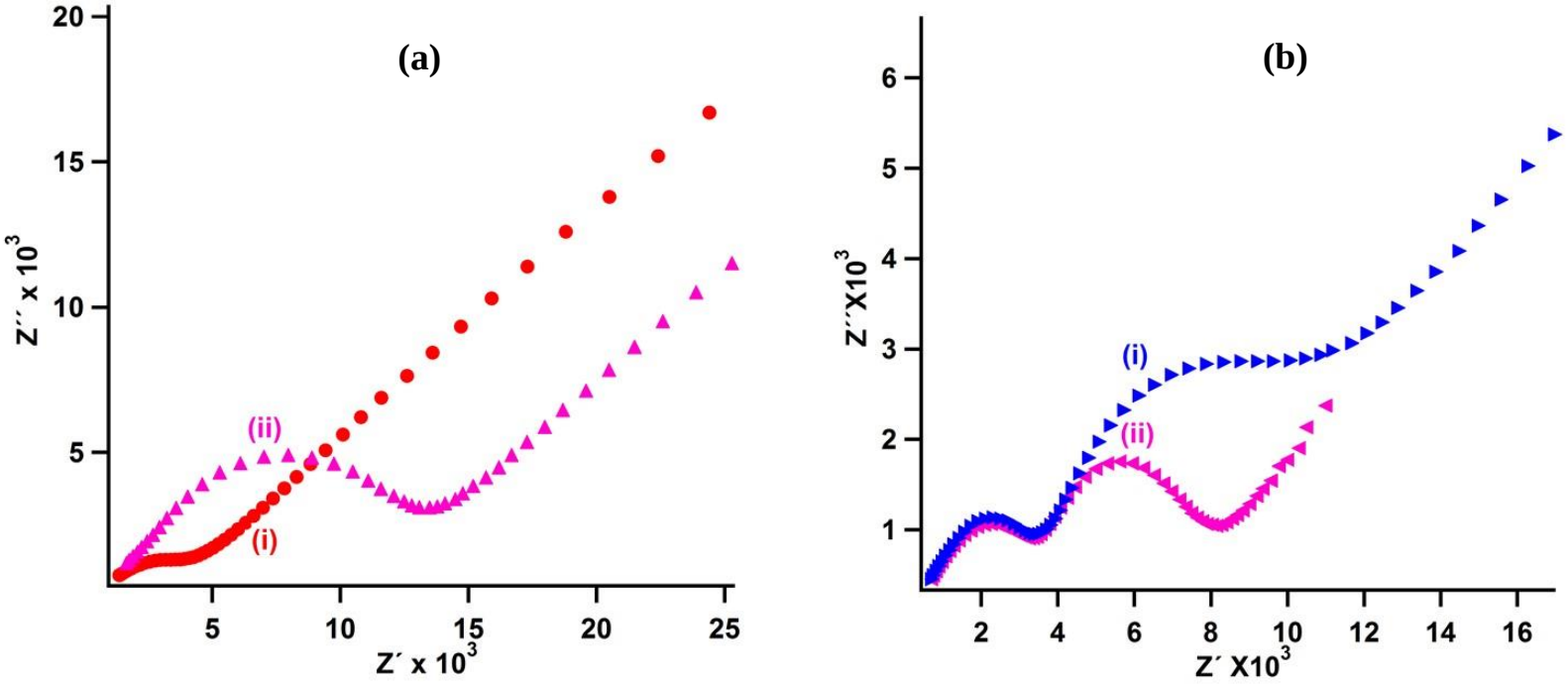

Figure 5.6 Nyquist plots of 1.0 mM $[Ru(NH_3)_6]^{3+}$ at electrode (a) Electrode I (trace i) and (trace ii) Electrode II; (b) Electrode III (trace i) and Electrode IV (trace ii) in 1.0 M KCl supporting electrolyte. Frequency range is 100 kHz – 0.1 Hz with 10 mV wave potential amplitude at the formal $E_{1/2}$ of 0.2 V.

5.8.3 Characterisation of Electrode IV by X-ray photoelectron spectroscopy

X-ray photoelectron spectroscopy was next conducted to further investigate the characteristics of Electrode II and Electrode IV. Both the survey X-ray photoelectron spectroscopy spectra and Gaussian-fitted results obtained at these electrodes are presented in Figure 5.7(a) and (b). These spectra show common distinct C1s, O1s, S2s and S2p peaks. However, in the survey spectra of Electrode II (Figure 5.7 (a)), an additional Na1s peak was observed, which was absent at Electrode IV. In contrast, a Si2p peak was also observed in Figure 5.7(b), as expected.

Based on deconvolution, the corresponding high-resolution spectra obtained at these electrodes are displayed in Figure 5.8(a). There were 3 peaks identified in the C1s spectrum of Electrode II. As discussed in Section 3.6.5, the peak centred at 284.8 eV was assigned to the carbon substrate including sp^2 like graphitic carbon and sp^3-hybridised diamond like carbon.[37,38] The other two peaks centred at 286.7 and 288.2 eV were assigned to carbon in 4-SB aromatic ring, and C-O species, respectively by comparing to the spectrum of a 4-SB modified glassy carbon electrode.[20,32] The C-O species would have been formed on the graphitic electrode surface during pyrolysis of carbon during the electrode fabrication process.[39]

As shown in Figure 5.8(b), the deconvoluted results at Electrode IV also yielded 3 peaks under C1s. Compared to 3 peaks shown in Figure 5.8(a), all three peaks have slightly shifted to 284.7, 286.6 and 288.1 eV due to an altered chemical environment on the hydrogenated electrode surface.[38] Similar to the spectrum of Electrode II, peaks centred at 284.7 and 286.6 eV were assigned to carbon materials and carbon in benzene ring of 4-SB. The remaining peak centred at 288.1 eV might have originated from C–O present within the butylsiloxane moity on a hydrogenated carbon electrode as previously reported by us.[40]

Most functional oxygen groups would reportedly yield O1s binding energies within a narrow 531-535 eV range.[38,41] In this work, the deconvolution of the O1s spectrum at

Electrode II yielded two peaks at 531.8 and 533.2 eV, as shown in Figure 5.9(a). These two peaks most likely originated from C–O functionalities on a carbon electrode substrate.[37] The peak at 533.2 eV could have arisen from oxygen in the $–SO_3$ group present in 4-SB.[42] At Electrode IV, binding energies arising from oxygen-bearing functionalities (carbonyl, carboxyl, epoxy, *etc*) associated with carbon on an electrode surface, except phenolic hydroxyl, are expected to diminish when hydrogen atoms replaced these functionalities during hydrogenation.[43] However, we observed a peak at 532.04 eV in Figure 5.9(b), which could have arisen from a large number of oxygen present in the dendrimeric butylsiloxane derivative formed during hydrogenation, as previously reported by us.[43] Another peak at 533.3 eV was assigned to oxygen present in the $–SO_3$ group of 4-SB. This peak is similar to the 533.2 eV peak observed in spectrum (Figure 5.9(a)) of Electrode II.[42]

Following the introduction of a sulfonate group through diazonium reaction, the expected S2s and S2p signals were observed in the X-ray photoelectron spectra of Electrode II and Electrode IV, as shown in Figure 5.10(a) and (b), respectively. Deconvolution of the broad S2p core-level spectrum yields two binding energies of 169.4 ($2p_{1/2}$) and 168.1 ($2p_{3/2}$) eV in Figure 5.10(a), and 169.5 ($2p_{1/2}$) and 168.2 ($2p_{3/2}$) eV in Figure 5.10(b), which are consistent with the expected 2:1 peak ratio between $S2p_{3/2}$ and $S2p_{1/2}$.[32,28]

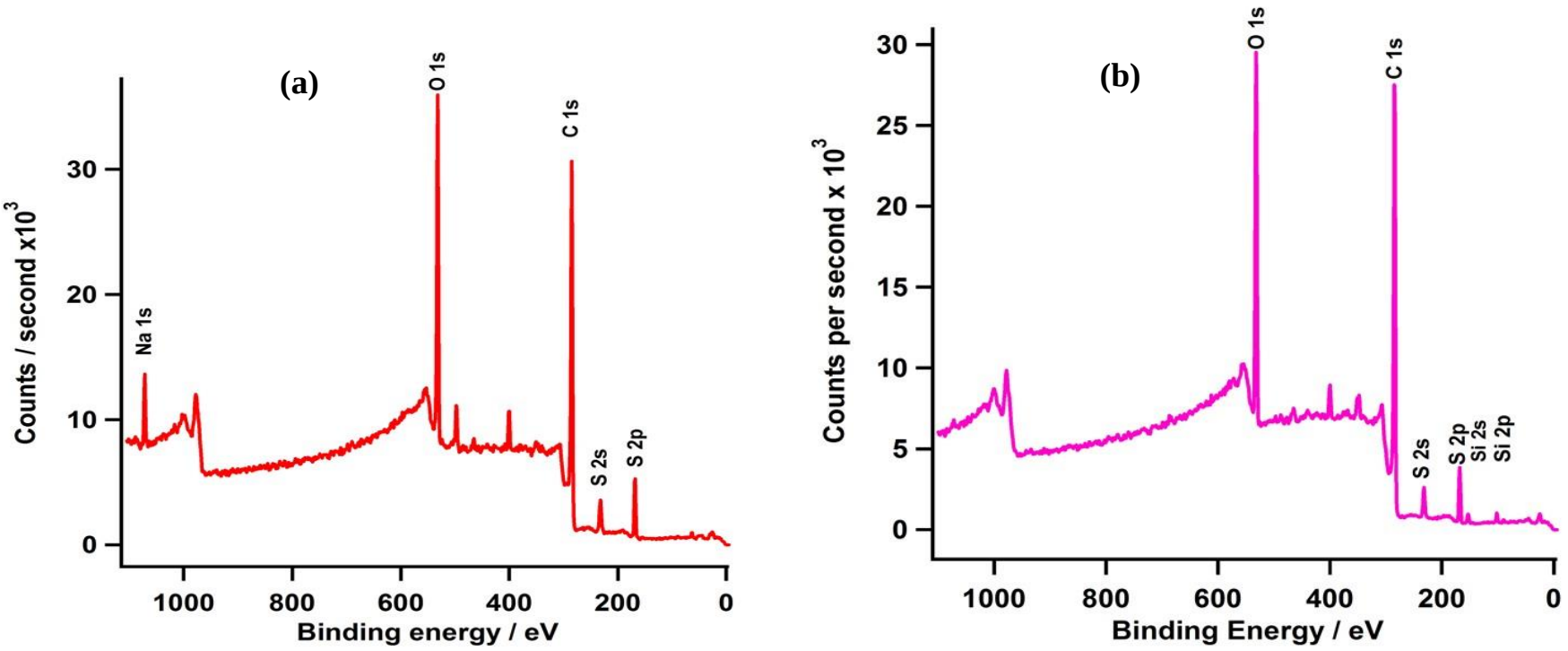

Figure 5.7. XPS survey spectra of (a) Electrode II and (b) Electrode IV.

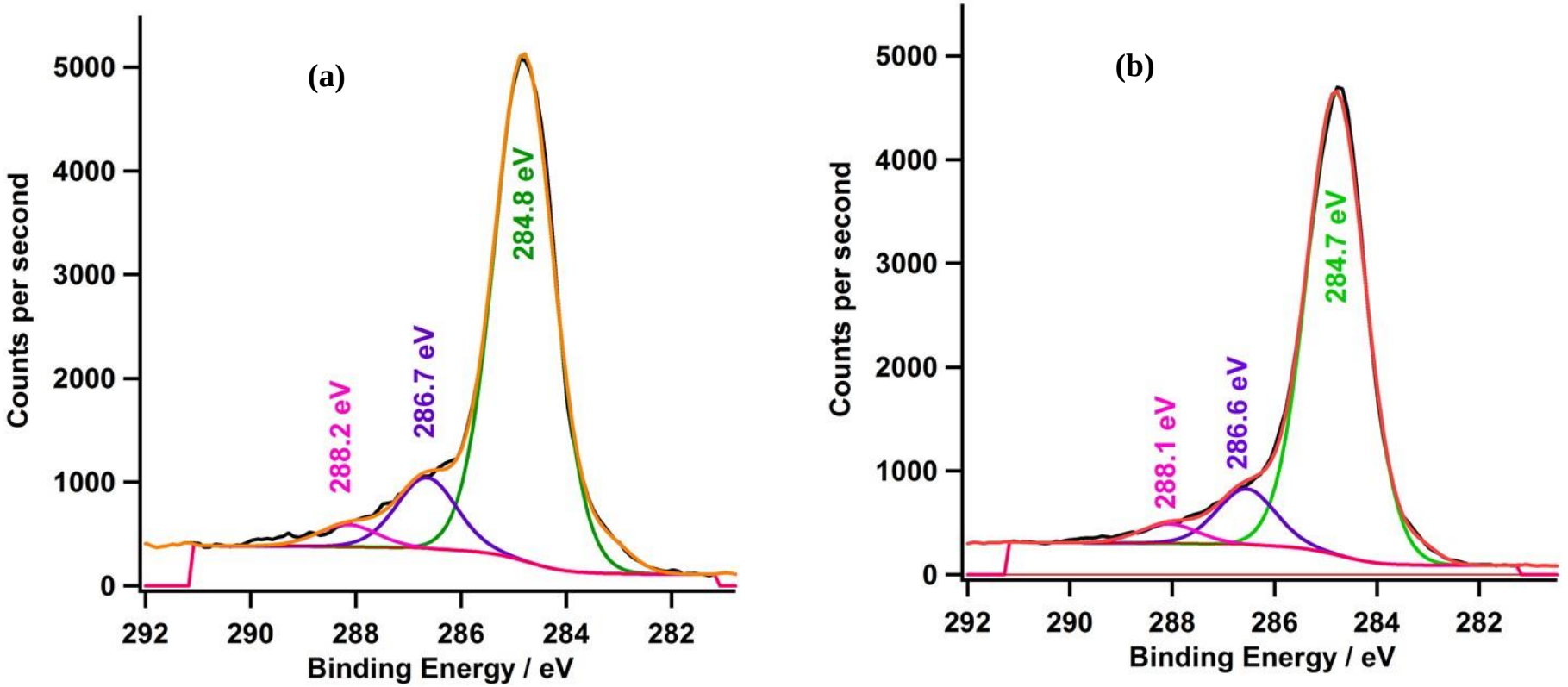

Figure 5.8 C1s peak fitting of spectra of (a) Electrode II and (b) Electrode IV.

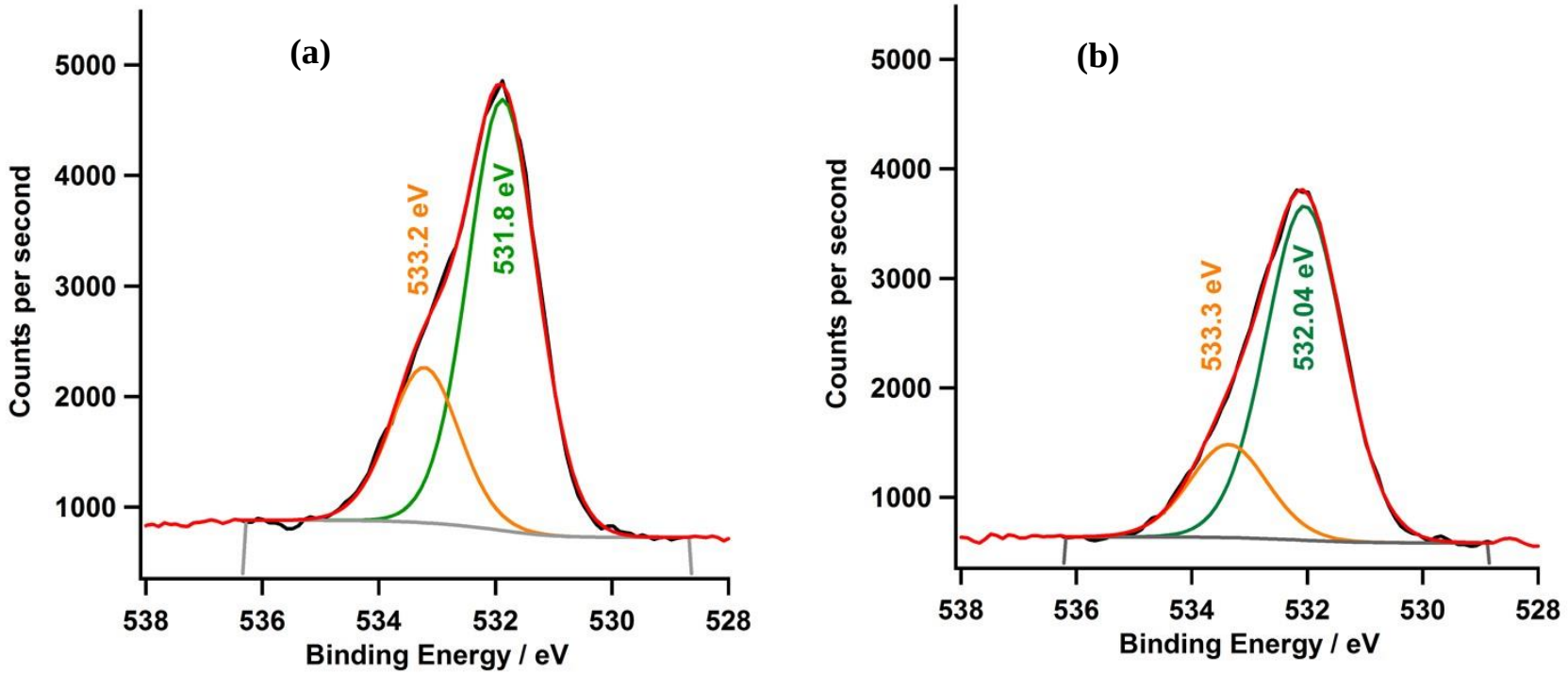

Figure 5.9. O1s peak fitting of spectra of (a) Electrode II and (b) Electrode IV.

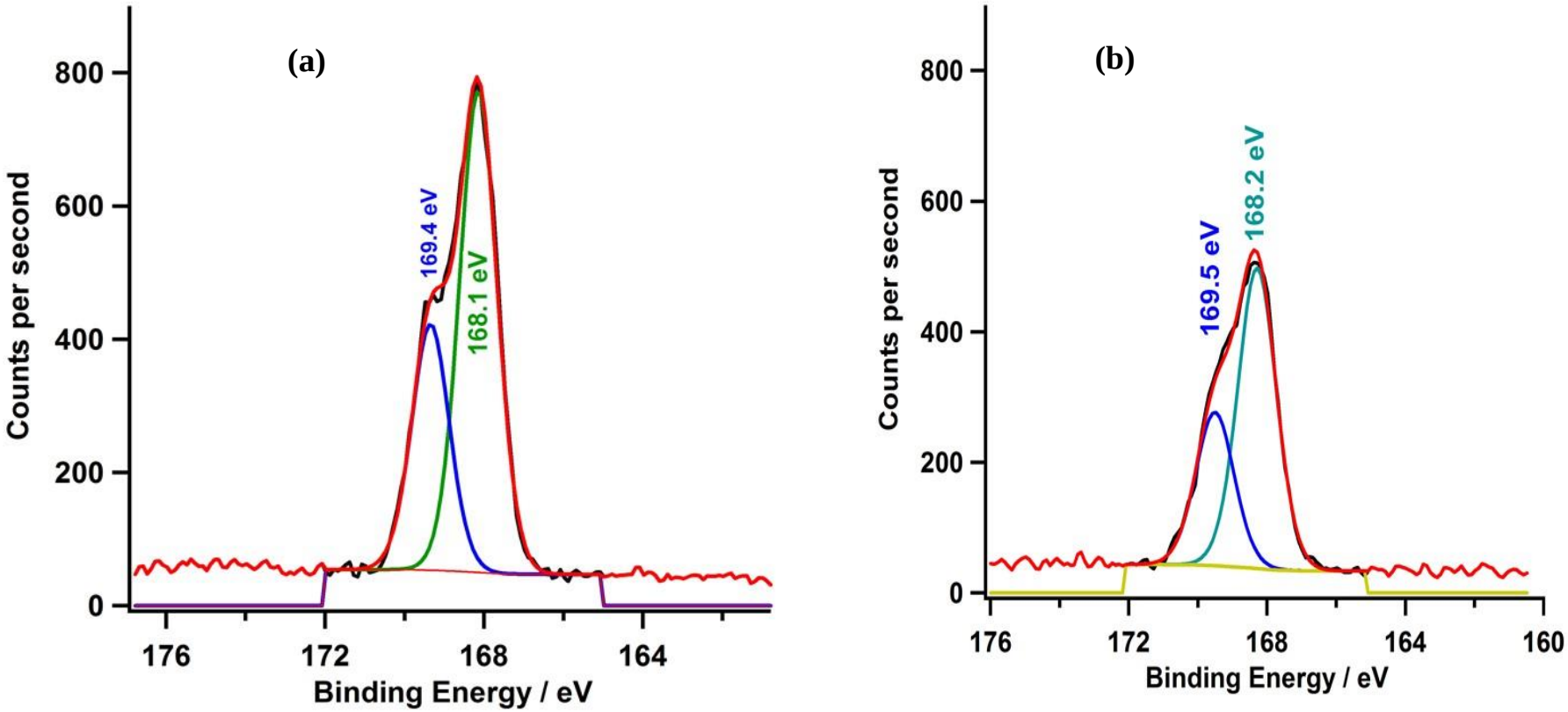

Figure 5.10. S2p peak fitting of spectra of (a) Electrode II and (b) Electrode IV.

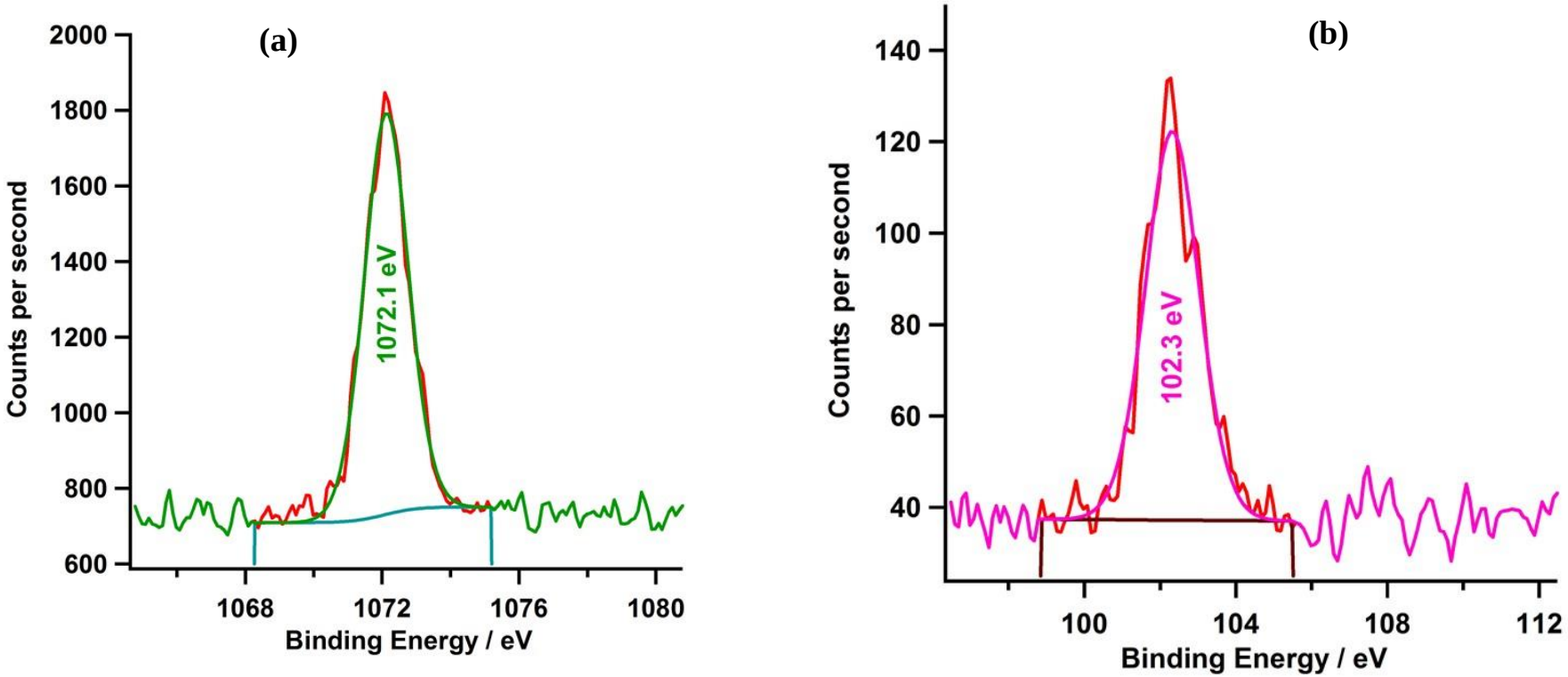

Figure 5.11. Na1s and Si2p peak fitting of spectra of (a) Electrode II and (b) Electrode IV.

Alternatively, a distinct Na peak centred at 1072.1 eV was observed in the spectrum (Figure 5.11(a)) of Electrode II, which was absent in the corresponding spectrum (Figure 5.7(b)) of Electrode IV. This peak indicates that Na^+ existed as counterions to neutralise the surface charge of $-SO_3^-$ at the bare carbon electrode, as suggested by Gui *et al.*[32] This was used to indicate that the negatively charged 4-SB was unavailable for electrostatic attraction towards such a positively charged analyte as dopamine. The Na^+ ion was likely to have originated from sodium tetrafluoroborate that was co-crystallised with 4-SBD during the synthesis, as reported previously.[26] However, the absence of this peak in the spectrum of Electrode IV may indicate that $-SO_3^-$ and a positively charged intermediate of *n*-butylsilane and carbon substrate (Scheme 5.2), formed during *n*-butylsilane hydrogenation as proposed by Nimmagadda and McRae[3], may have maintained an equal mole ratio on the electrode surface leaving $-SO_3^-$ available for electrostatic interaction with dopamine. In this respect, Gui *et al.*[32] reported similar observation on their $-SO_3^-$ and $-N^+(Me)_3$ (1:1 mole ratio) modified glassy carbon electrodes.

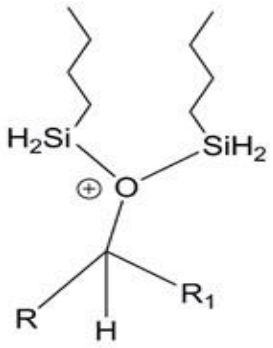

R = Alkyl, Aryl R_1 = Alkyl, Aryl, H

Scheme 5.2. Reaction intermediate in hydrogenation by *n*-butylsilane reduction. Adapted from reference 3.

On the other hand, a spectrum of Electrode IV in Figure 5.11(b) shows a characteristic Si2p peak at 102.3 eV as the sole observable signal. This Si peak would have originated from the butylsiloxane dendrimers formed by the hydrogenation process described in Section 3.6.5.

5.8.4 Evaluation of antifouling property of Electrode IV

In evaluating the antifouling capability of Electrode IV, we have conducted cyclic voltammetry of 1.0 mM dopamine at these electrodes after they were incubated in a laboratory synthetic fouling solution consisting of 4% (w/v) bovine serum albumin, 0.01% (w/v) cytochrome C (both are proteins), 1.0% (v/v) caproic acid (a lipid), and 0.002% (w/v) human fibrinopeptide B (a peptide) for a specified duration, as described in Section 4.9.5. The results obtained are shown in Figure 5.12. In this figure, trace i represents the cyclic voltammogram obtained at Electrode IV before any incubation in the fouling solution. After incubating the electrode in the fouling solution for 30 min, the cyclic voltammogram obtained is depicted in trace ii. Compared to trace i, there was a 15% decrease in the dopamine oxidation signal. In order to study the longer-term stability of these electrodes, they were incubated in the same fouling solution for 1 week before cyclic voltammetry of dopamine was repeated at these electrodes. As shown by the result in trace iii, the dopamine oxidation limiting current obtained was comparable to that in trace ii. In contrast, a 35% decrease in dopamine oxidation limiting current was observed at Electrode III, as previously reported in Section 4.9.5.

In the cyclic voltammograms of dopamine at electrodes incubated in the fouling solution for 30 min, there was a 20% positive shift of $E_{1/2}$ of dopamine oxidation at Electrode IV. In contrast, a corresponding 41% positive shift of $E_{1/2}$ was observed at Electrode III, indicating an enhanced resistance at the electrodes by the grafted 4-SB functionalities. In addition, there was no further discernible change of $E_{1/2}$ observed at Electrode IV even after incubating them in the fouling solution for one week. A comparable observation at Electrode III was reported in Section 4.9.5.

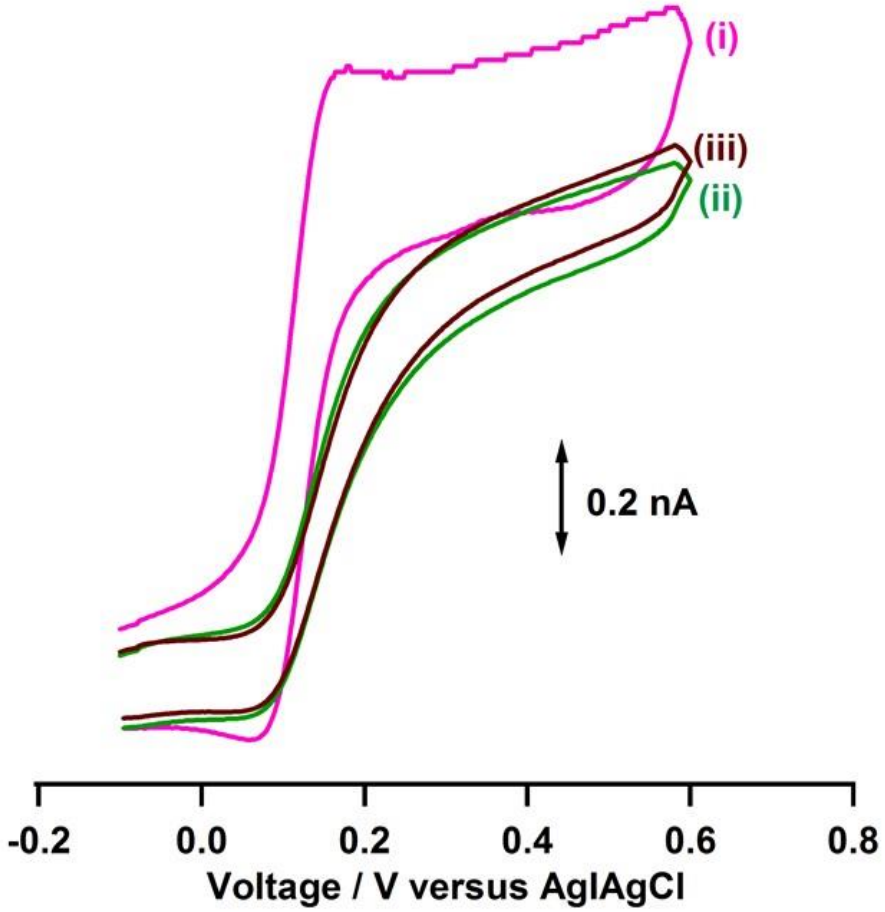

Figure 5.12 Cyclic voltammetry of 1.0 mM dopamine at (i) Electrode IV; (ii) Electrode IV after being incubated in the fouling solution for 30 min; (iii) Electrode IV after being incubated in the fouling solution for 1 week. In all experiments, pH 7.4 citrate / phosphate buffer was used as the supporting electrolyte. Scan rate: 100 mV s^{-1}.

Analogous to work reported in Chapter 4, electrochemical impedance spectroscopy was again conducted here to evaluate the effect of 4-SB in fouling resistance of electrodes. In Figure 5.13, trace i, ii and iii are the corresponding Nyquist plots of 1.0 mM $[Ru(NH_3)_6]^{3+}$ at Electrode IV without any incubation, after a 30-min incubation and after a 1-week incubation in the fouling solution using 1.0 KCl as the supporting electrolyte. In this experiment, there was no observable change in R_c, the resistance arising from the butylsiloxane film, under all experimental conditions. However, after

incubating Electrode IV in the fouling solution for 30 min, R_{ct} increased by only 13%, compared to 38% at Electrode III. After 1 week of incubation, an insignificant increase of R_{ct} was observed. These results are in agreement with those interpreted from cyclic voltammogram (Figure 5.12) at Electrode IV.

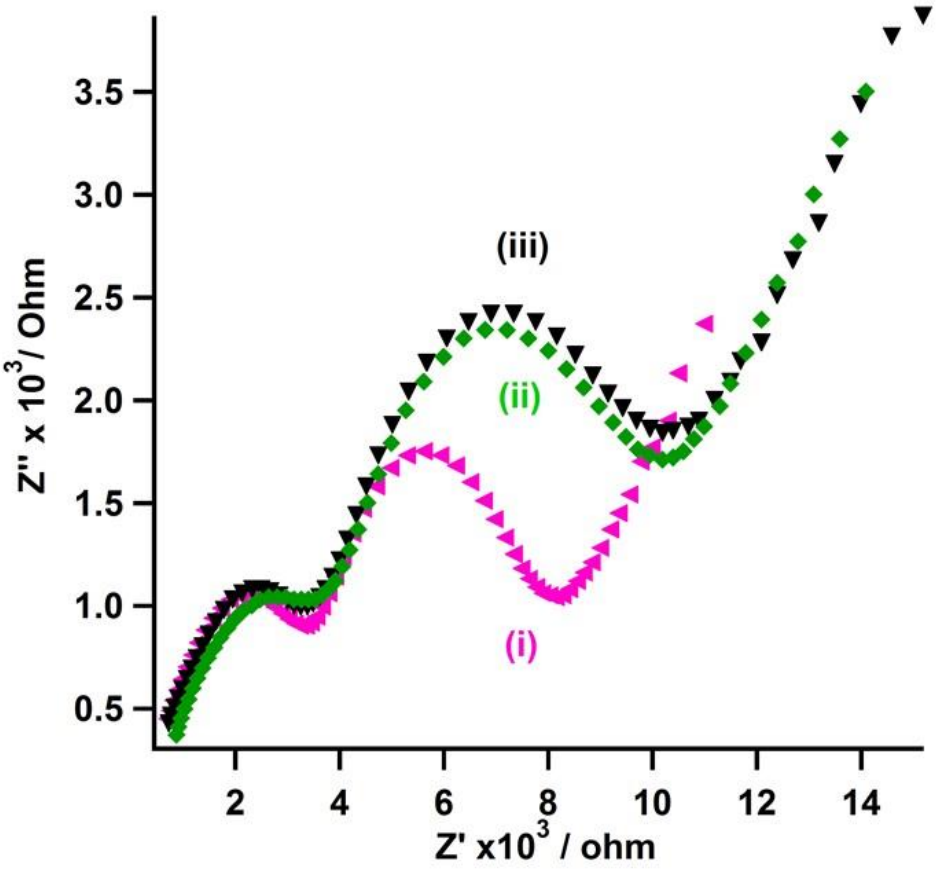

Figure 5.13 Nyquist plots of 1.0 mM $[Ru(NH_3)_6]^{3+}$ at Electrode IV without incubation (trace i), after a 30-min incubation (trace ii), and after a 1-week incubation (trace iii) in fouling solution using 1.0 M KCl supporting electrolyte. Frequency range is 100 kHz – 0.1 Hz with 10 mV wave potential amplitude at a formal half wave potential of - 0.2 V of the electrode.

5.8.5 Analytical detection of dopamine at Electrode IV

A sensor susceptible to fouling often suffers from distortion of the voltammetric signal and suppression of the electrode sensitivity. As a result, it is useful to evaluate and compare the sensitivity and limit of detection of Electrode IV before and after treatment in the fouling solution. Accordingly, a calibration plot based on the dopamine limiting current in the cyclic voltammograms at Electrode IV was constructed, as shown in trace (i) of Figure 5.14. A correlation coefficient of 0.9991 (N=7), which was found to be statistically significant at the 95% level, was obtained. This was also supported by the Wald-Wolfowitz runs test that showed a random distribution of the positive and negative residuals of the plot, indicating a linear calibration plot. In the linear relationship specified in the figure, the uncertainties associated with slope and the ordinate intercept represent the 95% confidence intervals. Based on the slope of the calibration plot, the sensitivity was determined to be 26.7 pA μM^{-1} dopamine, which is a 13% enhancement compared to that at Electrode III. Based on a signal-to-noise ratio of 3, the limit of detection at Electrode IV was estimated to be 52 ± 8 nM dopamine, compared to be 138 ± 12 nM at Electrode III.

Trace (ii) in Figure 5.14 shows the calibration plot (statistically significant correlation coefficient 0.9993, N=7; Wald-Wolfowitz runs test justified) of electrodes that were incubated in the fouling solution for 1 week. Similarly, the sensitivity of the electrode was determined to be 22.5 pA μM^{-1} dopamine, which is 15% lower than that at electrodes not treated by the fouling solution. A limit of detection at this electrode was estimated to be 46 ± 6 nM, which is not significantly different from the detection limit 52 ± 8 nM measured at the same electrode before they were incubated in fouling solution for 1 week.

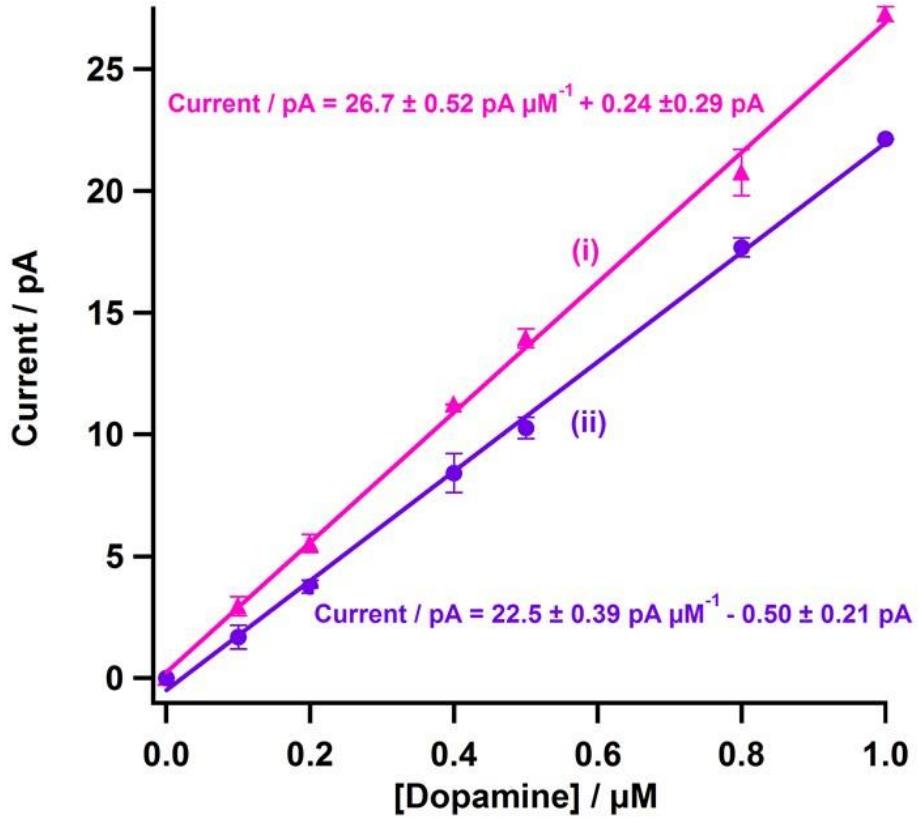

Figure 5.14. Calibration plots based on I_{lim} of dopamine cyclic voltammograms in pH 7.4 citrate / phosphate buffer at Electrode IV (trace i) and after incubation (trace ii) for 1 week in 1.0% (v/v) caproic acid (a lipid), 4% (w/v) bovine serum albumin and 0.01% (w/v) cytochrome C (both are proteins), and 0.002% (w/v) human fibrinopeptide B (a peptide). Scan rate: 100 mV s^{-1} in all voltammograms.

5.8.6 Characterisation of Electrode V and Electrode VI

In Chapter 4, we have demonstrated that Electrode III showed a degree of antifouling property. Earlier in this chapter, we again demonstrated Electrode IV offered more favourable antifouling activity compared to Electrode III. In this section, we have compared the effectiveness of conical-tip carbon electrodes hydrogenated by linear alky chain (*n*-butylsilane) and branched chain (diethylsilane) silane compounds against fouling. Finally, Electrode V were then modified by 4-SB to obtain Electrode VI. The antifouling property and analytical detection of dopamine at Electrode V and Electrode VI were also systematically studied.

5.8.7 Characterisation of Electrode V and Electrode VI

5.8.7.1 X-ray photoelectron spectroscopic characterisation of Electrode V and Electrode VI

Electrode V and Electrode VI were characterised using X-ray photoelectron spectroscopy and the results were compared to those obtained at Electrode III. As shown in the survey spectra in Figure 5.15, the common peaks C1s, O1s, Si2s and Si2p were observed for all electrodes. Similar S2s and S2p peaks to those obtained at Electrode IV (see Figure 5.10(b)) were also observed at Electrode VI in Figure 5.15(c). Here, we will focus on the C1s and O1s peaks to demonstrate the difference of these two elements on Electrode III, Electrode V and Electrode VI.

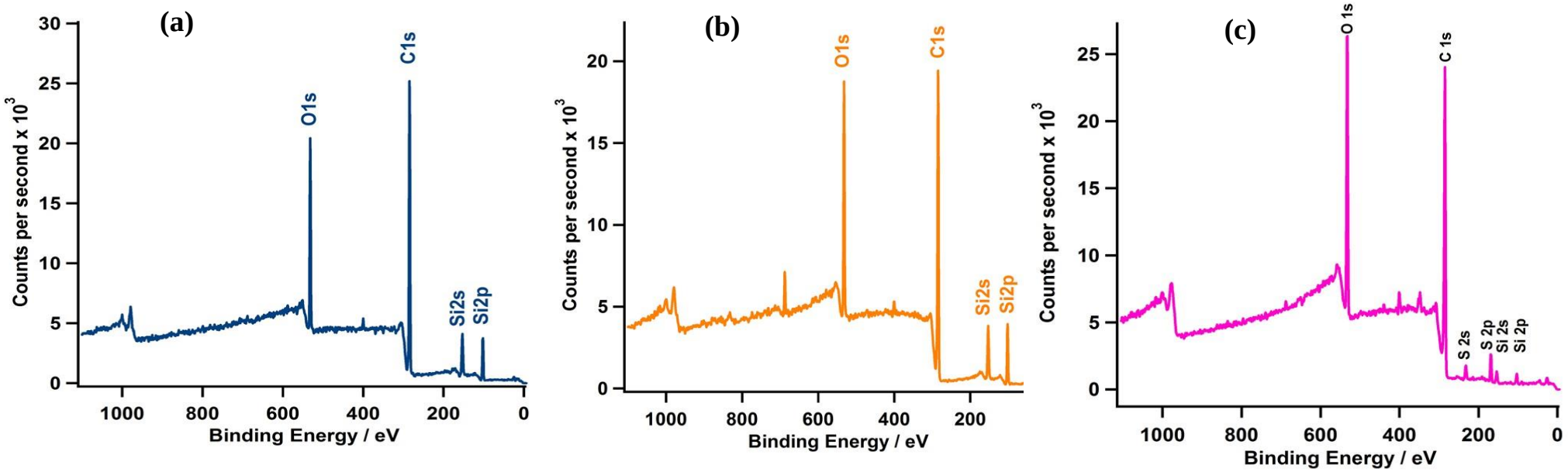

Figure 5.15. XPS survey spectrum of (a) Electrode III (b) Electrode V and (c) Electrode VI.

Qualitatively, the survey spectra shown in Figure 5.15 revealed that the intensity of O1s peak at Electrode VI is higher than that at Electrode V, followed by Electrode III. An O/C ratio of 0.23, 0.29 and 0.35 was obtained at the corresponding Electrode III, Electrode V and Electrode VI. The results obtained based on deconvolution of the C1s peak in Figure 5.15 are shown in Figure 5.16. In Figure 5.16(a), the peak at binding energy centred at 284.5 eV originated from the carbon material in the form of sp^2 and sp^3 carbons, as defined in Section 3.6.5. A small peak centred at 286.3 eV indicates the presence of carbon bonded with oxygen in butylsiloxane dendrimers (see Scheme 3.1 in Section 3.4) as also defined in Section 3.6.5. Other possible carbon peaks bonded with oxygen in carbon materials are absent as most of the C–O bonds have been replaced by C–H bonds after being hydrogenated by *n*-butylsilane.

However, following the deconvolution of C1s peak obtained at Electrode V, Figure 5.16(b) shows three sharp peaks centred at 284.8, 286.7 and 288.1 eV. The peak centred at 284.8 eV was assigned to carbon substrate present in the form of sp^2 and sp^3 carbons as described in the previous section on Electrode III. The 286.7 eV peak originated from the carbon bonded with oxygen in diethylsiloxane and other possible carbons in the form of phenols, alcohols or ether groups. The last peak centred at 288.1 eV represents carbon in carbonyl or quinone groups as assigned in Section 3.6.5. The presence of intense peaks at 286.7 and 288.1 eV indicates that not all C–O functionalities have been terminated by C–H as was found with Electrode III. Among the three peaks at 284.8, 286.7 and 288.4 eV in Figure 5.16(c) obtained at Electrode VI, only the intensity of the 286.7 eV peak has increased compared to that was obtained at Electrode V, which was attributable to carbons present in the benzene ring of 4-SB functionalities at Electrode IV as outlined in Section 5.8.3.

The intense O1s peak at 532.01 eV in the spectrum obtained at Electrode III shown in Figure 5.17(a) would have arisen from oxygen in the butylsiloxane dendrimers, as discussed in Section 3.6.5. However, the deconvolution of this O1s peak in the spectrum (Figure 5.17(b)) obtained at Electrode V yielded two peaks at 532.04 and 533.6 eV. The former peak indicates the presence of oxygen as diethylsiloxane and the

latter peak indicates other forms of oxygens (*e.g.*, oxygen present as ethers, alcohols, and esters in aromatic frames) as assigned for Electrode III in Section 3.6.5. This indicates that not all C–O functionalities were reduced to C–H at Electrode V. In the spectrum (Figure 5.17(c)) obtained at Electrode VI, we observed two peaks at 532.0 and 533.2 eV. The intensity of the 532.0 eV peak remained almost unchanged compared to Electrode III and Electrode V, while that of the 533.2 eV peak sharply increased due to the oxygen present in 4-SB moieties.

Previously, in their work on the reduction of aldehydes, ketones and primary, secondary and tertiary alcohols into their corresponding alkyl function, Nimmagadda *et al*.[3,5] reported 85%-95% and 50%-60% conversion rate of C–O to C–H, while the organic substrates (containing such functional groups as alcohol, phenol, aldehyde, carboxyl, and ketone) were reduced by *n*-butylsilane and diethylsilane, respectively (see Table 5.1). As discussed above, our results supported similar reduction of C–O functionalities to C–H bonds on the carbon electrode surface to C–H. Based on X-ray photoelectron spectroscopic characterisation of diethylsilane modified electrode, we propose Scheme 5.3 for diethylsilane hydrogenation, showing the conversion of C–O functionalities to corresponding C–H on carbon electrode. As shown in the Scheme 5.3, most of the C–O functionalities are terminated by C–H. In addition, phenolic hydroxyl groups are converted to diethylsiloxane dendrimers bulkier than butylsiloxane dendrimers formed during *n*-butylsilane hydrogenation, as described in Scheme 3.1.

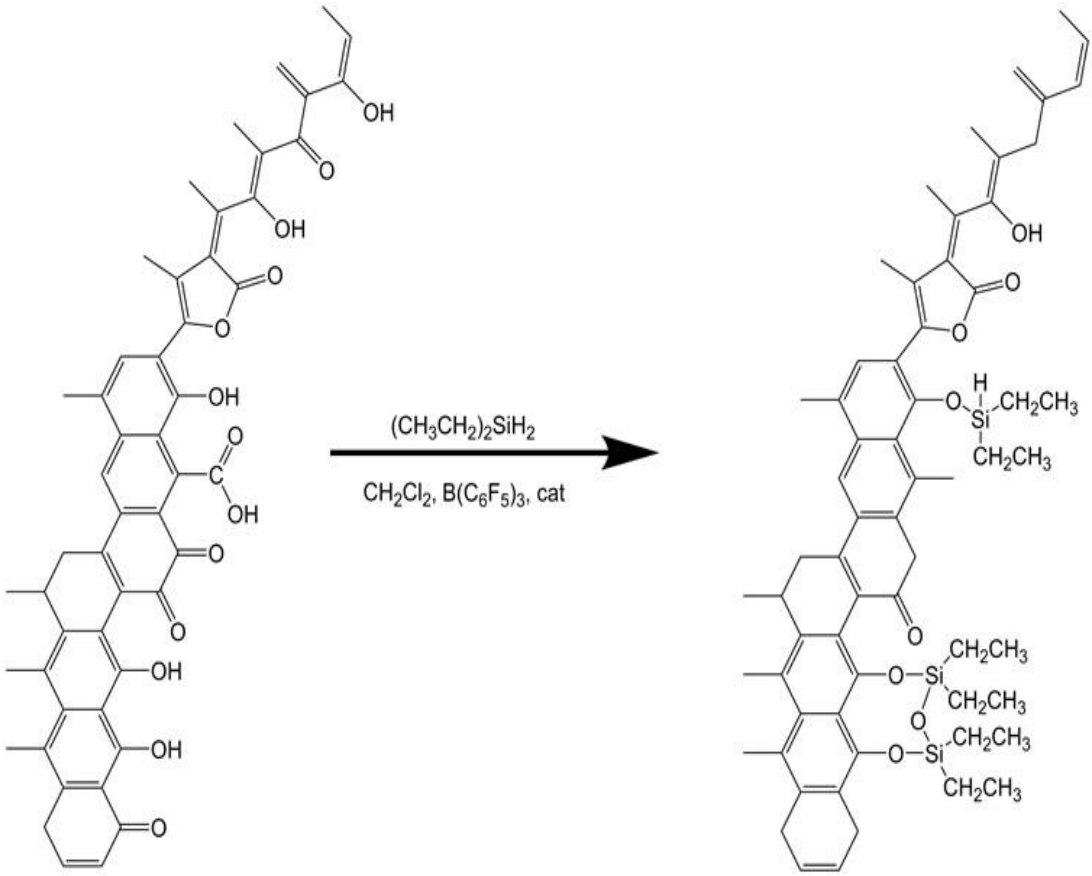

Scheme 5.3 Hydrogenation of carbon electrodes by diethylsilane reduction method.

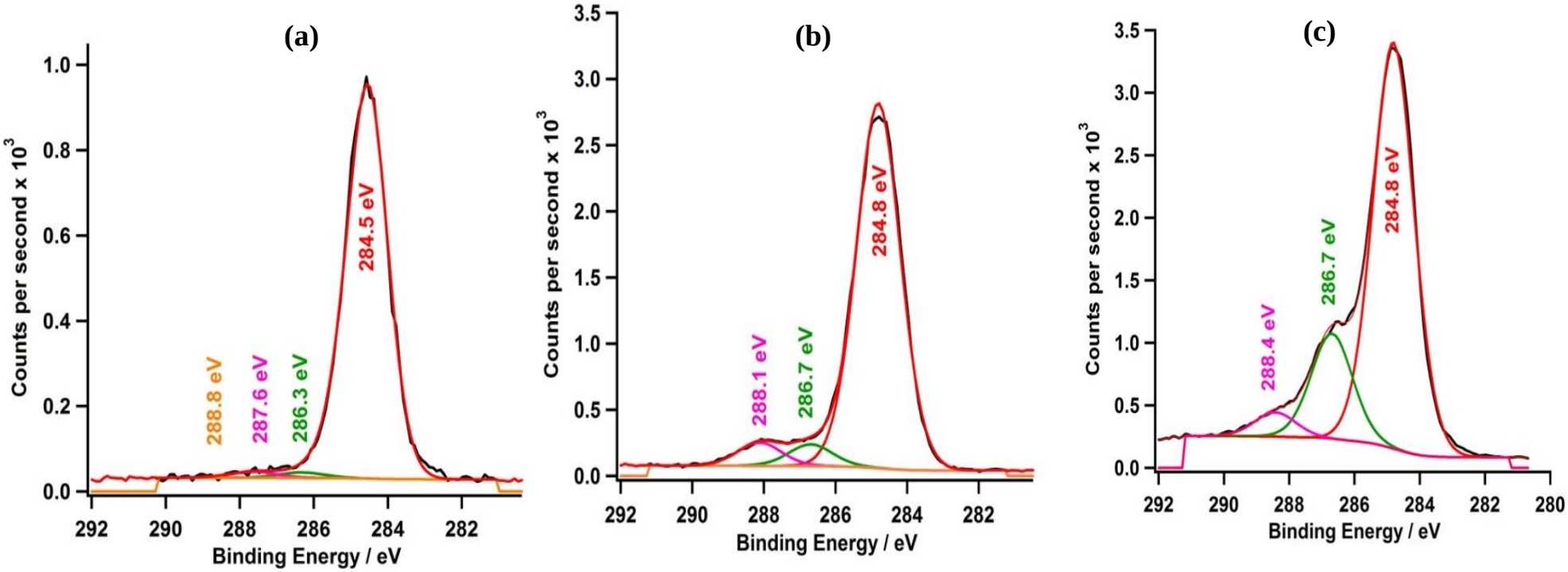

Figure 5.16 C1s peak fitting of spectrum of (a) Electrode III, (b) Electrode V and (c) Electrode VI.

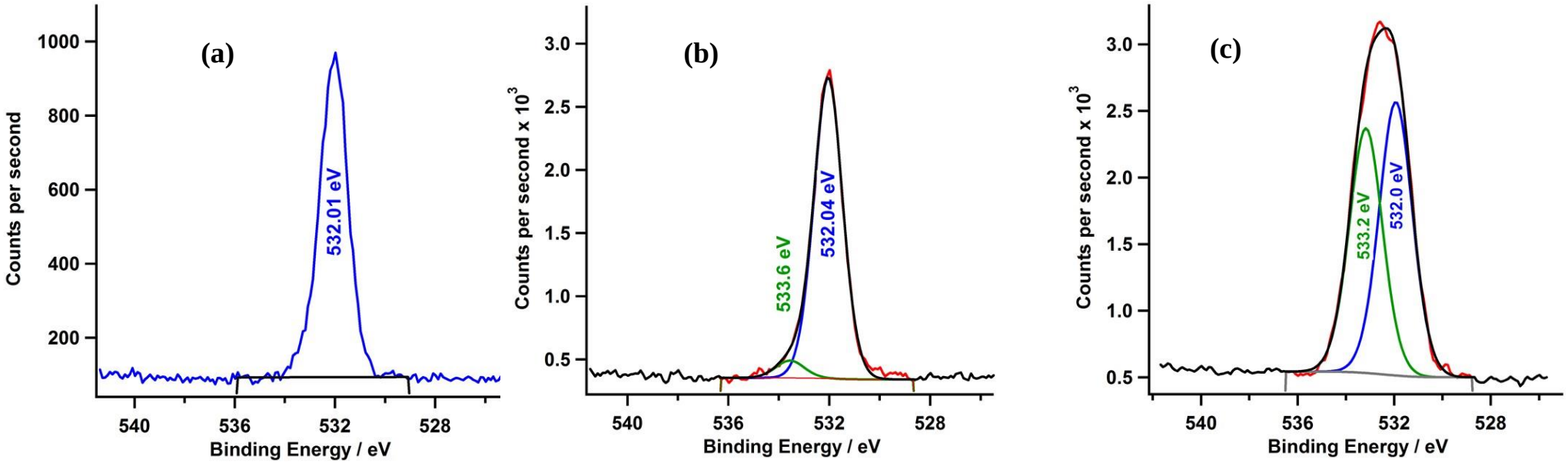

Figure 5.17 O1s peak fitting of spectrum of (a) Electrode III, (b) Electrode V and (c) Electrode VI.

5.8.7.2 Electrochemical characterisation of Electrode V and Electrode VI

At the carbon surface of Electrode V, some of the carbon-oxygen functionalities were shown by X-ray photoelectron spectroscopy to have diminished following the partial formation of C–H bonds on the electrode surface and diethylsiloxane dendrimers. As a result, the presence of residual C–O functionalities on modified surface offers faster electron transfer kinetics on Electrode V and Electrode VI compared to Electrode III and Electrode IV.

In this work, we have also conducted cyclic voltammetry of three redox markers, (i) 1.0 mM $[Ru(NH_3)_6]^{3+}$ in 1.0 M KCl, (ii) 1.0 mM $[Fe(CN)_6]^{3-}$ in 1.0 M KCl, and (iii) 1.0 mM dopamine in pH 7.4 citrate/phosphate buffer at Electrode V and Electrode VI. The results obtained show the expected sigmoidal-shaped cyclic voltammograms of 1.0 mM $[Ru(NH_3)_6]^{3+}$ (Figure 5.18(a)), 1.0 mM $[Fe(CN)_6]^{3-}$ (Figure 5.18(b)) and 1.0 mM dopamine (Figure 5.18(c)) at Electrode I (trace i), Electrode V (trace ii), and Electrode VI (trace iii) at a scan rate of 100 mV s^{-1}.

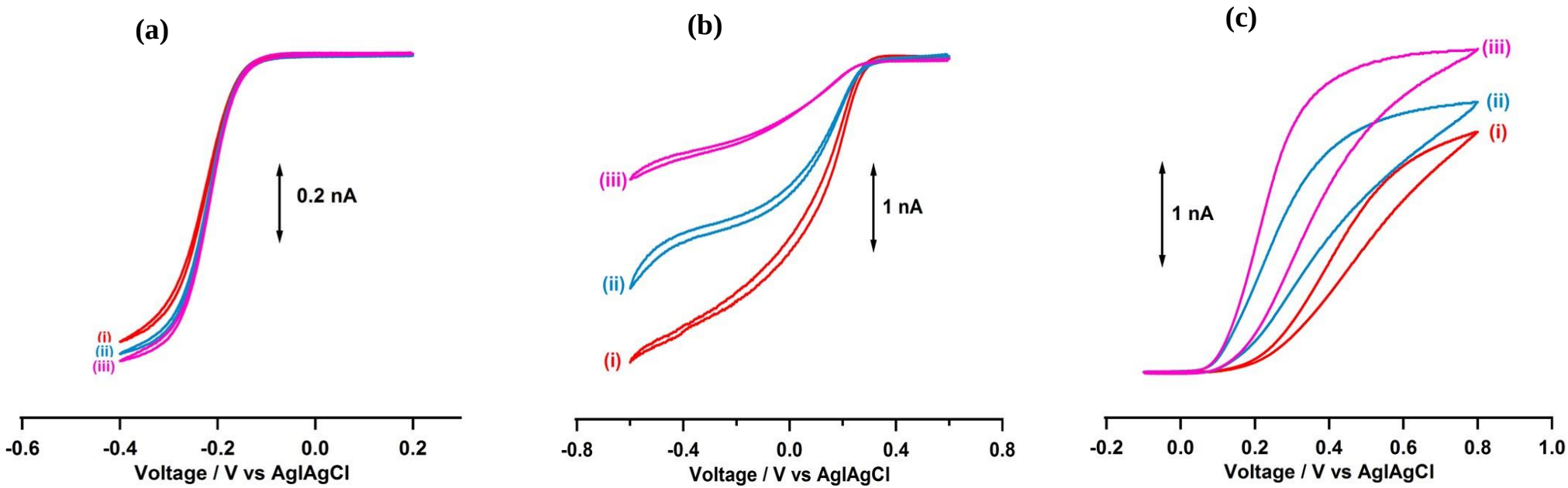

Figure 5.18 Cyclic voltammograms of (a) 1.0 mM $[Ru(NH_3)_6]^{3+}$ in 1.0 M KCl, (b) 1.0 mM $Fe(CN)_6^{3-}$ in 1.0 M KCl and (c) 1.0 mM dopamine in pH 7.4 citrate/phosphate buffer at (trace i) Electrode I, (trace ii) Electrode V and (trace iii) Electrode VI. Scan rate: 100 mV s^{-1}.

Compared to trace i in Figure 5.18(a), we observed a 5% increase in the reduction limiting current of $[Ru(NH_3)_6]^{3+}$ at Electrode V (trace ii). This could be due to preconcentration of $[Ru(NH_3)_6]^{3+}$ by the bulky diethylsiloxane that entrapped the analyte, which was not observed on Electrode III. The reduction signal of $[Ru(NH_3)_6]^{3+}$ was further increased by 2% due to electrostatic attraction by 4-SB on Electrode VI (trace iii). Notably, a similar observation was reported in work involving Electrode IV in Section 5.8.2.1. Based on the electrochemical parameters tabulated in Table 5.3, there is no significant change of $E_{1/2}$, waveslope and E_T in the cyclic voltammograms of the outer sphere redox marker $[Ru(NH_3)_6]^{3+}$ obtained at the Electrode V and Electrode VI, as expected.

In contrast, as an inner sphere complex ion, the reduction of $[Fe(CN)_6]^{3-}$ is very sensitive to monolayer adsorption on an electrode. In Figure 5.18(b), by comparing to the $[Fe(CN)_6]^{3-}$reduction limiting current at Electrode I in trace i, we observed a 20% decrease of the current at Electrode V in trace ii. In trace iii, the limiting current further decreased by 38% compared to trace ii at Electrode VI. We attribute the decreasing limiting current to the hindering of electron transfer by the presence of a diethylsiloxane monolayer and also the less favourable C–H terminated surface for $[Fe(CN)_6]^{3-}$ reduction, as observed at Electrode III in Section 4.9.1.2. In addition, the negatively charged 4-SB further repelled the anionic $[Fe(CN)_6]^{3-}$ away from the electrode surface, resulting in sluggish electron transfer kinetics. As tabulated in Table 5.3, there was a 145 mV negative shift of $E_{1/2}$ and a 68% increase waveslope (only a 8% difference in E_T) at Electrode VI compared to bare carbon electrodes, all supporting facile electron transfer kinetics at the modified electrodes.

Next, all electrodes were characterised in 1.0 mM of dopamine, a well-known surface sensitive/inner sphere redox marker, in pH 7.4 citrate/phosphate buffer. Compared to the voltammogram obtained at Electrode I in trace i, the corresponding voltammogram obtained at Electrode V in trace ii showed a 20% increase in dopamine oxidation limiting current due to preconcentration effect. We attribute that due to preconcentration effect offered by bulky diethylsiloxane layer, dopamine is

accumulated on the modified electrode surface that, in turn, enhanced the oxidation signal. The cyclic voltammogram (trace iii) obtained at Electrode VI, the dopamine oxidation signal has further increased by 13% relative to trace (ii) of Electrode V due to electrostatic attraction of 4-SB towards dopamine as described in Section 5.8.2.3. To investigate the preconcentration effect on Electrode V, we conducted nine consecutive differential pulse voltammetric scans of 1.0 mM dopamine in pH 7.4 citrate/phosphate buffer, while the electrodes were deliberately kept in dopamine solution from 0 to 25 min, to accumulate the dopamine on the modified surface. In this experiment, we have also plotted the corresponding dopamine oxidation peak current with the function accumulation time. The results obtained are shown in Figure 5.19(a) and (b). We observed that the oxidation current of dopamine increased to a threshold point and then remained almost constant. This experiment indicates that the Electrode V was likely to have been saturated with dopamine, providing a constant supply of dopamine for oxidation.

As tabulated in Table 5.3, there was a significant 109 mV negative shift of $E_{1/2}$ and a 15% decrease in waveslope, and 12% change in E_T of dopamine at Electrode V, and 123 mV negative shift of $E_{1/2}$ and a 22% decrease in waveslope, and 10% change in E_T of dopamine at Electrode VI, compared to the corresponding parameters estimated at Electrode I, all provided an indication of more facile electron transfer kinetics at both Electrode V and Electrode VI. At Electrode V, diethylsiloxane dendrimers on the modified surface, as shown in Scheme 5.3, played a key role in enhancing electron transfer reaction by preconcentrating the analyte on the electrode surface. At Electrode VI, in addition to preconcentration effect offered by diethylsiloxane dendrimers, 4-SB might have contributed to enhance the reaction rate through electrostatic attraction towards dopamine.

	Redox markers								
	$[Ru(NH_3)_6]^{3+}$ (N=5)			$[Fe(CN)_6]^{3-}$ (N=6)			Dopamine (N=6)		
Electrodes	$E_{1/2}$ / mV	Waveslope / mV decade^{-1}	E_T / mV	$E_{1/2}$ / mV	Waveslope / mV decade^{-1}	E_T / mV	$E_{1/2}$ / mV	Waveslope / mV decade^{-1}	E_T / mV
Electrode I	-221 (9)	67 (8)	66 (10)	98 (27)	153 (22)	271 (85)	398 (26)	192 (12)	188 (17)
Electrode V	-218 (6)	64 (4)	61 (6)	35 (57)	208 (45)	309 (106)	289 (65)	160 (34)	164 (35)
Electrode VI	-216 (5)	63 (4)	61 (5)	-47 (72)	258 (56)	293 (76)	275 (31)	148 (16)	165 (37)

Table 5.3. Summary of electrochemical parameters obtained for the three redox markers at Electrode I, Electrode V and Electrode VI. All values in parentheses are standard deviations.

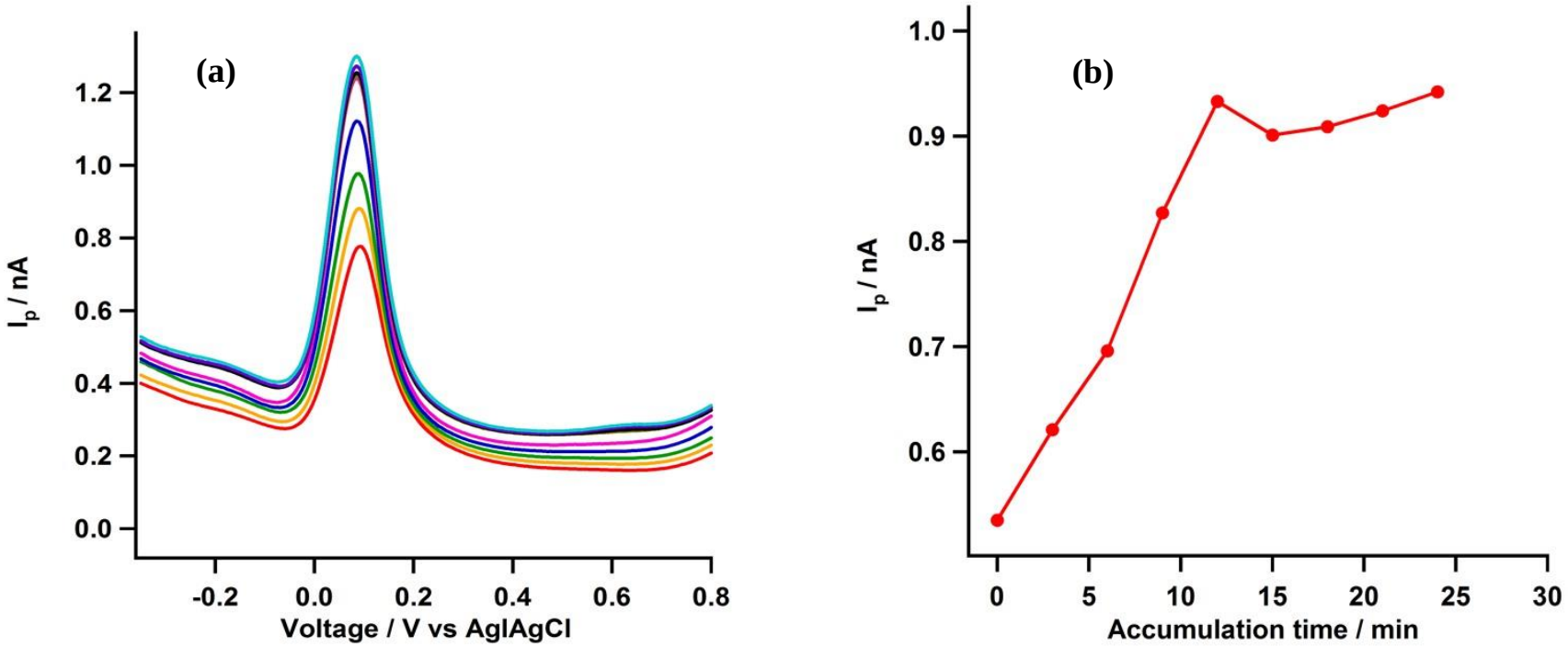

Figure 5.19 (a) Differential pulse voltammetry (scan rate 20 mV s^{-1}) of 1.0 mM dopamine in pH 7.4 citrate/phosphate buffer at Electrode V and (b) a corresponding plot based on dopamine oxidation current obtained from (a) versus dopamine accumulation time.

5.8.8 Evaluation of antifouling property of Electrode V and Electrode VI

In this section, we will study the antifouling property of Electrode V and Electrode VI in a laboratory synthetic fouling solution in a similar manner to that described in Section 4.9.5 and Section 5.8.4. Accordingly, cyclic voltammetry of 1.0 mM dopamine was conducted at these electrodes and the results obtained are shown in Figure 5.20(a) and (b). Data extracted from corresponding cyclic voltammogram are tabulated in Table 5.4 and compared to that with Electrode III and Electrode IV. In these figures, trace i, ii and iii represent the corresponding cyclic voltammograms of 1.0 mM dopamine at the corresponding electrodes in pH 7.4 citrate/phosphate buffer without incubation (trace i), after a 30-min (trace ii) and after a 1-week incubation (trace iii) in the fouling solution.

As expected, trace i in Figure 5.20(a) shows a sigmoidal-shaped cyclic voltammogram for the dopamine reaction at Electrode V. The cyclic voltammogram (trace ii) obtained at this electrode after a 30-min incubation revealed a 33% decrease of dopamine signal, compared to that in trace i. However, there was no discernible change of dopamine signal observed in trace iii after incubating them in the same fouling solution for one week.

Similarly, trace i in Figure 5.20(b) shows cyclic voltammogram for the dopamine reaction at Electrode VI. At this electrode, dopamine signal decreased by 36% (trace ii) after being incubated in the fouling solution for 30 min, compared to without any incubation (trace i. After 1 week of incubation, no appreciable change of dopamine was observed as shown in trace iii. Notably, these results are comparable to 33% obtained at Electrode III (see Section 4.9.5).

In contrast to positive shift of $E_{1/2}$ dopamine at both Electrode III and Electrode IV after being incubated in fouling solution, a negative $E_{1/2}$ shift was observed at both Electrode V and Electrode VI. At Electrode V and Electrode VI, $E_{1/2}$ shifted from 0.300 V to 0.257 V and from 0.303 V to 0.226 V respectively. The negative shift of

$E_{1/2}$ at Electrode V indicated enhanced electron transfer reaction of dopamine that might have been caused by preconcentration effect of bulky diethylsiloxane dendrimers as described in Section 5.8.7.2. Similarly, the negative shift of $E_{1/2}$ at Electrode VI might have caused by both diethylsiloxane dendrimers and electrostatic attraction of 4-SB towards dopamine.

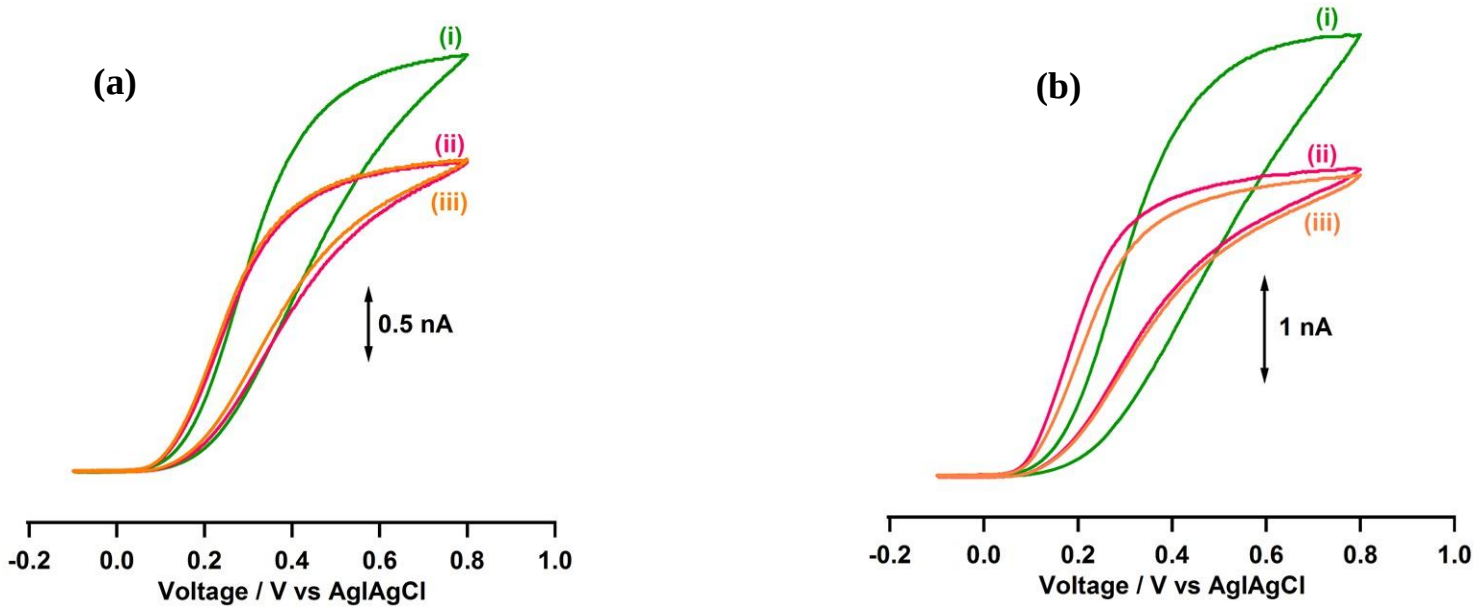

Figure 5.20 Cyclic voltammetry of 1.0 mM dopamine at (a) Electrode V without any incubation (trace i) in the fouling solution, Electrode V after incubation in the fouling solution for 30 min (trace ii); Electrode V after incubation in the fouling solution for 1 week (trace iii); (b) Electrode VI before incubation in the fouling solution (trace i), Electrode VI after incubation in the fouling solution for 30 min (trace ii); Electrode VI after incubation in the fouling solution for 1 week (trace iii).

Electrodes	Percentage decrease in dopamine I_{lim} after a 30-min incubation	Percentage decrease in dopamine I_{lim} after a 1-week incubation	$E_{1/2}$ shift after 1 week incubation / V
Electrode III	33% (9%)	35% (12%)	+0.27 to +0.38
Electrode IV	15% (6%)	12% (11%)	+0.12 to +0.14
Electrode V	33% (6%)	36% (9%)	+0.30 to +0.26
Electrode VI	36% (3%)	38% (7%)	+0.30 to +0.23

Table 5.4. Effect of fouling on dopamine oxidation signal and $E_{1/2}$ at modified electrodes. All values in parentheses are standard deviations estimated from seven electrodes for Electrode III and Electrode IV, six electrodes for Electrode V and Electrode VI.

In investigating the fouling resistance of all six electrode types, the percentage change of the dopamine limiting current between the incubation period was evaluated after an individual electrode of each electrode type was incubated in a fouling solution containing 4% bovine serum albumin, 0.01 % (w/v) cytochrome C, 0.002% (w/v) human fibrinopeptide, and 1.0% (v/v) caproic acid for 0, 10, 30 mins and 1 week. The results obtained at each individual electrode denoted by the electrode number on the abscissa are displayed in Figure 5.21. In Figure 5.21(a) and 5.21(b), approximately 33% of Electrode III and Electrode IV were relatively stable throughout the experiment. However, as shown in Figure 5.21(c), the results were improved to 66% at Electrode V. More significantly, as shown in Figure 5.21(d), 100% of the Electrode VI demonstrated consistent fouling resistance throughout the experiments.

To account for the above observation, apart from the conversion of C–O functionalities on an electrode to C–H bonds, we also need to consider the formation of diethylsiloxane dendrimers in the hydrogenation process. Owing to its side chains, a diethylsiloxane dendrimer is structurally bulkier than the corresponding butylsiloxane dendrimer. As a result, the diethylsiloxane dendrimers would form an even more

effective physical barrier towards large molecules that cause fouling and allow such small molecules as dopamine to access the electrode surface for electron transfer, relative to the butylsiloxane dendrimers. Previously, similar barrier effects were already reported for electrodes correspondingly modified by Nafion[16], cellulose acetate[15], and polypyrrole[44]. In addition, due to an sp^3 carbon enriched surface at a hydrogenated carbon electrode, the interactions between the electrode surface and the hydrophilic domains of proteins, peptide and lipid were minimised. Nonetheless, the initial 36-38% signal reduction might still have been caused by hydrophobic-hydrophobic interactions between the resultant hydrophobic electrode surface and the hydrophobic domains of proteins, peptide and lipid. In particular, as a common fouling agent, proteins are known to participate in hydrophobic-hydrophobic interaction and adhere to the hydrophobic surface and irreversibly foul a surface.[45]

A $-SO_3^-$ terminated electrode surface was previously demonstrated to be resistant to proteins including bovine serum albumin and cytochrome c[20] or fibrinogen and lysozyme[46]. In our work, we have observed an improved resistance to fouling at Electrode IV, as discussed in Section 5.8.4. As shown in Figure 5.21(d), our results showed that the corresponding Electrode VI yielded significantly improved antifouling resistance and these electrodes were therefore more stable in a fouling solution compared to Electrode III, Electrode IV and Electrode V. We attribute the enhanced stability to the synergistic effect of diethylsilane and 4-SB throughout the fouling experiment.

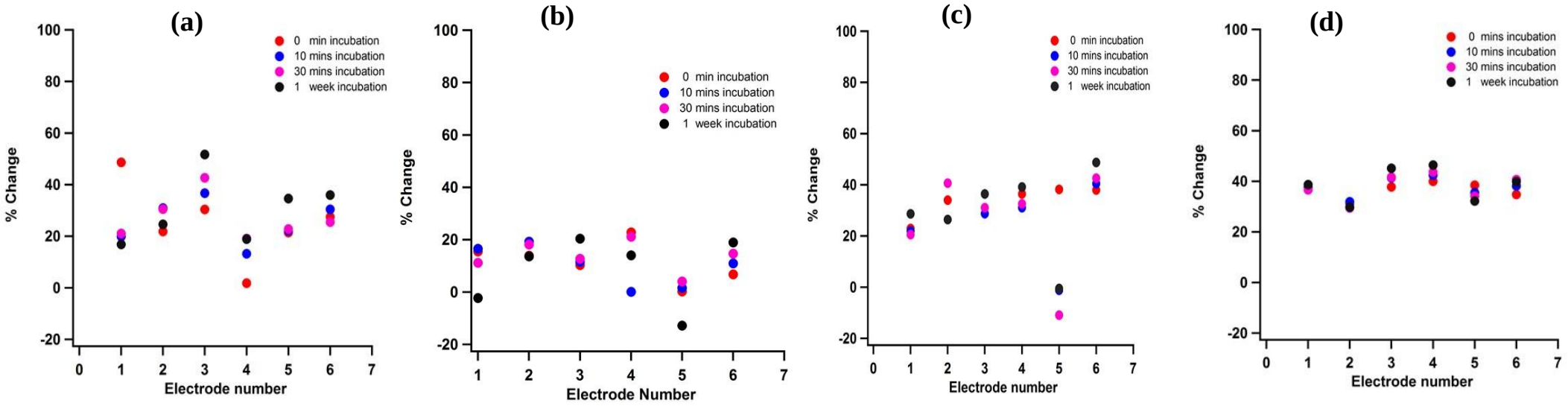

Figure 5.21. Antifouling experiment using (a) Electrode III, (b) Electrode IV, (c) Electrode V and (d) Electrode VI in 1.0% (v/v) caproic acid (a lipid), 4% (w/v) bovine serum albumin and 0.01% (w/v) cytochrome C (both are proteins), and 0.002% (w/v) human fibrinopeptide B (a peptide).

To evaluate and compare the sensitivity and limit of detection, two calibration plots were constructed, as shown in Figure 5.22(a) and (b) based on dopamine limiting current in the cyclic voltammograms of dopamine at Electrode V and Electrode VI, respectively, in pH 7.4 citrate/phosphate buffer. Using Student's *t*-test, the correlation coefficients indicated in Figure 5.22 were found to be statistically significant at the 95% confidence level. These results were also supported by a random distribution of the residuals, as assessed by the Wald-Wolfolwitz runs test. Based on the slopes of these calibration plots, the detection sensitivity was estimated to be 30.3 pA μM^{-1} dopamine for Electrode V and 42.4 pA μM^{-1} dopamine for Electrode VI before incubating them in the fouling solution. After a 1-week incubation, the corresponding detection sensitivity was estimated to be 20.4 and 26.1 pA μM^{-1}. Similarly, based on a signal-to-noise ratio of 3, a limit of detection of 176 ± 15 nM dopamine was estimated at Electrode V, and 94 ± 10 nM dopamine at Electrode VI. After incubating the respective modified electrodes in the fouling solution for 1 week, the limit of detection was determined to be as 208 ± 12 nM at Electrode V and 105 ± 8 nM at Electrode VI. The results are also tabulated in Table 5.5.

Electrodes	Incubation	Sensitivity / pA μM^{-1}	Detection limit / nM
Electrode V	Before	30.3	176 ± 15
Electrode V	After	20.4	208 ± 12
Electrode VI	Before	42.4	94 ± 10
Electrode VI	After	26.1	105 ± 8

Table 5.5 Sensitivity and limit of detection of Electrode V and Electrode VI

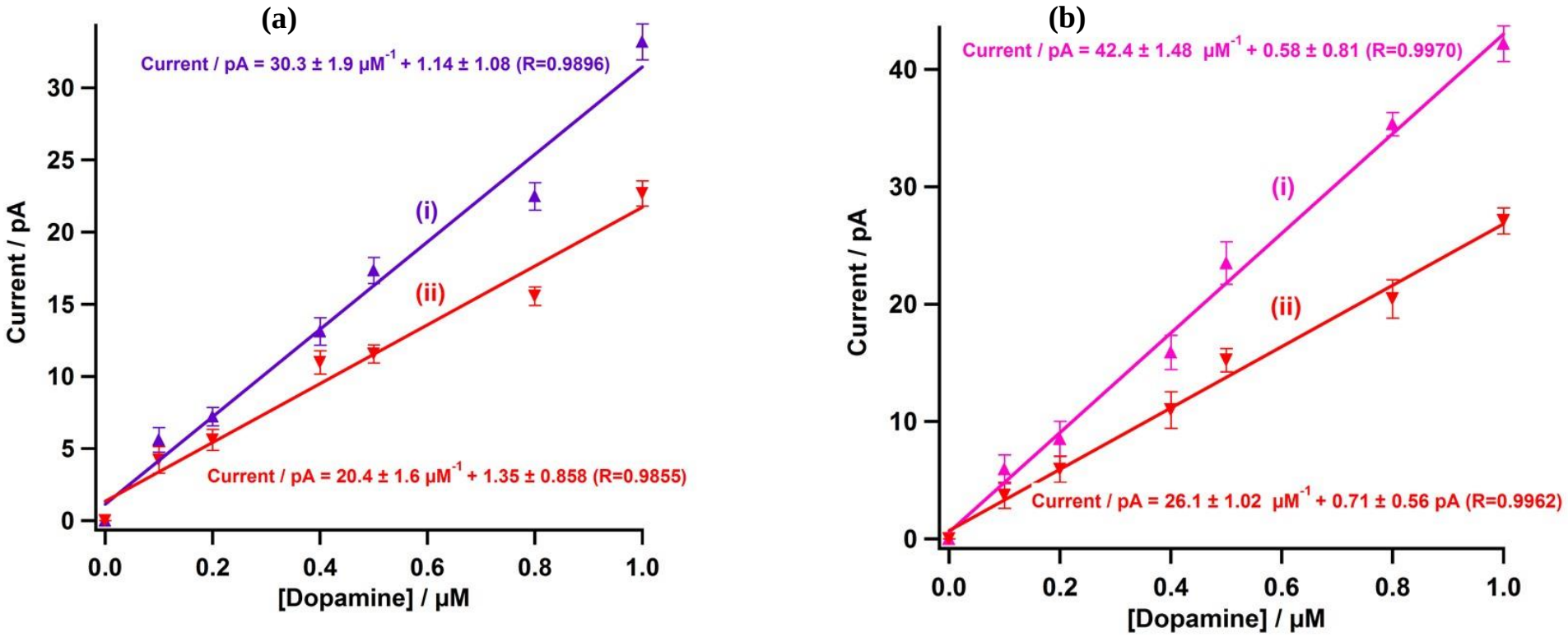

Figure 5.22 Calibration plots based on I_{lim} of dopamine cyclic voltammograms in pH 7.4 cittrate / phosphate buffer solution at (a) Electrode V and (b) Electrode VI before (trace i) and after incubation (trace ii) for 1 week in 1.0% (v/v) caproic acid (a lipid), 4% (w/v) bovine serum albumin and 0.01% (w/v) cytochrome C (both are proteins), and 0.002% (w/v) human fibrinopeptide B (a peptide). Scan rate: 100 mV s^{-1} in all voltammograms.

5.8.9 Real-life sample analysis

To illustrate the feasibility of all four types of electrodes for routine analysis, they were applied to the determination of dopamine spiked in human serum used as a real-life biological sample for analysis. In this experiment, the human serum sample was diluted 50 times using pH–7.4 citrate/phosphate buffer to reduce background current. Then, cyclic voltammetry of 0.5 μmol L^{-1} dopamine already spiked in diluted human serum was carried out at the modified electrodes. Based on the dopamine oxidation current measured, the corresponding dopamine concentration was estimated using the calibration plot. In this way, this concentration was compared to the known concentration in order to evaluate the recovery. According to the results tabulated in Table 5.6, the recovery of dopamine at Electrode III (99.7–114%; relative standard deviation 8.4%, (N=3)) is comparable to that at the corresponding Electrode IV (97.2–110%; relative standard deviation 6.2%, (N=3)). Similarly, the dopamine recovery at Electrode V (98.2–105%; relative standard deviation 3.3%, (N=3)) was found to be similar to that at Electrode VI (108–129%; relative standard deviation 10.7%, (N=3)). These results support the potential applications of all the above modified electrodes for determination of dopamine in real-life samples.

Modification	Electrode	Added / μM	Detected / μM	Recovery	Relative standard deviation
Electrode III	1	0.50	0.58	114%	7.69%
	2	0.50	0.49	99.3%	8.88%
	3	0.50	0.49	99.7%	8.85%
Electrode IV	1	0.50	0.55	110%	5.85%
	2	0.50	0.49	97.2%	6.62%
	3	0.50	0.51	102%	6.30%
Electrode V	1	0.50	0.52	103%	3.29%
	2	0.50	0.49	98.2%	3.45%
	3	0.50	0.52	105%	3.23%
Electrode VI	1	0.50	0.54	108%	11.3%
	2	0.50	0.54	107%	11.4%
	3	0.50	0.65	129%	9.49%

Table 5.6. Recovery test of dopamine spiked in human serum as a real-life sample.

5.9 Concluding remarks

Chapter 4 was devoted to the development of Electrode III to yield a hydrophobic surface to deter electrode fouling by amphiphilic proteins, peptides and lipids. However, these electrodes still exhibited a ~35% decrease in sensitivity towards dopamine after they were incubated in the fouling solution for 1 week. Therefore, we aimed in this chapter at improving fouling resistance of Electrode III by also grafting 4-SB on the electrode surface (Electrode IV). Initially, we have systematically characterised Electrode II and Electrode IV based on the electrochemistry of three redox markers ($Ru(NH_3)_6^{3+}$, $[Fe(CN)_6]^{3-}$ and dopamine), electrochemical impedance spectroscopy, and X-ray photoelectron spectroscopy. We observed a significant signal loss arising from the electrochemical activity of all three redox markers at Electrode II. This was attributed to rapidly growing 4-SB multilayers that passivated the electrode,

causing hindrance or repulsion of the redox markers from the electrode, and hence resulted in sluggish electron transfer kinetics. We then demonstrated the feasibility of controlled grafting of 4-SB on Electrode III. Unlike Electrode II, Electrode IV was found to remain active. We proposed that formation of 4-SB multilayers was avoided by butylsiloxane dendrimers already formed on Electrode III during the *n*-butylsilane hydrogenation process. Notably, at Electrode IV, we achieved ~10% enhanced dopamine oxidation signal and ~13% improved sensitivity due to electrostatic attraction between the negatively charged 4-SB modified electrode surface and positively charged dopamine. In addition, electrochemical impedance spectroscopic results were used to complement the above cyclic voltammetric results. X-ray photoelectron spectroscopic examination of the electrode surfaces confirmed the grafting of 4-SB on Electrode III surface. Differences in elemental composition on the electrodes were then systematically accounted for.

The antifouling property of Electrode IV was assessed in a laboratory synthetic fouling solution containing 4% bovine serum albumin, 0.01 % (w/v) cytochrome C, 0.002% (w/v) human fibrinopeptide, and 1.0% (v/v) caproic acid. After a 1-week incubation of these electrodes, a ~15% sensitivity loss was estimated, compared to ~35% at Electrode III. Therefore, Electrode IV have demonstrated more than a two-fold improvement in dopamine signal and sensitivity as they were more fouling resistant compared to Electrode III. In addition, a limit of detection of 52 ± 8 nM was estimated at Electrode IV, which is approximately a three-fold improvement relative to Electrode III.

Further work was also conducted in this chapter to study the electrochemical behaviour of Electrode V, hydrogenated carbon electrodes by the branch-chained alkylsilane, diethylsilane, so that we could also compare their antifouling capability with Electrode III hydrogenated by the straight-chained alkylsilane of *n*-butylsilane. Using X-ray photoelectron spectroscopy, the survey spectrum of Electrode III, Electrode V and Electrode VI appeared to indicate a similar process in diethylsilane hydrogenation to that in *n*-butylsilane hydrogenation. The presence of Si in the survey spectrum of Electrode V and Electrode VI also confirmed the formation of diethylsiloxane at

diethylsilane hydrogenation electrodes, just as the formation of butylsiloxane during *n*-butylsilane hydrogenation. The presence of S in the survey spectrum of Electrode VI also confirmed the successful grafting of 4-SB on Electrode V. In this work, we have deconvoluted the C and O peaks and the elemental composition of C and O at these electrodes to demonstrate that diethylsilane only partially hydrogenated the carbon electrode surface. The electrochemistry of dopamine at Electrode V, showed a preconcentration effect towards dopamine that has in turn enhanced dopamine oxidation signal. We attributed that the bulkier diethylsiloxane than butylsiloxane has played a key role in preconcentrating dopamine on the electrode surface, which was responsible for improved electron transfer reaction.

The antifouling performances of both Electrode V and Electrode VI were assessed by conducting similar experiment in a fouling solution, as described above for Electrode IV. We observed that the oxidation signal of dopamine decreased by ~36% at Electrode V and ~38% at Electrode VI after being incubated in the fouling solution for 1 week. The results are comparable to those obtained at Electrode III. However, there was an approximately three-fold decrease in dopamine oxidation signal at both electrodes compared to that Electrode IV. Meanwhile, $E_{1/2}$ of dopamine voltammograms at both Electrode V and Electrode VI shifted negatively after incubating them in the fouling solution for 1 week, compared to positive shifts at both Electrode III and Electrode IV.

In addition, several systematically conducted experiments in which Electrode III, Electrode IV, Electrode V and Electrode VI were incubated for 0, 10, 30 mins and 1 week to investigate their antifouling property and stability within the specified time-course. In these experiments, we concluded from the results that 100% Electrode VI (N=6) exhibited the strongest antifouling characteristics and were correspondingly the most stable electrodes among all the modified electrodes.

Finally, Electrode III, Electrode IV, Electrode V and Electrode VI were assessed in their feasibility in analysis of dopamine in a real-life sample such as human serum, into which dopamine was spiked and then recovery was evaluated. In this way, a 98.2 –

105% recovery of dopamine was obtained at Electrode V and 108 – 129% at Electrode VI, compared to 99.7 – 114% at Electrode III and 97.2 – 110% at Electrode IV.

5.10 References

1. Martin, E. L., The Clemmensen Reduction. In *Organic Reactions*, John Wiley & Sons, Inc.: 2004.
2. Bajracharya, G. B.; Nogami, T.; Jin, T.; Matsuda, K.; Gevorgyan, V.; Yamamoto, Y., Reduction of carbonyl function to a methyl group. *Synthesis* **2004,** *2004* (02), 308-311.
3. Nimmagadda, R. D.; McRae, C., A novel reduction reaction for the conversion of aldehydes, ketones and primary, secondary and tertiary alcohols into their corresponding alkanes. *Tetrahedron Letters* **2006,** *47* (32), 5755-5758.
4. Nimmagadda, R. D.; McRae, C., Characterisation of the backbone structures of several fulvic acids using a novel selective chemical reduction method. *Organic geochemistry* **2007,** *38* (7), 1061-1072.
5. Nimmagadda, R. D.; McRae, C., A novel reduction of polycarboxylic acids into their corresponding alkanes using n-butylsilane or diethylsilane as the reducing agent. *Tetrahedron letters* **2006,** *47* (21), 3505-3508.
6. Gerhardt, G. A.; Oke, A. F.; Nagy, G.; Moghaddam, B.; Adams, R. N., Nafion-coated electrodes with high selectivity for CNS electrochemistry. *Brain Research* **1984,** *290* (2), 390-395.
7. Yuan, S.; Hu, S., Characterization and electrochemical studies of Nafion/nano-TiO_2 film modified electrodes. *Electrochimica acta* **2004,** *49* (25), 4287-4293.
8. Li, S.-J.; He, J.-Z.; Zhang, M.-J.; Zhang, R.-X.; Lv, X.-L.; Li, S.-H.; Pang, H., Electrochemical detection of dopamine using water-soluble sulfonated graphene. *Electrochimica Acta* **2013,** *102*, 58-65.
9. Hu, S.; Huang, Q.; Lin, Y.; Wei, C.; Zhang, H.; Zhang, W.; Guo, Z.; Bao, X.; Shi, J.; Hao, A., Reduced graphene oxide-carbon dots composite as an enhanced material for electrochemical determination of dopamine. *Electrochimica Acta* **2014,** *130*, 805-809.

10. Zen, J.-M.; Ilangovan, G.; Jou, J.-J., Square-wave voltammetric determination and ac impedance study of dopamine on preanodized perfluorosulfonated ionomer-coated glassy carbon electrodes. *Analytical Chemistry* **1999,** *71* (14), 2797-2805.
11. Zhang, Y.; Pan, Y.; Su, S.; Zhang, L.; Li, S.; Shao, M., A Novel Functionalized Single-Wall Carbon Nanotube Modified Electrode and Its Application in Determination of Dopamine and Uric Acid in the Presence of High Concentrations of Ascorbic Acid. *Electroanalysis* **2007,** *19* (16), 1695-1701.
12. Li, W.; Ding, L.; Wang, Q.; Su, B., Differential pulse voltammetry detection of dopamine and ascorbic acid by permselective silica mesochannels vertically attached to the electrode surface. *The Analyst* **2014,** *139* (16), 3926-3931.
13. Razmi, H.; Heidari, H., Nafion/lead nitroprusside nanoparticles modified carbon ceramic electrode as a novel amperometric sensor for l-cysteine. *Analytical biochemistry* **2009,** *388* (1), 15-22.
14. Jolly, P.; Formisano, N.; Tkáč, J.; Kasák, P.; Frost, C. G.; Estrela, P., Label-free impedimetric aptasensor with antifouling surface chemistry: a prostate specific antigen case study. *Sensors and Actuators B: Chemical* **2015,** *209*, 306-312.
15. Trouillon, R.; Combs, Z.; Patel, B. A.; O'Hare, D., Comparative study of the effect of various electrode membranes on biofouling and electrochemical measurements. *Electrochemistry Communications* **2009,** *11* (7), 1409-1413.
16. Singh, Y. S.; Sawarynski, L. E.; Dabiri, P. D.; Choi, W. R.; Andrews, A. M., Head-to-head comparisons of carbon fiber microelectrode coatings for sensitive and selective neurotransmitter detection by voltammetry. *Analytical chemistry* **2011,** *83* (17), 6658-6666.
17. Marinesco, S.; Carew, T. J., Improved electrochemical detection of biogenic amines in Aplysia using base-hydrolyzed cellulose-coated carbon fiber microelectrodes. *Journal of neuroscience methods* **2002,** *117* (1), 87-97.
18. Chira, A.; Bucur, B.; Radulescu, M.-C.; Galaon, T.; Radu, G.-L., Study of Electrochemically Modified Electrode with Synthesized N-benzyl-4, 4'-bipyridine with Anti-Fouling Properties for Oxygen and Hydrogen Peroxide

Detection. *International Journal of Electrochemical Science* **2014,** *9*, 4493-4511.

19. Chandra, S.; Miller, A. D.; Wong, D. K. Y., Evaluation of physically small p-phenylacetate-modified carbon electrodes against fouling during dopamine detection in vivo. *Electrochimica Acta* **2013,** *101*, 225-231.
20. Gui, A. L.; Luais, E.; Peterson, J. R.; Gooding, J. J., Zwitterionic Phenyl Layers: Finally, Stable, Anti-Biofouling Coatings that Do Not Passivate Electrodes. *ACS applied materials & interfaces* **2013,** *5* (11), 4827-4835.
21. Lawal, O. S., Kosmotropes and chaotropes as they affect functionality of a protein isolate. *Food Chemistry* **2006,** *95* (1), 101-107.
22. Holmlin, R. E.; Chen, X. X.; Chapman, R. G.; Takayama, S.; Whitesides, G. M., *Langmuir* **2001,** *17*, 2841.
23. Trouillon, R.; Cheung, C.; Patel, B. A.; O'Hare, D., Comparative study of poly (styrene-sulfonate)/poly (L-lysine) and fibronectin as biofouling-preventing layers in dissolved oxygen electrochemical measurements. *The Analyst* **2009,** *134* (4), 784-793.
24. Hermans, A.; Seipel, A. T.; Miller, C. E.; Wightman, R. M., Carbon-fiber microelectrodes modified with 4-sulfobenzene have increased sensitivity and selectivity for catecholamines. *Langmuir* **2006,** *22* (5), 1964-1969.
25. Jin, G.; Zhang, Y.; Cheng, W., Poly(p-aminobenzene sulfonic acid)-modified glassy carbon electrode for simultaneous detection of dopamine and ascorbic acid. *Sensors and Actuators B: Chemical* **2005,** *107* (2), 528-534.
26. Gui, A. L.; Liu, G.; Chockalingam, M.; Le Saux, G.; Harper, J. B.; Gooding, J. J., A Comparative Study of Modifying Gold and Carbon Electrode with 4-Sulfophenyl Diazonium Salt. *Electroanalysis* **2010,** *22* (12), 1283-1289.
27. Combellas, C.; Kanoufi, F.; Pinson, J.; Podvorica, F. I., Sterically hindered diazonium salts for the grafting of a monolayer on metals. *Journal of the American Chemical Society* **2008,** *130* (27), 8576-8577.
28. Liu, W.; Tilley, T. D., Sterically Controlled Functionalization of Carbon Surfaces with− C6H4CH2X (X= OSO2Me or N3) Groups for Surface Attachment of Redox-Active Molecules. *Langmuir* **2015,** *31* (3), 1189-1195.

29. Kariuki, J. K.; McDermott, M. T., Nucleation and growth of functionalized aryl films on graphite electrodes. *Langmuir* **1999,** *15* (19), 6534-6540.

30. Kariuki, J. K.; McDermott, M. T., Formation of multilayers on glassy carbon electrodes via the reduction of diazonium salts. *Langmuir* **2001,** *17* (19), 5947-5951.

31. Allongue, P.; Delamar, M.; Desbat, B.; Fagebaume, O.; Hitmi, R.; Pinson, J.; Saveant, J.-M., Covalent modification of carbon surfaces by aryl radicals generated from the electrochemical reduction of diazonium salts. *Journal of the American Chemical Society* **1997,** *119* (1), 201-207.

32. Gui, A. L.; Yau, H. M.; Thomas, D. S.; Chockalingam, M.; Harper, J. B.; Gooding, J. J., Using Supramolecular Binding Motifs To Provide Precise Control over the Ratio and Distribution of Species in Multiple Component Films Grafted on Surfaces: Demonstration Using Electrochemical Assembly from Aryl Diazonium Salts. *Langmuir* **2013,** *29* (15), 4772-4781.

33. Randriamahazaka, H.; Ghilane, J., Electrografting and Controlled Surface Functionalization of Carbon based Surfaces for Electroanalysis. *Electroanalysis* **2016,** *28* (1), 13-26.

34. Combellas, C.; Kanoufi, F.; Pinson, J.; Podvorica, F. I., Time-of-Flight Secondary Ion Mass Spectroscopy Characterization of the Covalent Bonding between a Carbon Surface and Aryl Groups. *Langmuir* **2005,** *21* (1), 280-286.

35. Parviz, M.; Darwish, N.; Alam, M. T.; Parker, S. G.; Ciampi, S.; Gooding, J. J., Investigation of the Antifouling Properties of Phenyl Phosphorylcholine-Based Modified Gold Surfaces. *Electroanalysis* **2014**.

36. Sasso, L.; Heiskanen, A.; Diazzi, F.; Dimaki, M.; Castillo-León, J.; Vergani, M.; Landini, E.; Raiteri, R.; Ferrari, G.; Carminati, M., Doped overoxidized polypyrrole microelectrodes as sensors for the detection of dopamine released from cell populations. *The Analyst* **2013,** *138* (13), 3651-3659.

37. Ferro, S.; Dal Colle, M.; De Battisti, A., Chemical surface characterization of electrochemically and thermally oxidized boron-doped diamond film electrodes. *Carbon* **2005,** *43* (6), 1191-1203.

38. Filik, J.; May, P.; Pearce, S.; Wild, R.; Hallam, K., XPS and laser Raman analysis of hydrogenated amorphous carbon films. *Diamond and related Materials* **2003,** *12* (3), 974-978.

39. Zhou, J.-H.; Sui, Z.-J.; Zhu, J.; Li, P.; Chen, D.; Dai, Y.-C.; Yuan, W.-K., Characterization of surface oxygen complexes on carbon nanofibers by TPD, XPS and FT-IR. *Carbon* **2007,** *45* (4), 785-796.

40. Siraj, S.; McRae, C. R.; Wong, D. K., Effective activation of physically small carbon electrodes by n-butylsilane reduction. *Electrochemistry Communications* **2016,** *64*, 35-41.

41. Goeting, C. H.; Marken, F.; Gutiérrez-Sosa, A.; Compton, R. G.; Foord, J. S., Electrochemically induced surface modifications of boron-doped diamond electrodes: an X-ray photoelectron spectroscopy study. *Diamond and Related Materials* **2000,** *9* (3), 390-396.

42. Schulze, M.; Lorenz, M.; Wagner, N.; Gülzow, E., XPS analysis of the degradation of Nafion. *Fresenius' journal of analytical chemistry* **1999,** *365* (1-3), 106-113.

43. Siraj, S.; McRae, C. R.; Wong, D. K., Effective Activation of Physically Small Carbon Electrodes by n-Butylsilane Reduction. *Electrochemistry Communications* **2016**.

44. Pirvu, C.; Manole, C. C., Electrochemical surface plasmon resonance for in situ investigation of antifouling effect of ultra thin hybrid polypyrrole/PSS films. *Electrochimica Acta* **2013,** *89*, 63-71.

45. Wilson, C. J.; Clegg, R. E.; Leavesley, D. I.; Pearcy, M. J., Mediation of biomaterial-cell interactions by adsorbed proteins: a review. *Tissue engineering* **2005,** *11* (1-2), 1-18.

46. Holmlin, R. E.; Chen, X.; Chapman, R. G.; Takayama, S.; Whitesides, G. M., Zwitterionic SAMs that resist nonspecific adsorption of protein from aqueous buffer. *Langmuir* **2001,** *17* (9), 2841-2850.

Chapter 6

Concluding Remarks

6.1 Thesis summary and conclusion

The research in this thesis was motivated by the need of fouling resistant physically small electrodes for detecting dopamine in a complex biological environment without substantial transient loss of the signal. Dopamine is a ubiquitous neurotransmitter in the mammalian central nervous system that is strongly implicated in higher-order cognitive and motor functioning[1] and it also plays important physiological roles in the peripheral nervous system as the regulator of olfaction, retinal processes, hormonal regulation cardiovascular functions, sympathetic regulations, immune system and renal functions[2]. In the central nervous system, dopamine is found in basal ganglia where its extracellular concentration is approximately 10 nM, while fast burst neuronal firing can increase dopamine to a concentration level ranging from 0.1 µM to 1 µM.[3] Decrease in concentration of dopamine in the dorsal (caudate-putamen) and ventral striatum (nucleus accumbens) may cause extrapyramidal disorders and neuropsychiatric diseases such as Parkinson's, addiction, schizophrenia, obsessive compulsive disorder, and Tourette's syndrome.[4] Thus, it is of interest to neuroscientists to quantify dopamine in extracellular fluid in the mammalian brain in order to monitor neurotransmission processes and correlate neurochemistry with behaviour.

Some of the techniques for *in vivo* measurements involve microdialysis sampling techniques and analysis by chromatographic techniques, fluorescence techniques or electrochemical methods. Among these techniques, electrochemical techniques can be used to analyse dopamine easily because they offer high sensitivity, rapid response, simple operation, real time detection, and low expense, coupled with the fact that dopamine itself can be easily oxidised. In such detection techniques, conventional carbon fibre microelectrodes are commonly used to measure dopamine *in vivo*, as discussed in Section 1.2.4.2, because they are amenable to miniaturisation (5-30 µm in diameter). However, unsatisfactory sealing and leakage of epoxy, that arise during

fabrication processes, often compromise quality of carbon fibre microelectrodes, resulting in high noise, low sensitivity, short electrode life span and sometimes contamination of solution of interest.[5]

Previously, our group[6] reported the development of Electrode I that was fabricated using already pulled quartz capillary as a substrate. In this fabrication, carbon was deposited on and in the shank of the pulled quartz capillary by pyrolysing C_2H_2 in the presence of N_2 as outlined in Section 2.4.1. Compared to carbon fibre electrodes, the quartz substrate of Electrode I provides the mechanical strength, whilst the sharp tips aid in easy biological membrane penetration during implantation.[7] In addition, the open-ended base edge on Electrode I is more accessible to the mass transport of analyte to the electrode, compared to an insulating plane at the finite fibre-capillary junction on carbon fibre electrodes. Therefore, Electrode I of a similar dimension to carbon fibre electrodes were found to show an improved signal-to-noise ratio in detecting dopamine *in vivo*.[8] Notably, there is also no epoxy sealing at the carbon-capillary junction, which could otherwise have polluted solution of interest in a biological environment.[5]

In general, upon fabrication of microelectrodes, cyclic voltammetry of well-behaved redox systems is commonly performed at the electrodes to assess their integrity. For example, the outer-sphere complex ion $[Ru(NH_3)_6]^{3+}$ is often used to characterise carbon surfaces because of its independence on the type of carbon surface.[9] Similar to microelectrodes with other geometries, a typical response of $[Ru(NH_3)_6]^{3+}$ in KCl supporting electrolyte showing (1) a sigmoidal shaped cyclic voltammogram and, (2) a small capacitive charging current between the forward and backward scans, is used to indicate a functioning Electrode I. Once a typical sigmoidal-shaped voltammogram with a small charging current was obtained, the electrodes were subjected to evaluate the dimensions using chronoamperometry and scanning electron microscopy. In this work, the mean tip diameter of the electrodes was estimated to be ~2 μm and the mean axial length of deposited carbon was ~15 μm. However, due to non-uniform deposition of carbon on the quartz surface during pyrolysis, a non-sigmoidal shaped cyclic

voltammogram with an appreciable charging current was occasionally obtained, yielding a non-functioning conical-tip carbon electrode.

The study, outlined in Chapter 3, was aimed at activating non-functional Electrode I by hydrogenating the electrodes using an *n*-butylsilane reduction method. In this hydrogenation process, non-functional Electrode I was treated by *n*-butylsilane, in the presence of the catalyst $B(C_6F_5)_3$, to obtain a hydrogenated Electrode I, which is denoted as Electrode III, by converting carbon–oxygen functionalities present on carbon materials, *e.g*. aldehydes, ketones and primary, secondary and tertiary alcohols, polycarboxylic acid group to their corresponding alkyl functionalities, leaving carbon–carbon double bonds and the graphitic structure undisturbed. Phenolic hydroxyl groups were instead silanised to form a dendrimeric butylsiloxane.

Electrode III was similarly characterised by the cyclic voltammetry of 1.0 mM $[Ru(NH_3)_6]^{3+}$ in 1.0 M KCl and the corresponding non-sigmoidal shaped cyclic voltammogram at a non-functional electrode with high charging current would now appear as a sigmoidal shaped cyclic voltammogram with negligible charging current, indicating a characteristic functioning microelectrode. In this way, the fabrication success rate of carbon microelectrodes by *n*-butylsilane hydrogenation has been improved to nearly 100%. After repeated hydrogenation, the limiting current of $[Ru(NH_3)_6]^{3+}$ diminished by ~30-50%, which was attributed to the formation of butylsiloxane dendrimers on the hydrogenated surface, leading to an increased electron tunnelling distance. We attributed the reduction of charging current at Electrode III to the removal of carbon-oxygen functionalities from the electrode surface, followed by terminating defect sites with carbon-hydrogen. To support this, a cyclic voltammetry of 1.0 mM anthraquinone-2,6-disulfonate (AQDS) in 0.1 M $HClO_4$ at Electrode I and Electrode III was conducted. At Electrode I, a sigmoidal cyclic voltammogram of AQDS was obtained. However, a featureless CV at the corresponding Electrode III, provided strong evidence for the removal of the functionalities from the edge planes of the electrode surface.

In addition, X-ray photoelectron spectroscopy was conducted to further probe the characteristics of the carbon surface of Electrode III and compared to that of Electrode I. The spectrum of Electrode I revealed that the carbon obtained from the pyrolysis of C_2H_2 comprised sp^2-like graphitic carbon and sp^3-hybridised diamond-like carbon. In addition, as a result of exposure to air during pyrolysis, various oxidation products could also be found on the carbon electrode. A relative abundance of 10.2% oxygen at Electrode I also supported the presence of oxidation products on the bare electrode surface. In contrast, the spectrum of Electrode III confirmed that oxygen-bearing functionalities (carbonyl, carboxyl, epoxy, *etc*) associated with carbon on a bare electrode surface, except phenolic hydroxyl, were reduced after the surface was hydrogenated. Phenolic hydroxyl groups were, however, silanised to form a dendrimeric butylsiloxane. An intense oxygen peak and silicon peak originated from a –C–O–Si– group was observed at Electrode III, confirming the formation of dendrimeric butylsiloxane derivative at Electrode III.

To investigate the electrode stability, 20 cyclic voltammetric scans of 1.0 mM $[Ru(NH_3)_6]^{3+}$ in 1.0 M KCl was conducted at Electrode III. Repeatable sigmoidal-shaped voltammograms with negligible changes in charging current were obtained in this experiment, confirming the stability of the Electrode III surface. To further establish the integrity of modified electrodes, cyclic voltammetry of $[Ru(NH_3)_6]^{3+}$ was conducted at Electrode III that were separately stored in air and in a pH 7.4 citrate/phosphate buffer for one week. Very minimal detection signal change was observed at Electrode III in air (1.1%) and the buffer (2.8%), indicating that Electrode III was less prone to both air and buffer exposure because of the H-terminated hydrophobic surface formed in *n*-butylsilane reduction. This also revealed the long-term stability of Electrode III in air and in citrate/phosphate buffer.

In Chapter 4, the stability and antifouling capability of Electrode III was evaluated in a laboratory synthetic fouling solution that mimics a complex biological environment. Very often, the detection of dopamine *in vivo* using conventional carbon microelectrodes is often compromised after being implanted in such an environment.

High molecular weight proteins, peptides and lipids present in the extracellular fluid irreversibly adsorb onto the bare carbon surface, preventing dopamine from making contact with electrode. This then led to a transient attenuated dopamine response. The study in Chapter 4 was focussed on studying the antifouling performance of Electrode III. In addition to characterisation of Electrode III by $[Ru(NH_3)_6]^{3+}$ and AQDS as presented in Chapter 3, the electrodes were further characterised using $[Fe(CN)_6]^{3-}$ and dopamine. The electrochemistry of $[Ru(NH_3)_6]^{3+}$ and AQDS supported the respective formation of butylsiloxane and termination of C–O functionalities by C–H at the edge planes on Electrode III. A ~40% reduction of limiting current and ~38% negative shift of $E_{1/2}$ of $[Fe(CN)_6]^{3-}$ indicated sluggish electron transfer kinetics and a H–terminated hydrophobic surface is not favourable for the polar analyte. In addition, a ~15% decrease in oxidation current and also the reduced electron transfer kinetics (~40% positive shift of $E_{1/2}$) of dopamine was observed at Electrode III, attributed to the absence of ionisable carbon-oxygen functional groups on a hydrogenated surface that facilitate dopamine oxidation. A three-fold increased charge transfer resistance of $[Ru(NH_3)_6]^{3+}$ at Electrode III, determined by electrochemical impedance spectroscopy, compared to Electrode I, also supported sluggish electron transfer kinetics at Electrode III.

Electrode III was further characterised using atomic force microscopy and Raman spectroscopy. A 50% smoother and flatter surface of Electrode III, compared to Electrode I, was observed at atomic force micrograph, making it as less prone to fouling caused by biomolecular adsorption. By Raman spectroscopy, the characteristic D peak (arises from sp^3 hybridised carbon) and G peak (arises from sp^2 hybridised carbon) ratio was found to higher at Electrode III (4.72) compared to Electrode I (3.82), supporting an sp^3 enriched H–terminated surface originated from reduced C–O functionalities and butylsiloxane dendrimers on Electrode III.

As the hydrophobic sp^3 enriched H–terminated surface is not favourable for anionic ascorbic acid, which is a common interferent co-existing with dopamine in extracellular fluid, Electrode III was capable of detecting dopamine while completely blocking the

ascorbic acid oxidation at a concentration as high as 500 μM, which is generally expected in extracellular fluid. Besides, Electrode III was found to exhibit antifouling behaviour in the presence of amphiphilic, high molecular weight entities that often adsorb on the surface of an implanted sensor. This leads to severe effects on the analytical characteristics of a technique or a sensor and thus compromise its sensitivity, detection limit, reproducibility, and overall reliability. In an *in vitro* experiment, Electrode III was subjected to incubation in a synthetic laboratory fouling solution comprising 4% (w/v) bovine serum albumin, 0.01% (w/v) cytochrome C (both are proteins), 1.0% (v/v) caproic acid (a lipid), and 0.002% (w/v) human fibrinopeptide B (a peptide). After a 30-min incubation, the dopamine oxidation limiting current decreased by ~35% at Electrode III, compared to featureless dopamine oxidation cyclic voltammogram with a high charging current at Electrode I because of severe electrode surface degradation by fouling. However, after a 1-week incubation, there was no noticeable change in the limiting current measured. The findings that charge transfer resistance, determined by electrochemical impedance spectroscopy, increased by ~37% after 30 min incubation and remained almost unchanged after 1 week incubation also supported the results obtained by cyclic voltammetry. The performance of Electrode III was found to be affected by slight fouling with sensitivity decreasing from 23.7 pA μM^{-1} to 14.5 pA μM^{-1}. Similarly, the limit of detection was observed to increase only slightly from 138 ± 12 nM to 154 ± 10 nM after a one-week incubation in the fouling solution. In addition, oxidation signal in the cyclic voltammogram of 1.0 μM dopamine at Electrode III remained stable without any obvious change even after 20 consecutive scans. By this, the effectiveness of Electrode III was demonstrated in determining up to 1.0 μM dopamine without any significant fouling caused by polymeric dopamine oxidation product. The antifouling property of Electrode III was attributed to either a modified flat/smooth surface or an sp^3 enriched electrode with H–terminated edge plane. The antifouling capability of Electrode III was promoted by butylsiloxane dendrimers that restricted structurally large fouling molecules to approach the electrode surface, while dopamine was able to penetrate the butylsiloxane layer to participate in electron transfer reaction at the electrode surface.

Next, we aimed in Chapter 5 at achieving enhanced dopamine detection signal by further modifying Electrode III with a negatively charged 4-sulfobenzene (4-SB) layer that exerted electrostatic attraction towards positively charged dopamine. This electrode was termed as Electrode IV. Results obtained from X-ray photoelectron spectroscopy confirmed the successful grafting of 4-SB on Electrode III. Voltammetric studies in $[Ru(NH_3)_6]^{3+}$ and dopamine at Electrode IV resulted 4% and 10% enhanced reduction and oxidation limiting current compared to Electrode III, as expected, indicating enhanced sensitivity of Electrode IV. In electrochemical impedance spectroscopy, a 50% reduced charge transfer resistance (R_{ct}) of $[Ru(NH_3)_6]^{3+}$ at Electrode IV compared to Electrode III also supported improved sensitivity of the modified electrodes. Based on the slope of the calibration plot constructed using dopamine oxidation limiting current at different concentrations, the sensitivity of Electrode IV was determined as 26.7 pA μM^{-1}, which was a 13% improved sensitivity compared to that at Electrode III. Based on a signal-to-noise ratio of 3, the limit of detection at Electrode IV was estimated to be 52±8 nM of dopamine, approximately three times lower than that at Electrode III.

Due to the unique antifouling capability of the $-SO_3^-$ functional group, the antifouling property of Electrode III was enhanced by three fold after grafting 4-sulfobenzene on it. In the fouling experiment, dopamine oxidation limiting current decreased by only 12% at Electrode IV, compared to 35% at Electrode III, after being incubated in the same fouling solution as described above. R_{ct} increased by only 13% at Electrode IV, compared to 38% at Electrode III. This also supported the results obtained from cyclic voltammetry. In addition, the sensitivity of Electrode IV was determined to be 22.5 pA μM^{-1} dopamine, which was 15% lower than that at electrodes not treated by the fouling solution. A corresponding decrease in the limit of detection from 52±8 nM to 46±3 nM was also observed at Electrode IV treated in the fouling solution.

We have also compared the antifouling effectiveness of both Electrode III, a conical-tip carbon electrode hydrogenated by a linear alky chain (*n*-butylsilane), and Electrode V, a conical-tip carbon electrode hydrogenated by branched chain (diethylsilane) silane

compound. Finally, Electrode V was modified by 4-SB to obtain Electrode VI. The antifouling property and analytical detection of dopamine were also systematically studied. Similar to Electrode III and Electrode IV, electrochemistry of $[Ru(NH_3)_6]^{3+}$, $[Fe(CN)_6]^{3-}$ and dopamine was studied at Electrode V and Electrode VI. Both types of electrodes were found to be unfavourable for electron transfer reaction of $[Fe(CN)_6]^{3-}$. However, a 5% increase in the $[Ru(NH_3)_6]^{3+}$ reduction limiting current and a 20% increase in the dopamine oxidation limiting current were observed at Electrode V, compared to Electrode I, due to preconcentration of analyte by the bulky diethylsiloxane. There was a corresponding 2% increase and 13% increase at Electrode VI, compared to Electrode V, due to electrostatic interaction exhibited by the $-SO_3^-$ functional group with $[Ru(NH_3)_6]^{3+}$ and dopamine (a cation under physiological pH). X-ray photoelectron spectroscopy conducted at Electrode V and Electrode VI confirmed the presence of diethylsiloxane dendrimers at the modified surfaces, as well as 4-SB on Electrode VI.

Similar to Electrode III and Electrode IV, the antifouling property of Electrode V and Electrode VI in a laboratory synthetic fouling solution was also studied. A 36% and 38% lower dopamine oxidation signal observed at Electrode V and Electrode VI, compared to 35% at Electrode III and 12% at Electrode IV, after a one-week incubation in the fouling solution was conducted. In contrast to a positive shift of $E_{1/2}$ of dopamine after fouling at Electrode III and Electrode IV, a negative shift was observed at Electrode V and Electrode VI indicating faster kinetics of dopamine at these latter electrodes.

At Electrode V and Electrode VI, the detection sensitivity was estimated to be 30.3 pA μM^{-1} dopamine and 42.4 pA μM^{-1} dopamine, respectively, before incubating them in the fouling solution. After a 1-week incubation, the corresponding detection sensitivity was estimated to be 20.4 and 26.1 pA μM^{-1}. Similarly, based on a signal-to-noise ratio of 3, a limit of detection of 176±15 nM dopamine was estimated at Electrode V, and 94±10 nM dopamine at Electrode VI. After incubating the respective modified

electrodes in the fouling solution for 1 week, the limit of detection was determined to be as 208 nM±12 at Electrode V and 105±8 nM at Electrode VI.

In investigating the fouling resistance of all electrode types, the percentage change of the dopamine limiting current between the incubation period was evaluated after they were incubated in a fouling solution for 0, 10, 30 mins and 1 week. Approximately 33% of Electrode III and Electrode IV were relatively stable throughout the experiment. However, the results were improved to 66% at Electrode V. More significantly, 100% of Electrode VI demonstrated consistent fouling resistance throughout the experiments. We attributed the enhanced stability of Electrode VI to the synergistic effect of diethylsilane and 4-SB in the fouling experiment.

To illustrate the feasibility of all four types of electrodes for routine analysis, they were applied to the determination of dopamine spiked in a real-life sample of human serum. The recovery of dopamine at Electrode III (99.7–114%) was comparable to that at the corresponding Electrode IV (97.2–110%). Similarly, the dopamine recovery at Electrode V (98.2–105%) was found to be similar to that at Electrode VI (108–129%). These results supported the potential applications of all the above modified electrodes for determination of dopamine in real-life samples.

6.2 Future directions

This study has hitherto been devoted to the development of physically small conical-tip carbon electrodes of ~2 μm diameter and ~15 μm axial length with antifouling capability. A long-term goal of this work is therefore to apply these electrodes to monitoring of neurotransmitter secretion in single cells, neurons, membrane pores, and liposome. Physically small electrodes will reduce the rate of damage of cells and allow investigations at single cells or single vesicles in a cell during an exocytosis event. As a neuronal synapse is typically a ~20 nm gap, the sensing electrode must be at least smaller than the synaptic gap to conduct an uninterrupted experiment in the synapse.[10] High spatial resolution can be obtained during non-invasive analysis of single living

cells and intracellular detection of neurotransmitter using nanometre-sized electrodes. Ewing's group[11] has very recently developed nanotip conical carbon fibre microelectrodes by thermally etching a carbon fibre in a blue butane flame for less than 2 s to obtain 50-100 nm tip diameter. Morton *et al*.[12] also developed a carbon electrode using parylene as a carbon source. They conducted the pyrolysis in a furnace of 900^{o}C for 1 h to deposit carbon at the tip of a pulled pipette with an inner diameter of 150 nm. Rees *et al*.[13] fabricated a carbon electrode using an already pulled conical tip glass nanopipette of 50 to 400 nm diameter. In their work, the pulled pipette was placed in a chemical vapour deposition chamber with a flow of methane and argon at 900^{o}C such that carbon was selectively deposited inside the pipette. Similarly, to obtain high spatial resolution at our conical-tip carbon electrode, the tip dimeter and axial length can be manipulated by pulling quartz capillary such that an appropriate dimension down to several nanometre size is obtained. We have mainly concentrated our effort on the pioneering work of developing antifouling electrodes using *n*-butylsilane and diethylsilane reduction method based on conical-tip carbon electrodes of micrometres in tip diameters and axial lengths. Although these electrodes are relatively large compared to others reported in the literature, their appreciable detection signals are essential for convenient evaluation of their characteristics. According to the instruction manual of the Sutter P2000 Micropipette Puller[14], quartz capillaries can be pulled down to 10 nm in tip diameters. Therefore, a further development in this project is to fabricate even smaller conical-tip carbon electrodes than those reported in this work, which will be hydrogenated by adopting the alkylsilane reduction method, followed by attachment of 4-SB to enhance dopamine detection.

In our work, C_2H_2 gas was used a carbon source, which was pyrolysed to obtain a carbon deposit at the tip and on the shank of already pulled capillaries. C-C and C-H bonds (sp^3 hybridised) with a relative abundance of ~56% was revealed in X-ray photoelectron spectroscopy. In addition, graphitic carbon (sp^2 hybridised) and oxygen (as impurities) with a relative abundance of ~13.8% and 10.2% were also observed at the pyrolysed carbon. Therefore, these results clearly indicated that the type and composition of carbon formed depends on the hydrocarbon gas source. Previously,

parylene[12], hexane vapour[15], methane/hydrogen[16], methane/nitrogen[17] or ammonia/acetylene[18] gas/gas mixture were reported as a carbon source in the fabrication of carbon microelectrode by chemical vapour deposition method. A hydrogen stream was often used in conjunction with a carbon source in the furnace to convert the deposited carbon to an H-terminated surface, if there were any C–O impurities present on the surface.[19] Therefore, other types of carbon sources can be chosen in our research to obtain other possible sp^3 enriched pyrolysed carbon.

In this study, we employed *n*-butylsilane reduction method to hydrogenate C–O functionalities to obtain a sp^3 carbon surface. In this way, we also activated non-functional conical-tip carbon electrodes to functional conical-tip carbon electrodes with minimised charging current. However, occasionally we observed that repeated hydrogenation steps were required to improve the success rate of electrode activation. This might stem from the occasional inefficiency of the hydrogenating agent, *n*-butylsilane and the catalyst, tris(pentafluorophenyl)borane, which is highly sensitive to moisture/air[20]. Although an airtight condition was maintained and measures were taken to avoid any interference from moisture that could otherwise lower the efficiency of the catalyst, hydrogenation might be improved by conducting the experiment in a sealed bag.

In assessing the stability of hydrogenated carbon electrodes, they were found to be quite stable in air or in citrate/phosphate buffer for one week. However, these electrodes are expected to be stable for a longer period. A systematic study in this aspect is essential in the future. In addition, the stability of butylsiloxane film, formed during *n*-butylsilane and diethylsilane reduction, in unconventional conditions (*e.g.* acidic or basic extremes), will need to be examined in order to assess the robustness of these hydrogenated carbon electrodes.

This study has also demonstrated that *n*-butylsilane hydrogenated electrodes exhibited a degree of antifouling resistance after being incubated in a simulated fouling solution. Similarly, in the later part of the study, electrodes hydrogenated by diethylsilane were

also subjected to the fouling experiment. Between these two modified electrodes, diethylsilane hydrogenated electrodes showed improved fouling resistance compared to *n*-butylsilane hydrogenated electrodes. Owing to its side chains, a diethylsiloxane dendrimer is structurally bulkier than the corresponding butylsiloxane dendrimer. As a result, the diethylsiloxane dendrimers would form an even more effective physical barrier towards large molecules that cause fouling and allow such small molecules as dopamine to access the electrode surface for electron transfer, relative to the butylsiloxane dendrimers. In future, dimethylethylsilane, triethylsilane or triphenylsilane can be further studied to obtain bulkier siloxane than butylsiloxane or diethylsiloxane on the electrode surface to evaluate their fouling resistance.

In the present study, we have further immobilised 4-SB on *n*-butylsilane and diethylsilane hydrogenated electrodes and approximately a 3-fold improved fouling resistance was achieved at these electrodes. Nonetheless, a 15-35% reduction of dopamine oxidation signal was still observed at our electrodes. Clearly, the electrodes must desirably improve their antifouling property. Carbon-based materials, such as carbon nanotubes and graphene, are commonly used due to their large surface area, electrical conductivity, and electrocatalytic properties.[21] Both of them exhibited antifouling properties in electrochemical analysis *in vivo*. For example, by using vertically aligned carbon nanotube immobilised carbon fibres to monitor ascorbate in cerebrospinal fluid *in vivo*, Xiang *et al*.[22] achieved only 2% loss of sensitivity in a 30-min experiment. Similarly, Zestos *et al*.[23] also applied a carbon nanotube fibre electrode to measure exogenous serotonin concentration in rat brain slices, the dopamine oxidation peak current remained unchanged after a 10 min experiment. Alwarappan *et al*.[24] studied the direct electrochemical activity of cytochrome *c* at a chemically reduced graphene-modified glassy carbon electrode. Analogously, carbon nanotubes or graphene can be immobilised on conical-tip carbon electrodes, so that their sensitivity and antifouling can be compared to those achieved by *n*-butylsilane or diethylsilane reduction method.

In addition to carbon-based materials, electrodes can also be modified with polymeric or nonpolymeric materials to provide a physical barrier between fouling agents and the electrode surface. However, such films, including Nafion[25], thiols[26] also give rise to an increased background electrode capacitance and impedance, which is not favourable for the detection of trace analyte concentrations. Moreover, some self-assembled monolayers, for example poly(ethylene glycol), can be self-oxidised and the oxidation products can be toxic to tissues upon implantation.[27] Therefore, alternative to self-oxidising films and high capacitance / impedance films, low impedance phenyl phosphorylcholine have been developed.[28] This low impedance phenyl phosphorylcholine can be considered as a potential antifouling layer that can be immobilised on conical-tip carbon electrodes so that the analytical performance and antifouling capability of the resultant electrodes can also be evaluated and compared to the hydrogenated carbon electrodes.

Antifouling strategies should be tested against a variety of fouling agents and fouling matrices, particularly biological samples and matrices, which can be a complex and often unknown mixture of proteins, peptides, lipids, and carbohydrates. In this study, we have employed a synthetic fouling solution containing 4% bovine serum albumin, 0.01% (w/v) cytochrome *c*, 0.002% (w/v) human fibrinopeptide, and 1.0% (v/v) caproic acid to investigate antifouling property of 4-SB modified conical-tip carbon electrodes that were already hydrogenated by *n*-butylsilane or diethylsilane reduction. Although these may be representative fouling agents, it does not indicate how the antifouling strategy will perform in more complex environments. Where possible, antifouling strategies should be tested against a wide variety of fouling agents and complex matrices appropriate to the intended application, for example, blood, serum, or urine. In this aspect, we investigated the feasibility of our modified electrodes for detection of dopamine spiked in human serum. However, the relationship between fouling agent concentration and extent of fouling should not be overlooked, as fouling can occur with some antifouling strategies above a certain concentration. Also, owing to time constraint, 4-SB modified carbon electrodes that were hydrogenated by *n*-butylsilane and diethylsilane reduction have yet to be applied in the current work to detection of

dopamine *in vivo*. Therefore, work is also required in assessing fouling resistance of our modified conical-tip carbon electrodes in more complex matrices including detection of dopamine *in vivo*.

6.3 References

1. Bäckman, L.; Lindenberger, U.; Li, S.-C.; Nyberg, L., Linking cognitive aging to alterations in dopamine neurotransmitter functioning: Recent data and future avenues. *Neuroscience & Biobehavioral Reviews* **2010,** *34* (5), 670-677.
2. Beaulieu, J.-M.; Gainetdinov, R. R., The physiology, signaling, and pharmacology of dopamine receptors. *Pharmacological reviews* **2011,** *63* (1), 182-217.
3. Jacobs, C. B.; Peairs, M. J.; Venton, B. J., Review: Carbon nanotube based electrochemical sensors for biomolecules. *Analytica chimica acta* **2010,** *662* (2), 105-127.
4. (a) Tritsch, Nicolas X.; Sabatini, Bernardo L., Dopaminergic Modulation of Synaptic Transmission in Cortex and Striatum. *Neuron* **2012,** *76* (1), 33-50; (b) Kurian, M. A.; Gissen, P.; Smith, M.; Heales, S. J. R.; Clayton, P. T., The monoamine neurotransmitter disorders: an expanding range of neurological syndromes. *The Lancet Neurology* **2011,** *10* (8), 721-733.
5. Huang, W.-H.; Pang, D.-W.; Tong, H.; Wang, Z.-L.; Cheng, J.-K., A method for the fabrication of low-noise carbon fiber nanoelectrodes. *Analytical chemistry* **2001,** *73* (5), 1048-1052.
6. McNally, M.; Wong, D. K., An in vivo probe based on mechanically strong but structurally small carbon electrodes with an appreciable surface area. *Analytical chemistry* **2001,** *73* (20), 4793-4800.
7. Chen, S.; Kucernak, A., Fabrication of carbon microelectrodes with an effective radius of 1 nm. *Electrochemistry communications* **2002,** *4* (1), 80-85.
8. Wong, D. K. Y.; Charles, D. B.; McNally, M., Amperometric detection of dopamine release. *Chemistry in Australia, Royal Australian Chemical Institute, Australia* **2003,** (12), 12-15.

9. Chen, P.; McCreery, R. L., Control of electron transfer kinetics at glassy carbon electrodes by specific surface modification. *Analytical Chemistry* **1996,** *68* (22), 3958-3965.

10. Paul, D. W.; Stenken, J. A., A review of flux considerations for in vivo neurochemical measurements. *The Analyst* **2015,** *140* (11), 3709-3730.

11. Li, X.; Majdi, S.; Dunevall, J.; Fathali, H.; Ewing, A. G., Quantitative measurement of transmitters in individual vesicles in the cytoplasm of single cells with nanotip electrodes. *Angewandte Chemie International Edition* **2015,** *54* (41), 11978-11982.

12. Morton, K. C.; Morris, C. A.; Derylo, M. A.; Thakar, R.; Baker, L. A., Carbon Electrode Fabrication from Pyrolyzed Parylene C. *Analytical Chemistry* **2011,** *83* (13), 5447-5452.

13. Rees, H. R.; Anderson, S. E.; Privman, E.; Bau, H. H.; Venton, B. J., Carbon nanopipette electrodes for dopamine detection in Drosophila. *Analytical chemistry* **2015,** *87* (7), 3849-3855.

14. P-2000 Laser-based micropipette puller system operation manual. **2012**, 55.

15. Zhao, X.; Lu, X.; Tze, W. T. Y.; Wang, P., A single carbon fiber microelectrode with branching carbon nanotubes for bioelectrochemical processes. *Biosensors and Bioelectronics* **2010,** *25* (10), 2343-2350.

16. Park, J.; Quaiserová-Mocko, V.; Patel, B. A.; Novotný, M.; Liu, A.; Bian, X.; Galligan, J. J.; Swain, G. M., Diamond microelectrodes for in vitro electroanalytical measurements: current status and remaining challenges. *The Analyst* **2008,** *133* (1), 17-24.

17. Shalini, J.; Sankaran, K. J.; Dong, C.-L.; Lee, C.-Y.; Tai, N.-H.; Lin, I.-N., In situ detection of dopamine using nitrogen incorporated diamond nanowire electrode. *Nanoscale* **2013,** *5* (3), 1159-1167.

18. Zestos, A. G.; Yang, C.; Jacobs, C. B.; Hensley, D.; Venton, B. J., Carbon nanospikes grown on metal wires as microelectrode sensors for dopamine. *The Analyst* **2015,** *140* (21), 7283-7292.

19. Silva, E. L.; Bastos, A. C.; Neto, M. A.; Silva, R. F.; Ferreira, M. G. S.; Zheludkevich, M. L.; Oliveira, F. J., Novel diamond microelectrode for pH sensing. *Electrochemistry Communications* **2014,** *40*, 31-34.

20. Nimmagadda, R. D.; McRae, C., Characterisation of the backbone structures of several fulvic acids using a novel selective chemical reduction method. *Organic geochemistry* **2007,** *38* (7), 1061-1072.

21. Gasnier, A.; Pedano, M. L.; Gutierrez, F.; Labbé, P.; Rivas, G. A.; Rubianes, M. D., Glassy carbon electrodes modified with a dispersion of multi-wall carbon nanotubes in dopamine-functionalized polyethylenimine: Characterization and analytical applications for nicotinamide adenine dinucleotide quantification. *Electrochimica Acta* **2012,** *71*, 73-81.

22. Xiang, L.; Yu, P.; Hao, J.; Zhang, M.; Zhu, L.; Dai, L.; Mao, L., Vertically aligned carbon nanotube-sheathed carbon fibers as pristine microelectrodes for selective monitoring of ascorbate in vivo. *Analytical chemistry* **2014,** *86* (8), 3909-3914.

23. Zestos, A. G.; Jacobs, C. B.; Trikantzopoulos, E.; Ross, A. E.; Venton, B. J., Polyethylenimine Carbon Nanotube Fiber Electrodes for Enhanced Detection of Neurotransmitters. *Analytical chemistry* **2014,** *86* (17), 8568-8575.

24. Alwarappan, S.; Joshi, R. K.; Ram, M. K.; Kumar, A., Electron transfer mechanism of cytochrome c at graphene electrode. *Applied Physics Letters* **2010,** *96* (26), 263702.

25. Trouillon, R.; Combs, Z.; Patel, B. A.; O'Hare, D., Comparative study of the effect of various electrode membranes on biofouling and electrochemical measurements. *Electrochemistry Communications* **2009,** *11* (7), 1409-1413.

26. McQuistan, A.; Zaitouna, A. J.; Echeverria, E.; Lai, R. Y., Use of thiolated oligonucleotides as anti-fouling diluents in electrochemical peptide-based sensors. *Chemical Communications* **2014,** *50* (36), 4690-4692.

27. Li, W.; Liu, Q.; Liu, L., Antifouling gold surfaces grafted with aspartic acid and glutamic acid based zwitterionic polymer brushes. *Langmuir* **2014,** *30* (42), 12619-12626.

28. Gui, A. L.; Luais, E.; Peterson, J. R.; Gooding, J. J., Zwitterionic Phenyl Layers: Finally, Stable, Anti-Biofouling Coatings that Do Not Passivate Electrodes. *ACS applied materials & interfaces* **2013,** *5* (11), 4827-4835.

Appendices

Appendix 1 Publications and presentations arising from work presented in this thesis

Appendix 2 Journal article

Siraj, S.; McRae, C. R.; Wong, D. K., Effective activation of physically small carbon electrodes by n-butylsilane reduction. *Electrochemistry Communications* **2016,** *64*, 35-41.

A copy of the above journal article is included in the following pages.

Appendix 3 Review article

Hanssen, B. L.; Siraj, S.; Wong, D. K., Recent strategies to minimise fouling in electrochemical detection systems. *Reviews in Analytical Chemistry* **2016,** *35* (1), 1-28.

A copy of the above review article is included in the following pages.

Appendix 4 Conference presentations

Siraj, S., Wong, D. K. Y.,"Hydrogenated and 4-sulfobenzene modified conical-tip carbon electrodes with antifouling property for sensitive detection of dopamine" 66th Annual Meeting of the International Society of Electrochemistry, Taipei, Taiwan, 4-9 October, 2015, p131.

Siraj, S., Wong, D. K. Y., "Antifouling property of hydrogenated conical-tip carbon electrodes modified with 4-sulfobenzene for sensitive detection of dopamine" International Chemical and Biological Sensing Analysis Symposium in 2015, National Taipei University of Technology, Taipei, Taiwan, 12-13 October, 2015, p12

Siraj, S., McRae, C. R., Wong, D. K. Y., "Fouling resistant hydrogenated carbon electrodes fabricated using n-butyl silane reduction" RACI National Congress, Adelaide, Australia, 7-12 December 2014, p507.

Siraj, S., McRae, C. R., Wong, D. K. Y.,"Analytical characteristics of physically small, antifouling carbon electrodes during dopamine detection" 22nd RACI Annual Research and Development Topics Conference, Adelaide, Australia, 13-15 December 2014, p38.

Wong, D.K.Y., Chandra, S., Siraj, S., McRae, C. R., Miller, A. D., Bendavid, A., P. Martin, J., "In vivo Dopamine Detection with Minimal Fouling at Hydrogenated Conical-tip Carbon Electrodes" 65th Annual Meeting of the International Society of Electrochemistry, Lausanne, Switzerland, 31 August – 5 September, 2014.

Siraj, S., McRae, C. R., Wong, D. K. Y., Wong"Electrochemistry at Physically Small Carbon Electrodes Subjected to n-Butyl Silane Reduction" ISE Satellite Student Regional Symposium on Electrochemistry and 19th Australian/New Zealand Electrochemistry Symposium (19ANZES), Melbourne, Australia, 25-26 November 2013, p67.

Siraj, S., McRae, C. R., Wong, D. K. Y., "Using n-butyl silane reduction to introduce a hydrophobic carbon surface on physically small electrodes to resist fouling" 21st Annual Research and Development Topics Conference, Canberra, Australia, 11-13 December 2013, p56.

Electrochemistry Communications 64 (2016) 35–41

Contents lists available at ScienceDirect

Electrochemistry Communications

journal homepage: www.elsevier.com/locate/elecom

Effective activation of physically small carbon electrodes by *n*-butylsilane reduction

Shajahan Siraj, Christopher R. McRae, Danny K.Y. Wong *

Department of Chemistry and Biomolecular Sciences, Macquarie University, Sydney, NSW 2109, Australia

ARTICLE INFO

Article history:
Received 9 December 2015
Received in revised form 15 January 2016
Accepted 15 January 2016
Available online 22 January 2016

Keywords:
Conical-tip carbon microelectrodes
Electrode activation
Reduction
Hydrogenated carbon electrodes
Hexaammineruthenium(III) reduction
Cyclic voltammetry

ABSTRACT

In this work, we report a simple, effective activation of structurally small carbon electrodes by forming an H-terminated carbon surface using *n*-butylsilane reduction. The electrode surface modification was confirmed by electrochemistry and X-ray photoelectron spectroscopy. Cyclic voltammetry of $[Ru(NH_3)_6]^{3+}$ at these hydrogenated carbon electrodes yielded sigmoidal-shaped cyclic voltammograms with minimal charging current. They also exhibited superb stability after one-week storage in air or citrate/phosphate buffer.

1. Introduction

Microelectrodes (*i.e.* electrodes with ≤100 μm in at least one dimension) are of general interest owing to their capability in spatially resolved measurement of a small volume of a resistant analyte and investigating the chemistry of an analyte at a submicrosecond time scale [1]. Similarly, microelectrodes are particularly useful for applications in biological micro-environments. For example, diamond microelectrodes were used to measure norepinephrine release from the mesenteric artery of a rat [2] and serotonin uptake at lymphocytes extracted in monkey's blood [3]. These diamond microelectrodes exhibit high temporal and spatial resolutions with improved sensitivity, reproducibility and response stability required to monitor small changes of analyte concentration during the analytical detection of neurotransmitters.

Many different techniques have been developed for physically small electrode fabrication. Microelectrodes with ~2 nm diameter, fabricated by insulating electrochemically etched carbon fibres using a paint layer, showed steady-state voltammetric behaviour of different redox markers with and without a supporting electrolyte [4]. Using microwave-assisted chemical vapour deposition in a diborane-CH_4/H_2 mixture, boron-doped diamond microelectrodes with low, stable and pH-independent background current were constructed [2,3]. Carbon nanotube yarn microelectrodes were also fabricated for fast scan voltammetric detection of neurotransmitters by sealing carbon nanotube yarn in pulled glass capillaries [5]. Meanwhile, carbon-ring microelectrode arrays were constructed by pyrolysing acetylene gas inside a cluster of quartz capillaries to record individual exocytotic events from cultured cells [6].

In our laboratory, conical-tip carbon electrodes (~2 μm diameter, ~15 μm axial length) are routinely fabricated [7]. Briefly, after pulling a quartz capillary down to a fine tip, it is placed in a nuclear magnetic resonance tube such that acetylene gas is delivered through the larger end of the capillary and a nitrogen stream is counter-flowing through the nuclear magnetic resonance tube. In this way, the acetylene gas is thermally pyrolysed to deposit carbon in and on the shank of the pulled capillary. To accomplish electrical connection, graphite powder is packed and a wire is introduced through the larger end of the capillary before it is sealed with epoxy. Compared to carbon fibre electrodes, the quartz substrate of conical-tip carbon electrodes makes them mechanically stronger, whilst the sharp tips aid in easy biological membrane penetration during implantation [4]. In addition, the open-ended base edge on a conical-tip electrode is more accessible to the mass transport of analyte to the electrode, compared to an insulating plane at the finite fibre-capillary junction on carbon fibre electrodes. Therefore, conical-tip carbon electrodes of a similar dimension to carbon fibre electrodes were found to show an improved signal-to-noise ratio in detecting dopamine *in vivo* [8]. Notably, there is also no epoxy sealing at the carbon-capillary junction, which could otherwise have polluted solution of interest in a biological environment [9]. Recently, our laboratory has also applied conical-tip carbon electrodes with a hydrophobic surface to deter biological fouling during dopamine detection *in vivo* [10].

Upon fabrication, cyclic voltammetry of well-behaved redox systems is commonly performed at the electrodes to assess their

* Corresponding author. Tel.: +61 2 9850 8300.
E-mail address: Danny.Wong@mq.edu.au (D.K.Y. Wong).

http://dx.doi.org/10.1016/j.elecom.2016.01.007
1388-2481/

integrity. For example, the outer-sphere complex ion $[Ru(NH_3)_6]^{3+}$ is often used to characterise carbon surfaces because of its independence on the type of carbon surface [11]. Similar to microelectrodes with other geometries, a typical response of $[Ru(NH_3)_6]^{3+}$ in KCl supporting electrolyte showing (1) a sigmoidal shaped cyclic voltammogram (CV) and, (2) a small capacitive charging current between the forward and backward scans, is used to indicate a functioning conical-tip carbon microelectrode. Owing to the small electrode surface area, in addition to linear diffusion, edge diffusion of $[Ru(NH_3)_6]^{3+}$ becomes more prominent in the vicinity of the electrode, which maintains a constant supply of $[Ru(NH_3)_6]^{3+}$ to the electrode for reduction. This constant supply of $[Ru(NH_3)_6]^{3+}$ results in a steady-state diffusion current, giving rise to a sigmoidal shaped CV. Moreover, a good seal between the carbon film and the quartz substrate with minimal cracks and crevices on the carbon surface yields a small capacitive charging current between the forward and backward cyclic voltammetric scan. In many cases, pinholes, cracks or crevices arising from carbon surface imperfections and/or poor epoxy sealing, for example, between a fibre and the glass substrate in carbon fibre microelectrodes, will yield non-sigmoidal CVs with appreciable charging current between the forward and backward scans. When non-sigmoidal CVs were obtained at Pt and Au microdisc electrodes, they were often mechanically polished to minimise the imperfections, which could sometimes aid in subsequently achieving a sigmoidal-shape CV. Alternatively, a pre-treatment involving scanning the potential from −0.2 V to 1.8 V and back to −0.2 V (against a sodium saturated calomel reference electrode) at 200 mV s^{-1} was previously used to activate physically small, fragile carbon electrodes [12]. However, this pre-treatment was not known to yield a long-lasting improved characteristic. In the event of unsuccessful activation of these microelectrodes, they were simply discarded.

Previously, Nimmagadda and McRae [13,14] reported a one-pot reaction involving *n*-butylsilane reduction capable of reducing carbon–oxygen functionalities to chemically modify an analyte for chromatographic separation. As shown in Scheme 1, in the *n*-butylsilane reduction method catalysed by $B(C_6F_5)_3$, carbon–oxygen functionalities present on carbon materials, *e.g.* aldehydes, ketones and primary, secondary and tertiary alcohols, polycarboxylic acid group were converted to their corresponding alkyl functionalities, leaving carbon–carbon double bonds and the graphitic structure undisturbed. Phenolic hydroxyl groups are, however not reduced but are instead silanised to form a dendrimeric butylsiloxane [13]. This work aims at investigating the feasibility of activating non-functional conical-tip carbon electrodes by hydrogenating the electrodes using the *n*-butylsilane reduction method. X-ray photoelectron spectroscopy (XPS) will be used to characterise the surface of the hydrogenated carbon electrodes. We will also study the electrochemistry of $[Ru(NH_3)_6]^{3+}$ and anthraquinone-2,6-disulfonate (AQDS) at the hydrogenated carbon electrodes.

2. Experimental

All conical-tip carbon electrodes were fabricated as described previously [7,10]. In the *n*-butylsilane reduction, 5.0 mg of $B(C_6F_5)_3$ was dissolved in 5.0 mL anhydrous CH_2Cl_2 by stirring for 10 min before 20 μL (0.156 mmol) of *n*-butylsilane (99% pure) was added. A conical-tip carbon electrode was placed in the reaction solution that was continuously purged by N_2, before the setup was sealed with parafilm. Hydrogenation at the electrode was continued for 2 h at room temperature.

The fabricated electrodes were next characterised by a cyclic voltammetry of 1.0 mM $[Ru(NH_3)_6]^{3+}$ in 1.0 M KCl supporting electrolyte between +0.2 V and −0.4 V, and 1.0 mM AQDS in 0.1 M $HClO_4$ supporting electrolyte between +1.0 V and −1.2 V, both at 100 mV s^{-1}, using a low-current potentiostat (eDAQ Pty Ltd., Sydney, Australia) operated by EChem version 2.1.2 software on a PC *via* an E-corder interface (eDAQ Pty Ltd.). A single compartment, three-electrode cell accommodating a Ag|AgCl reference electrode and a platinum wire counter electrode was used for electrochemical measurement. All measurements were performed at room temperature in a Faraday cage to minimise any noise interference.

XPS was conducted using an ESCALAB250Xi spectrometer (Thermo Scientific, Loughborough, UK) interfaced to a computer with data acquisition and processing software (Avantage; Thermo Scientific). The samples were irradiated with a monochromatic Al Kα X-ray source of 1486.68 eV energy. A vacuum system at 2×10^{-9} mbar was operating at 73 W (13.8 kV × 5.25 mA) power. A sample of ~320 μm spot size was used. The photoelectron takeoff angle was 90° with a pass energy of 100 eV for survey scans or 20 eV for region scans.

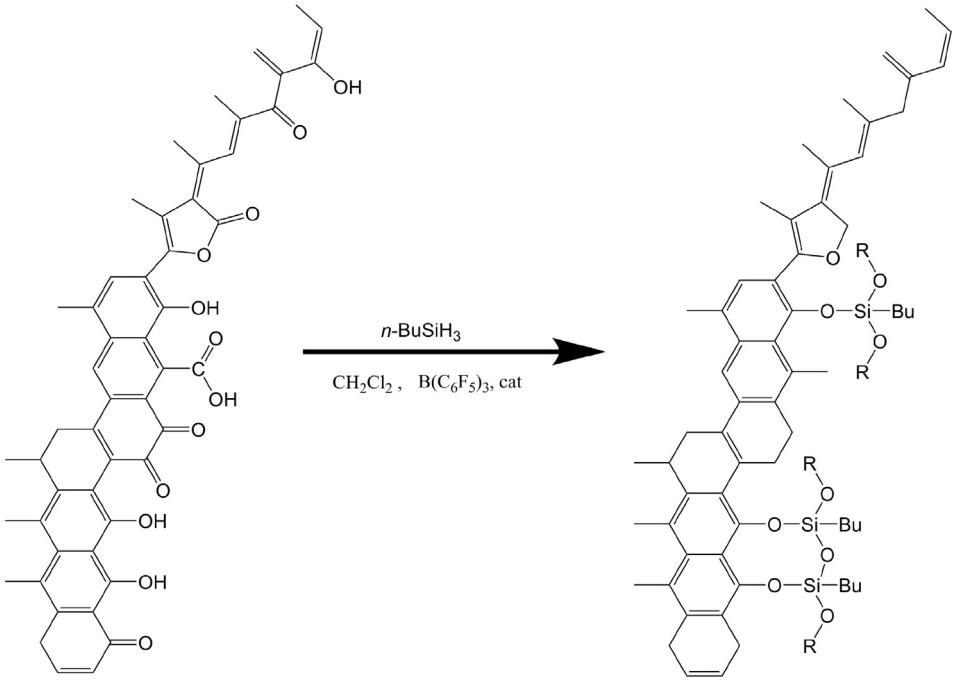

Scheme 1. Hydrogenation of carbon electrodes by *n*-butylsilane reduction method.

3. Results and discussion

After assembling a conical-tip carbon electrode together, cyclic voltammetry of 1.0 mM $[Ru(NH_3)_6]^{3+}$ in 1.0 M KCl is always conducted. A sigmoidal-shaped voltammogram, shown in Fig. 1(a), is used to indicate a functioning electrode. In Fig. 1(b), trace i shows an example of a non-sigmoidal shaped CV with an appreciable charging current obtained at a conical-tip carbon electrode. At these electrodes, non-uniform deposition of electroactive carbon on the quartz surface during pyrolysis would have resulted in cracks and crevices on the electrode surface, allowing $[Ru(NH_3)_6]^{3+}$ to travel through by capillary action. Such "leaky" electrodes would exhibit a large charging current. On a carbon electrode, edge planes resulting from cracks and crevices on the electrode surface contain many oxygen functionalities, which would contribute to a large background current [15]. Similarly, oxygen functionalities present on hexagonal rings of sp^2 carbon atoms on an electrode surface [11] will also contribute to a significant charging current. This feature becomes undesirable when microelectrodes are used in detecting low concentration analytes with the small detection signal masked by a large background current. Similar to other microelectrodes, conical-tip carbon electrodes that produced such non-sigmoidal-shaped CVs were just discarded, contributing to their unsuccessful fabrication rate.

After hydrogenating the bare conical-tip carbon electrode that yielded trace i in Fig. 1(b) by *n*-butylsilane reduction, the CV of 1.0 mM $[Ru(NH_3)_6]^{3+}$ at the electrode (trace ii) in 1.0 M KCl appears sigmoidal in shape with negligible charging current, indicating a characteristic functioning microelectrode. In our work, cyclic voltammetry of 1.0 mM AQDS in 0.1 M $HClO_4$, often used to show the presence of carbon–oxygen functionalities at edge plane of highly ordered pyrolytic graphite and other carbon surfaces [16,17], was also conducted. As shown by trace i of Fig. 1(c), the CV obtained depicts a reduction current

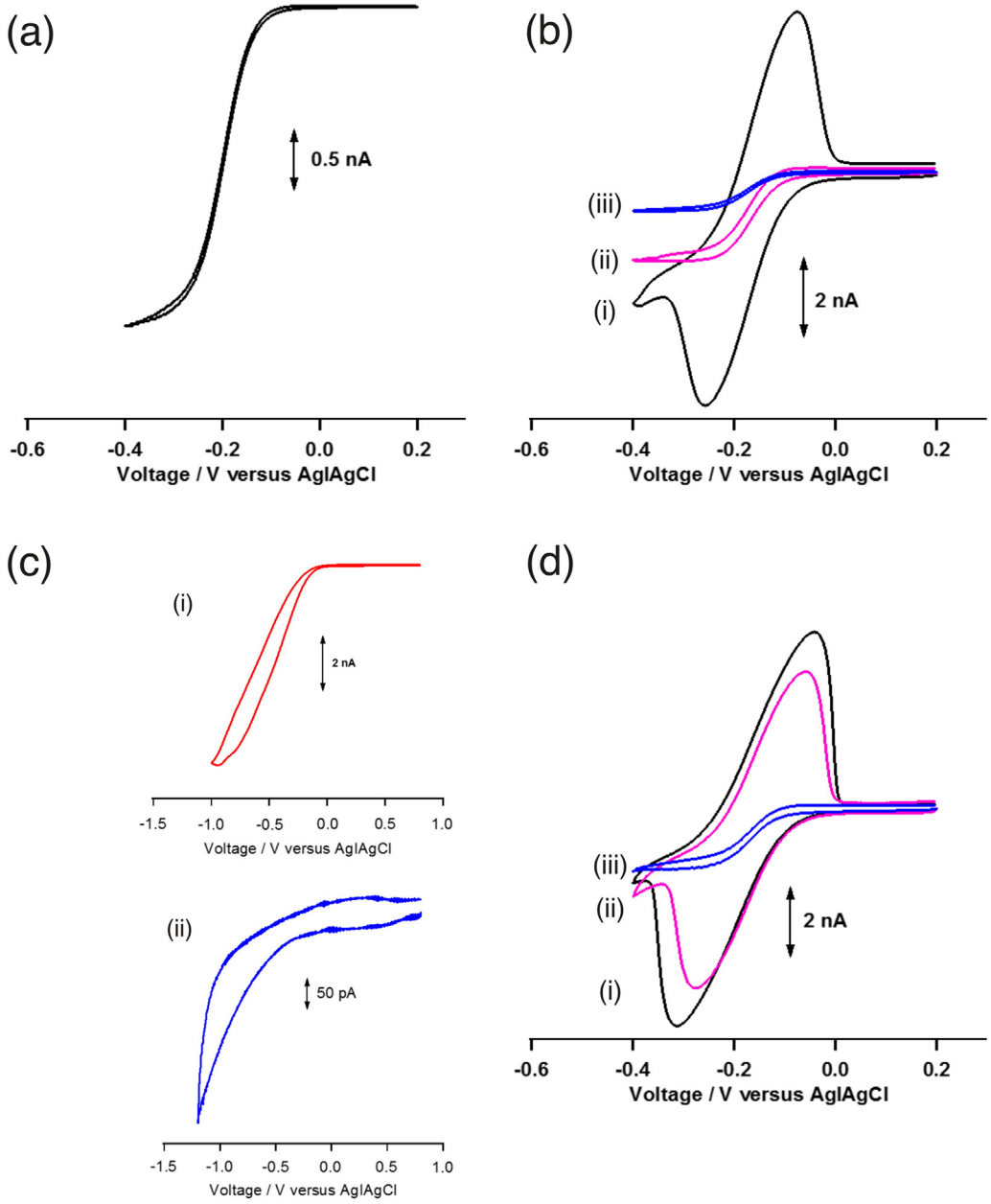

Fig. 1. Cyclic voltammetry of 1.0 mM $[Ru(NH_3)_6]^{3+}$ at (a) a conical-tip carbon electrode; (b) (i) a non-functioning conical-tip carbon electrode that was (ii) hydrogenated and (iii) twice hydrogenated in 1.0 M KCl; (c) cyclic voltammetry of 1.0 mM AQDS in 0.1 M $HClO_4$ at (i) a carbon electrode and (ii) a hydrogenated carbon electrode; (d) Cyclic voltammetry of 1.0 mM $[Ru(NH_3)_6]^{3+}$ at (i) a non-functioning conical-tip carbon electrode that was (ii) hydrogenated and (iii) twice hydrogenated in 1.0 M KCl. Scan rate: 100 mV s^{-1}.

arising from physisorbed AQDS on carbon–oxygen functionalities at carbon electrodes. However, a featureless CV (trace ii of Fig. 1(c)) at the corresponding hydrogenated electrodes has provided strong evidence for the removal of the functionalities from the electrode surface.

XPS was next conducted to further probe the characteristics of the hydrogenated carbon surface. Both the survey XPS spectra and Gaussian-fitted results obtained using bare and hydrogenated carbon electrodes are presented in Fig. 2. In Fig. 2(a)(i), the survey XPS spectrum of a bare carbon electrode shows distinct C1s and O1s peaks. However, in Fig. 2(a)(ii), after hydrogenation, an additional Si2p peak was also observed. By deconvolution, the corresponding high-resolution spectra obtained at these electrodes are displayed in Fig. 2(b) and (c). In Fig. 2(b)(i), 5 peaks were identified in the C1s spectrum of a bare carbon electrode. It is therefore apparent that the carbon obtained from the pyrolysis of C_2H_2 contributed several peaks under C1s including sp^2-like graphitic carbon and sp^3-hybridised diamond-like carbon. Amongst the fitted results in Fig. 2(b)(i), the most intense peak at ~285.0 eV is attributable to aliphatic, sp^3-like carbon (explicitly, quaternary C in long aliphatic chain) by comparing to a peak at the same binding energy obtained using an electrochemically and thermally oxidised boron-doped diamond film on a silicon substrate [18]. The peak at 284.5 eV is assigned to the presence of sp^2 graphitised carbon as this is analogous to that obtained using amorphous carbon films deposited by plasma on a single crystal silicon substrate [19]. Notably, the carbon film was exposed to air whilst being deposited during pyrolysis, giving rise to oxidation products on the electrode, which may account for carbon binding energies at 286.6, 288.0, and 289.2 eV. According to Zhou et al. [20], who examined chemically and thermally functionalised carbon nanofibres, the 286.6 eV peak represents carbon in the form of phenols, alcohols or ether groups, the 288.0 eV peak represents carbon in carbonyl or quinone groups, and the 289.2 eV peak indicates the presence of carbon as carboxyl groups on the electrode surface.

As shown in Fig. 2(b)(ii), the deconvoluted results at a hydrogenated carbon electrode also yielded 5 peaks under C1s. Compared to Fig. 2(b)(i), a peak of similar intensity is observable at 285.0 eV. However, the 284.5 eV peak in Fig. 2(b)(i) has slightly shifted to 284.4 eV after hydrogenation due to an altered chemical environment on the electrode surface [19]. Moreover, at the hydrogenated carbon electrode, the 284.4 eV peak becomes ~60% more intense than that obtained at the bare electrode. This is attributed to the composition of carbon films with mixed sp^2 carbon as graphite and silane-like carbon (−C–Si–O–) formed after hydrogenation, as illustrated in Scheme 1. This is further supported by the presence of both the Si2p and O1s signals obtained at the hydrogenated electrode surface, in agreement with Ferro et al.'s work involving a boron-doped diamond film electrode grown on a single-crystal, *p*-silicon wafer [18]. However, as expected, the intensity of the remaining three peaks is significantly lower after hydrogenation and these peaks have correspondingly shifted to 286.4, 287.3 and 288.8 eV due to different chemical environment after hydrogenation [19].

Most functional oxygen groups would reportedly yield O1s binding energies within a narrow 531–535 eV range [19,21]. In this work, the deconvolution of the O1s spectrum at a bare electrode yielded two peaks at 532.25 and 533.7 eV, as shown in Fig. 2(c)(i), with a relative abundance of ~7.13% and 3.10%, respectively. Using Ferro et al.'s work [18] as a guide, the 532.25 eV peak is assigned to etheric/alcoholic aliphatic functionalities and, to a lesser extent, to carbonylic aliphatic groups, most likely originated from dangling bonds on the sp^3-carbon skeleton. On the other hand, the 533.7 eV peak is assigned to oxygen present as ethers, alcohols, and esters in aromatic frames [18,20]. After hydrogenation, binding energies arising from oxygen-bearing functionalities (carbonyl, carboxyl, epoxy, *etc.*) associated with carbon on an electrode surface, except phenolic hydroxyl, have diminished when hydrogen atoms replaced these functionalities. However, we observed a separate intense oxygen peak at 532.0 eV in Fig. 2(c)(ii), possibly arising from a large number of oxygen present in the dendrimeric butylsiloxane derivative formed during hydrogenation shown in Scheme 1. Ferro et al. [18] also obtained a sharp oxygen peak at 532.8 eV that was assigned as oxygen present in aliphatic –C–O–Si– group when a boron-doped diamond film was deposited on a single-crystal *p*-silicon wafer. On the other hand, a characteristic Si2p peak at 102.18 eV is notably observable in Fig. 2(d), which was absent in the spectrum of the bare electrode. According to Ferro et al. [18], Si in aliphatic and aromatic species is expected to appear respectively at 102.1 and 102.0 eV, whilst the Si peak originated from the quartz substrate (SiO_2) is expected to be located between 103.21 and 103.9 eV. Therefore, the Si2p signal at the hydrogenated electrodes could be confidently assigned to aliphatic bonded silicon, indicating the formation of a butylsiloxane group on electrode surface by hydrogenation shown in Scheme 1. All XPS data above provided strong support for the proposed electrode surface structure obtained by *n*-butylsilane reduction in Scheme 1.

In some experiments, the hydrogenation of a non-functioning carbon electrode, represented by trace i in Fig. 1(d), still produced a peak-shaped CV for $[Ru(NH_3)_6]^{3+}$, as denoted by trace ii in Fig. 1(d), indicating unsuccessful modification in single hydrogenation. In this case, after repeating an identical hydrogenation step at such an electrode, a similarly sigmoidal shaped CV to that depicted in trace iii in Fig. 1(d) was obtained. In trace ii of Fig. 1b, the half-wave potential ($E_{½}$) and waveslope ($0.0592/n$) were estimated (based on the equation [22], $E = E_{½} + (0.0592/n)\log_{10}[(I_{lim} - I)/I]$, where E denotes the potential, n is the number of electrons transferred, I_{lim} is the limiting current and I is the current) to be −171 mV (standard deviation (SD) 15 mV; $N = 10$) and 60.2 mV decade^{-1} (SD 4.2 mV decade^{-1}; $N = 10$), respectively. After a repeated hydrogenation at the same electrode used to acquire trace ii in Fig. 1(b), the $E_{½}$ and waveslope of the corresponding CV (trace iii) in Fig. 1(b) were −177 mV (SD 12 mV; $N = 10$) and 63.9 mV decade^{-1} (SD 5.6 mV decade^{-1}; $N = 10$). Therefore, no discernible $E_{½}$ and waveslope shift was observed after repeated hydrogenation, which supports the insensitivity of $[Ru(NH_3)_6]^{3+}$ to the electrode surface chemistry. Moreover, the good agreement in waveslope to the expected 59 mV decade^{-1} for a one-electron transfer at hydrogenated electrodes indicates a reversible electron transfer reaction of $[Ru(NH_3)_6]^{3+}$. Further, the charging current in the sigmoidal-shaped CV became almost negligible after repeated hydrogenation. In their work involving the activation of glassy carbon electrodes by vacuum heat-treatment, Fagan et al. [23] suggested that the reduced charging current is due to removed surface redox species and microscopic surface structure changes. Notably, the limiting current diminished by ~30%–50% after repeated hydrogenation, which is attributable to the silanisation of phenolic hydroxyl groups on the electrode surface, leading to an increased electron tunnelling distance [11]. Therefore, this clearly demonstrates the ability of *n*-butylsilane reduction to activate electrodes by potentially filling in microfractures on the electrode surface. As the electrochemistry of $[Ru(NH_3)_6]^{3+}$ is independent of surface chemistry, the transform of a peak-shaped voltammogram to a sigmoidal shape can be attributed to a range of physical changes on the electrode surface. For example, the hydrogenation process can result in the bonding of the silicon atom in a butylsiloxane group to the carbon structure and this might function as a mechanical support for carbons on electrode surface, as described by Amato et al. [24].

In the next experiment, 20 cyclic voltammetric scans of 1.0 mM $[Ru(NH_3)_6]^{3+}$ in 1.0 M KCl were conducted at hydrogenated electrodes. The results obtained after hydrogenating a non-functioning bare carbon electrode, depicted in Fig. 3(a), show repeatable sigmoidal-shaped voltammograms with negligible changes of charging current. These results demonstrate the stability of hydrogenated electrode surface. To further establish the integrity of modified electrodes, cyclic voltammetry of $[Ru(NH_3)_6]^{3+}$ was conducted at both bare and hydrogenated electrodes that were separately stored in air and in a pH 7.4 citrate/phosphate buffer. The changes in the $[Ru(NH_3)_6]^{3+}$ reduction signal obtained at these electrodes after a week of storage are shown in Fig. 3(b) and (c). After storage, the reduction current at bare electrodes stored in air increased

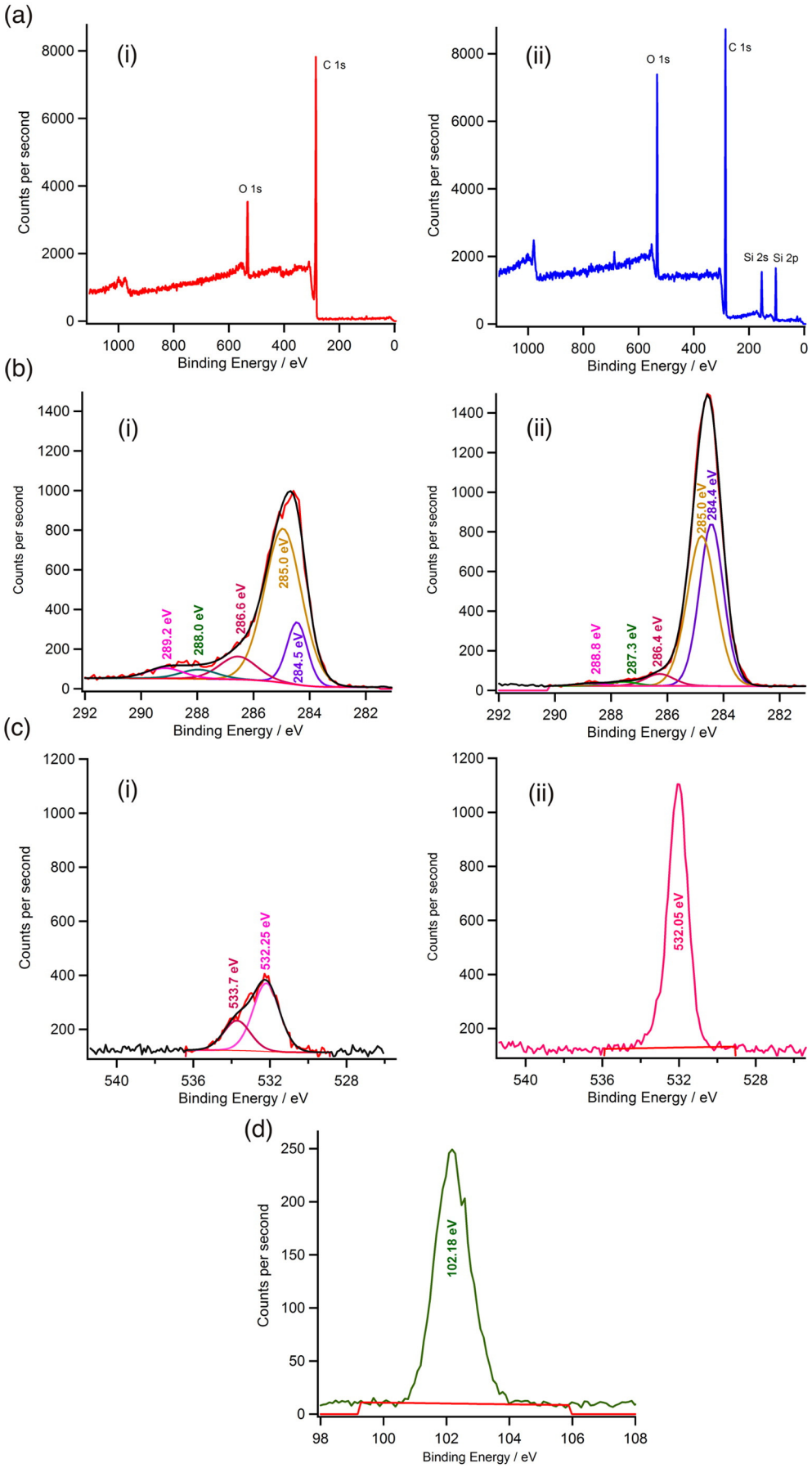

Fig. 2. (a) XPS survey spectrum of a bare carbon electrode (i) and a hydrogenated carbon electrode (ii); (b) C1s peak fitting of spectrum of a bare carbon electrode (i) and a hydrogenated electrode (ii); (c) O1s peak fitting of spectrum of a bare electrode (i) and a hydrogenated electrode (ii); (d) Si2p peak fitting of a spectrum of a hydrogenated electrode.

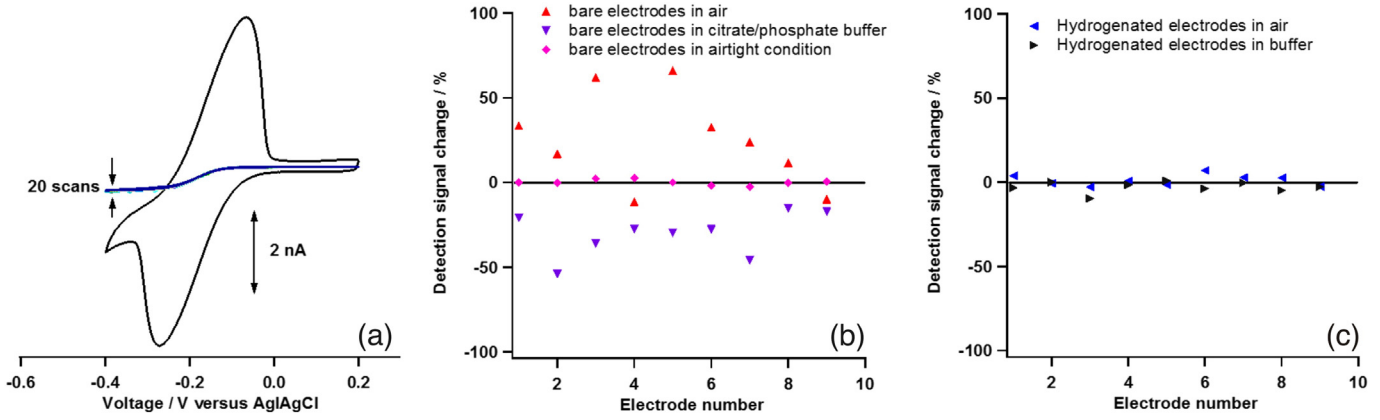

Fig. 3. (a) Twenty CVs of 1.0 mM $[Ru(NH_3)_6]^{3+}$ in 1.0 M KCl. Scan rate: 100 mV s^{-1}; $[Ru(NH_3)_6]^{3+}$ detection signal change at (b) bare and (c) hydrogenated carbon electrodes in air and in pH 7.4 citrate/phosphate buffer.

by 25% (SD 27%; $N = 9$). In this experiment, the exposure of carbon surface to air might have increased the specific surface area by surface fragmentation, roughening and channels originated through the deposited carbon, leading to the formation of surface oxides, as reported by Toebes et al. [25]. According to Lee et al. [26], upon exposure to air, the number of functional groups substantially increased on a carbon fibre surface, which would in turn enlarge the surface area of a carbon fibre and thus the enhanced detection signal. In addition, the charging current has clearly increased between the forward and backward scan in the voltammogram after storage. This may serve as evidence for surface oxide formation after exposure to air [27]. Similarly, the bare electrodes were also stored in an airtight condition as a control and their detection signal remained almost unchanged at 0.11% (SD 1.6%; $N = 9$) with a small charging current over the same period. In contrast, the bare electrodes stored in buffer showed a diminished detection signal by 30% (SD 13%; $N = 9$). Wang et al. [28] also observed a gradual decrease in detection signal and up to 50% loss of the detection signal after storing iridium and glucose oxidase modified carbon fibre microelectrodes in phosphate buffer for 1 week. Previously, polar functional groups (*e.g.* –OH) on a carbon surface reportedly provide coordination sites for phosphate to bind onto a carbon surface [29]. Anions can bind on a polar functional group-containing carbon surface by electrostatic interaction or ligand exchange mechanism and therefore, carbon was previously used as an adsorbent for removal of phosphate from aqueous waste [30]. In our work, we assume that citrate/phosphate ions in buffer can bind to the electrode surface and block the active surface area that ultimately causes diminishing detection signal at the electrodes. Hydrogenated electrodes were similarly stored in both air and buffer for 1 week. As shown in Fig. 3(c), very minimal detection signal change was observed at the hydrogenated electrodes in air (1.1% (SD 3.3%; $N = 9$)) and the buffer (2.8% (SD 3.2%; $N = 9$)). These results clearly indicated that hydrogenated electrodes were less prone to both air and buffer exposure because of H-terminated hydrophobic surface resulted in *n*-butylsilane reduction. Previously, H-terminated glassy carbon electrodes showed long-term surface stability towards air oxidation and also demonstrated weaker adsorption to polar compounds compared to bare glassy carbon electrodes. The absence of surface oxide might have enhanced the stability of H-terminated glassy carbon, which would otherwise increase adsorption to carbon promoted by local electron withdrawal by oxygen and the possibility of ionic and covalent bonding of adsorbates [31].

As illustrated in Scheme 1, during *n*-butylsilane hydrogenation, the carbon–oxygen functional groups on electrode surface are eliminated, except the phenolic hydroxyl groups, and are replaced by sp^3 carbon-hydrogen. We attribute the reduction of charging current at the hydrogenated carbon electrodes to the removal of the carbon–oxygen functionalities from the electrode surface, followed by terminating defect sites with carbon–hydrogen, as described by Xu et al. [16] for glassy carbon electrodes hydrogenated by microwave plasma. Similarly, H-terminated diamond electrodes also show low background current due to a lack of detectable electroactive surface carbon–oxygen functionalities [2]. In this way, we postulate that hydrogenated conical tip carbon electrodes surface behave similarly to a diamond electrode surface and produced CVs with minimal charging current.

4. Conclusion

In summary, this work has demonstrated the application of the *n*-butylsilane reduction as an effective activation of non-functional carbon microelectrodes to obtain sigmoidal-shaped voltammograms with minimal charging current at these electrodes. Chemical modification of these microelectrodes was confirmed by electrochemistry and XPS. In this way, the fabrication success rate of carbon microelectrodes has been improved to nearly 100%. Equally significant, these activated carbon electrodes have shown long-term stability in air and in citrate/phosphate buffer.

References

[1] R.M. Wightman, Probing cellular chemistry in biological systems with microelectrodes, Science 311 (2006) 1570–1574.
[2] J. Park, Y. Show, V. Quaiserova, J.J. Galligan, G.D. Fink, G.M. Swain, Diamond microelectrodes for use in biological environments, J. Electroanal. Chem. 583 (2005) 56–68.
[3] Y.S. Singh, L.E. Sawarynski, H.M. Michael, R.E. Ferrell, M.A. Murphey-Corb, G.M. Swain, B.A. Patel, A.M. Andrews, Boron-doped diamond microelectrodes reveal reduced serotonin uptake rates in lymphocytes from adult rhesus monkeys carrying the short allele of the 5-HTTLPR, ACS Chem. Neurosci. 1 (2010) 49–64.
[4] S. Chen, A. Kucernak, Fabrication of carbon microelectrodes with an effective radius of 1 nm, Electrochem. Commun. 4 (2002) 80–85.
[5] A.C. Schmidt, X. Wang, Y. Zhu, L.A. Sombers, Carbon nanotube yarn electrodes for enhanced detection of neurotransmitter dynamics in live brain tissue, ACS Nano 7 (2013) 7864–7873.
[6] Y. Lin, R. Trouillon, M.I. Svensson, J.D. Keighron, A.S. Cans, A.G. Ewing, Carbon-ring microelectrode arrays for electrochemical imaging of single cell exocytosis: fabrication and characterization, Anal. Chem. 84 (2012) 2949–2954.
[7] M. McNally, D.K.Y. Wong, An *in vivo* probe based on mechanically strong but structurally small carbon electrodes with an appreciable surface area, Anal. Chem. 73 (2001) 4793–4800.
[8] D.K.Y. Wong, D.B. Charles, M. McNally, Amperometric detection of dopamine release, Chemistry in Australia, Royal Australian Chemical Institute, Australia, 2003 12–15 issue 12.
[9] W.-H. Huang, D.-W. Pang, H. Tong, Z.-L. Wang, J.-K. Cheng, A method for the fabrication of low-noise carbon fiber nanoelectrodes, Anal. Chem. 73 (2001) 1048–1052.
[10] S. Chandra, A.D. Miller, A. Bendavid, P.J. Martin, D.K.Y. Wong, Minimizing fouling at hydrogenated conical-tip carbon electrodes during dopamine detection *in vivo*, Anal. Chem. 86 (2014) 2443–2450.
[11] P. Chen, R.L. McCreery, Control of electron transfer kinetics at glassy carbon electrodes by specific surface modification, Anal. Chem. 68 (1996) 3958–3965.
[12] J.B. Chien, R.A. Saraceno, A.G. Ewing, Intracellular voltammetry with ultrasmall carbon ring electrodes, Redox Chemistry and Interfacial Behavior of Biological Molecules, Springer, US 1988, pp. 417–424.

[13] R.D. Nimmagadda, C. McRae, Characterisation of the backbone structures of several fulvic acids using a novel selective chemical reduction method, Org. Geochem. 38 (2007) 1061–1072.
[14] R.D. Nimmagadda, C. McRae, A novel reduction reaction for the conversion of aldehydes, ketones and primary, secondary and tertiary alcohols into their corresponding alkanes, Tetrahedron Lett. 47 (2006) 5755–5758.
[15] B.K. Swamy, B.J. Venton, Carbon nanotube-modified microelectrodes for simultaneous detection of dopamine and serotonin *in vivo*, Analyst 132 (2007) 876–884.
[16] J. Xu, Q. Chen, G.M. Swain, Anthraquinonedisulfonate electrochemistry: a comparison of glassy carbon, hydrogenated glassy carbon, highly oriented pyrolytic graphite, and diamond electrodes, Anal. Chem. 70 (1998) 3146–3154.
[17] K.R. Kneten, R.L. McCreery, Effects of redox system structure on electron-transfer kinetics at ordered graphite and glassy carbon electrodes, Anal. Chem. 64 (1992) 2518–2524.
[18] S. Ferro, M. Dal Colle, A. De Battisti, Chemical surface characterization of electrochemically and thermally oxidized boron-doped diamond film electrodes, Carbon 43 (2005) 1191–1203.
[19] J. Filik, P.W. May, S.R.J. Pearce, R.K. Wild, K.R. Hallam, XPS and laser Raman analysis of hydrogenated amorphous carbon films, Diam. Relat. Mater. 12 (2003) 974–978.
[20] J.-H. Zhou, Z.-J. Sui, J. Zhu, P. Li, D. Chen, Y.-C. Dai, W.-K. Yuan, Characterization of surface oxygen complexes on carbon nanofibers by TPD, XPS and FT-IR, Carbon 45 (2007) 785–796.
[21] C.H. Goeting, F. Marken, A. Gutiérrez-Sosa, R.G. Compton, J.S. Foord, Electrochemically induced surface modifications of boron-doped diamond electrodes: an X-ray photoelectron spectroscopy study, Diam. Relat. Mater. 9 (2000) 390–396.
[22] J. Wang, Analytical Electrochemistry, third ed. John Wiley & Sons, 2006 73.
[23] D.T. Fagan, I.F. Hu, T. Kuwana, Vacuum heat-treatment for activation of glassy carbon electrodes, Anal. Chem. 57 (1985) 2759–2763.
[24] L. Amato, L. Schulte, A. Heiskanen, S.S. Keller, S. Ndoni, J. Emnéus, Novel nanostructured electrodes obtained by pyrolysis of composite polymeric materials, Electroanalysis 27 (2015) 1544–1549.
[25] M.L. Toebes, J.M.P. van Heeswijk, J.H. Bitter, A.J.van Dillen, K.P.de Jong, The influence of oxidation on the texture and the number of oxygen-containing surface groups of carbon nanofibers, Carbon 42 (2004) 307–315.
[26] J.-S. Lee, T.-J. Kang, Changes in physico-chemical and morphological properties of carbon fiber by surface treatment, Carbon 35 (1997) 209–216.
[27] M.J. Bleda-Martínez, J.A. Maciá-Agulló, D. Lozano-Castelló, E. Morallón, D. Cazorla-Amorós, A. Linares-Solano, Role of surface chemistry on electric double layer capacitance of carbon materials, Carbon 43 (2005) 2677–2684.
[28] J. Wang, G. Rivas, M. Chicharro, Glucose microsensor based on electrochemical deposition of iridium and glucose oxidase onto carbon fiber electrodes, J. Electroanal. Chem. 439 (1997) 55–61.
[29] L. Zhang, Q. Zhou, J. Liu, N. Chang, L. Wan, J. Chen, Phosphate adsorption on lanthanum hydroxide-doped activated carbon fiber, J. Chem. Eng. 185 (2012) 160–167.
[30] Z. Wang, E. Nie, J. Li, M. Yang, Y. Zhao, X. Luo, Z. Zheng, Equilibrium and kinetics of adsorption of phosphate onto iron-doped activated carbon, Environ. Sci. Pollut. Res. 19 (2012) 2908–2917.
[31] T.-C. Kuo, R.L. McCreery, Surface chemistry and electron-transfer kinetics of hydrogen-modified glassy carbon electrodes, Anal. Chem. 71 (1999) 1553–1560.

Benjamin L. Hanssen, Shajahan Siraj and Danny K.Y. Wong*

Recent strategies to minimise fouling in electrochemical detection systems

DOI 10.1515/revac-2015-0008
Received May 19, 2015; accepted December 2, 2015

Abstract: Electrode fouling is a phenomenon that can severely affect the analytical characteristics of a technique or a sensor, such as sensitivity, detection limit, reproducibility, and overall reliability. Electrode fouling generally involves the passivation of an electrode surface by a fouling agent that forms an increasingly impermeable layer on the electrode, inhibiting the direct contact of an analyte of interest with the electrode surface for electron transfer. Some potential fouling agents include proteins, phenols, amino acids, neurotransmitters, and other biological molecules. Various antifouling strategies have been reported to reduce or eliminate electrode fouling. Most antifouling strategies exploit a protective layer or barrier on an electrode substrate to prevent the fouling agent from reaching the electrode surface. Although such strategies can be quite effective, they are inappropriate for systems in which the analyte itself is also the fouling agent. In such cases, other strategies must be used, including electrode surface modification and electrochemical activation. In this review, recent strategies to minimise and efforts to overcome electrode fouling across a diverse range of analytes and fouling agents will be presented.

Keywords: chemical fouling; fouling during neurotransmitter detection; strategies for minimising electrode fouling.

Introduction

Fouling of an electrode surface is often a serious problem encountered in some electrochemical analyses. This phenomenon may negatively affect the analytical characteristics of a technique or a sensor, such as sensitivity, detection limit, reproducibility, and overall reliability (Godino et al. 2010, Gao et al. 2011, Gasnier et al. 2012, Teymourian et al. 2012, Roeser et al. 2013, Sharp 2013, Brocenschi et al. 2014, Cavanillas et al. 2014, Chira et al. 2014, Schmidt et al. 2014, Stoytcheva et al. 2014). Electrode fouling can thus significantly affect the performance and reliability of electrochemical techniques and sensors in many applications.

Electrode fouling is a broad term generally describing the passivation of an electrode surface by a fouling agent that forms an increasingly impermeable layer on the electrode (Gattrell and Kirk 1992, Gao et al. 2011, Casella and Contursi 2012, Gasnier et al. 2012). This occurs by a wide range of mechanisms predominantly depending on the identity of the responsible fouling agent. The fouling agent may be a component of the matrix, the analyte itself, or a product of the electrochemical reaction. Electrode fouling prevents an analyte of interest from making physical contact with the electrode for electron transfer to elicit an electrochemical response (Narmadha et al. 2011, Mudrinić et al. 2014, Muna et al. 2014, Stoytcheva et al. 2014). The fouling agent may specifically adhere to certain structural features present on the electrode surface, such as edges and grain boundaries (Wilson et al. 2005, Goto et al. 2011, Zhuiykov and Kalantar-zadeh 2012). The fouling agent tends to adhere to the electrode surface as a result of favourable interactions between the fouling agent and the electrode surface. This includes hydrophobic, hydrophilic, and electrostatic interactions depending on the particular chemistries of the fouling agent and the electrode surface.

Electrodes that tend to have hydrophobic surfaces, such as diamond, carbon nanotubes, and some other carbon-based electrodes (Shin et al. 2005, McCreery 2008, Goto et al. 2011, Roeser et al. 2013), can promote species possessing hydrophobic components, including aromatic compounds, saturated or aliphatic compounds, and proteins to adhere to and foul the electrode. The hydrophobic interactions are entropically favourable in an aqueous electrolyte because water molecules are released from the solvation shell around hydrophobic compounds or components (Malmsten 2003, Wilson et al. 2005). These interactions are sufficiently favourable such that fouling

***Corresponding author: Danny K.Y. Wong,** Department of Chemistry and Biomolecular Sciences, Macquarie University, Sydney, New South Wales 2109, Australia, e-mail: Danny.Wong@mq.edu.au. http://orcid.org/0000-0003-2435-5140
Benjamin L. Hanssen and Shajahan Siraj: Department of Chemistry and Biomolecular Sciences, Macquarie University, Sydney, New South Wales 2109, Australia

by a hydrophobic mechanism is typically irreversible in an aqueous electrolyte under mild conditions (Grinnell and Feld 1981, Malmsten 2003).

Fouling that occurs by hydrophilic interactions tends to be more reversible than fouling involving hydrophobic interactions (Grinnell and Feld 1981, Hess and Vogel 2001, Malmsten 2003, Wilson et al. 2005, Thevenot et al. 2008). This greater reversibility in aqueous electrolytes containing a strong polar solvent, for example, water, is because the hydrophilic and electrostatic interactions are not exclusive to the fouling agent and the electrode surface, as water also has compatible hydrophilic (dipole-dipole interactions or hydrogen bonding) and electrostatic properties (ion-dipole interactions). In the case of electrostatic interactions, the electrode surface may possess ionisable functional groups, such as carboxylic acids, which will bind with a suitable fouling agent (Shin et al. 2005, McCreery 2008). Electrode fouling that occurs by a hydrophilic or electrostatic interaction is associated with polar, hydrophilic, or charged species, including proteins and other biological molecules.

Electrode fouling that occurs by the adsorption of biological macromolecules is frequently due to proteins as a result of their abundance in biological samples and tendency to cause fouling. The adsorption of other biological materials, such as cells, cell fragments, and DNA/RNA, can also foul an electrode. The binding of cells to an electrode surface is often mediated by proteins (Wilson et al. 2005). Soluble proteins are interesting fouling agents, as they are often hydrophilic on the surface to interact with an aqueous environment as well as hydrophobic on the inside to maintain protein folding or the binding of hydrophobic materials (Malmsten 2003). As a result of the dual nature of most proteins, they can foul electrodes through both hydrophilic and hydrophobic interactions. To foul a hydrophobic electrode surface, many proteins will unfold to allow the hydrophobic residues to interact with the hydrophobic surface (Grinnell and Feld 1981, Malmsten 2003, Wilson et al. 2005, Thevenot et al. 2008). Due to the greater strength of hydrophobic interactions in aqueous systems (Grinnell and Feld 1981, Hess and Vogel 2001, Malmsten 2003, Wilson et al. 2005, Thevenot et al. 2008), many antifouling strategies aimed at reducing fouling by biological materials involve increasing the hydrophilicity of the electrode surface.

Fouling agents discussed thus far have been monomeric species, where it is more energetically favourable for the fouling agent to adsorb to the electrode surface rather than be in solution. A fouling agent may also be a polymeric species that forms in the electrolyte, usually as a result of an electrochemical reaction (Gattrell and Kirk 1992, 1993, Anandhakumar et al. 2010, Narmadha et al. 2011, Pirvu and Manole 2013, Yang et al. 2013, Muna et al. 2014, Quynh et al. 2014). The product of an electrochemical reaction may be reactive, such that it forms dimers or larger polymeric structures. These polymeric structures are often insoluble due to their large size and high molecular weight and will precipitate from solution on the nearest surface, such as the electrode surface. Such adhesion of a polymer to the electrode surface obstructs the ability of the analyte to reach the electrode surface, thereby fouling the electrode (Gattrell and Kirk 1992, Anandhakumar et al. 2010, Narmadha et al. 2011, Pirvu and Manole 2013, Yang et al. 2013, Quynh et al. 2014). The polymer may be a dense and closed structure that is impermeable, or it may be lighter and more open such that the polymer is permeable or semipermeable (Paul et al. 2013, Pirvu and Manole 2013, Yang et al. 2013). The permeability of the polymeric species will depend on the starting monomer and the electrochemical system conditions (Anandhakumar et al. 2010, Narmadha et al. 2011). The important analytes of interest that foul electrodes by this route are phenols and neurotransmitters. In the case of phenols, following anodic oxidation, radicals are formed. Further reactions involving the radicals may produce soluble species, such as hydroquinone/benzoquinone or catechol, or may undergo coupling reactions to form dimers, then oligomers, and finally polymers (Gattrell and Kirk 1992, 1993). During the detection of the neurotransmitter, dopamine, the reaction products, including leukodopaminechrome (LDC) and dopaminechrome (DC), can lead to the formation of melanin-like polymeric molecules of ~3.8 Å in size that foul the electrode (Lee et al. 2007, Harreither et al. 2013, Trouillon et al. 2014). Specifically, dopamine is electrochemically oxidised to *o*-dopaminoquinone that is subsequently cyclised leading to the formation of LDC. In the following step, LDC is further oxidised to yield DC that may polymerise into a melanin-like molecule, as depicted by the mechanism shown in Scheme 1. These molecules can form strong covalent bonds with organic moieties and noncovalent bonds with inorganic groups present on an electrode surface (Lee et al. 2007, Harreither et al. 2013, Trouillon et al. 2014).

The types of fouling agents and the ways in which they cause electrode fouling are exceedingly broad. Equally broad are the strategies that have been used to reduce electrode fouling or impart some fouling resistance to an electrochemical technique or sensor. Most antifouling strategies use a modified electrode that has greater fouling resistance than an unmodified electrode. With the tendency

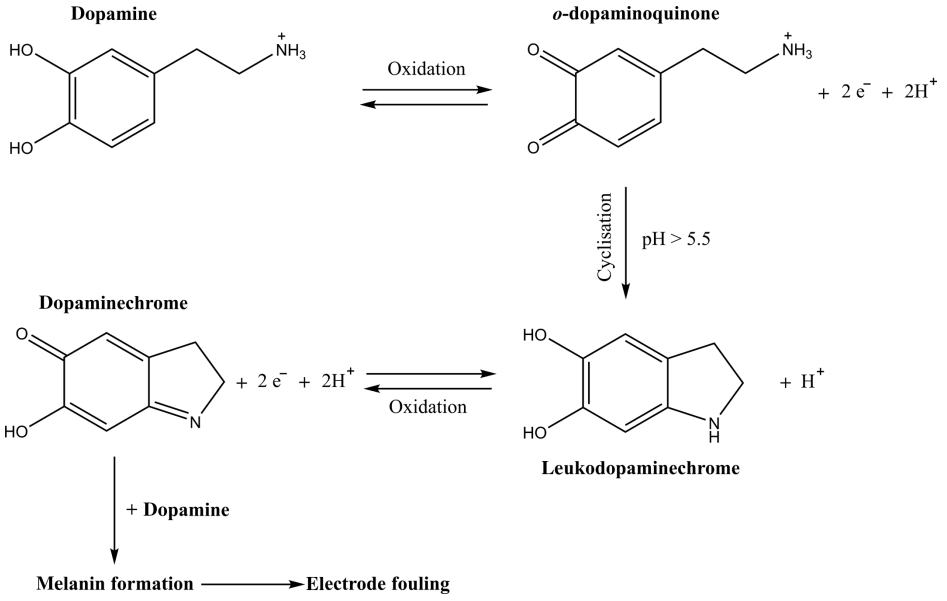

Scheme 1: A mechanism proposed by Harreither et al. (2013) for electrode fouling during the electrochemical oxidation of dopamine in aqueous solutions.

of glassy carbon, graphite, and metallic electrodes to be heavily fouled by a large variety of fouling agents, these electrode materials are commonly modified to increase fouling resistance (Gao et al. 2011, Gasnier et al. 2012, Teymourian et al. 2012, Roeser et al. 2013, Chira et al. 2014). Carbon-based materials, such as carbon nanotubes or graphene, have been used as electrode coatings due to their large surface area, electrocatalytic properties, and fouling resistance (Shan et al. 2009, Zhou et al. 2009, Gasnier et al. 2012, Teymourian et al. 2012). Metallic nanoparticles also possess important electrocatalytic properties and high electrical conductivity and can exhibit antifouling properties (Safavi and Momeni 2010, Muna et al. 2014). Polymers including Nafion (Razmi and Heidari 2009, Trouillon et al. 2009, Singh et al. 2011), poly(ethylene glycol) (Liu et al. 2011, Picher et al. 2013), poly(vinyl chloride) (Kivlehan et al. 2012), poly(3,4-ethylenedioxythiophene) (PEDOT; Yang et al. 2013), and polypyrrole (Pirvu and Manole 2013, Sasso et al. 2013) may be used as a coating to prevent the fouling agent from reaching the electrode surface. Although proteins are often fouling agents, they have been immobilised on electrode surfaces to prevent the nonspecific adsorption of other proteins or fouling agents (Picher et al. 2013, Qiu et al. 2013). Another potential benefit of this antifouling strategy is that enzymes can be immobilised to catalyse a reaction as part of the detection process, such as horseradish peroxidase and the detection of 4-chlorophenol (Qiu et al. 2013). Enzyme immobilisation can thus reduce both enzyme loss and the adsorption of potential fouling agents.

Electrochemical analyses are increasingly utilising uncoated electrodes with antifouling properties, especially boron-doped diamond electrodes. While pure diamond has a very low electrical conductivity due to a completely sp^3 structure, doping with boron sufficiently increases the conductivity for use as an electrode material (McCreery 2008). The extensive sp^3 structure of boron-doped diamond together with the typically low surface polar functional groups results in a dramatic decrease in the adsorption of certain fouling agents (Shin et al. 2005, McCreery 2008). Nanoporous gold electrodes are another type of uncoated electrode with strong antifouling properties as a result of their increased electrode porosity and surface area compared to the frequently fouled planar gold electrodes (Summerlot et al. 2011, Patel et al. 2013b, Tavakkoli and Nasrollahi 2013, Quynh et al. 2014).

Although many antifouling strategies rely on the electrode material or coating to alleviate fouling, there are also other strategies for minimising electrode fouling during analyses using conventional electrodes. In electrochemical activation, a single potential or a train of pulses is applied to modify the electrode surface chemistry or remove adsorbed material through physical or oxidative processes (Dejmkova et al. 2009, da Silva et al. 2013). Surfactants or organic solvents can be included in the electrolyte to increase the solubility of reaction products that may adsorb on the electrode surface (Anandhakumar et al. 2010, Narmadha et al. 2011). The surfactants may also adsorb on the electrode surface, providing a physical barrier between the surface and potential fouling agents

(Malmsten 2003, Anandhakumar et al. 2010). Analogous to the process of electrode fouling, the choice and success of any antifouling strategy will depend on the particular analyte, potential fouling agents, matrix, and conditions used.

In this review, we have described the selected progresses in reducing electrode fouling published over the period from 2009 to early 2015. Due to the diversity of fouling agents and antifouling strategies investigated in this period, the evaluation or comparison of one strategy over another for a particular application is not straightforward. This review is not intended to be a comprehensive review covering all developments in this period, but instead we have sought to provide an overview and discussion of recent significant strategies for reducing fouling. No previous review is known to focus on the multiple aspects of electrode fouling and discuss diverse antifouling strategies in the one article. This review has been organised by categorising antifouling strategies into three main sections: electrode coatings and modifications, electrochemical activation, and electrolyte and flow systems. In each section, we have provided as many relevant examples as possible to illustrate the feasibility and effectiveness of the developed strategies for electrode fouling prevention or reduction. Examples involving more than one antifouling strategy were placed in the section for the most important or effective strategy.

Electrode coatings and modifications

Carbon-based materials

Carbon nanotubes

Carbon nanotubes are commonly immobilised on electrode surfaces due to their large surface area, electrical conductivity, and electrocatalytic properties (Gasnier et al. 2012, Teymourian et al. 2012). Carbon nanotube-modified electrodes also exhibit antifouling properties. For example, a multiwalled carbon nanotube-modified glassy carbon electrode was successfully used in the analysis of Sudan I, which is a phenolic azo dye (Yang et al. 2010). This modified electrode significantly reduced fouling due to the polymeric products of Sudan I compared to a bare glassy carbon electrode. In an amperometric analysis, the modified electrode lost only 15% of the initial current after 90 min compared to the bare glassy carbon electrode in which the current decreased more than 50% in <20 min. In addition to the greater fouling resistance of the carbon nanotube-modified electrode, the high surface area of the carbon nanotubes increased the measured current (Yang et al. 2010). Carbon nanotubes have also shown antifouling properties in an electrochemical analysis *in vivo*, where proteins of all sizes could potentially foul the electrode surface. For an *in vivo* analysis, Xiang et al. (2014) immobilised vertically aligned carbon nanotubes on SiO_2 passivated carbon fibres. This electrode was prepared by the pyrolysis of iron phthalocyanine under an Ar/H_2 atmosphere at 800°C to 1100°C. In applying the electrode to selectively monitor 0.5 mM ascorbate in cerebrospinal fluid *in vivo*, the authors reported a 2% loss of sensitivity in a 30-min experiment. In contrast, a corresponding 21% loss was observed at a bare carbon fibre microelectrode. The modified electrode was also used to successively detect ascorbate in the striatum of anesthetised rat brain every 5 min (Xiang et al. 2014). Excellent reproducibility and durability, along with well-defined sigmoidal voltammograms of ascorbate in the rat brain, supported an antifouling capability of the carbon nanotube-modified electrode in a complex sample. The antifouling properties of carbon nanotubes may be due to their electrocatalytic activity that arises from various defects at the ends of the nanotubes or on the cylindrical walls (McCreery 2008, Gasnier et al. 2012, Teymourian et al. 2012). These defects often undergo oxidation or other reactions producing a variety of functional groups.

Although the carbon nanotube-modified electrodes prepared by Yang et al. (2010) and Xiang et al. (2014) used a suspension of the nanotubes in *N*,*N*-dimethylformamide and pyrolysis of iron phthalocyanine, respectively, a polymer is frequently used to reduce the aggregation of the nanotubes (Gasnier et al. 2012, Teymourian et al. 2012). For the analysis of phenolic flavones, Sheng et al. (2014) and Chen et al. (2011b) prepared multiwalled carbon nanotube composite electrodes using two different polymers. In the analysis of 5,7-dihydroxychromone and luteolin, an electrode with the polymer poly(ethylene terephthalate) was used in conjunction with capillary electrophoresis (Sheng et al. 2014). It was found that the current at this electrode diminished by 7.1% [relative SD (RSD) 2.6%] after 15 repetitive runs. The electrode prepared by Chen et al. (2011b) showed a very similar performance in the analysis of various phenolic flavones. The electrode was prepared by the water vapour-initiated polymerisation of ethyl 2-cyanoacrylate with multiwalled carbon nanotubes. Coupled with capillary electrophoresis, the current at this electrode decreased by up to 7.8% after 15 runs (RSD 2.7%). In both studies, the antifouling properties

of carbon nanotubes were illustrated with an analogous composite electrode where the carbon nanotubes were replaced with graphite. These graphite composite electrodes experienced 42% to 43% (RSD 18–19%) decrease in current. These results suggest that the observed fouling resistance is due to the carbon nanotubes and the particular polymer used to construct the electrode has little impact on the fouling resistance. The electrodes used by Sheng et al. (2014) and Chen et al. (2011b) were constructed without a solid electrode substrate by placing the carbon nanotube-polymer mixtures inside fused silica capillaries. This avoids issues with possible detachment of the carbon nanotube-polymer layer from an electrode surface.

Although carbon nanotubes have been shown to be resistant to fouling from phenolic analytes that polymerise during electrochemical detection, such as Sudan I (Yang et al. 2010) and phenolic flavones (Chen et al. 2011b, Sheng et al. 2014), they are also resistant to polyphenols present in white wine. Although these polyphenols are not a product of the electrochemical process, they can nevertheless adsorb on the electrode surface. To analyse the polyphenols present in white wine, Moreno et al. (2011) used multiwalled carbon nanotubes dispersed in the polymer polyethylenimine on a glassy carbon substrate. With the use of capillary zone electrophoresis, no decrease in current was observed after eight runs. The presence of the carbon nanotubes significantly improved the fouling resistance of the electrode, as the current at a bare glassy carbon electrode decreased by 82% after eight runs.

In addition to polymers, other materials have been used to increase carbon nanotube dispersion to improve electrode performance. Gasnier et al. (2012) observed that the presence of the neurotransmitter, dopamine, could improve the dispersion and mechanical strength of carbon nanotubes when applied to an electrode surface. This electrode was prepared by immobilising multiwalled carbon nanotubes dispersed in a solution of polyethylenimine functionalised with dopamine on a glassy carbon electrode (Gasnier et al. 2012). The addition of dopamine also resulted in a lower oxidation potential of nicotinamide adenine dinucleotide (NADH; Gasnier et al. 2012). Using the modified electrode, a series of 10 amperometric calibrations was performed. Between the 1st and 10th calibrations, the sensitivity to NADH decreased by only 12% (Gasnier et al. 2012). These results demonstrate the resistance of the modified glassy carbon electrode to fouling by NAD^+. Although dopamine has a tendency to cause electrode fouling, its use significantly improved the dispersion of the carbon nanotubes in solution through hydrophobic interactions and thus may have contributed to the good antifouling properties. Zestos et al. (2014) also developed a modified electrode using polyethylenimine and carbon nanotubes. A carbon nanotube fibre electrode was prepared by suspending single-walled carbon nanotubes in water with sodium dodecylbenzenesulfonic acid and pumping the suspension into a rotating solution of polyethylenimine in a custom-built rotating stage. The fouling resistance of the polyethylenimine-carbon nanotube fibre electrodes was examined by measuring serotonin in the presence of the metabolite of serotonin, 5-hydroxyindolacetic acid, which is also known to cause electrode fouling during the detection of serotonin *in vivo*. Electrode fouling from the metabolite of serotonin is particularly important because its physiological concentration is often 10 times higher than that of serotonin. The serotonin oxidation peak at the polyethylenimine-carbon nanotube electrode was reported to remain almost constant upon incubation in 5-hydroxyindolacetic acid for 2 h. The polyethylenimine-carbon nanotube fibre electrodes have also exhibited antifouling properties towards the oxidation product of dopamine, as no significant change in dopamine oxidation current was observed when a bolus of dopamine was injected every 2 h over a 10-h period (Zestos et al. 2014). When the polyethylenimine-carbon nanotube fibre electrodes were applied to measure exogenous serotonin in rat brain slices of the caudate putamen for 10 min, the peak-shaped cyclic voltammograms and the dopamine oxidation peak current remained unchanged. The authors proposed that the antifouling properties of the electrode are due to the presence of additional edge plane sites arising from carbon nanotubes. Similarly, Harreither et al. (2013) developed a 35 μm diameter carbon nanotube fibre by continuously spinning single-walled carbon nanotubes dispersed in sodium dodecyl sulfate in a coflowing stream of aqueous poly(vinyl alcohol). Based on a steady-state amperometric measurement of 1 mM and 100 μM dopamine at the fabricated electrode, as shown in Figure 1, they found that the electrode lost half of its initial steady-state current in 15 min at the high concentration (Harreither et al. 2013). However, the steady-state current obtained in 100 μM dopamine was unchanged for 2 h. The experiment may be a good indication of the potential application of carbon nanotube fibres in the brain, where the concentration of dopamine (0.01–1 μM) is much lower than that used in this experiment. These results also indicated that fouling of dopamine is concentration dependent and a lower concentration of dopamine may lead to decreased chemical fouling. The authors also explained that the insulating patches grew at a slower rate on carbon nanotube fibre compared to traditional carbon fibre.

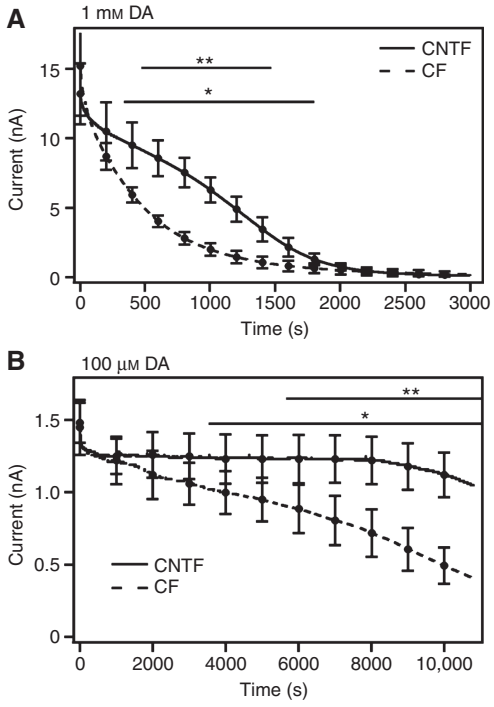

Figure 1: Amperometric currents for 1 mM dopamine (A) and 100 μM dopamine (B) obtained at 0.8 V versus Ag|AgCl with a carbon nanotube fibre microelectrode (solid line) and a carbon fibre microelectrode (dashed line) in phosphate-buffered saline (pH 7.4).
Mean±SD (n=4–7). The results were compared using Student's t-test, *p<0.05, **p<0.01. Reproduced with permission from Harreither et al. (2013).

Without the use of a polymer, Zheng et al. (2012) constructed a glassy carbon electrode modified with multiwalled carbon nanotubes dispersed in a gel containing the ionic liquid, 1-butyl-3-methyl-imidazolium hexafluorophosphate. This ionic liquid-modified electrode was used for the analysis of *o*-sec-butylphenol and displayed moderate antifouling properties. The current density was observed to have decreased by 25% in the second cycle relative to the first cycle. Despite being a large decrease in current density, a 51% and 49% decrease in current density was measured at a bare glassy carbon electrode and a multiwalled carbon nanotube-modified glassy carbon electrode, respectively. In this study, the carbon nanotube-modified electrode without the ionic liquid showed virtually identical fouling resistance to a bare glassy carbon electrode. This is in contrast to the study of Yang et al. (2010), where a similarly prepared carbon nanotube electrode was found to have good antifouling properties towards Sudan I. The observed difference in fouling resistance appears to be due to the properties of the particular analytes involved.

As the walls of carbon nanotubes are generally hydrophobic with strong π-π interactions between their aromatic rings (Gasnier et al. 2012), fouling resistance to some aromatic fouling agents may be improved by increasing the hydrophilicity of the carbon nanotubes. Merli et al. (2012) and Thomas et al. (2013) both prepared electrodes with oxidised carbon nanotubes that resisted fouling agents possessing aromatic functional groups. Olanzapine and risperidone are two pharmaceutical drugs that can form oligomers during electrochemical analysis (Merli et al. 2012). Merli et al. (2012) developed an oxidised single-walled carbon nanotube-modified gold electrode for the analysis of these drugs. They found that, after more than 20 differential pulse voltammetric scans, there was no apparent fouling of the modified electrode for both drugs. Similarly, for the analysis of the amino acid tryptophan, Thomas et al. (2013) constructed an oxidised multiwalled carbon nanotube-modified carbon paste electrode that demonstrated good antifouling properties, with a negligible change in current after 30-min continuous amperometry. The oxidation of the carbon nanotubes would have increased the hydrophilicity with a greater number of surface oxygen functional groups, which may have reduced the adsorption of these aromatic species on the carbon nanotubes.

Graphene

Graphene is a two-dimensional single layer of sp^2 carbon atoms with very high electrical conductivity, surface area, and mechanical strength (Shan et al. 2009, Zhou et al. 2009). It can be considered as an individual layer of graphite or an unrolled carbon nanotube and has been shown to reduce electrode fouling. The most common method to prepare graphene is by oxidising graphite and separating into single layers to form graphene oxide, which is then chemically or electrochemically transformed to reduced graphene oxide. For example, Alwarappan et al. (2010) studied the direct electrochemical activity of cytochrome *c* at a chemically reduced graphene-modified glassy carbon electrode. In addition to improved electron transfer kinetics, the current at the modified electrode decreased by only 7.5±0.3% after 50 repetitive cycles (Alwarappan et al. 2010). The presence of graphene protected the electrode from fouling by preventing cytochrome *c* from reaching the glassy carbon electrode surface and provided electrocatalytic sites for the efficient detection of the protein. Similar to carbon nanotubes, electrocatalytic sites may be made up of the various surface oxygen functional groups and defects on

the graphene. Although reduced graphene is obtained in the graphene oxide route, not all oxygen functionalities are removed and defects in the carbon lattice may still be present. Graphene that is more hydrophobic with fewer oxygen functionalities could be advantageous for minimising fouling from certain species. Keeley et al. (2011) prepared such low-oxygenated graphene by the *N*,*N*-dimethylformamide exfoliation of graphite powder. After 60-min continuous amperometry, a glassy carbon electrode modified with this exfoliated graphene showed only a 15% decrease in the oxidation current of NADH, whereas an analogous graphene oxide-modified electrode showed a corresponding 63% decrease. These results support the suggestion that the absence of oxygen functionalities in this exfoliated graphene significantly reduce the adsorption of NAD^+, minimising electrode fouling (Keeley et al. 2011).

Similar to carbon nanotubes, graphene can be combined with polymers and other materials to improve the stability and performance of a graphene-modified electrode. Chen et al. (2011a) developed a graphene/poly(urea-formaldehyde) composite platinum electrode for the determination of salidroside and tyrosol phenols. After 15 measurements, the current decreased by 8.1% and 43.9% at the composite electrode and bare platinum electrode, respectively. The polymer used in this graphene composite electrode assisted in binding the carbon material to the electrode surface and ensuring the surface was completely protected from fouling agents. In place of a polymer, Raj and John (2014) pretreated a glassy carbon electrode with 1,6-hexadiamine before adding graphene oxide to the treated surface and then electrochemically reducing the graphene oxide. This modified electrode was shown to be resistant to fouling by the oxidation products of theophylline, a methylxanthine derivative used as a pharmaceutical drug. In their work, there was a negligible change in current (RSD 0.85±0.04%) at the graphene-modified glassy carbon electrode after 25 cycles, indicating minimal fouling by the oxidation of theophylline (Raj and John 2014). The modified electrode showed higher fouling resistance than the corresponding bare glassy carbon and graphene oxide-modified glassy carbon electrodes. The lower fouling resistance of the graphene oxide-modified electrode is probably due to the many hydrophilic functional groups, which would increase the adsorption of the polar theophylline molecule and oxidation products. Similar to poly(urea-formaldehyde), 1,6-hexadiamine has enhanced the adsorption of reduced graphene oxide to the surface, which formed a barrier between the underlying electrode surface and the theophylline oxidation products.

Diamond and other carbon-based materials

Diamond has a very low electrical conductivity due to a completely sp^3 structure, but doping with boron sufficiently increases the conductivity for use as an electrode material (McCreery 2008). The extensive sp^3 structure of boron-doped diamond, together with the typically low surface polar functional groups, results in a dramatic decrease in the adsorption of certain fouling agents (Shin et al. 2005, McCreery 2008). The surface chemistry and shape of an electrode can, however, have a major effect on the electrochemical performance and antifouling characteristics. Indeed, Trouillon et al. (2011) demonstrated that the boron doping level affects the antifouling properties of boron-doped diamond electrodes. They investigated a range of boron doping levels (0.1, 1, and 5%, v/v) to investigate the stability of the electrodes for the detection of dopamine with bovine serum albumin as a biological fouling agent. Albumin is commonly used to test the antifouling properties of electrodes and sensors because it is often considered a biological fouling standard (Grinnell and Feld 1981, Wilson et al. 2005, Thevenot et al. 2008, Trouillon et al. 2009). A nonsignificant decrease of dopamine oxidation current was observed at the 0.1% and 1% doping levels. However, a corresponding 25% decrease was observed when the doping level was increased to 5%. These results indicate that high-density boron-doped diamond electrodes are more prone to fouling. A high level of boron doping would facilitate the formation of a high density of defect sites that are electrocatalytically active. Consequently, the inactivation of these defect sites by fouling agents would result in diminished electrochemical detection of the analyte. Therefore, low-level boron-doped diamond electrodes should limit the adsorption of fouling agents on an electrode surface. For example, Zhao et al. (2010) fabricated a conical-tip boron-doped diamond microelectrode with a low doping level. No significant attenuation in the oxidation signal was observed during the amperometric detection of serotonin in guinea pig mucosa *in vitro* for 100 min. As well as the doping level, the surface termination and roughness affect the fouling resistance of boron-doped diamond electrodes. Shpilevaya and Foord (2014) examined the extent of fouling by methyl viologen dichloride hydrate and 9,10-anthraquinone-2,6-disulfonic acid disodium salt and their products on various diamond electrodes, including microcrystalline boron-doped diamond, boron-doped diamond powder, and detonation nanodiamond powder. The effect of electrode fouling was also investigated at H- and O-terminated electrodes, which have low and high proportions of surface oxygen functionalities,

respectively. There was no observable adsorption of both compounds or products at O-terminated diamond electrodes (Shpilevaya and Foord 2014). On the contrary, there was a significant adsorption at the H-terminated electrodes. For methyl viologen, although the microcrystalline boron-doped diamond electrode showed the highest quantity of adsorbed product at 10.8 nmol cm^{-2}, it was the boron-doped diamond powder and detonation nanodiamond powder electrodes that exhibited a greater tendency to permanently adsorb the methyl viologen product (Shpilevaya and Foord 2014). After rinsing all three electrodes with water, the quantity of remaining adsorbed product was 0.4 and 1.2 nmol cm^{-2} for the boron-doped diamond powder and detonation nanodiamond powder electrodes, respectively, compared to only 0.1 nmol cm^{-2} for the microcrystalline boron-doped diamond electrode. For anthraquinonedisulfonate, however, the detonation nanodiamond powder electrode showed the highest quantity of adsorbed material at 18 and 15 nmol cm^{-2} for the reduction and oxidation scans, respectively, whereas the boron-doped diamond powder and detonation nanodiamond powder electrodes again showed a greater tendency to permanently adsorb material (Shpilevaya and Foord 2014). From the results, it is apparent that the hydrophobicity of the H-termination increases the extent of electrode fouling for these analytes as well as the greater surface roughness of the diamond powder electrodes compared to the microcrystalline boron-doped diamond (Shpilevaya and Foord 2014). For the analysis of serotonin, Güell et al. (2010) also observed that O-terminated boron-doped diamond electrodes had superior antifouling properties compared to a carbon nanotube network electrode after 10 consecutive scans.

In comparing the fouling resistance of boron-doped diamond (sp^3-hybridised carbon), undoped graphene (sp^2-hybridised carbon), and boron-doped graphene (sp^2-hybridised carbon) electrodes, Tan et al. (2013) found that, after 20 consecutive cyclic voltammetric scans in NADH, the boron-doped diamond electrode had a greater fouling resistance than both graphene-modified electrodes. These results support that the more inert sp^3 surface of diamond has lower surface oxygen functionalities and higher hydrophobicity than graphene. Similarly, Patel et al. (2013a) compared a boron-doped diamond electrode to several other carbon-based electrodes in the analysis of dopamine. The O-terminated polycrystalline boron-doped diamond electrode was considered the least susceptible to fouling even in a high concentration of 1 mM dopamine compared to glassy carbon, edge plane pyrolytic graphite, basal plane pyrolytic graphite, and basal plane highly oriented pyrolytic graphite, as depicted in Figure 2.

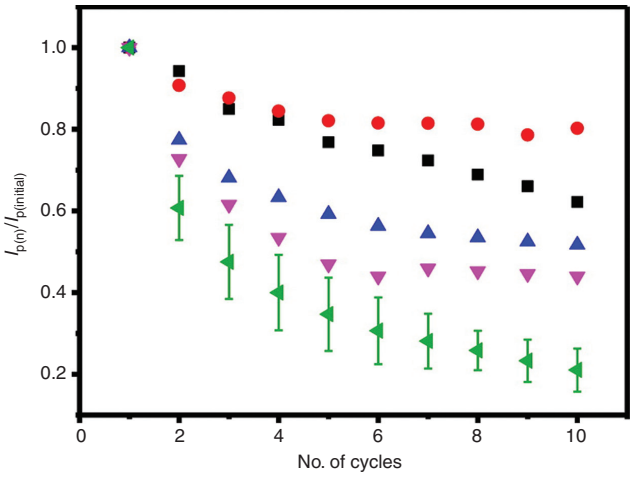

Figure 2: $I_{p(n)}/I_{p(initial)}$ against number of cycles (n) for the electrooxidation of dopamine at polycrystalline boron-doped diamond (red), glassy carbon (black), edge plane pyrolytic graphite (blue), basal plane pyrolytic graphite (pink), and basal plane highly oriented pyrolytic graphite (green).
The five grades of basal plane highly oriented pyrolytic graphite are plotted as mean±SD. Reproduced with permission from Patel et al. (2013a).

Similar to boron-doped diamond electrodes, diamond-like carbon electrodes are amorphous carbon with a high proportion of diamond-like bonds (sp^3), which provides good resistance to electrode fouling (Goto et al. 2011). The fouling resistance of a diamond-like carbon electrode treated with oxygen plasma to increase hydrophilicity has been investigated using bovine serum albumin, DNA, and human serum (Goto et al. 2011). There was a negligible change in the current response to ferricyanide/ferrocyanide after incubation in solutions of bovine serum albumin, DNA, and human serum for up to 24 h. The very strong resistance to fouling at the electrode is likely the result of the generally inert sp^3 diamond-like structure that reduces adsorption. Similar to Shpilevaya and Foord (2014) and Tan et al. (2013), where hydrophilicity was considered to be important for fouling resistance, increasing the surface hydrophilicity of the diamond-like carbon electrode with oxygen plasma treatment has likely improved the fouling resistance to these biological fouling agents and matrices. This would minimise the tendency of proteins to unfold and foul by hydrophobic mechanisms, which is considered to be stronger than hydrophilic adsorption (Grinnell and Feld 1981, Hess and Vogel 2001, Malmsten 2003, Wilson et al. 2005, Thevenot et al. 2008). On the contrary, Chandra et al. (2014) reported physically small conical-tip carbon electrodes (~2–5 µm diameter and ~4 µm axial length) that were hydrogenated by plasma-enhanced chemical vapour deposition to achieve

an H-terminated diamond-like sp^3 electrode surface. These electrodes retained 65% of dopamine oxidation current after they were incubated in a laboratory synthetic fouling solution containing caproic acid (a lipid), bovine serum albumin (a protein), cytochrome *c* (a protein), and human fibrinopeptide B (a peptide) for 7 days. By implanting the electrode in the left striatum of a male Sprague-Dawley rat during 60-min *in vivo* experiments, more than 70% of the dopamine oxidation current remained after the first 30 min and 50% remained over the next half period of the experiment, as shown in Figure 3. Although these results can be attributed to the H-terminated hydrophobic surface, the hydrophilic oxygen plasma-treated diamond-like electrode appeared to have a greater resistance to fouling.

An electron cyclotron resonance-sputtered nanocarbon film is a carbon electrode with similar properties to diamond-like carbon electrodes and has both sp^2 and sp^3 characteristics (Kato et al. 2011, Xue et al. 2012). Kato et al. (2011) and Xue et al. (2012) both prepared oxidised electron cyclotron resonance-sputtered nanocarbon films to resist fouling by bovine serum albumin and 8-hydroxy-2′-deoxyguanosine, respectively. The electrode used by Kato et al. (2011) was anodically pretreated to oxidise the electrode surface. Coupled with flow injection analysis, there was a negligible decrease in the current at this electrode after 12 injections (RSD 0.75%). At a bare glassy carbon electrode, the current was highly variable, fluctuating over the 12 injections (RSD 9.28%). The authors suggested that the greater fouling resistance of the pretreated nanocarbon film electrode was due to the increased hydrophilicity from oxidation. To oxidise their nanocarbon film, Xue et al. (2012) treated the electrode with oxygen plasma to partially oxidise the electrode surface. After a 30-min incubation in bovine serum albumin, the peak separation of ferricyanide/ferrocyanide increased from 80 to 120 mV and the peak current decreased to 92.0% of the initial value. On the contrary, for a pristine electron cyclotron resonance-sputtered nanocarbon film electrode without the oxygen plasma treatment, the peak separation increased from 217 to 620 mV and the peak current decreased to 71.7% of the initial value, which illustrated the requirement of a partially oxidised surface for antifouling properties. Compared to glassy carbon electrodes, the treated nanocarbon film electrode also demonstrated superior fouling resistance and was slightly improved compared to diamond-like carbon electrodes. The nanocarbon film electrode treated with oxygen plasma remained relatively hydrophobic compared to glassy carbon electrodes and diamond-like carbon electrodes, which suggests that, in addition to hydrophilicity, there are other important factors influencing the antifouling properties (Xue et al. 2012). For example, surface flatness is also believed to contribute to the observed fouling resistance, as the nanocarbon films were much smoother than diamond-like carbon electrodes (Kato et al. 2011, Xue et al. 2012).

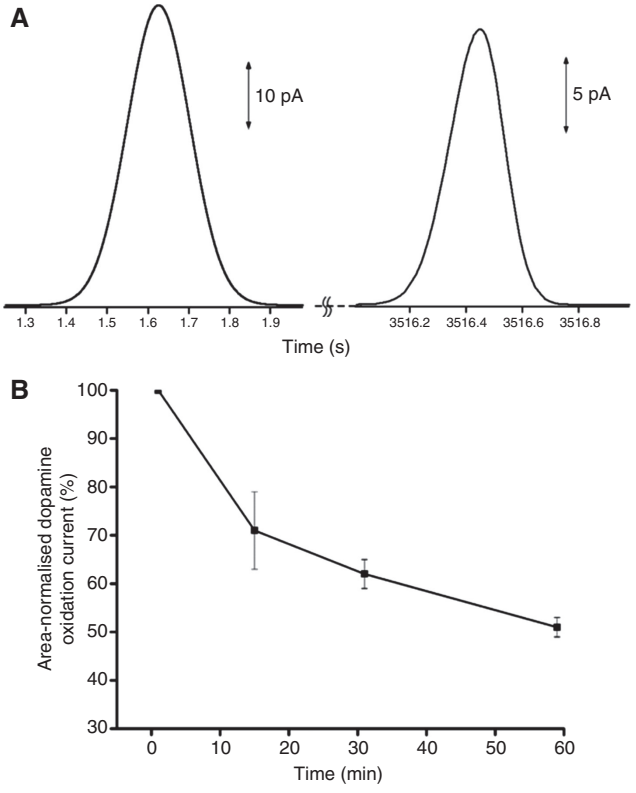

Figure 3: Gaussian-fitted dopamine oxidation signals obtained upon repeated electrical stimulations in the rat striatum at the start (left) and after 60 min (right) of monitoring at a hydrogenated carbon electrode (A) and a plot of electrode area normalised current measured over a 60-min period at hydrogenated carbon electrodes implanted in the rat striatum (B).
Reproduced with permission from Chandra et al. (2014).

Although sp^2-hybridised carbon materials, such as graphite and glassy carbon, are often found to significantly foul with a variety of species, some sp^2 carbon materials have shown strong antifouling properties, such as the NADH sensor developed by Gao et al. (2011) using a carbon double-shelled hollow sphere-modified glassy carbon electrode. The current at this modified electrode decreased by 16.0% after 4000 s, whereas the current at a bare glassy carbon electrode decreased by 52.6% (Gao et al. 2011). The antifouling and electrocatalytic properties of the carbon hollow spheres were suspected to be due to the presence of a glassy carbon surface with surface oxygen functionalities and defects. Although such surface features have been considered to contribute

to increased fouling with other species, the spherical shape and small size of the carbon hollow spheres may have resisted the adsorption of NAD^+. Similarly, Hadi and Rouhollahi (2011) analysed the thiols cysteine, homocysteine, and *N*-acetylcysteine using a nanocrystalline graphite-like pyrolytic carbon film electrode. These thiols or their electrochemical reaction products can cause electrode fouling. The pyrolytic carbon film was obtained by a noncatalytic thermal chemical vapour deposition method using methane as the carbon source. The electrode produced from a temperature of 1100°C proved to have superior electrochemical performance. For this electrode, the amperometric current for cysteine decreased by only 2% after 900 s (Hadi and Rouhollahi 2011). The antifouling properties of the pyrolytic carbon film is likely due to the high density of edge plane sites that promote the efficient oxidation of the thiols, and similar electrocatalytic oxygen functionalities to those on carbon hollow spheres may be present.

Polymeric films

The formation or presence of a polymeric film on an electrode surface can be detrimental to the electrode performance, such as during the analysis of phenols and neurotransmitters. However, conductive polymers have been demonstrated to show antifouling properties. For example, PEDOT was synergistically immobilised with the surfactant poly(sodium-4-styrenesulfonate) (PSS) on a glassy carbon electrode for the indirect analysis of tricresyl phosphate by detecting cresol that was formed from the hydrolysis of tricresyl phosphate (Yang et al. 2013). Using the modified glassy carbon electrode, the current after 20 repetitive measurements was 85% of the initial value, but the corresponding current was only 30% at a bare electrode. While the PEDOT polymer prevents cresol and its products from directly adsorbing on the glassy carbon electrode surface, the amphiphilic nature of PSS is also believed to aid in minimising electrode fouling by reducing the adsorption of the products of cresol (Yang et al. 2013). In another study, Pirvu and Manole (2013) used an alternative conductive polymer, polypyrrole, also with PSS to reduce fouling during the analysis of phenol. The extent of fouling was determined by surface plasmon resonance, in which the quantity of adsorbed material on the electrode surface is measured. With an ultrathin hybrid polypyrrole/PSS film on a gold electrode, the surface plasmon resonance signal was found to increase by an average of 22 m° per scan over 10 scans. Although this value indicates that the electrode was being progressively fouled, the value is significantly lower than that of a polypyrrole film electrode without PSS, where the corresponding signal increased by an average of 205 m° per scan for the first five scans and then 80 m° per scan for the last five scans. The scanning electron micrographs in Figure 4 visually show the different degrees of electrode fouling between the two electrode films. Although there is clearly less fouling with the polypyrrole/PSS film, it was not able to completely eliminate the electrode fouling. An interdigitated gold microelectrode surface was also modified with a PSS-doped polypyrrole film and used for the detection of dopamine released from pheochromocytoma (PC12) cells (Sasso et al. 2013). The modified electrode was stable under cell culture conditions for long-term amperometric experiments. In this work, the three-dimensional polypyrrole structure was speculated to decrease the freedom of movement of the protonated positively charged amino group tail of dopamine molecules and hence reduce polydopamine fouling. There could also be a combination of steric and electrostatic hindrance, limiting the intermolecular cyclisation, which is the prerequisite for the polymerisation of dopamine on an

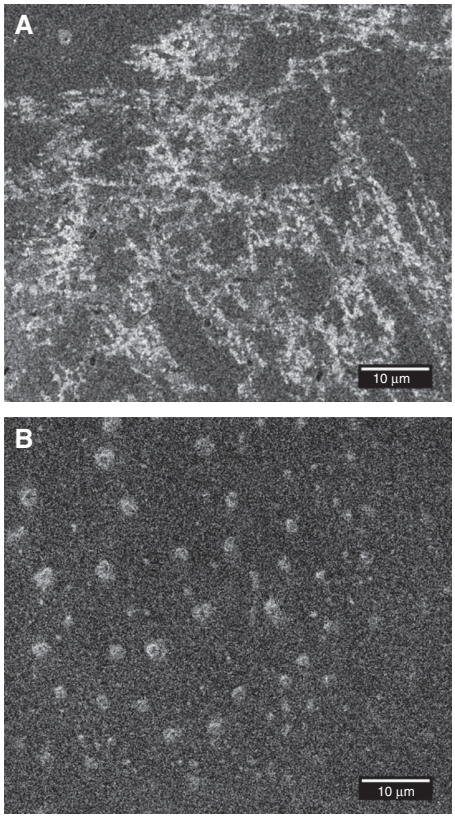

Figure 4: Scanning electron micrographs of (A) polypyrrole and (B) polypyrrole/PSS after 10 cyclic voltammetry scans in a solution of phenol.
Reproduced with permission from Pirvu and Manole (2013).

electrode surface. These results further demonstrate the greater antifouling properties of the PSS surfactant combined with conductive polymers compared to bare conventional electrodes. PSS, however, is not a requirement for an effective conductive polymer electrode. For example, for the detection of 2-(2-nitrophenyl)-1H-benzimidazole, a film of 1-naphtylamine was electropolymerised on a glassy carbon electrode surface followed by overoxidation by cycling in an aqueous sodium hydroxide solution (D'Eramo et al. 2010). Using this modified electrode, there was a 6% decrease in the reduction current after the first cycle and was then stable in subsequent cycles. At a bare electrode, however, there was a corresponding 34% decrease in current after the first cycle (D'Eramo et al. 2010). Evidently, the modified electrode was capable of reducing the extent of adsorption by the reduction product of the analyte, but the previous two conductive polymers with PSS seemed to provide greater fouling protection relative to bare conventional electrodes. This may be due to the presence of PSS or the particular analytes and fouling agents. Heterocyclic conductive polymeric films have also shown antifouling properties without the use of a surfactant such as PSS. To reduce electrode fouling, 3-amino-5-mercapto-1,2,4-triazole films were electropolymerised on glassy carbon electrodes for the detection of riboflavin, ascorbic acid, and folic acid (Revin and John 2012d), inosine (Revin and John 2012b), tyrosine (Revin and John 2012c), and norepinephrine and serotonin (Revin and John 2012a). In all analyses, there was a negligible change in current after 20 cycles with RSD values of 1.4% to 2.0%. These results indicate that electropolymerised films of heterocyclic conductive polymers can provide antifouling protection against a range of small biologically relevant molecules.

In addition to conductive polymers, nonconducting polymers may also be useful provided they are porous, allowing the analyte to reach the electrode surface while restricting the access of larger fouling agents, or mediate the electrochemical reaction on the polymer rather than the electrode surface. The polymer formed from the electropolymerisation of eugenol is known to be a nonconducting, porous polymer (Paul et al. 2013). The application of this polyeugenol coating to a gold electrode preserved the sensitivity of the electrode for oxygen detection in the presence of bovine serum albumin for 16 h (Paul et al. 2013). Without the polyeugenol coating, the sensitivity of a bare gold electrode to oxygen decreased by 80%. The pores in the polyeugenol film were too small to allow bovine serum albumin to reach the electrode surface, but oxygen was able to travel through the pores. Another nonconducting, porous polymer, chitosan, was immobilised on an electrode simply by incubating carbon fibre microelectrodes in chitosan solution for 15 s (Özel et al. 2011). The fabricated electrodes showed no decrease in signal after four consecutive measurements of serotonin. These modified electrodes were also satisfactorily used in four repeated determinations of serotonin in a live embryonic zebrafish intestine with minimum interference, while brief electrochemical reconditioning was performed between determinations. The authors observed similar current response after the four consecutive determinations. As chitosan has excellent sieving properties, the chitosan layer was likely acting as a protective barrier against the direct adsorption of biological molecules or large polymeric molecules formed during the oxidation of serotonin. To protect the underlying gold electrode surface, the electrode prepared by Milczarek (2009) relied on an adsorbed layer of iodine in addition to a nonconducting, porous polymeric film to prevent NAD^+ fouling. On top of this chemisorbed iodine layer, hydrolytic lignin was allowed to adsorb followed by the electrooxidation of the adsorbed lignin. Interestingly, lignin, a phenolic polymer, was used as part of an electrode to minimise fouling given that such polymers often rapidly cause fouling. A negligible decrease in current was observed after 45-min continuous amperometry (Milczarek 2009). Milczarek (2009) suggested that the adsorbed iodine minimised the oxidation of NADH on the surface of the gold electrode, but the oxidation of NADH was mediated by the adsorbed lignin polymeric film, thereby preventing the fouling of the electrode surface by NAD^+.

Nafion is a porous membrane that contains sulfonic acid functional groups, which gives the membrane a negative charge when exposed to an aqueous electrolyte. As an electrode coating, Nafion has demonstrated some antifouling properties due to it acting as a physical barrier to fouling agents and electrostatic repulsion of negatively charged fouling agents. Razmi and Heidari (2009) constructed a lead nitroprusside nanoparticle-modified carbon ceramic electrode coated with Nafion. Cyclic voltammetry and amperometry of 5 mM and 10 μM cysteine, respectively, were used to assess the performance of the electrode. The cyclic voltammetric current decreased by 12% after 10 cycles and then a further 8% after 40 cycles, and the amperometric current decreased by 10% after 10 min and then a further 5% after 20 min (Razmi and Heidari 2009). Without the Nafion coating, however, the cyclic voltammetric current decreased by 45% after 10 cycles and then a further 20% after 40 cycles, and the amperometric current decreased by 20% after 10 min and then a further 15% after 20 min (Razmi and Heidari 2009). Although nanoparticles can also have antifouling properties, these results clearly illustrate that the Nafion coating improved the fouling resistance of the electrode to

cysteine and its products. As cysteine and its products can reach the electrode surface and nanoparticles by permeating the Nafion membrane, the ability of Nafion to reduce electrode fouling suggests that the fouling agent responsible may be negatively charged and is repelled by the negatively charged Nafion film.

Individual polymer chains, such as poly(ethylene glycol), can be attached to an electrode surface to provide a dense polymeric film that resists fouling by a diversity of fouling agents. To protect against protein fouling, various poly(ethylene glycol) monomethyl ether moieties were grafted on a hydrogenated silicon surface by Perez et al. (2012) to investigate the adsorption of bovine serum albumin. The modified electrode exhibited excellent antifouling properties toward bovine serum albumin after being incubated in a solution for 1 h. With grafted moieties, the chain length, rather than the number of ethylene oxide monomers, was reportedly related to the antifouling behaviour. Similarly, Zhang et al. (2009) investigated the use of oligo(ethylene glycol) thiols as an electrode coating for an electrochemiluminescent sequence-specific DNA sensor. The use of oligo(ethylene glycol) thiols was found to reduce the nonspecific adsorption of the glucose oxidase enzyme label. After incubating an oligo(ethylene glycol) thiol-modified electrode in glucose oxidase for 30 min, there was only a minimal increase in the electrochemiluminescent signal compared to the signal before enzyme incubation. On the contrary, there was a 10-fold increase in signal at a comparable electrode modified with the commonly used antifouling agent, 6-mercaptohexanol, indicating significant nonspecific adsorption of glucose oxidase (Zhang et al. 2009). In addition to neutrally charged polymer chains such as poly(ethylene glycol), charged chains can be attached to an electrode to provide fouling resistance. Li et al. (2014) have used surface-initiated photoiniferter-mediated polymerisation to guide the growth of the amino acid-based zwitterionic polymers, poly[N^4-(2-methacrylamidoethyl)asparagine] and poly[N^5-(2-methacrylamidoethyl)glutamine], on gold surfaces. Using surface plasmon resonance, the authors reported the effective resistance to nonspecific protein adsorption from human blood serum and plasma when the polymer thickness was <11 nm. Moreover, the surface was also resistant to cell adhesion after incubating these polymer-coated electrodes in a culture medium with a concentration of 10^5 cells ml^{-1} (Li et al. 2014). These polymers could be resistant to fouling due to the net balanced charge, which increases hydrophilicity without placing a net charge on the electrode surface.

Although many antifouling strategies to reduce electrode fouling have involved increasing surface hydrophilicity, this is not a feasible strategy for all applications. As an example, a hydrophobic coating is needed to reduce friction in digital microfluidics, where droplets are manipulated electrodynamically between electrodes (Sarvothaman et al. 2014). Due to the hydrophobic coating of digital microfluidics, they are prone to fouling by hydrophobic species, such as unfolded proteins. Sarvothaman et al. (2014) improved the fouling resistance of a digital microfluidics coating through the use of a fluorinated poly(ethylene glycol) and perfluorinated methacrylate copolymer. The use of the new copolymer increased the lifetime of a device from 102 to 580 actuation steps compared to the standard amorphous fluorinated copolymer, Teflon-AF, used with serum and cellular materials (Sarvothaman et al. 2014). The addition of the fluorinated poly(ethylene glycol) was suggested to increase elasticity and lubricity, which improves the fouling resistance to components in serum and cellular samples. Similarly, a hydrophobic, highly plasticised poly(vinyl chloride) membrane was used to improve the selectivity and fouling resistance of glassy carbon electrodes for the analysis of the hydrophobic compound, propofol (Kivlehan et al. 2012). The poly(vinyl chloride)-modified electrode reduced the fouling of the electrode surface by the products of the oxidation of propofol, as no decrease in the current was observed after six repetitive cycles (Kivlehan et al. 2012). Furthermore, due to the large difference in hydrophobicity of the propofol analyte and common interfering species, only the analyte of interest could penetrate the poly(vinyl chloride) membrane to be detected at the electrode surface.

Many other polymeric films can be used to protect electrodes from fouling species. Trouillon et al. (2009) investigated the performance of many polymeric membrane coatings including Nafion, cellulose acetate, chitosan, fibronectin, and PSS/poly(L-lysine) for a gold electrode in resisting fouling by bovine serum albumin. Their ability to resist fouling was evaluated by performing cyclic voltammetry of $[Ru(NH_3)_6]^{2+/3+}$ and dissolved oxygen in the presence and absence of bovine serum albumin. Based on the peak potential, peak width, peak current, and capacitance, fibronectin coating was the only membrane that was not significantly different in the presence of bovine serum albumin from a pristine bare gold electrode (Trouillon et al. 2009). All other coated electrodes showed some significant difference from a pristine bare gold electrode in the presence of bovine serum albumin, suggesting that the other membrane coatings provided less fouling protection. However, all of the tested membrane coatings provided some protection from fouling by bovine serum albumin compared to a bare gold electrode. Singh et al. (2011) also investigated several different

polymeric films to prepare fouling-resistant dopamine selective sensors for detection in brain tissues. Nafion, base-hydrolysed cellulose acetate, and fibronectin-modified carbon fibre electrodes were prepared. The authors observed that approximately 70% to 80% of dopamine oxidation current was retained at all types of modified electrodes after a 2-h incubation in bovine serum albumin and brain tissue. Among the electrodes, base-hydrolysed cellulose acetate-modified electrodes were found to be most resistant to fouling. The cellulose film offers a steric barrier that prevents macromolecules from diffusing to the surface and its porosity can be progressively increased by controlled hydrolysis (Marinesco and Carew 2002).

Nonpolymeric films

Nonpolymeric thiol (mercapto) films or other sulfur-based films can be efficiently and strongly attached to gold electrodes through gold-sulfur bonds, such as the commonly used 6-mercaptohexanol, to reduce electrode fouling. However, Jolly et al. (2015) found that a 6-mercaptohexanol-modified electrode did not provide as much fouling protection as a novel sulfur-based film electrode. In this study, an aptamer-based biosensor was developed for the determination of prostate-specific antigen. On this sensor, a thiol-terminated sulfobetaine, the structure of which is shown in Figure 5, was used as an antifouling agent to reduce the fouling of the sensor by human serum albumin. After the incubation of the sensor in human serum albumin, there was a negligible change in the electron transfer resistance (R_{ct}; <1%) estimated using electrochemical impedance spectroscopy (Jolly et al. 2015). However, the use of 6-mercaptohexanol resulted in an increase of 12.5% in R_{ct} upon incubation in human serum albumin. With both the oligo(ethylene glycol) thiol-modified electrode (Zhang et al. 2009) and the sulfobetaine-modified electrode, the poorer fouling resistance of 6-mercaptohexanol may be due to its shorter chain length, which could result in a greater number of surface defects exposing the gold surface (Jolly et al. 2015). Similarly, Kuralay et al. (2011) and McQuistan et al. (2014) investigated the improvement in fouling resistance when 6-mercaptohexanol was combined with other sulfur-based materials. Kuralay et al. (2011) constructed a ternary monolayer on a screen-printed gold electrode. This ternary monolayer consisted of hexanedithiol, a specific thiolated capture probe, and 6-mercaptohexanol (HDT/SHCP/MCH electrode) and was used to detect nucleic acid hybridisation events. After 24-h incubation in serum and urine, the current was 80% to 85% of the initial value. There was a significant reduction in current and increase in noise when hexanedithiol was not used (SHCP/MCH electrode), as shown in Figure 6. The authors suggested that the use

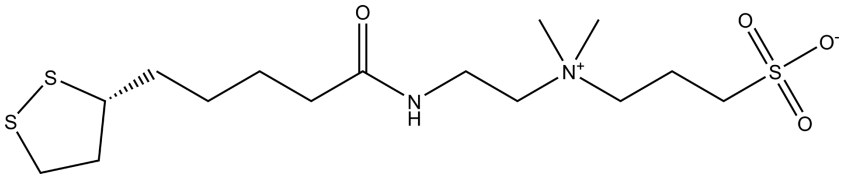

Figure 5: Chemical structure of the thiol-terminated sulfobetaine used by Jolly et al. (2015): (*R*)-3-((2-(5-(1,2-dithiolan-3-yl)pentanamido)-ethyl)dimethylammonio)propane-1-sulfonate).

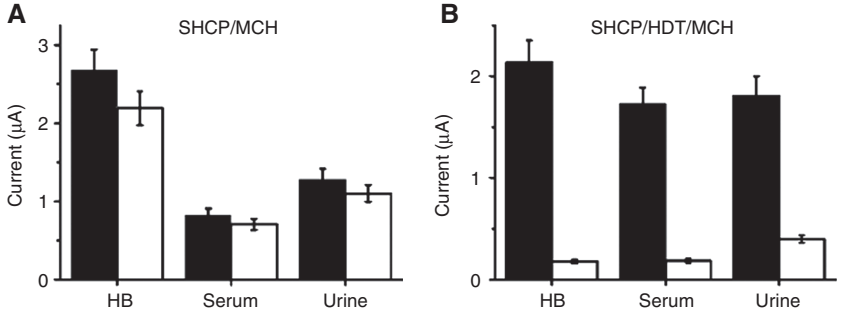

Figure 6: Antifouling properties of the SHCP/MCH electrode (A) and SHCP/HDT/MCH electrode (B) after 24 h in hybridisation buffer (HB), serum, and urine.
Black columns represent response from 1 nM of target DNA and white columns represent blank response (0 nM of target DNA). Reproduced with permission from Kuralay et al. (2011).

of hexanedithiol leads to more dense monolayers with fewer pinholes and surface defects. In addition to 6-mercaptohexanol, McQuistan et al. (2014) incorporated short thiolated oligonucleotides (containing varied numbers of thymines) as antifouling diluents in an electrochemical peptide-based sensor to minimise the nonspecific adsorption of nontarget immunoglobulin G. With the use of thiolated oligonucleotides, there was only a 5% signal suppression after being incubated in nontarget immunoglobulin G. Without the thymines (only 6-mercaptohexanol), there was significant fouling of the electrode, resulting in a 35% signal suppression. The negatively charged backbone of the oligonucleotides may help limit the electrode fouling as a result of unfavourable electrostatic interactions or increased hydrophilicity (McQuistan et al. 2014). Although these results demonstrate that 6-mercaptohexanol generally has poor antifouling properties, other sulfur-based films can be used alone or in combination with 6-mercaptohexanol to minimise electrode fouling. Instead of a thiol, Motaghedifard et al. (2012) employed a thiophene to immobilise a self-assembled monolayer of 2-hydroxy-*N*′1-[(*E*)-1-(3-methyl-2-thienyl)methylidene] benzohydrazide and used the electrode in the determination of epinephrine. The authors demonstrated excellent antifouling properties of the electrode after no change in the oxidation current of epinephrine was observed upon 20 repetitive scans.

Without the formation of gold-sulfur bonds, nonpolymeric films that do not contain thiols or similar sulfur-based functional groups must be attached to an electrode surface by other methods, such as diazonium chemistry. To protect a glassy carbon electrode from a large range of fouling agents, Chira et al. (2014) used diazonium chemistry to covalently attach 1-[(4-nitrophenyl)methyl]-4,4′-bipyridinium to the electrode surface, yielding a stable 1-phenylmethyl-4,4′-bipyridine film. Following the incubation of the modified glassy carbon electrode in solutions of bovine serum albumin, phenol, casein, riboflavin, pectin, sodium dodecyl sulfate, linoleic acid, and pepsin for 20 min, the change in R_{ct} before and after incubation was estimated to be <2.5 kΩ by electrochemical impedance spectroscopy (Chira et al. 2014). The change in R_{ct} was significantly greater at a bare glassy carbon electrode. The authors suggested that the antifouling properties of the modified glassy carbon electrode were due to the reduction of surface hydrophobicity, masking of functional groups on the electrode surface, and steric repulsion of fouling agents from the 1-phenylmethyl-4,4′-bipyridine. Similarly, Chandra et al. (2013) electrochemically deposited a *p*-phenylacetate film on conical-tip carbon electrodes using diazonium chemistry to enhance the antifouling properties of the electrodes. Their modified electrodes offered a degree of protection for carbon electrodes against fouling during dopamine detection. The modified electrode was demonstrated to retain 75% of the initial detection signal after being incubated for 7 days in a simulated fouling solution containing caproic acid (a lipid), bovine serum albumin (a protein), cytochrome *c* (a protein), and human fibrinopeptide B (a peptide) that partially mimics the environment of extracellular fluid. During their *in vivo* experiments involving Sprague-Dawley rats, 70% to 95% of the dopamine oxidation current remained after the first 40 min and 50% remained over the next 20 min, indicating that the electrodes may not be as fouling resistant as in the *in vitro* experiments. Therefore, the complex environment *in vivo* may need to be taken into consideration in the development of electrodes for *in vivo* detection.

A polymer layer that passivates an electrode surface will tend to increase the impedance. Therefore, the compromise between impedance and fouling resistance must be assessed in considering the use of such films. As an alternative, Gui et al. (2013) reported a low impedance phenyl phosphorylcholine-based zwitterionic layer immobilised on a glassy carbon electrode. Owing to the influence of the charge of proteins on fouling, the adsorption of anionic bovine serum albumin and cationic cytochrome *c* was monitored at this modified electrode by fluorescence microscopy. Although the phenyl phosphorylcholine-modified electrode demonstrated greater or similar resistance to fouling by the two proteins compared to oligo(ethylene glycol)-modified glassy carbon or gold electrodes, the impedance was much lower than that at the oligo(ethylene glycol)-modified electrodes (Gui et al. 2013). The results of this work suggest that complete charge balancing and packing of the charged groups of phophorylcholine zwitterions provided resistance to electrode fouling without creating high impedance.

Antifouling nonpolymeric films can also be attached to the surface by noncovalent interactions. Such an electrode utilising a film of electrogenerated oxidation products of NAD^+ has been shown to exhibit good antifouling properties against NAD^+ adsorption (Teymourian et al. 2012). The modified glassy carbon electrode was constructed by immobilising multiwalled carbon nanotubes dispersed in an ionic liquid on a glassy carbon electrode followed by electrooxidising NAD^+ on the electrode surface. The ionic liquid was included to bind the carbon nanotubes and oxidised NAD^+ to the electrode surface, whereas the carbon nanotubes acted as an electrical conductor between the electrode surface and the oxidised NAD^+, which served as a redox mediator (Teymourian et al. 2012). As illustrated in Figure 7, for the analysis of

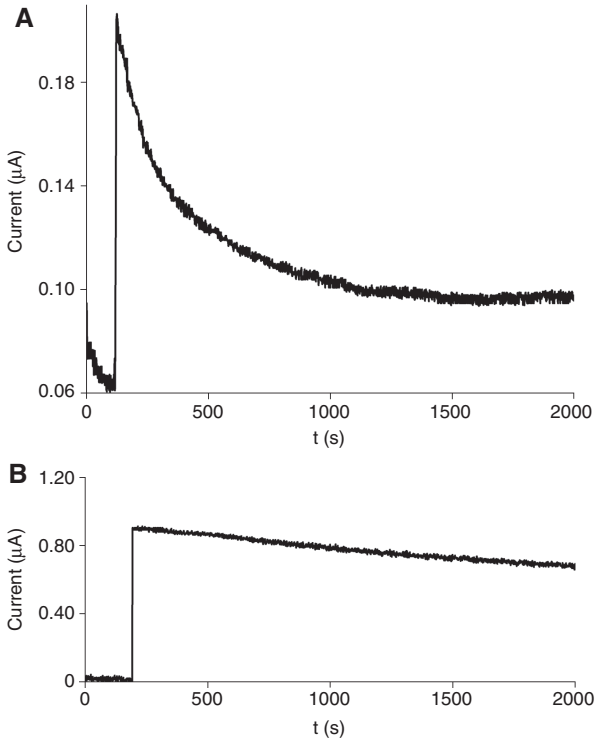

Figure 7: Amperometric response of a bare glassy carbon electrode (A) and the oxidised NAD^+/multiwalled carbon nanotube/ionic liquid-modified glassy carbon electrode (B) to a solution of NADH over 1800 s.
Reproduced with permission from Teymourian et al. (2012).

NADH, the current at the modified electrode decreased by 15% after 1800 s, whereas a corresponding current decrease of up to 70% was obtained at a bare glassy carbon electrode (Teymourian et al. 2012). The authors attributed the antifouling properties of this modified electrode to the improved electron transfer kinetics and more negative oxidation potential of the electrooxidised NAD^+ film, which reduced the formation of adsorbing radical intermediates.

Protein films and coatings

Many antifouling strategies seek to prevent a fouling agent, such as a protein, from reaching the electrode surface by establishing a barrier that is only permeable to the analyte. In some cases, the barrier that prevents fouling can actually be a protein attached to the electrode surface. The S-layer protein, SbpA, isolated from *Lysinibacillus sphaericus* CCM 2177, was used to provide an antifouling monolayer on a platinum electrode with pore sizes of 4 to 5 nm (Picher et al. 2013). After incubation in human serum albumin, human serum, and human blood, the corresponding mass density of adsorbed molecules was measured to be 0, 0.18, and 0.46 ng mm^{-2} on the electrode surface by surface plasmon resonance. The SbpA layer substantially reduced the electrode fouling compared to a bare gold electrode as well as poly(ethylene glycol) and bovine serum albumin coatings (Picher et al. 2013). In addition to the greater fouling resistance, pores in the SbpA layer allow small analytes to reach the electrode surface while excluding large fouling agents, unlike poly(ethylene glycol) and bovine serum albumin coatings. Protein films or coatings can also be immobilised on an electrode surface to impart targeted functionalities or properties. For example, Qiu et al. (2013) constructed a horseradish peroxidase-modified nanostructured gold thin-film electrode for the analysis of 4-chlorophenol. The presence of horseradish peroxidase significantly improved the fouling resistance with 81.5% of the initial current remaining after 30 cycles compared to a corresponding 9.9% at a bare gold thin film (Qiu et al. 2013). The presence of the horseradish peroxidase has likely increased fouling resistance because the phenol oxidation does not occur directly on the gold electrode surface and the enzyme provides a physical barrier against the adsorption of the phenol or reaction products on the surface.

Metallic nanoparticles and catalytic redox couples

The nanoscale size of metallic nanoparticles imparts useful electrocatalytic properties as well as a high electrical conductivity (Safavi and Momeni 2010, Muna et al. 2014). Nanoparticles have also been shown to exhibit antifouling properties and may be used alone or in combination with other materials. Indeed, Safavi and Momeni (2010) combined gold nanoparticles with a carbon ionic liquid electrode. This electrode was shown to be resistant to fouling by the products of tryptophan, as there was only a slow decrease in oxidation current over five cycles. This fouling resistance was somewhat greater than a bare ionic liquid carbon paste electrode and much greater than a bare glassy carbon electrode or conventional carbon paste electrode, both of which showed rapid electrode fouling (Safavi and Momeni 2010). The antifouling properties of the modified electrode could be attributed to the particular electrocatalytic properties of the gold nanoparticles, which mediated the electrochemical reactions. The polarity of the ionic liquid may have also contributed by increasing the surface hydrophilicity.

Similarly, Adams et al. (2010) combined a sol-gel network of (3-mercaptopropyl)trimethoxysilane (MPTS) with gold nanoparticles to measure dopamine secreted during single-cell exocytotic events in PC12 cells. In fabricating these electrodes, gold was electrochemically deposited on carbon fibre microdisc electrodes before the deposited gold was chemically functionalised by MPTS for 20 min. Subsequently, gold nanoparticles were immobilised on a thiol-terminated three-dimensional sol-gel network of MPTS. The fabricated electrode was stored for both short term (2–10 days) and long term (38–46 days) after the amperometric detection of dopamine in PC12 cells. At the end of both storage durations, the measured current remained fairly constant without any electrode pretreatment, indicating a low level of fouling during exposure to PC12 cells. The sol-gel network of MPTS on the electrode surface was proposed to have formed a barrier towards cellular debris adhesion and direct molecular adsorption on the electrode surface. The electrocatalytic and antifouling properties of the gold nanoparticles would also have contributed to the observed resistance to fouling. For the analysis of norepinephrine and dopamine, aminophenyl grafted gold nanoparticles on glassy carbon electrodes provided good protection from the polymeric fouling products of the neurotransmitters. Kesavan et al. (2012) immobilised β-D-glucose-capped gold nanoparticles on an aminophenyl grafted glassy carbon electrode and used the electrode to detect norepinephrine in the presence of uric acid. This modified electrode demonstrated antifouling properties against norepinephrine after 15 repetitive measurements at 5-min intervals. Similarly, Kesavan and John (2014) prepared a layer of aminophenyl grafted gold nanoparticles on a glassy carbon electrode without capping the nanoparticles with β-D-glucose. In addition to an enhancement of the oxidation of dopamine, the authors also found the electrode to be resistant to fouling caused by the oxidation products in 15 repeated scans, which suggests that capping the nanoparticles does not improve the fouling resistance of the electrode. Alternatively, Guo et al. (2014) constructed a palladium-nickel bimetallic alloy nanoparticle-modified carbon nanofibre electrode, in place of monometallic nanoparticles, to exploit the generally higher electrocatalytic activity, selectivity, and stability of bimetallic alloy nanoparticles (Guo et al. 2014). This electrode was constructed by electrospinning a solution of polyacrylonitrile, palladium(II) acetylacetonate, and nickel(II) acetylacetonate followed by the reduction of the metals and carbonisation of the polyacrylonitrile fibres by a controlled thermal process. Coupled with flow injection analysis, the electrode showed a minimal decrease in current after 60 injections of glucose (RSD 1.45%). For a bare nickel electrode, the current decreased by 38% after 60 injections (RSD 10.3%; Guo et al. 2014). These results demonstrate that the electrode exhibits a good resistance to fouling by the products of glucose oxidation and this could be attributed to improved electrocatalytic and antifouling properties from the synergistic effect of nanoscale palladium and nickel. Maiyalagan et al. (2013) also prepared an electrode by electrospinning and carbonisation, which appeared to induce the formation of small crystalline α-Fe_2O_3 nanoparticles on the surface of carbon nanofibres. This α-Fe_2O_3 nanofibre-modified glassy carbon electrode showed good resistance to fouling by the products of folic acid during its analysis. After 20 cycles in a solution of folic acid, there was a negligible change in current (RSD 2.1%) at the modified electrode. On the contrary, at a bare glassy carbon electrode and bulk Fe_2O_3 electrode, the oxidation peak of folic acid continuously decreased after each cycle (Maiyalagan et al. 2013). This difference in fouling resistance is likely due to the presence of nanoparticles with the particular crystal structure of α-Fe_2O_3, which catalyses the efficient oxidation of folic acid, minimising the adsorption of fouling species.

Similar to nanoparticles, metallic redox couples can exhibit important electrocatalytic properties and resistance to electrode fouling. Both Muna et al. (2014) and Safavi et al. (2009) investigated the electrocatalytic and antifouling properties of the $Ni(OH)_2$/NiOOH redox system. Coupled with flow injection analysis, Muna et al. (2014) detected estrone (a phenolic steroid) at a nickel nanoparticle-modified glassy carbon electrode and observed a negligible change in the current after 20 consecutive injections of estrone (RSD 0.5%). The authors attributed the fouling resistance to the catalytic $Ni(OH)_2$/NiOOH redox system, which forms on the electrode surface after cycling in alkaline electrolyte. Safavi et al. (2009) combined the catalytic $Ni(OH)_2$/NiOOH redox couple with graphite and an ionic liquid to produce an antifouling electrode for the detection of glucose (Safavi et al. 2009). The $Ni(OH)_2$ nanoscale carbon ionic liquid composite electrode exhibited good antifouling properties with six repetitive amperometric measurements having an RSD of 3.4%. The current and peak potential of repetitive cyclic voltammetric scans did not change, which also showed that the electrode did not foul (Safavi et al. 2009). Similar to Muna et al. (2014), the observed antifouling properties of this composite electrode are likely due to the nickel redox couple, but the presence of the ionic liquid could also have contributed to the fouling resistance by increasing the hydrophilicity of the electrode.

Nanoporous electrodes

Nanoporous electrodes have numerous nanoscale pores through the electrode structure that are separate from the bulk solution, but diffusion from the bulk solution into the pores is possible for species of a defined size. Nanoporous electrodes have been demonstrated to show a higher fouling resistance than planar electrodes; however, the observed antifouling properties strongly depend on the size of the pores. To investigate the relationship between pore size and electrode fouling, Patel et al. (2013b) investigated the performance of planar, macroporous (1200 nm pore size), hierarchical (1200 and 60 nm pore size), and nanoporous (<50 nm pore size) gold electrodes in the presence of bovine serum albumin and fibrinogen. As expected, the antifouling performance of these electrodes was found to be highly dependent on the pore size, with the nanoporous electrode having the greatest fouling resistance (Patel et al. 2013b). Figure 8 shows cyclic voltammograms obtained over the course of 60 min in the presence of bovine serum albumin. Clearly, the nanoporous electrode offers the greatest protection, with only a small decrease in current and a small increase in peak separation. The antifouling properties of nanoporous electrodes appear to be due to their high surface area and nanoporosity. While fouling agents in the bulk solution can readily adsorb on the gold surface in contact with the bulk solution, fouling of the inner surfaces would be slower due to restricted mass transport of larger species through small pores in the nanoporous electrode. With the other porous electrodes, there were sufficiently large pores for bovine serum albumin to reach the inner electrode surface, indicating that a pore size of <50 nm is required for fouling resistance to bovine serum albumin and similar-sized proteins. Fouling by smaller proteins and protein fragments can also be greatly minimised with the use of nanoporous electrodes, as illustrated by Summerlot et al. (2011) using fragmented amyloid-β protein. After a 30-min incubation in a protein solution, the current at a nanoporous gold electrode decreased by only 13%, whereas the current at a planar bare gold electrode decreased by 96.5% (Summerlot et al. 2011). Although the experiment was conducted for 30 min, the electrodes reached the above values within ~10 and 2 min for the nanoporous and planar electrodes, respectively. Despite the fragmented amyloid-β proteins being smaller than most proteins (e.g. albumin), the pores are still sufficiently small to restrict the fragmented proteins without affecting analyte detection. Similarly, Quynh et al. (2014) showed that a nanoporous gold electrode could resist fouling by the polymeric oxidation products of aniline and hydroxylamine. This electrode was prepared by dealloying silicon from an Au_xSi_{1-x} film. After five repetitive measurements, a maximum of 10% deviation in current was observed. In contrast, a bare planar gold electrode was fouled even after only one measurement. Due to the nanoporosity of the electrode, the analysis of small analytes can continue even if the very outer surface is fouled. In this case, as the analytes aniline and hydroxylamine can reach the inner surfaces of the

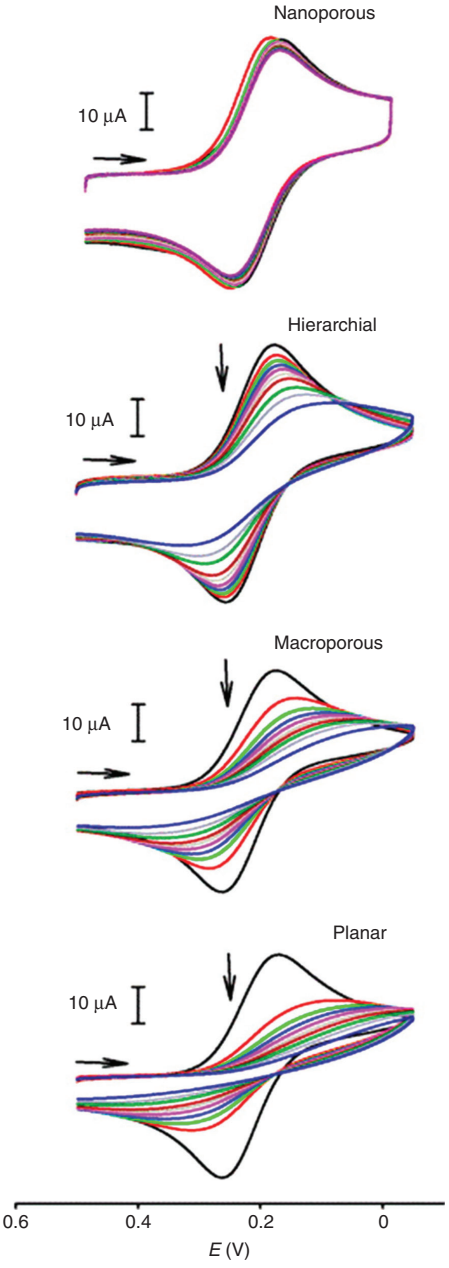

Figure 8: Cyclic voltammograms at nanoporous, hierarchical, macroporous, and planar gold electrodes in a solution of ferricyanide and bovine serum albumin.
Cyclic voltammograms were obtained between ~1 and 60 min. Reproduced with permission from Patel et al. (2013b).

nanoporous electrode, the polymeric oxidation products may even be deposited within the pores. Although five satisfactory repetitive measurements could be obtained, the nanoporous electrode may have become fouled with additional use if the oxidation products could not diffuse out of the nanoporous structure before polymerisation.

In addition to these bare nanoporous gold electrodes, a nanoporous gold electrode can be coated to change the particular properties of the electrode. Tavakkoli and Nasrollahi (2013) combined the catalytic properties of palladium with the fouling resistance of a nanoporous gold electrode for the analysis of glucose. After 15 repetitive cycles with the palladium-coated nanoporous gold electrode, there was a negligible change in current. To demonstrate the fouling resistance of the electrode to glucose products, a bulk palladium electrode was also tested and was found to be rapidly fouled (Tavakkoli and Nasrollahi 2013).

Other effective electrode modifications

Coatings, films, or membranes can be used on an electrode to separate the susceptible electrode surface from fouling agents in the bulk solution. More simply, the distance between the electrode surface and the bulk solution can be increased with the use of a recessed electrode. Anastasova et al. (2012) combined recessed electrodes with polyurethane membranes to minimise electrode fouling by bovine serum albumin. These recessed electrodes were prepared by etching gold inside a fused silica capillary to the required depth and finally coating with polyurethane. Anastasova et al. (2012) observed that greater fouling resistance could be gained by increasing the recess depth of an electrode. After incubation with bovine serum albumin for 17 h, the reduction in oxygen response was 6±0.4% at an 880 μm recess electrode, and the reduction in glucose response was 11±0.5% at a 546 μm recess electrode both with polyurethane membranes. The benefit of using a recessed electrode was illustrated by comparing to planar electrodes. The authors observed a 45±2.7% reduction in oxygen response at a bare planar electrode and 13±1.4% at a membrane planar electrode as well as a 48±2.3% reduction in glucose response at a bare planar electrode and 17±1.2% at a membrane planar electrode. These results demonstrate that the polyurethane membrane alone has reasonable antifouling properties but, in combination with the recessed electrode, fouling by bovine serum albumin is further reduced. Although the fouling resistance of recessed electrodes is likely a result of the greater separation between the electrode surface and the bovine serum albumin in the bulk solution, the delay in signal response increases with greater recess depth.

Electrodes can be made more hydrophobic without using carbon-based materials, such as diamond and electron cyclotron resonance-sputtered nanocarbon. The hydrophobicity of the carbon paste electrode prepared by Safavi et al. (2010) was increased using the chromatography stationary phase, SE-30, as the carbon paste binder instead of an organic oil or liquid. The antifouling properties of this carbon paste electrode were investigated by amperometry in a solution of NADH. After 10 min, a 15% decrease in the oxidation current was observed at the carbon paste electrode, whereas a conventional carbon paste electrode produced a corresponding current reduction of up to 80% (Safavi et al. 2010). The fouling resistance of the modified carbon paste electrode could be a result of the low surface energy and hydrophobicity of the SE-30 binder, which reduced the adsorption of NAD^+. Zhuiykov and Kalantar-zadeh (2012) prepared an even more hydrophobic surface with a superhydrophobic 20 mol% Cu_2O-doped RuO_2 electrode ($Cu_{0.4}Ru_{3.4}O_7$+RuO_2), which was shown to exhibit high fouling resistance against biological materials. Following a 3-month field trial in a sewerage environment, the extent of electrode fouling was examined by scanning electron microscopy and potentiometry. The scanning electron micrographs showed that there was negligible fouling by biological material, and potentiometry determined that the sensitivity to oxygen detection only decreased from -46 to -43 mV $decade^{-1}$ (Zhuiykov and Kalantar-zadeh 2012). Although a hydrophobic electrode surface can be considered prone to fouling, this superhydrophobic electrode demonstrated good resistance to fouling. Similar to the electron cyclotron resonance-sputtered nanocarbon film used by Xue et al. (2012), surface roughness or smoothness was considered to contribute to the observed antifouling properties of the superhydrophobic electrode.

Analogous to nanoporous electrodes, Mudrinić et al. (2014) developed a micropore electrode with antifouling properties by polymeric phenol products. They used bentonite clay as part of an electrode coating with carbon black and Nafion on a glassy carbon electrode. The bentonite clay was modified by pillaring, which allowed particular metal cations to be incorporated into the clay. The electrode constructed with a pillaring solution containing 90 mol% Al^{3+}, 5 mol% Fe^{3+}, and 5 mol% Ni^{2+} was shown to exhibit the highest fouling resistance. The Fe-to-Ni proportion was also shown to have an important effect on the fouling resistance. The current density at this electrode decreased by 5.4% after the first 10 cycles and 17.8% after 20 cycles (Mudrinić et al. 2014). The authors suggested

that the antifouling properties may be due to a specific Al-Fe-Ni pillar structure that does not favour the formation of polymeric structures. Similarly, Hasanzadeh et al. (2013) applied silica-based mesoporous materials to the simultaneous determination of dopamine and serotonin. In their work, porous mobile crystalline material-41 functionalised by amine was immobilised on a glassy carbon electrode. A 1.2- and 3-fold enhancement in the electron transfer kinetics of dopamine and serotonin, respectively, was achieved at the modified electrode. Moreover, seven successive differential pulse voltammetric scans of 10 nM dopamine and 2 nM serotonin showed similar oxidation peak currents (RSD 3.2% and 2.0%, respectively). The fabricated electrodes also demonstrated antifouling properties during the analysis of dopamine and serotonin spiked in human serum, and the recovery of both analytes was 94% to 100% (Hasanzadeh et al. 2013). The micropores and mesopores present in the modified electrodes may have acted similarly to other porous electrodes and excluded potential fouling agents from the inner pore structures.

In an effort to reduce electrode fouling by NAD^+, Chumbimuni-Torres and Wang (2009) used a copper-ion selective electrode with potentiometric detection. The concentration of NADH was measured by monitoring the NADH-mediated reduction of copper ions in the presence of gold nanoparticle seeds. The amperommogram obtained at a bare glassy carbon electrode, depicted in Figure 9A, shows that the current decreased by 75% over the course of a continuous 50-min experiment as a result of fouling by NAD^+. On the contrary, the corresponding potentiometric response obtained at the copper-ion selective electrode, depicted in Figure 9B, shows a negligible change in the measured potential (Chumbimuni-Torres and Wang 2009). Although the greater fouling resistance of the copper-ion selective electrode may be due to the copper-ion selective membrane preventing the adsorption of NAD^+ on the underlying electrode surface, a combination of the membrane, gold nanoparticles, and reduction of copper ions might be required to yield the observed resistance to electrode fouling.

Electrochemical activation

Electrochemical activation involves the use of single anodic and/or cathodic potentials or a train of pulses to periodically clean the electrode surface. Depending on the particular conditions of the electrochemical activation, adsorbed material may be removed or the surface chemistry can be altered to reduce the adsorption of fouling agents. For example, Dejmkova et al. (2009) employed electrochemical activation to remove adsorbed material during the analysis of the phenolic flavanol, quercetin, at a boron-doped diamond electrode. The application of anodic and cathodic activation pulses (up to ±3 V) before each cyclic voltammetric scan achieved an RSD of <2% after 10 repetitive cycles of quercetin. An identically treated glassy carbon electrode suffered from continuous signal drift due to electrode fouling. Similarly, Kiran et al. (2013) found that anodic and cathodic activation pulses could be applied to remove fouling resulting from contact with urine. After placing a boron-doped diamond electrode in human urine, the electron transfer rate constant (k_0) for ferricyanide/ferrocyanide was reduced to <0.001 cm s^{-1}, indicating significant fouling of the electrode surface by components in urine (Kiran et al. 2013). By applying a set of 150 current pulses of alternating amplitude, k_0 was restored to >0.2 cm s^{-1}, which is a similar value to that of the pristine electrode (0.27 cm s^{-1}; Kiran et al. 2013). Anodic and cathodic activation pulses

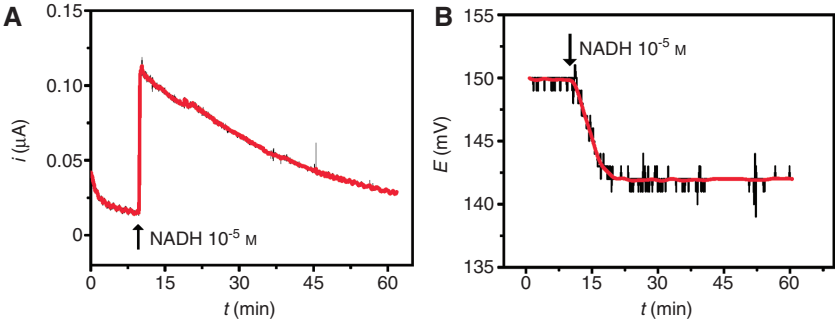

Figure 9: Amperometric response of a bare glassy carbon electrode (A) and potentiometric response of the copper-ion selective electrode (B) to a solution of NADH over 60 min.
Reproduced with permission from Chumbimuni-Torres and Wang (2009).

have also been used to remove serotonin and biological fouling agents from a boron-doped diamond electrode. Duran et al. (2014) anodically treated the electrode at 250 mA cm^{-2} for 30 s and then cathodically treated at 250 mA cm^{-2} for 180 s to activate fouled electrodes. This electrochemical activation was also capable of reactivating fouled electrodes *in situ*. To investigate this, a pristine and a fouled (after incubating in 100 μM serotonin) electrode were positioned in the extracellular space of the enterochromaffin cells in mouse ileum to detect the stimulated release of serotonin. The fouled electrode yielded a chronoamperometric signal half the magnitude of that obtained at the pristine electrode. Only by cathodically treating the fouled electrode were the authors able to achieve a signal of comparable magnitude to that at the pristine electrode. The large positive and negative potentials used in electrochemical activation can generate reactive oxygen species, such as hydroxyl radicals, as well as oxygen or hydrogen gas (Stoytcheva et al. 2014). The evolution of gas and reactive oxygen species helps to physically dislodge and oxidise adsorbed organic material, respectively.

By incorporating electrochemical activation as part of the analysis procedure, the effects of fouling can be sufficiently minimised to achieve reliable measurements. For example, by exploiting pulsed amperometry and differential pulse voltammetry, electrochemical activation can be performed at regular intervals to minimise the accumulation of a fouling layer on the electrode. This was demonstrated by Stoytcheva et al. (2014), where an anodic activation potential of +1.40 V was applied as part of a pulsed amperometric analysis of catechol at a graphite electrode. Based on five measurements of catechol, they estimated an RSD of 2.97% compared to 6.53% without the activation potential (Stoytcheva et al. 2014). da Silva et al. (2013) similarly examined the effect of an electrochemical activation potential in reducing electrode fouling during differential pulse voltammetry and multiple pulse amperometry analysis of the pharmaceutical drug, nimesulide. There was a negligible change in current after three scans by applying electrochemical activation before each scan (RSD 1.52%), but the corresponding current decreased by 16.6% without electrochemical activation (da Silva et al. 2013). Also, with multiple pulse amperometry and flow injection analysis, there was a negligible change in current after 14 injections (RSD 1.02%). However, a corresponding 15% current decrease was estimated when single potential amperometry was conducted (da Silva et al. 2013). To reduce analysis time with multiple pulse amperometry, a new two-step potential waveform (activation potential -2.0 V and detection potential +0.2 V) was employed in conjunction with flow injection analysis in the detection of carbohydrates at a gold electrode and compared to the conventional four-step potential waveform (activation potential -2.0 V, gold oxidation and reduction potentials +0.6 and -0.1 V, and detection potential +0.2 V; Kotnik et al. 2011). After 60 injections of glucose, there was a negligible change in current for both the two-step (RSD 0.16%) and four-step (RSD 0.18%) pulsed amperometric detection, demonstrating that a short cathodic pulse in the two-step detection was sufficient to activate the electrode (Kotnik et al. 2011). A careful selection of the fast scan voltammetry parameters has avoided electrode fouling during the measurement of serotonin. Agnesi et al. (2009) found that the use of a wireless instantaneous neurotransmitter concentration system comprising fast scan cyclic voltammetry from a resting potential of +0.2 to +1.0 V and then to -0.1 V and back to +0.2 V at a rate of 1000 V s^{-1} yielded a constant oxidation current amplitude after 10 sequential injections of serotonin. Subsequently, serotonin was measured using the same waveform after electrically stimulating the dorsal raphe nucleus of rat brain slices and the results indicated that high electrode sensitivity was retained throughout the measurement. Similarly, Schmidt et al. (2014) developed a modified sawhorse waveform with two different anodic scan rates and a short holding period at the switching potential to minimise fouling. The authors detected the small peptide, methionine-enkephalin, in the presence of interfering species without electrode fouling caused by the products of the peptide oxidation. Coupled with flow injection analysis, a negligible change in current was observed after 10 injections compared to a corresponding ~10% current decrease when a more conventional triangular waveform was used (Schmidt et al. 2014). As part of the modified waveform, +1.2 V was applied for only 3 ms, which must have been sufficiently anodic to remove any adsorbed material.

By applying a high anodic or cathodic potential, the surface chemistry of an electrode can be altered because of the different number of oxygen functionalities, which affects hydrophilicity. Roeser et al. (2013) and Brocenschi et al. (2014) both cathodically pretreated boron-doped diamond electrodes to modify the surface chemistry and minimise electrode fouling. During the electrochemical oxidation and cleavage of the tripeptide leucine-phenylalanine-leucine, a significant adsorption of the products of the tripeptide, including dimers, was found on a glassy carbon electrode (Roeser et al. 2013). In contrast, a boron-doped diamond electrode exhibited a more satisfactory performance, albeit the oxidation yields decreased to 20% to 30% after several days of use from an initial yield of 60% to 70%. Fouling resistance of the boron-doped

diamond electrode was found to be further increased by the cathodic pretreatment of the electrode. Subsequently, there was no significant change in oxidation yield or performance after 24-h operation (Roeser et al. 2013). Similarly, Brocenschi et al. (2014) estimated RSDs of 9.6% for estrone, 11.4% for 17-β-estradiol, and 10.8% for estriol at a cathodically pretreated boron-doped diamond electrode upon 20 injections. Despite the high RSDs, the authors emphasised that these should be considered as the worst-case values, as an RSD of 2.3% was measured for estrone from 10 injections. In such work, the cathodic treatment of boron-doped diamond electrodes increases the H-termination and hydrophobicity, which would reduce the adsorption of small polar peptides and the oxidised steroid products, provided that they were sufficiently polar.

In addition to altering the surface chemistry, the application of high anodic or cathodic potentials can aid in exposing a pristine surface. Takmakov et al. (2010) electrochemically etched carbon fibre microelectrodes using cyclic voltammetry between -0.4 and 1.3 V at 400 V s^{-1} for 15 min to constantly regenerate a fresh carbon surface. The sensitivity could be restored even after an intensive fouling of electrode surfaces with dopamine. The authors used electrochemical etching to exfoliate graphite oxide and carbon particle to generate new active sites for use in subsequent experiments. This method of reactivating electrodes will keep the electrodes active *in vivo* in a prolonged experiment, as the electrodes can be regenerated by a simple electrochemical procedure *in situ*.

Although Hu et al. (2011) did not use electrochemical activation to clean an electrode surface, they instead used an analogous process to treat already fouled carbon-doped TiO_2 nanotube arrays. This process involved irradiating the electrode surface with ultraviolet and visible radiation, which is similar to electrochemical activation in that a clean electrode surface is generated by removing adsorbed fouling species. These electrodes were prepared by rapid annealing in argon as-anodised TiO_2-nanotube arrays that were deliberately fouled after obtaining featureless voltammograms at the end of 20 cyclic voltammetric scans of serotonin. The authors were able to reactivate the electrodes and achieve the original detection using ultraviolet and visible irradiation for 30 and 120 min, respectively, in doubly distilled water at room temperature. This work has demonstrated the application of ultraviolet or visible radiation to decompose the intermediate products of serotonin adsorbed on an electrode surface into H_2O, CO_2, and NO_x without damaging the surface microstructure and is analogous to applying high anodic or cathodic potentials to chemically degrade material adsorbed on the electrode surface.

Electrolyte and flow systems

The composition of the electrolyte can be modified to remove adsorbed fouling agents during electrochemical analysis. Both Anandhakumar et al. (2010) and Narmadha et al. (2011) investigated different electrolyte compositions to solubilise polymeric products from the electrochemical analysis of phenols, reducing adsorption on the electrode surface. Anandhakumar et al. (2010) compared aqueous sodium hydroxide, aqueous sodium hydroxide-sodium dodecyl sulfate micellar solution, and sodium dodecyl sulfate/hexane/butanol/water microemulsion in the analysis of several chlorophenols at a glassy carbon electrode. The authors found that, with aqueous sodium hydroxide, fouling was apparent at a 2,4-dichlorophenol concentration lower than 2 mM. On the contrary, no fouling was observed up to 10 and 20 mM 2,4-dichlorophenol with the micellar solution and microemulsion, respectively. The micellar solution and microemulsion were expected to solubilise the phenols and intermediates, as well as the surfactant forming adsorbed layers on the electrode, which reduces the extent of electrode fouling. Similarly, Narmadha et al. (2011) investigated the fouling resistance of acidic methanol, acidic aqueous, neutral microemulsion, and acidic microemulsion electrolytes for the oxidation of phenols at glassy carbon and boron-doped diamond electrodes. Narmadha et al. (2011) found that the acidic methanol electrolyte provided the greatest fouling resistance. For the acidic methanol electrolyte, the ratio of anodic peak current after four cycles compared to the first cycle (I^4_{pa}/I^1_{pa}) is shown in Table 1. These results show

Table 1: I^4_{pa}/I^1_{pa} values for selected phenols at a glassy carbon electrode and a boron-doped diamond electrode with an acidic methanol electrolyte (Narmadha et al. 2011).

	Electrode	2,6-Dichlorophenol	2,6-Dimethylphenol	2,6-Dimethoxyphenol
I^4_{pa}/I^1_{pa}	Glassy carbon electrode	0.94	0.99	0.98
	Boron-doped diamond electrode	0.93	0.82	0.99

that, under the experimental conditions, glassy carbon electrodes exhibited ~20% greater fouling resistance against 2,6-dimethylphenol than boron-doped diamond electrodes, although boron-doped diamond electrodes are often regarded as having greater fouling resistance compared to glassy carbon electrodes (Shin et al. 2005, Narmadha et al. 2011). In light of these results, Narmadha et al. (2011) recommended the use of a glassy carbon electrode instead of a boron-doped diamond electrode because the glassy carbon electrode can be easily cleaned by mechanical polishing. The more satisfactory performance of the acidic methanol electrolyte is most likely due to the greater solubility of the phenols and their products in the organic solvent.

In addition to aqueous/nonaqueous solvents and surfactants, the effect of supporting electrolyte salts in minimising electrode fouling has also been studied. Two electrolyte salts were investigated for use in the complete mineralisation of trichloroethene at a Ti/IrO_2-Ta_2O_5 electrode (Lakshmipathiraj et al. 2012). Using Na_2SO_4, the current changed between the first two cycles, but there was only a minimal change in current in the subsequent four cycles. On the contrary, using $NaNO_3$, the current decreased after every cycle. The higher fouling resistance associated with Na_2SO_4 was attributed to the *in situ* generation of sulfur-based oxidants, such as $S_2O_8^{2-}$ and SO_4^{2-}, which would remove material adsorbed on the surface of the electrode (Lakshmipathiraj et al. 2012). Such oxidant generation was not believed to occur when $NaNO_3$ was used (Lakshmipathiraj et al. 2012).

The contact between a susceptible electrode and fouling agents can be minimised or even eliminated in some cases through the use of a flow system. To reduce the adsorption of enzymes to electrode surfaces, Godino et al. (2010) developed a novel zero dead volume rotary switch valve that allowed for the enzyme β-galactosidase and the electrode to be separated at all stages of the assay. This involved immobilising the enzyme on streptavidin-coated magnetic particles and removing nonspecifically bound enzyme before introducing the substrate. When the electrode was directly incubated with the enzyme solution for 10 min, the background current increased from 3.5 to 8 nA. As the enzyme and the electrode never come into contact, there is no possibility for fouling of the electrodes by the enzyme, which is the most ideal solution to electrode fouling. However, it is not possible to completely separate the electrode from fouling agents in most situations. Instead of preventing the electrode from coming in contact with fouling agents, Casella and Contursi (2012), Tormin et al. (2014), and Sansuk et al. (2012) used flow systems to minimise the adsorption of fouling agents. Casella and Contursi (2012) used a cobalt oxide/oxyhydroxide redox couple (CoO_2/CoOOH)-modified glassy carbon electrode to resist fouling during the electrooxidation of hydrazines. Under stirring chronoamperometric conditions, the current at the modified electrode decreased very rapidly after the addition of phenylhydrazine owing to rapid fouling by the analyte (Casella and Contursi 2012). However, using the same modified electrode with flow injection analysis, a negligible change in oxidation current of both phenylhydrazine and hydrazine was achieved over multiple injections. While a similar redox couple to the previously reported $Ni(OH)_2$/NiOOH was used (Safavi et al. 2009, Muna et al. 2014), the observed resistance to fouling involving CoO_2/CoOOH was likely due to more efficient desorption of analytes and products from the electrode surface under flowing conditions as well as to the continuous electrodeposition of new cobalt oxide/oxyhydroxide species to replace lost or poisoned species (Casella and Contursi 2012). Continuous electrodeposition was possible because the detection and deposition potentials were similar and cobalt-gluconate complex was present in solution. Similar to flow injection analysis, batch injection analysis is a simpler version without the tubes, pumps, and injection valves. A batch injection analysis system combined with carbon screen-printed electrodes modified with graphene has been used for the detection of diclofenac (Tormin et al. 2014). There was a minimal decrease in the oxidation current after 10 runs (RSD 1.3%), as shown in Figure 10. Under steady-state conditions with square wave voltammetry, however, Figure 10 illustrates that the current decreased rapidly over the first six runs and was highly variable in subsequent runs (RSD 6.2%). In their work, the authors exploited the injection of

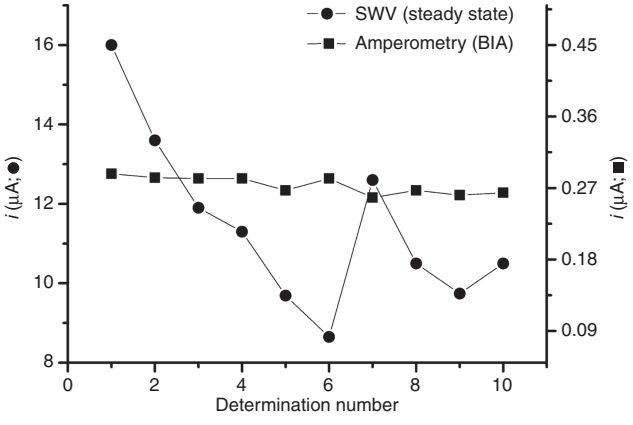

Figure 10: Current data over 10 runs of a solution of diclofenac using square wave voltammetry (steady-state conditions; •) and batch injection analysis with amperometry (■).
Reproduced with permission from Tormin et al. (2014).

a minimum solution volume under a high dispensing rate with constant stirring to reduce fouling by the products of diclofenac (Tormin et al. 2014). Sansuk et al. (2012) also used a small sample volume and high flow rate to minimise fouling. They employed single-walled carbon nanotubes as an amperometric detector in a microfluidic cell for dopamine. In this work, these electrodes showed no fouling over the concentration range of 5 to 1000 nM for a period of 20 days. The absence of fouling was attributed to the relatively fast continuous flow of electrolyte (1 ml min^{-1}) that sweeps possible fouling products away from the electrode surface and also the small volume of analyte in contact with electrode. Notably, the electrode was only in contact with a very small volume of dopamine (50 µl) for a short period of time. Polymer growth from dopamine is a slow step process that may take longer than the residence time of the analyte around the fabricated fluidic cell (Harreither et al. 2013).

Conclusion

Electrode fouling can often complicate the electrochemical analysis of many analytes, particularly those of biological and medical interest. Fouling agents, such as proteins, phenols, and neurotransmitters, can adsorb on the surface of unprotected electrodes, giving rise to deteriorating transient detection signals and thus strongly affect the performance of the electrochemical technique or sensor.

Many antifouling strategies have been discussed in this review. However, more research into antifouling strategies is needed to minimise the impact of electrode fouling in practical applications. Due to the diversity of analytes that foul electrodes and the abundance of other fouling agents in some samples, care should be taken when interpreting results where a decrease in signal is observed with repeated analysis as electrode fouling may be a cause. Therefore, antifouling strategies should be tested against a variety of fouling agents and fouling matrices, particularly biological samples and matrices, which can be a complex and often unknown mixture of proteins, peptides, lipids, and carbohydrates. However, when testing the fouling resistance of a particular strategy, sometimes only one analyte, such as phenol, or one protein, such as bovine serum albumin, is investigated. Although these may be representative fouling agents, it does not indicate how the antifouling strategy will perform in more complex environments. Where possible, antifouling strategies should be tested against the widest variety of fouling agents and complex matrices appropriate to the intended application, for example, different chlorophenol isomers and blood, serum, or urine. Similarly, the relationship between fouling agent concentration and extent of fouling should not be overlooked, as fouling can occur with some antifouling strategies above a certain concentration.

The majority of antifouling strategies involve modifying the electrode with a coating or film to increase fouling resistance. Carbon-based materials, such as carbon nanotubes and graphene, are commonly used due to their large surface area, electrical conductivity, and electrocatalytic properties (Shan et al. 2009, Zhou et al. 2009, Gasnier et al. 2012, Teymourian et al. 2012). Although research into the antifouling properties of such materials should be continued, new carbon-based materials must also be investigated, as they may be resistant to fouling. For example, electron cyclotron resonance-sputtered nanocarbon (Kato et al. 2011, Xue et al. 2012) and carbon double-shelled hollow spheres (Gao et al. 2011) have been shown to have good antifouling properties. Boron-doped diamond electrodes are often touted as having high fouling resistance, but this has been shown to depend on the analyte, system conditions, and the surface of the electrode. The surface chemistry of boron-doped diamond electrodes can be altered to produce either H- or O-termination. There is some disagreement as to which type of termination has superior resistance to fouling, with some studies indicating O-termination (Güell et al. 2010, Shpilevaya and Foord 2014) and another suggesting H-termination (Brocenschi et al. 2014). Although H- or O-termination can have a significant impact on the fouling resistance of boron-doped diamond electrodes, few studies have investigated the use of oxidised carbon nanotubes or other oxidised carbon-based materials. Oxidation increases the number of oxygen functionalities on the electrode surface and thus hydrophilicity. It is debatable whether surface hydrophilicity or hydrophobicity increase fouling resistance, as it tends to depend on the analyte and fouling agents. Surface roughness has also been identified as a possible cause of electrode fouling (Zhuiykov and Kalantar-zadeh 2012, Xue et al. 2012, Shpilevaya and Foord 2014).

In addition to carbon-based materials, electrodes can also be modified with polymeric, nonpolymeric, and protein films that are not carbon allotropes to provide a physical barrier between fouling agents and the electrode surface. Such films, including Nafion (Razmi and Heidari 2009, Trouillon et al. 2009, Singh et al. 2011), thiols (Kuralay et al. 2011, McQuistan et al. 2014), and proteins (Picher et al. 2013, Qiu et al. 2013), also give rise to an increased background electrode capacitance and impedance, which is not favourable for the detection of

trace analyte concentrations. Moreover, some self-assembled monolayers, including poly(ethylene glycol), can be self-oxidised and the oxidation products can be toxic for tissues upon implantation (Li et al. 2014). Therefore, alternatives to self-oxidising films and high capacitance/impedance films should be developed, such as the low impedance phenyl phosphorylcholine-modified electrode used by Gui et al. (2013). Although many of the polymeric film-modified electrodes discussed in this review were a single type of polymer with no additives, some studies that incorporated the PSS surfactant into the polymer showed good antifouling properties (Trouillon et al. 2009, Pirvu and Manole 2013, Sasso et al. 2013, Yang et al. 2013). Although the use of PSS is not necessary to provide protection from fouling, the incorporation of PSS or similar surfactants or compounds may improve the surface hydrophilicity and fouling resistance of a polymeric film.

Electrodes can also be modified with metallic nanoparticles or catalytic redox couples to improve the electrochemical response and fouling resistance. Several different types of nanoparticle were discussed in this review, including gold, nickel, palladium-nickel, and α-Fe_2O_3. To continue improving the antifouling properties of nanoparticles, new types of nanoparticles should be developed as well as improved attachment and functionalisation of the nanoparticles. Although two catalytic redox couples were specifically discussed, only the $Ni(OH)_2$/NiOOH redox couple was shown to impart antifouling properties (Safavi et al. 2009, Muna et al. 2014). Other metallic redox couples should be investigated for similar antifouling properties to $Ni(OH)_2$/NiOOH.

Nanoporous electrodes are resistant to fouling without the use of an electrode coating or film. The presence of nanoscale pores in the electrode structure prevents large fouling agents from reaching the inner surface of the electrode. Patel et al. (2013b) showed that only the presence of nanopores can effectively eliminate fouling from bovine serum albumin, as macroporous and hierarchical electrodes experienced fouling. Such a study, however, does not identify whether there is an upper or lower threshold pore size beyond which fouling occurs.

Electrochemical activation and electrolyte and flow systems do not involve the direct modification of the electrode but can also provide protection from fouling by removing adsorbed material or resisting its adsorption. Similar to the debate over whether H- or O-termination is superior for resisting fouling with boron-doped diamond electrodes, sometimes anodic pulses are superior for electrochemical activation, whereas, in other cases, cathodic pulses or a combination of anodic and cathodic pulses may be more appropriate. The choice could depend on the analyte, system conditions, and the type of electrode. Overall, this is indicative of the generally poor understanding of the pathways involved in electrode fouling and the mechanisms by which antifouling strategies are able to minimise or eliminate fouling. Therefore, research should be directed towards enhancing our understanding of fouling pathways and the specific mechanisms involved in resistance to fouling to develop more effective and versatile antifouling strategies.

References

Adams, K. L.; Jena, B. K.; Percival, S. J.; Zhang, B. Highly sensitive detection of exocytotic dopamine release using a gold-nanoparticle-network microelectrode. *Anal. Chem.* **2010**, *83*, 920–927.

Agnesi, F.; Tye, S. J.; Bledsoe, J. M.; Griessenauer, C. J.; Kimble, C. J.; Sieck, G. C.; Bennet, K. E.; Garris, P. A.; Blaha, C. D.; Lee, K. H. Wireless instantaneous neurotransmitter concentration system-based amperometric detection of dopamine, adenosine, and glutamate for intraoperative neurochemical monitoring. *J. Neurosurg.* **2009**, *111*, 701–711.

Alwarappan, S.; Joshi, R. K.; Ram, M. K.; Kumar, A. Electron transfer mechanism of cytochrome *c* at graphene electrode. *Appl. Phys. Lett.* **2010**, *96*, 263702-1–263702-3.

Anandhakumar, S.; Chandrasekaran, M.; Noel, M. Anodic oxidation of chlorophenols in micelles and microemulsions on glassy carbon electrode: the medium effect on electroanalysis and electrochemical detoxification. *J. Appl. Electrochem.* **2010**, *40*, 303–310.

Anastasova, S.; Spehar-Délèze, A. M.; Bickham, D.; Uebel, P.; Schmidt, M.; Russell, P.; Vadgama, P. Stabilised biosensing using needle-based recess electrodes. *Electroanalysis* **2012**, *24*, 529–538.

Brocenschi, R. F.; Rocha-Filho, R. C.; Duran, B.; Swain, G. M. The analysis of estrogenic compounds by flow injection analysis with amperometric detection using a boron-doped diamond electrode. *Talanta* **2014**, *126*, 12–19.

Casella, I. G.; Contursi, M. Electrocatalytic oxidation of some hydrazine compounds at glassy carbon electrode modified with Co-gluconate complex. *Electroanalysis* **2012**, *24*, 752–758.

Cavanillas, S.; Winquist, F.; Eriksson, M. A self-polishing platinum ring voltammetric sensor and its application to complex media. *Anal. Chim. Acta* **2014**, *859*, 29–36.

Chandra, S.; Miller, A. D.; Wong, D. K. Evaluation of physically small *p*-phenylacetate-modified carbon electrodes against fouling during dopamine detection *in vivo*. *Electrochim. Acta* **2013**, *101*, 225–231.

Chandra, S.; Miller, A. D.; Bendavid, A.; Martin, P. J.; Wong, D. K. Minimizing fouling at hydrogenated conical-tip carbon electrodes during dopamine detection *in vivo*. *Anal. Chem.* **2014**, *86*, 2443–2450.

Chen, B.; Zhang, L.; Chen, G. Determination of salidroside and tyrosol in *Rhodiola* by capillary electrophoresis with graphene/poly (urea-formaldehyde) composite modified electrode. *Electrophoresis* **2011a**, *32*, 870–876.

Chen, Q.; Gan, Z.; Wang, J.; Chen, G. Facile preparation of carbon nanotube/poly (ethyl 2-cyanoacrylate) composite electrode by water-vapor-initiated polymerization for enhanced amperometric detection. *Chem. Eur. J.* **2011b**, *17*, 12458–12464.

Chira, A.; Bucur, B.; Radulescu, M.-C.; Galaon, T.; Radu, G.-L. Study of electrochemically modified electrode with synthesized *N*-benzyl-4,4′-bipyridine with anti-fouling properties for oxygen and hydrogen peroxide detection. *Int. J. Electrochem. Sci.* **2014**, *9*, 4493–4511.

Chumbimuni-Torres, K. Y.; Wang, J. Nanoparticle-induced potentiometric biosensing of NADH at copper ion-selective electrodes. *Analyst* **2009**, *134*, 1614–1617.

D'Eramo, F.; Moressi, M. B.; Fernández, H.; Zón, M. A.; Arévalo, A. H.; Sereno, L. E.; Álvarez-Lueje, A. Studies based on the electrochemical response of 2-(2-nitrophenyl)-1H-benzimidazole at chemically modified electrodes with over-oxidized poly-1-naphthylamine. *Electrochim. Acta* **2010**, *55*, 4421–4427.

da Silva, I. S.; Capovilla, B.; Freitas, K. H. G.; Angnes, L. Strategies to avoid electrode fouling for nimesulide detection using unmodified electrodes. *Anal. Methods* **2013**, *5*, 3546–3551.

Dejmkova, H.; Scampicchio, M.; Zima, J.; Barek, J.; Mannino, S. Determination of total phenols in foods by boron doped diamond electrode. *Electroanalysis* **2009**, *21*, 1014–1018.

Duran, B.; Brocenschi, R. F.; France, M.; Galligan, J. J.; Swain, G. M. Electrochemical activation of diamond microelectrodes: implications for the *in vitro* measurement of serotonin in the bowel. *Analyst* **2014**, *139*, 3160–3166.

Gao, F.; Guo, X.; Yin, J.; Zhao, D.; Li, M.; Wang, L. Electrocatalytic activity of carbon spheres towards NADH oxidation at low overpotential and its applications in biosensors and biofuel cells. *RSC Adv.* **2011**, *1*, 1301–1309.

Gasnier, A.; Pedano, M. L.; Gutierrez, F.; Labbé, P.; Rivas, G. A.; Rubianes, M. D. Glassy carbon electrodes modified with a dispersion of multi-wall carbon nanotubes in dopamine-functionalized polyethylenimine: characterization and analytical applications for nicotinamide adenine dinucleotide quantification. *Electrochim. Acta* **2012**, *71*, 73–81.

Gattrell, M.; Kirk, D. A Fourier transform infrared spectroscopy study of the passive film produced during aqueous acidic phenol electro-oxidation. *J. Electrochem. Soc.* **1992**, *139*, 2736–2744.

Gattrell, M.; Kirk, D. A study of the oxidation of phenol at platinum and preoxidized platinum surfaces. *J. Electrochem. Soc.* **1993**, *140*, 1534–1540.

Godino, N.; del Campo, F. J.; Munoz, F. X.; Hansen, M. F.; Kutter, J. P.; Snakenborg, D. Integration of a zero dead-volume PDMS rotary switch valve in a miniaturised (bio) electroanalytical system. *Lab. Chip.* **2010**, *10*, 1841–1847.

Goto, T.; Yasukawa, T.; Kanda, K.; Matsui, S.; Mizutani, F. Inhibition of electrochemical fouling against biomolecules on a diamond-like carbon electrode. *Anal. Sci.* **2011**, *27*, 91–94.

Grinnell, F.; Feld, M. K. Adsorption characteristics of plasma fibronectin in relationship to biological activity. *J. Biomed. Mater. Res.* **1981**, *15*, 363–381.

Güell, A. G.; Meadows, K. E.; Unwin, P. R.; Macpherson, J. V. Trace voltammetric detection of serotonin at carbon electrodes: comparison of glassy carbon, boron doped diamond and carbon nanotube network electrodes. *Phys. Chem. Chem. Phys.* **2010**, *12*, 10108–10114.

Gui, A. L.; Luais, E.; Peterson, J. R.; Gooding, J. J. Zwitterionic phenyl layers: finally, stable, anti-biofouling coatings that do not passivate electrodes. *ACS Appl. Mater. Interfaces* **2013**, *5*, 4827–4835.

Guo, Q.; Liu, D.; Zhang, X.; Li, L.; Hou, H.; Niwa, O.; You, T. Pd-Ni alloy nanoparticle/carbon nanofiber composites: preparation, structure, and superior electrocatalytic properties for sugar analysis. *Anal. Chem.* **2014**, *86*, 5898–5905.

Hadi, M.; Rouhollahi, A. Application of nanocrystalline graphite-like pyrolytic carbon film electrode for determination of thiols. *Electrochim. Acta* **2011**, *58*, 647–653.

Harreither, W.; Trouillon, R. l.; Poulin, P.; Neri, W.; Ewing, A. G.; Safina, G. Carbon nanotube fiber microelectrodes show a higher resistance to dopamine fouling. *Anal. Chem.* **2013**, *85*, 7447–7453.

Hasanzadeh, M.; Shadjou, N.; Omidinia, E. A novel electroanalytical method for simultaneous detection of two neurotransmitter dopamine and serotonin in human serum. *J. Neurosci. Methods* **2013**, *219*, 52–60.

Hess, H.; Vogel, V. Molecular shuttles based on motor proteins: active transport in synthetic environments. *Rev. Mol. Biotechnol.* **2001**, *82*, 67–85.

Hu, L.; Huo, K.; Chen, R.; Gao, B.; Fu, J.; Chu, P. K. Recyclable and high-sensitivity electrochemical biosensing platform composed of carbon-doped TiO_2 nanotube arrays. *Anal. Chem.* **2011**, *83*, 8138–8144.

Jolly, P.; Formisano, N.; Tkáč, J.; Kasák, P.; Frost, C. G.; Estrela, P. Label-free impedimetric aptasensor with antifouling surface chemistry: a prostate specific antigen case study. *Sens. Actuators B Chem.* **2015**, *209*, 306–312.

Kato, D.; Komoriya, M.; Nakamoto, K.; Kurita, R.; Hirono, S.; Niwa, O. Electrochemical determination of oxidative damaged DNA with high sensitivity and stability using a nanocarbon film. *Anal. Sci.* **2011**, *27*, 703.

Keeley, G. P.; O'Neill, A.; Holzinger, M.; Cosnier, S.; Coleman, J. N.; Duesberg, G. S. DMF-exfoliated graphene for electrochemical NADH detection. *Phys. Chem. Chem. Phys.* **2011**, *13*, 7747–7750.

Kesavan, S.; John, S. A. Simultaneous determination of neurotransmitters and a neuroprotector in human blood serum and urine samples using a diazonium grafted gold nanoparticle film electrode. *Anal. Methods* **2014**, *6*, 9022–9029.

Kesavan, S.; Revin, S. B.; John, S. A. Fabrication, characterization and application of a grafting based gold nanoparticles electrode for the selective determination of an important neurotransmitter. *J. Mater. Chem.* **2012**, *22*, 17560–17567.

Kiran, R.; Scorsone, E.; de Sanoit, J.; Arnault, J.-C.; Mailley, P.; Bergonzo, P. Boron doped diamond electrodes for direct measurement in biological fluids: an *in situ* regeneration approach. *J. Electrochem. Soc.* **2013**, *160*, H67–H73.

Kivlehan, F.; Garay, F.; Guo, J.; Chaum, E.; Lindner, E. Toward feedback-controlled anesthesia: voltammetric measurement of propofol (2,6-diisopropylphenol) in serum-like electrolyte solutions. *Anal. Chem.* **2012**, *84*, 7670–7676.

Kotnik, D.; Novič, M.; LaCourse, W. R.; Pihlar, B. Cathodic re-activation of the gold electrode in pulsed electrochemical detection of carbohydrates. *J. Electroanal. Chem.* **2011**, *663*, 30–35.

Kuralay, F.; Campuzano, S.; Haake, D. A.; Wang, J. Highly sensitive disposable nucleic acid biosensors for direct bioelectronic detection in raw biological samples. *Talanta* **2011**, *85*, 1330–1337.

Lakshmipathiraj, P.; Bhaskar Raju, G.; Sakai, Y.; Takuma, Y.; Yamasaki, A.; Kato, S.; Kojima, T. Studies on electrochemical detoxification of trichloroethene (TCE) on Ti/IrO_2-Ta_2O_5 electrode from aqueous solution. *Chem. Eng. J.* **2012**, *198*, 211–218.

Lee, H.; Dellatore, S. M.; Miller, W. M.; Messersmith, P. B. Mussel-inspired surface chemistry for multifunctional coatings. *Science* **2007**, *318*, 426–430.

Li, W.; Liu, Q.; Liu, L. Antifouling gold surfaces grafted with aspartic acid and glutamic acid based zwitterionic polymer brushes. *Langmuir* **2014**, *30*, 12619–12626.

Liu, X.; Barizuddin, S.; Shin, W.; Mathai, C. J.; Gangopadhyay, S.; Gillis, K. D. Microwell device for targeting single cells to electrochemical microelectrodes for high-throughput amperometric detection of quantal exocytosis. *Anal. Chem.* **2011**, *83*, 2445–2451.

Maiyalagan, T.; Sundaramurthy, J.; Kumar, P. S.; Kannan, P.; Opallo, M.; Ramakrishna, S. Nanostructured α-Fe_2O_3 platform for the electrochemical sensing of folic acid. *Analyst* **2013**, *138*, 1779–1786.

Malmsten, M. *Biopolymers at Interfaces*, 2nd ed., Vol. 110. Marcel Dekker: New York, 2003.

Marinesco, S.; Carew, T. J. Improved electrochemical detection of biogenic amines in *Aplysia* using base-hydrolyzed cellulose-coated carbon fiber microelectrodes. *J. Neurosci. Methods* **2002**, *117*, 87–97.

McCreery, R. L. Advanced carbon electrode materials for molecular electrochemistry. *Chem. Rev.* **2008**, *108*, 2646–2687.

McQuistan, A.; Zaitouna, A. J.; Echeverria, E.; Lai, R. Y. Use of thiolated oligonucleotides as anti-fouling diluents in electrochemical peptide-based sensors. *Chem. Commun.* **2014**, *50*, 4690–4692.

Merli, D.; Dondi, D.; Pesavento, M.; Profumo, A. Electrochemistry of olanzapine and risperidone at carbon nanotubes modified gold electrode through classical and DFT approaches. *J. Electroanal. Chem.* **2012**, *683*, 103–111.

Milczarek, G. Preparation, characterization and electrocatalytic properties of an iodine|lignin-modified gold electrode. *Electrochim. Acta* **2009**, *54*, 3199–3205.

Moreno, M.; Arribas, A. S.; Bermejo, E.; Zapardiel, A.; Chicharro, M. Analysis of polyphenols in white wine by CZE with amperometric detection using carbon nanotube-modified electrodes. *Electrophoresis* **2011**, *32*, 877–883.

Motaghedifard, M.; Ghoreishi, S. M.; Behpour, M.; Moghadam, Z.; Salavati-Niasari, M. Electrochemical study of new self-assembled monolayer of 2-hydroxy-*N*′ 1-[(*E*)-1-(3-methyl-2-thienyl) methylidene] benzohydrazide on gold electrode as an epinephrine sensor element. *J. Electroanal. Chem.* **2012**, *682*, 14–22.

Mudrinić, T.; Mojović, Z.; Milutinović-Nikolić, A.; Banković, P.; Dojčinović, B.; Vukelić, N.; Jovanović, D. Beneficial effect of Ni in pillared bentonite based electrodes on the electrochemical oxidation of phenol. *Electrochim. Acta* **2014**, *144*, 92–99.

Muna, G. W.; Partridge, M.; Sirhan, H.; VerVaet, B.; Guerra, N.; Garner, H. Electrochemical detection of steroid hormones using a nickel-modified glassy carbon electrode. *Electroanalysis* **2014**, *26*, 2145–2151.

Narmadha, M.; Noel, M.; Suryanarayanan, V. Relative deactivation of boron-doped diamond (BDD) and glassy carbon (GC) electrodes in different electrolyte media containing substituted phenols–voltammetric and surface morphologic studies. *J. Electroanal. Chem.* **2011**, *655*, 103–110.

Özel, R. E.; Wallace, K. N.; Andreescu, S. Chitosan coated carbon fiber microelectrode for selective *in vivo* detection of neurotransmitters in live zebrafish embryos. *Anal. Chim. Acta* **2011**, *695*, 89–95.

Patel, A. N.; Tan, S.-y.; Miller, T. S.; Macpherson, J. V.; Unwin, P. R. Comparison and reappraisal of carbon electrodes for the voltammetric detection of dopamine. *Anal. Chem.* **2013a**, *85*, 11755–11764.

Patel, J.; Radhakrishnan, L.; Zhao, B.; Uppalapati, B.; Daniels, R. C.; Ward, K. R.; Collinson, M. M. Electrochemical properties of nanostructured porous gold electrodes in biofouling solutions. *Anal. Chem.* **2013b**, *85*, 11610–11618.

Paul, D. W.; Prajapati, I.; Reed, M. L. Electropolymerized eugenol: evaluation as a protective film for oxygen sensing. *Sens. Actuators B Chem.* **2013**, *183*, 129–135.

Perez, E.; Lahlil, K.; Rougeau, C.; Moraillon, A.; Chazalviel, J.-N. L.; Ozanam, F. O.; Gouget-Laemmel, A. C. Influence of the molecular design on the antifouling performance of poly (ethylene glycol) monolayers grafted on (111) Si. *Langmuir* **2012**, *28*, 14654–14664.

Picher, M. M.; Küpcü, S.; Huang, C.-J.; Dostalek, J.; Pum, D.; Sleytr, U. B.; Ertl, P. Nanobiotechnology advanced antifouling surfaces for the continuous electrochemical monitoring of glucose in whole blood using a lab-on-a-chip. *Lab. Chip.* **2013**, *13*, 1780–1789.

Pirvu, C.; Manole, C. C. Electrochemical surface plasmon resonance for *in situ* investigation of antifouling effect of ultra thin hybrid polypyrrole/PSS films. *Electrochim. Acta* **2013**, *89*, 63–71.

Qiu, C.; Chen, T.; Wang, X.; Li, Y.; Ma, H. Application of horseradish peroxidase modified nanostructured Au thin films for the amperometric detection of 4-chlorophenol. *Colloids Surf. B Biointerfaces* **2013**, *103*, 129–135.

Quynh, B. T. P.; Byun, J. Y.; Kim, S. H. Nanoporous gold for amperometric detection of amino-containing compounds. *Sens. Actuators B Chem.* **2014**, *193*, 1–9.

Raj, M. A.; John, S. A. Graphene layer modified glassy carbon electrode for the determination of norepinephrine and theophylline in pharmaceutical formulations. *Anal. Methods* **2014**, *6*, 2181–2188.

Razmi, H.; Heidari, H. Nafion/lead nitroprusside nanoparticles modified carbon ceramic electrode as a novel amperometric sensor for L-cysteine. *Anal. Biochem.* **2009**, *388*, 15–22.

Revin, S. B.; John, S. A. Electrochemical sensor for neurotransmitters at physiological pH using a heterocyclic conducting polymer modified electrode. *Analyst* **2012a**, *137*, 209–215.

Revin, S. B.; John, S. A. Selective determination of inosine in the presence of uric acid and hypoxanthine using modified electrode. *Anal. Biochem.* **2012b**, *421*, 278–284.

Revin, S. B.; John, S. A. Selective determination of L-tyrosine in the presence of ascorbic and uric acids at physiological pH using the electropolymerized film of 3-amino-5-mercapto-1,2,4-triazole. *Sens. Actuators B Chem.* **2012c**, *161*, 1059–1066.

Revin, S. B.; John, S. A. Simultaneous determination of vitamins B2, B9 and C using a heterocyclic conducting polymer modified electrode. *Electrochim. Acta* **2012d**, *75*, 35–41.

Roeser, J.; Alting, N. F.; Permentier, H. P.; Bruins, A. P.; Bischoff, R. Boron-doped diamond electrodes for the electrochemical oxidation and cleavage of peptides. *Anal. Chem.* **2013**, *85*, 6626–6632.

Safavi, A.; Maleki, N.; Farjami, E. Fabrication of a glucose sensor based on a novel nanocomposite electrode. *Biosens. Bioelectron.* **2009**, *24*, 1655–1660.

Safavi, A.; Maleki, N.; Tajabadi, F. SE-30 graphite composite electrode: an alternative for the development of electrochemical biosensors. *Electroanalysis* **2010**, *22*, 2460–2466.

Safavi, A.; Momeni, S. Electrocatalytic oxidation of tryptophan at gold nanoparticle-modified carbon ionic liquid electrode. *Electroanalysis* **2010**, *22*, 2848–2855.

Sansuk, S.; Bitziou, E.; Joseph, M. B.; Covington, J. A.; Boutelle, M. G.; Unwin, P. R.; Macpherson, J. V. Ultrasensitive detection of dopamine using a carbon nanotube network microfluidic flow electrode. *Anal. Chem.* **2012**, *85*, 163–169.

Sarvothaman, M. K.; Kim, K. S.; Seale, B.; Brodersen, P. M.; Walker, G. C.; Wheeler, A. R. Dynamic fluoroalkyl polyethylene glycol co-polymers: a new strategy for reducing protein adhesion in lab-on-a-chip devices. *Adv. Funct. Mater.* **2015**, *25*, 506–515.

Sasso, L.; Heiskanen, A.; Diazzi, F.; Dimaki, M.; Castillo-León, J.; Vergani, M.; Landini, E.; Raiteri, R.; Ferrari, G.; Carminati, M. Doped overoxidized polypyrrole microelectrodes as sensors for the detection of dopamine released from cell populations. *Analyst* **2013**, *138*, 3651–3659.

Schmidt, A. C.; Dunaway, L. E.; Roberts, J. G.; McCarty, G. S.; Sombers, L. A. Multiple scan rate voltammetry for selective quantification of real-time enkephalin dynamics. *Anal. Chem.* **2014**, *86*, 7806–7812.

Shan, C.; Yang, H.; Song, J.; Han, D.; Ivaska, A.; Niu, L. Direct electrochemistry of glucose oxidase and biosensing for glucose based on graphene. *Anal. Chem.* **2009**, *81*, 2378–2382.

Sharp, D. Printed composite electrodes for in-situ wound pH monitoring. *Biosens. Bioelectron.* **2013**, *50*, 399–405.

Sheng, S.; Zhang, L.; Chen, G. Determination of 5,7-dihydroxychromone and luteolin in peanut hulls by capillary electrophoresis with a multiwall carbon nanotube/poly (ethylene terephthalate) composite electrode. *Food Chemistry* **2014**, *145*, 555–561.

Shin, D.; Tryk, D. A.; Fujishima, A.; Merkoçi, A.; Wang, J. Resistance to surfactant and protein fouling effects at conducting diamond electrodes. *Electroanalysis* **2005**, *17*, 305–311.

Shpilevaya, I.; Foord, J. S. Electrochemistry of methyl viologen and anthraquinonedisulfonate at diamond and diamond powder electrodes: the influence of surface chemistry. *Electroanalysis* **2014**, *26*, 2088–2099.

Singh, Y. S.; Sawarynski, L. E.; Dabiri, P. D.; Choi, W. R.; Andrews, A. M. Head-to-head comparisons of carbon fiber microelectrode coatings for sensitive and selective neurotransmitter detection by voltammetry. *Anal. Chem.* **2011**, *83*, 6658–6666.

Stoytcheva, M.; Zlatev, R.; Gochev, V.; Velkova, Z.; Montero, G.; Beleño, M. Amperometric biosensors precision improvement. Application to phenolic pollutants determination. *Electrochim. Acta* **2014**, *147*, 25–30.

Summerlot, D.; Kumar, A.; Das, S.; Goldstein, L.; Seal, S.; Diaz, D.; Cho, H. J. Nanoporous gold electrode for electrochemical sensors in biological environment. *Proc. Eng.* **2011**, *25*, 1457–1460.

Takmakov, P.; Zachek, M. K.; Keithley, R. B.; Walsh, P. L.; Donley, C.; McCarty, G. S.; Wightman, R. M. Carbon microelectrodes with a renewable surface. *Anal. Chem.* **2010**, *82*, 2020–2028.

Tan, S. M.; Poh, H. L.; Sofer, Z.; Pumera, M. Boron-doped graphene and boron-doped diamond electrodes: detection of biomarkers and resistance to fouling. *Analyst* **2013**, *138*, 4885–4891.

Tavakkoli, N.; Nasrollahi, S. Non-enzymatic glucose sensor based on palladium coated nanoporous gold film electrode. *Aust. J. Chem.* **2013**, *66*, 1097–1104.

Teymourian, H.; Salimi, A.; Hallaj, R. Electrocatalytic oxidation of NADH at electrogenerated NAD^+ oxidation product immobilized onto multiwalled carbon nanotubes/ionic liquid nanocomposite: application to ethanol biosensing. *Talanta* **2012**, *90*, 91–98.

Thevenot, P.; Hu, W.; Tang, L. Surface chemistry influence implant biocompatibility. *Curr. Top. Med. Chem.* **2008**, *8*, 270.

Thomas, T.; Mascarenhas, R. J.; D'Souza, O. J.; Martis, P.; Dalhalle, J.; Swamy, B. Multi-walled carbon nanotube modified carbon paste electrode as a sensor for the amperometric detection of L-tryptophan in biological samples. *J. Colloid Interface Sci.* **2013**, *402*, 223–229.

Tormin, T. F.; Cunha, R. R.; Silva, R. A. B. d.; Munoz, R. A. A.; Richter, E. M. Combination of screen-printed electrodes and batch injection analysis: a simple, robust, high-throughput, and portable electrochemical system. *Sens. Actuators B Chem.* **2014**, *202*, 93–98.

Trouillon, R.; Combs, Z.; Patel, B. A.; O'Hare, D. Comparative study of the effect of various electrode membranes on biofouling and electrochemical measurements. *Electrochem. Commun.* **2009**, *11*, 1409–1413.

Trouillon, R.; O'Hare, D.; Einaga, Y. Effect of the doping level on the biological stability of hydrogenated boron doped diamond electrodes. *Phys. Chem. Chem. Phys.* **2011**, *13*, 5422–5429.

Trouillon, R.; Einaga, Y.; Gijs, M. A. Cathodic pretreatment improves the resistance of boron-doped diamond electrodes to dopamine fouling. *Electrochem. Commun.* **2014**, *47*, 92–95.

Wilson, C. J.; Clegg, R. E.; Leavesley, D. I.; Pearcy, M. J. Mediation of biomaterial-cell interactions by adsorbed proteins: a review. *Tissue Eng.* **2005**, *11*, 1–18.

Xiang, L.; Yu, P.; Hao, J.; Zhang, M.; Zhu, L.; Dai, L.; Mao, L. Vertically aligned carbon nanotube-sheathed carbon fibers as pristine microelectrodes for selective monitoring of ascorbate *in vivo*. *Anal. Chem.* **2014**, *86*, 3909–3914.

Xue, Q.; Kato, D.; Kamata, T.; Umemura, S.; Hirono, S.; Niwa, O. Electron cyclotron resonance-sputtered nanocarbon film electrode compared with diamond-like carbon and glassy carbon electrodes as regards electrochemical properties and biomolecule adsorption. *Jpn. J. Appl. Phys.* **2012**, *51*, 090124.

Yang, D.; Zhu, L.; Jiang, X. Electrochemical reaction mechanism and determination of Sudan I at a multi wall carbon nanotubes modified glassy carbon electrode. *J. Electroanal. Chem.* **2010**, *640*, 17–22.

Yang, X.; Kirsch, J.; Olsen, E. V.; Fergus, J. W.; Simonian, A. L. Anti-fouling PEDOT: PSS modification on glassy carbon electrodes for continuous monitoring of tricresyl phosphate. *Sens. Actuators B Chem.* **2013**, *177*, 659–667.

Zestos, A. G.; Jacobs, C. B.; Trikantzopoulos, E.; Ross, A. E.; Venton, B. J. Polyethylenimine carbon nanotube fiber electrodes for enhanced detection of neurotransmitters. *Anal. Chem.* **2014**, *86*, 8568–8575.

Zhang, L.; Li, D.; Meng, W.; Huang, Q.; Su, Y.; Wang, L.; Song, S.; Fan, C. Sequence-specific DNA detection by using biocatalyzed electrochemiluminescence and non-fouling surfaces. *Biosens. Bioelectron.* **2009**, *25*, 368–372.

Zhao, H.; Bian, X.; Galligan, J. J.; Swain, G. M. Electrochemical measurements of serotonin (5-HT) release from the guinea pig

mucosa using continuous amperometry with a boron-doped diamond microelectrode. *Diamond Relat. Mater.* **2010**, *19*, 182–185.

Zheng, S.; Huang, Y.; Chen, G. Electrochemical behavior of *o*-sec-butylphenol at glassy carbon electrode modified with multiwalled carbon nanotubes and 1-butyl-3-methylimidazolium hexafluorophosphate. *Analyst* **2012**, *137*, 4335–4342.

Zhou, M.; Zhai, Y.; Dong, S. Electrochemical sensing and biosensing platform based on chemically reduced graphene oxide. *Anal. Chem.* **2009**, *81*, 5603–5613.

Zhuiykov, S.; Kalantar-zadeh, K. Development of antifouling of electrochemical solid-state dissolved oxygen sensors based on nanostructured $Cu_{0.4}Ru_{3.4}O_7$+RuO_2 sensing electrodes. *Electrochim. Acta* **2012**, *73*, 105–111.